

# **Anti-Stokes Spectroscopy of Crystalline Plasmonic Metals**

**Daniel Abraham Elmaleh**

Semester Project  
Master's in Microengineering



**Professor:** Olivier Martin

**Supervisors:** Sergejs Boroviks, Siarhei Zavatski

**Location:** Nano-Photonics and Metrology Laboratory

**Date:** January 3, 2025

## **Abstract**

The physical mechanism of photoluminescence (PL) in crystalline plasmonic metals, particularly the anti-Stokes (AS) emission, remains a subject of debate and intrigue within the plasmonics research community. While Stokes PL has been extensively studied, the AS counterpart offers promising applications, such as precision nanoscale thermometry. This project investigates the PL emission characteristics of chemically synthesized gold (Au) and silver (Ag) crystalline flakes, with a focus on the thickness-dependent behavior of the AS spectrum. Employing advanced nanofabrication, microscopy, spectroscopy, and computational simulation techniques, the study aims to elucidate the quantum mechanical effects underpinning AS emission. The outcomes are expected to provide insights into hot electron dynamics and pave the way for innovative applications in nanophotonics, potentially contributing to the scientific understanding of metal photoluminescence and electronic Raman scattering mechanisms.

# Contents

<b>Acknowledgments</b>	ii
<b>1 Introduction</b>	1
1.1 Literature review . . . . .	2
1.2 Anti-Stokes Thermometry in Nanoplasmonics . . . . .	2
<b>2 Methodology</b>	4
2.1 Growth of Gold Flakes . . . . .	4
2.2 Metrology . . . . .	5
2.3 Etching . . . . .	5
2.4 Optical Measurements . . . . .	6
2.4.1 Experimental Methodology . . . . .	7
2.5 Analysis & data processing procedure . . . . .	7
2.6 Color to Thickness Mapping for Gold Flakes . . . . .	8
2.7 Modeling and Predictions for Thickness . . . . .	9
2.7.1 Data Preprocessing . . . . .	9
2.7.2 Exponential Fit . . . . .	9
2.7.3 Other models . . . . .	10
<b>3 Results &amp; Discussion</b>	12
3.1 Growth, Etching & Metrology . . . . .	12
3.1.1 Color-to-Thickness and Etching Rate Extraction . . . . .	12
3.2 Optical measurements . . . . .	14
3.2.1 532nm/633nm analysis . . . . .	15
3.3 Computation of Transmitted Power in COMSOL . . . . .	16
3.4 Atomic Force Microscopy (AFM) Analysis . . . . .	19
<b>4 Conclusion</b>	20
<b>A Appendix A (Figures)</b>	22
<b>B Appendix B (Reports)</b>	26

# Acknowledgments

I would like to express my deepest gratitude to all the individuals and institutions who supported me throughout this project.

Firstly, I am grateful to the **Nam Lab** and **Professor Olivier Martin** for their guidance, expertise that greatly enriched this work. Special thanks also go to **Sergejs Boroviks** and **Siarhei Zavatski** for their technical assistance and insightful contributions during the experimental phases.

I extend my appreciation to the **Center of MicroNanoTechnology (CMi)** and the **School of Engineering (STI)** at EPFL, whose state-of-the-art facilities and tools provided the necessary resources for this research. Their support and access to advanced equipment made this work possible.

Finally, I am deeply thankful for the collaborative and intellectually stimulating environment at EPFL, which fostered the successful completion of this project.

# 1 Introduction

A distinction should be made between photoluminescence and Raman scattering, particularly electronic Raman scattering. The choice of terminology is critical, as there are clear differences between molecular spectroscopy, semiconductors, and metals. For metals, the high density of free electrons is thought to screen the potential interaction of light with nuclei. This highlights the importance of terms like *electronic* and *scattering*, as the interaction is not understood as transitions between electronic states, like in *luminescence*, but between a state and a virtual state, inelastic scattering. This conceptualization differentiates scattering from luminescence, where no light is generated by the material (absorption and re-emission).

This distinction makes experiments like these essential for exploring light-matter interactions, especially at the quantum scale, since energy level discretization may arise due to quantum confinement. The goal is to better understand phenomena like anti-Stokes Raman electronic scattering, assuming the terminology reflects the observed behavior.

Photoluminescence (PL) in plasmonic metals has garnered significant attention due to its implications for understanding hot electron dynamics and electronic band structures. The anti-Stokes (AS) component of PL, characterized by emission at wavelengths shorter than the excitation source, presents an intriguing avenue for research. Recent advancements highlight its potential in precision thermometry and its ability to reveal quantum mechanical effects. Despite these prospects, AS PL in crystalline plasmonic metals remains under-explored.

This project focuses on the synthesis, characterization, and analysis of thin crystalline flakes of gold (Au), employing anisotropic etching to control flake thickness. By leveraging techniques such as optical microscopy, atomic force microscopy (AFM), and numerical electromagnetic simulations (COMSOL), I aim to investigate the thickness-dependent AS PL behavior. Furthermore, this work integrates both experimental and theoretical approaches to provide a comprehensive understanding of the AS emission phenomena. The findings are expected to deepen the theoretical knowledge in plasmonics and contribute to practical applications in nanoscale thermometry and nanophotonics. As part of the project the growth and etching optimization were part of the analysis and results.

## 1.1 Literature review

## 1.2 Anti-Stokes Thermometry in Nanoplasmonics

Anti-Stokes spectroscopy has emerged as a powerful technique for probing nanoscale temperature distributions and light-matter interactions in plasmonic systems. By leveraging inelastic scattering processes, particularly anti-Stokes emission, researchers can explore thermal dynamics and electronic states of plasmonic nanoparticles. This report highlights recent advancements in anti-Stokes thermometry, focusing on its principles, mechanisms, and applications, as outlined by Baffou (2021) [1].

Anti-Stokes thermometry operates on the temperature-dependent properties of anti-Stokes emission, where scattered photons gain energy from thermally excited states, resulting in emission at shorter wavelengths than the incident light. The intensity of this emission, governed by a Boltzmann distribution, is given by:

$$I_{AS} \propto e^{-\Delta E/k_B T}, [2] \quad (1.1)$$

where  $I_{AS}$  is the anti-Stokes intensity,  $\Delta E$  is the energy difference,  $k_B$  is Boltzmann's constant, and  $T$  is the temperature. Compared to fluorescence-based thermometry, which is sensitive to environmental conditions (e.g., pH, ionicity), anti-Stokes thermometry provides a robust, label-free approach, directly measuring nanoparticle temperature.

Anti-Stokes emission arises primarily from two mechanisms:

- **Electronic Raman Scattering (ERS):** Coherent, inelastic scattering involving conduction band transitions.
- **Photoluminescence (PL):** Incoherent emission from electronic excitations and radiative relaxation.

Applications of anti-Stokes thermometry span:

- **Plasmonic Heating:** Quantifying nanoscale temperature changes in plasmonic systems.
- **Photocatalysis:** Investigating thermal effects in plasmon-assisted reactions.
- **Thermal Imaging:** Achieving sub-diffraction spatial resolution for temperature mapping.

Despite its advantages, challenges include accurate modeling of photonic density states, enhancing signal-to-noise ratios for smaller nanoparticles, and extending the method to non-gold materials. Future work aims to refine theoretical models and experimental techniques, broadening the applicability of anti-Stokes spectroscopy in nanoplasmonics.

The advancement of nanophotonics and plasmonics has heavily relied on the development of novel materials with exceptional optical and electronic properties. Among these, gold nanostructures have emerged as a cornerstone due to their unique plasmonic behavior, tunability, and biocompatibility. Recent efforts have focused on enhancing the understanding and applications of gold-based materials in nanoscale thermometry, ultrathin structures, and quantum-mechanical phenomena.

One significant area of progress is the use of gold nanoparticles for absolute temperature measurements at the nanoscale. Carattino et al. [2] demonstrated the feasibility of using gold nanorods as calibration-free nanothermometers based on anti-Stokes emission. Their work established a robust theoretical and experimental framework, showing that precise temperature measurements could be achieved through intrinsic photoluminescence properties, making them highly suitable for photothermal therapy and drug delivery applications.

Another breakthrough in nanophotonics is the controlled synthesis of ultrathin, single-crystalline gold structures. Krauss et al. [3] developed a wet-chemical approach to grow high-aspect-ratio gold platelets with tunable lateral sizes and thicknesses. Their systematic analysis of growth dynamics revealed critical factors for achieving aspect ratios exceeding 10,000. These platelets exhibit exceptional plasmonic properties, making them suitable for transparent conductive substrates and advanced optoelectronic devices.

Additionally, Hogan et al. [4] explored the steady-state dynamics of hot electrons in plasmonic gold nanostructures under continuous optical excitation. Their findings elucidated the persistence of non-equilibrium hot electron populations, extending our understanding of electron-phonon interactions and their implications for photochemical and optoelectronic processes.

Finally, Bowman et al. [5] delved into the quantum-mechanical effects of photoluminescence from ultrathin crystalline gold films. Their study identified enhanced pre-scattered luminescence driven by quantum confinement near the Fermi level, providing insights into the electronic band structure of gold films and their potential in label-free nanoscale thermometry.

These advancements collectively underscore the transformative potential of gold-based nanomaterials. From nanoscale thermometry to the development of ultrathin gold structures. These studies provide the foundation for this project.

## 2 Methodology

To achieve the project's goals, the following processes were carried out:

- Growth of 2D crystallin gold flakes and optimization of production methods.
- Etching processes aimed at controlled rates (ideally below 5 nm).
- Optical measurements using laser station and a spectrometer to study responses to wavelength, power, polarization, and sample orientation.

As part of the project, understanding the growth mechanism and optimizing it as well as the etching and extracting etching rates was important. To do so additionally to the usual metrology technics, a code that stores a lookup table that maps RGB color and Lab color space info was developed and used to then build a model that fits an exponential to this processed data. and thus a different way to extract thickness data and etching rates was tested.

### 2.1 Growth of Gold Flakes

The fabrication and characterization of gold flakes were carried out using the following steps:

#### Materials and Setup

Gold crystal growth was performed using 50 mL polypropylene centrifuge tubes, with ethylene glycol (EG) as the solvent. Chloroauric acid ( $\text{HAuCl}_4$ ) served as the gold source, dissolved in a mixture of ethylene glycol and water. Chemical concentrations were calculated relative to the ethylene glycol volume and varied to optimize growth conditions.

#### Substrates and Preparation

Float glass, D263 glass, and Menzel coverslips (24 mm × 24 mm, 1.5 thickness) were employed as substrates. Coverslips were cleaned with acetone and isopropanol (IPA), followed by rinsing with ultrapure water.

#### Growth Process and Handling

The substrates were immersed in the growth solution, with some placed back-to-back for testing. The solution was heated to 80°C in a closed centrifuge tube for durations

ranging from 12 to 60 hours to promote crystal growth. Post-growth, substrates were rinsed with acetone, IPA, and ultrapure water, then dried with nitrogen gas.

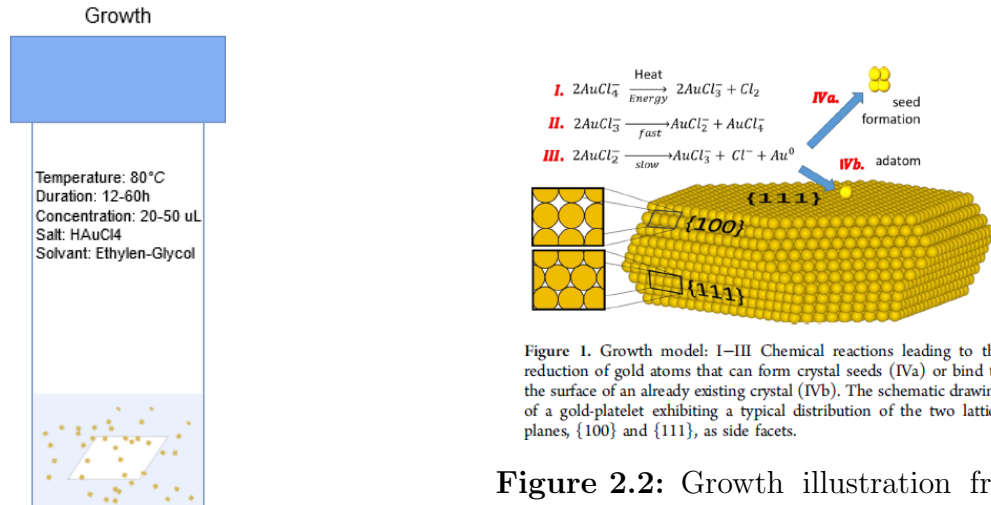


**Figure 2.1:** Experimental growth experiment.

Growth was tested on various substrates. A roughness experiment with glass substrates assessed the correlation between roughness and the quality, size, and number of gold flakes. Techniques such as growing the flakes in the gap between two substrates, described in [6], were tested but proved ineffective due to uncontrolled gap sizes and potentially gases evaporating from the surface and detaching the two substrates. Most growth experiments I carried utilized float glass, some cover slips and D263 glass were also used.

## 2.2 Metrology

Analysis tools included:

- Optical microscope with a camera for localization and selection of the flakes.
- Atomic Force Microscope (AFM) (Bruker FastScan) for flake quality and thickness analysis.

## 2.3 Etching

Etching experiments were conducted to refine the etching process and achieve a controlled etching rate, ideally below 5 nm. Despite challenges in precision, these experiments provided valuable insights into improving the procedure.

Two etching recipes were tested. Initially, Cysteamine hydrochloride and water were used, but it did not yield satisfactory results, likely due to issues in the experimental setup (described in Figure 3.4). Later the exact method described in [7] was employed.

Etching was conducted in plastic bottles, which introduced two significant problems:

- **Material Contamination:** Melting of the plastic added residues to the solution, contaminating the experiment.
- **Volatility Issues:** Chloroform evaporation through the bottle caps caused concentration variations, compromising the consistency of the etching rate.

These issues provoked the change to glass sealed bottles that were a more robust setup. (Figure 2.3)

The etching process for 2D gold films (2DGFs) involved immersing gold flakes in cysteamine solutions (150/200/250 mM in chloroform). The chloroform solvent ensured uniform etching, while cysteamine reacted with oxygen to form radicals that created soluble gold-thiolate complexes, enabling layer-by-layer etching at an approximate rate of 0.2 nm/min [7]. Notably, the lateral size of the flakes remained unchanged during the process.

**Crystalline Structure and Orientation:** As observed in Figure 2.2, the gold crystalline flakes predominantly exhibit the (100) plane on the surface. This structural feature allows for layer-by-layer etching due to the significant differences in bond energy across different planes. The (100) plane displays a six-fold polygonal symmetry, corresponding to a rotational period of  $360^\circ/6 = 60^\circ$ . Consequently, by rotating the sample by  $90^\circ$ , it is possible to achieve an intermediate orientation compared to the parallel side plane.



**Figure 2.3:** Etching process experiment.

**Figure 2.4:** Etching illustration from [7].

## 2.4 Optical Measurements

Optical measurements were performed using a laser station and a spectrometer to study the material's response to various parameters, including wavelength, power, polarization, and sample orientation. These experiments were designed to characterize the flakes' optical properties under controlled conditions.

The optical measurements, forming the core of this research, were conducted in the optical laboratory using two lasers: a red laser with a wavelength of 633 nm and a green laser with a wavelength of 532 nm. The setup, illustrated in Figure 2.5, included mirrors, polarizers, a microscope, a grating spectrometer, filters, and lenses. This configuration allowed for the calibration, alignment, and measurement of the optical response of Si, Ag, and Au mirrors, as well as three selected gold flakes with known thicknesses, previously measured using an AFM machine in the cleanroom.

A powermeter was utilized to measure laser intensities, enabling variation in both the intensity and polarization of the incoming light. These adjustments extended to the light entering the spectrometer, allowing for comprehensive testing of various responses

from the two-dimensional (2D) gold flakes. Using two polarizers in the setup facilitated precise control of the polarization, enabling experiments with co-polarized (maximum response) and cross-polarized (minimum response) configurations.

### 2.4.1 Experimental Methodology

The laser light was directed perpendicular (90 degrees) to the gold flake surface. However, the Gaussian nature of the beam introduces a slight angular spread due to focalization by the lens, resulting in revolution symmetry on the target. Key experiments included:

- **Red Laser (633 nm):** Laser power and thickness variation tests were conducted.
- **Green Laser (532 nm):** Experiments involved variations in laser power, flake thickness, light polarization at the spectrometer, and sample orientation.

Silicon was used to calibrate the spectrum by leveraging the known Raman peak of Si at  $[520.2 \text{ cm}^{-1}]$ . Separate wavelength shifts were applied for the red and green laser analyses to ensure accurate spectrum calibration. Background subtraction was employed to eliminate laser artifacts caused by filtering issues or other laser modes.

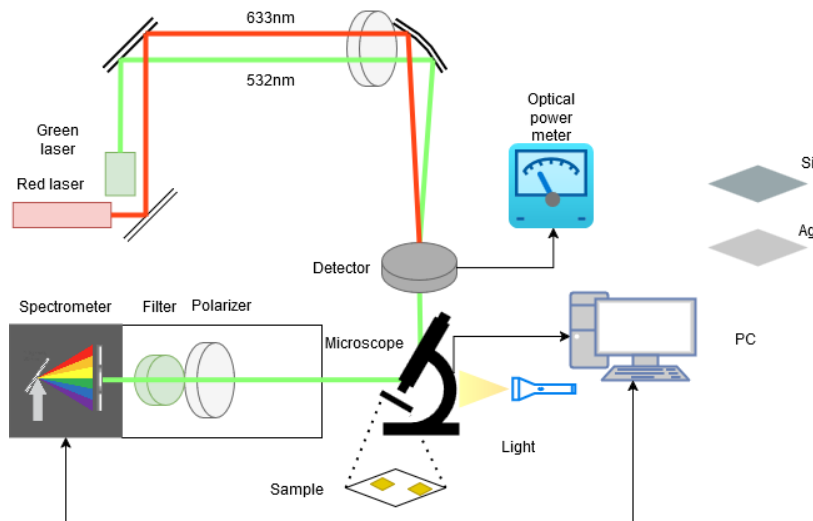


**Figure 2.5:** Schematic representation of the optical setup used for measurements. The diagram illustrates the arrangement of key components and their interconnections (The detector is removed after measuring and only one of the 2 lasers operate at once).

## 2.5 Analysis & data processing procedure

I developed a Python script [8] to process raw Raman/PL spectra, remove cosmic-ray artifacts, subtract background signals using Ag mirror, filter the laser line and integrate the Stokes/Anti-Stokes spectral regions. I also calibrated the wavelength axis using a silicon reference (Si peak at  $\sim 520 \text{ cm}^{-1}$ ) following the relationship:  $\text{shift} = \lambda_{\text{expected,Si}} - \lambda_{\text{detected,Si}}$ . Then produced a PDF report showing each plot and relevant metadata As seen in Appendix B.

**Background Subtraction & Non-Negative Shift:** I measured a background spectrum (from an *Ag* mirror) with the same acquisition settings. For each data file:

- I interpolated the background onto the main wavelength grid and subtract it:

$$I_{\text{corrected}, i} = I_i - I_{\text{bkg}, i}.$$

- Where  $\{(x_i, I_i)\}$  is the sample spectrum and  $\{(x_i, I_{\text{bkg}, i})\}$  the corresponding background.
- For intensities below zero, the entire spectrum is shifted upwards to have a minimum at 0. Namely,

$$I_{\text{final}, i} = I_{\text{corrected}, i} - \min(\{I_{\text{corrected}, i}\}),$$

if  $\min(I_{\text{corrected}}) < 0$ .

This ensures no nonsense negative intensities, which can appear from slight over-subtraction.

**Stokes and Anti-Stokes Separation & Integration:** After background subtraction and cosmic-ray removal, each spectrum is split around the laser line  $\lambda_{\text{laser}}$ . A typical  $\pm 5\text{nm}$  window around the laser line to avoid any direct laser signal or edge filters. Then:

- **Stokes region:**  $\lambda > \lambda_{\text{laser}}$ .
- **Anti-Stokes region:**  $\lambda < \lambda_{\text{laser}}$ .

For each region, the data is smoothed to reduce noise and then compute the fast Fourier transform (FFT) for spectral analysis of any periodic modulations. An integral of the final Stokes and Anti-Stokes intensities is calculated:

$$\text{Area}_{\text{Stokes}} = \int \text{counts}_{\text{Stokes}}(\lambda) d\lambda, \quad \text{Area}_{\text{Anti-Stokes}} = \int \text{counts}_{\text{Anti-Stokes}}(\lambda) d\lambda,$$

using the trapezoidal rule. These integrals are reported in the final PDF to quantify the overall spectral intensity in each region. They are of dimension  $\text{counts} * WL$ , which is not directly the energy related but is sufficient since we are later on looking at the ratio of  $(I_{as})/(I_s)$ .

## 2.6 Color to Thickness Mapping for Gold Flakes

A Python-based graphical user interface (GUI) was developed [9] to map the observed colors of gold flakes, captured via optical microscopy, to their corresponding thicknesses. The tool efficiently maps RGB and LAB color values to thickness measurements using substrate-specific lookup tables, aiding experimental analysis and validation.

The GUI allows users to:

- Select substrate types (e.g., Float, Borofloat, Si, D263).
- Input color values and thicknesses manually or extract them from images, saving the data as a CSV lookup table specific to the substrate.
- Analyze images by selecting regions of interest (ROI), averaging RGB values, and matching them with the lookup table. Results are saved as a separate CSV file.

The program generates:

- **Lookup Tables:** CSV files mapping RGB and LAB color values to thicknesses.
- **Results Files:** CSV files documenting thickness mappings derived from analyzed images, using normalized RGB and LAB values matched to the image background.

This tool proved invaluable for this project, particularly given time constraints and the unavailability of the AFM machine due to maintenance. Despite these challenges, the pre-collected lookup tables provided a solid foundation for developing a prediction model to estimate the thicknesses of etched flakes. This model simultaneously optimized the GUI tool and offered insights into etching rates derived from these predictions.

In the next section, a tool to predict from the lookup tables will be presented.

## 2.7 Modeling and Predictions for Thickness

For the mapping of the flakes from color to thickness I explored the modeling process for predicting the thickness. The goal was to establish a relationship between the features of the flakes and their corresponding thickness. I employed both machine learning models and an analytical exponential fit, evaluating the results to identify the most suitable approach.

### 2.7.1 Data Preprocessing

The dataset consisted of multiple features including  $R$ ,  $G$ ,  $B$ ,  $L$ ,  $a$ , and  $b$  and their AFM measured thickness (Figures 2.6 & 2.7). The data was cleaned and transformed to enhance its predictive power. In particular, I introduced new features such as  $L \times G$ ,  $L + G$ , and  $(L \times G) - B$ , to explore potential relationships between the thickness and combinations of these variables.

### 2.7.2 Exponential Fit

Initially, I attempted to model the relationship between thickness and certain feature combinations using an exponential function of the form:

$$\text{Thickness} = a \cdot \exp(b \cdot X) + c$$

where  $X$  represents the chosen feature combination, and  $a$ ,  $b$ , and  $c$  are the parameters to be optimized. I tried different combinations, including  $L \times G$ ,  $(L \times G) - B$ , and others. The optimal exponential fit was obtained for  $(L \times G) - B$ , yielding a model with a Mean Squared Error (MSE) of 14.80, which showed a reasonable fit to the data. The resulting parameters lead to this exponential expression:

$$\text{Thickness} = 1.63 \cdot \exp(0.34 \cdot ((L \times G) - B)) + 25.22$$

In Figure 2.8 the parameter importance, as well as Outlier removal and the data in the  $L \times G$ ,  $(L \times G) - B$  spaces can be visualized, with the selected exponential fit as well.

### 2.7.3 Other models

Random Forest Regressor, Support Vector Regressor (SVR) were also tried to predict the thickness.

The Random Forest model achieved the lowest MSE of 8.68 in the original feature space, outperforming the exponential fit and the SVR model had higher MSE values.

**In conclusion:** Based on the results from both the exponential model and the Random Forest model, I concluded that the exponential fit for the feature combination ( $L \times G$ ) –  $B$  is a robust and interpretable model for predicting the thickness of the gold flakes. Despite the Random Forest model providing slightly better predictive accuracy, the exponential model's simplicity and theoretical foundation make it a valuable tool for understanding the relationship between the flakes' features and their thickness.

For future work, it may be worthwhile to refine the exponential fit with additional data or explore other feature combinations.

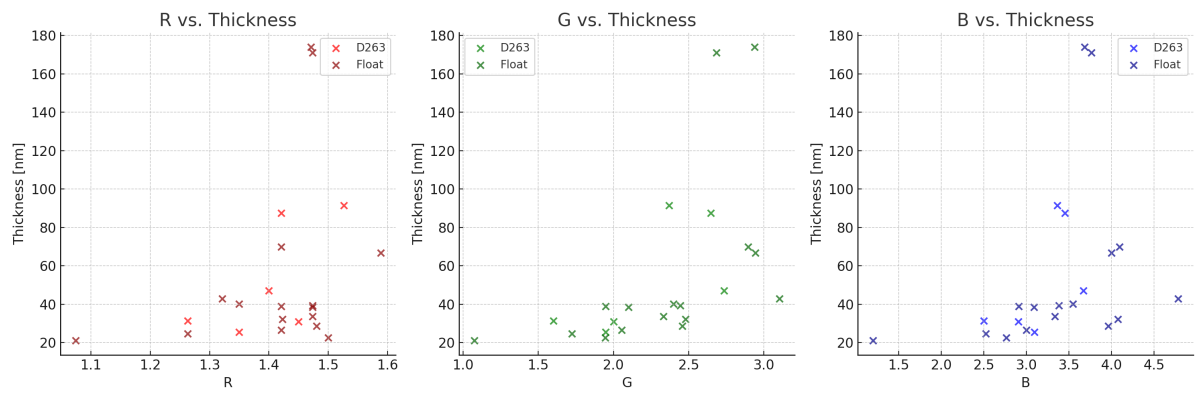


**Figure 2.6:** Comparison of data against RGB color space predictions, highlighting the relationship between data points and their RGB representation.

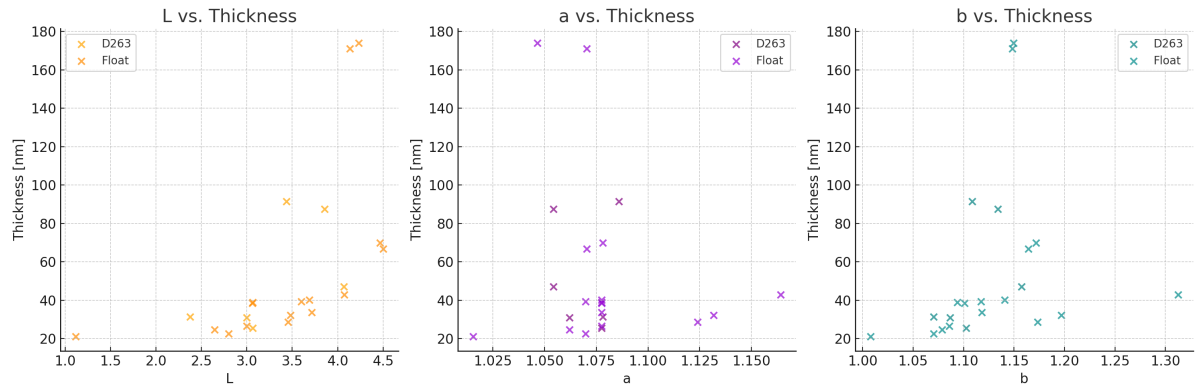
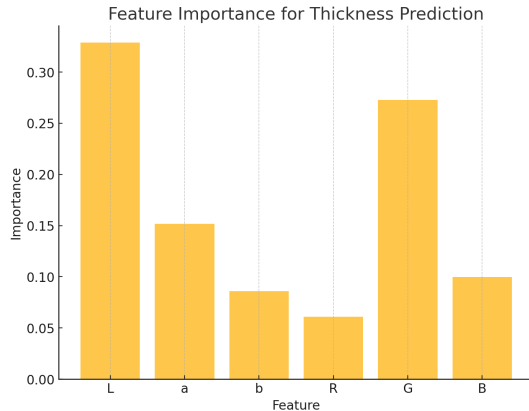
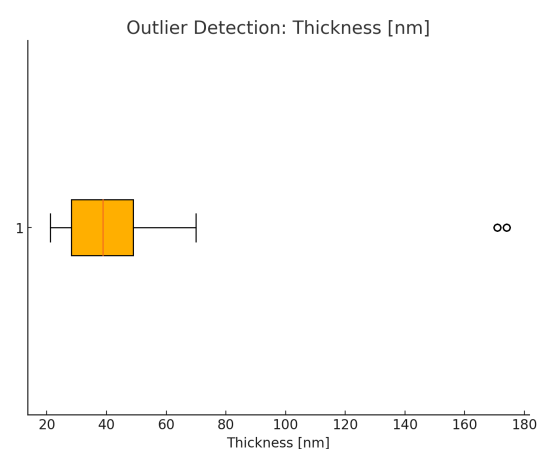


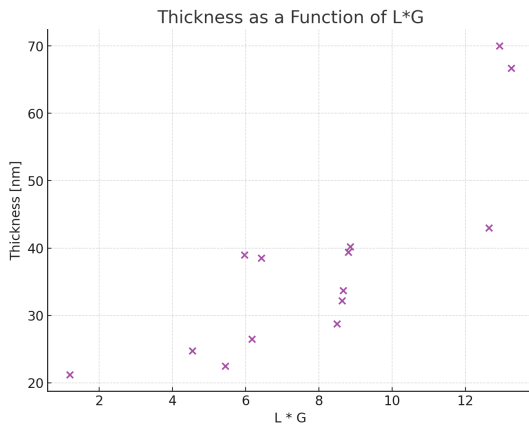
**Figure 2.7:** Comparison of data against Lab color space predictions, demonstrating how data maps within this perceptually uniform color space.



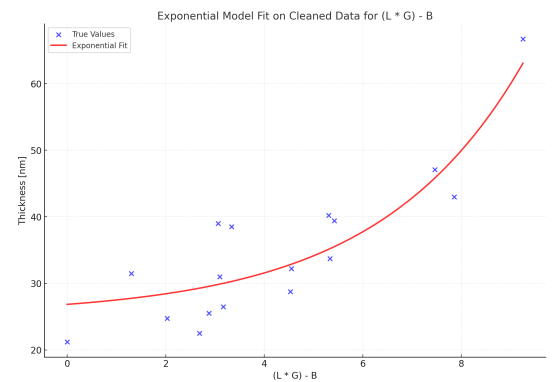
(a) Parameter importance analysis, showing the contribution of each variable to prediction accuracy.



(b) Outlier removal.



(c) Thickness mapping to  $L \cdot G$  space.



(d) Thickness mapping to  $(L \cdot G) - B$  space.

**Figure 2.8:** Analysis of various parameters and mappings: (a) Parameter importance, (b) Outlier removal, (c) Thickness mapping to  $L \cdot G$  space, and (d) Thickness mapping to  $(L \cdot G) - B$  space.

# 3 Results & Discussion

## 3.1 Growth, Etching & Metrology

The grown Flakes can be visualized in Figure 3.3, and their AFM measurements in Figure 3.11

**Unsuccessful etching:** The first etching experiment that led to bad results as discussed in 2.7.3 can be visualized with the seemingly damaged samples or unevenly etched in Figure 3.1.

### 3.1.1 Color-to-Thickness and Etching Rate Extraction

The current predictions, with a standard deviation exceeding 15 nm, are insufficient for the precision required in this study, despite being adequate for less demanding applications. Improvements are necessary to enhance the accuracy of the predictions. Specifically:

- Increasing the number of data points to improve the robustness of the model.
- Establishing a more controlled lighting environment and using a higher-quality camera to reduce noise and variability in the input data.
- Employing more sophisticated machine learning models, such as neural networks, to achieve better precision.

Currently, the model achieves a mean squared error (MSE) of 14 nm with only 20 data points. While this is significant for preliminary studies, it underscores the potential for higher precision with optimized parameters.

The exponential model was used to approximate thicknesses and etching rates, with results shown in Figure 3.2. As illustrated, an MSE of approximately 15 nm is too large for this application and thus unsuitable for precise etching rate calculations. However, the tool demonstrates potential for less precise applications, given that it achieved this result using only 20 data points and a microscope camera.

An additional observation is related to the calculated thickness values. The final column in the dataset represents the predicted thickness of the flake, assuming an etching rate of 0.2 nm/min for 200 mM cysteamine, as reported in [7]. For some flakes, this predicted rate implies negative thickness values, suggesting that these flakes should have been completely etched. This discrepancy indicates that the assumed etching rate is inconsistent with the results of the experiments conducted in this study and cannot be confirmed.

Images of the etched flakes are presented in Figure 3.3.

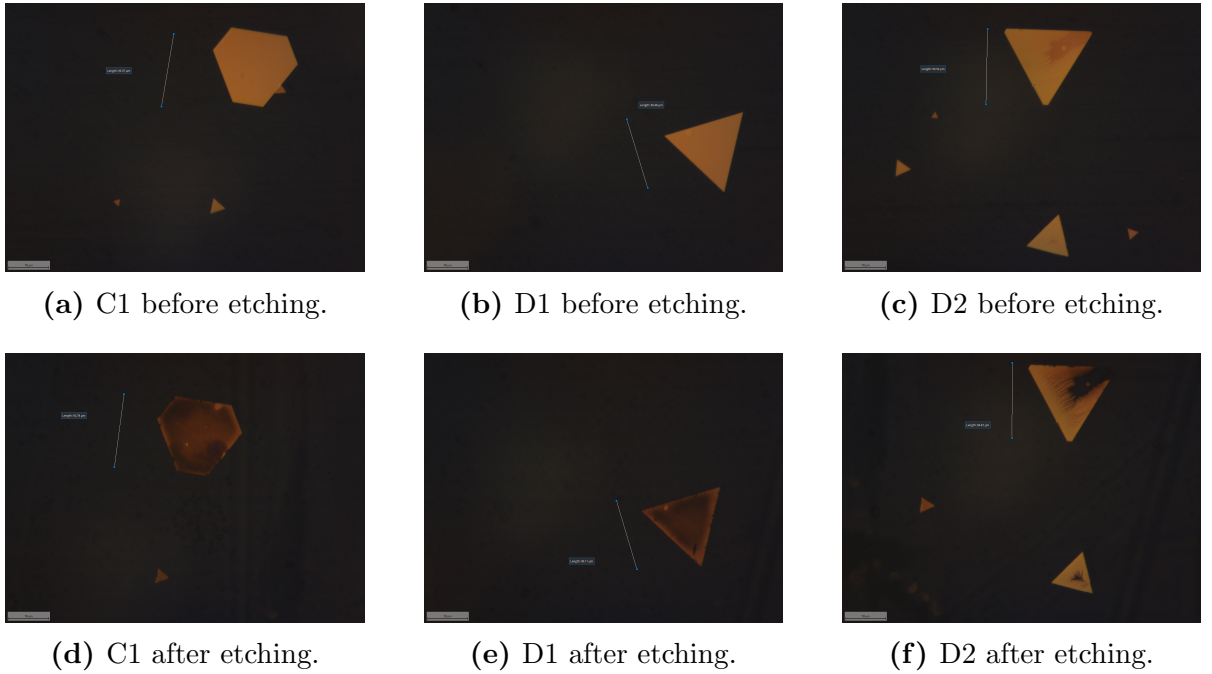


**Figure 3.1:** Comparison of samples before and after etching: Top row shows the pre-etching state, while the bottom row shows the post-etching results for samples C1, D1, and D2.

sample	flake	R	G	B	L	a	b	thickness	t etching	tir etching	cot (L*G)-B	predicted thickness with exponential	etching rate nm/min with exp	Expected thickness with 0.2nm/min (200mM)
DE2_S1_flip	A1_above	1.89655	4.03226	5.90909	4.83875	1.16406	1.35659	66.7	170	150	13.60185	191.4226657	-0.73366274	32.7
DE2_S1_flip	H11	1.76667	2.9	4.36364	3.63333	1.15625	1.22656	33.7	170	150	6.173017	38.51523626	-0.028324919	-0.3
DE2_S1_flip	M19	1.27778	1.86842	3	2.3	1.15504	1.17829	22.5	170	150	1.297366	27.75370955	-0.303904174	-11.5
DE2_S2	A21	1.58333	4	5.57143	5.04167	1.12403	1.32812	174	290	250	14.59525	258.2028894	-0.290354791	116
DE2_S2	G6	1.68	3.72	5.17241	4.79167	1.12308	1.29688	171	290	250	12.6526	145.5773014	0.087664478	113
DE2_S2	D15	1.44	2.48	4.07143	3.4166	1.14729	1.19531	26.5	290	250	4.401738	32.50029173	-0.020690661	-31.5
DE2_S5	B5	1.46667	2.36667	3.90625	3.17241	1.15625	1.19531	39	170	250	3.601798	30.76663363	0.048431567	5
DE2_S5	T12	1.3	1.96774	3.21212	2.51613	1.13281	1.15504	24.74	170	250	1.73897	28.1641781	-0.020142224	-9.26
DE2_S5	U11	1.83333	3.70968	5.27273	4.41939	1.13281	1.31008	70	170	250	11.12164	96.73727862	-0.152727811	36
DE2_S6_flip	H7	1.6	3.04	4.62068	4.08333	1.15504	1.23256	39.4	300	200	7.792633	48.27944168	-0.029598139	-20.6
DE2_S6_flip	H18	1.68	3.11538	4.82759	4.33333	1.15504	1.24031	40.2	300	200	8.67238	56.31941734	-0.053731391	-19.8
DE2_S6_flip	R17	1.625	2.95833	4.88462	4	1.14729	1.22656	38.5	300	200	6.9487	42.52746679	-0.013424889	-21.5
DE2_S3_flip	A14_right	1.5	2.84615	4.55172	3.88	1.15504	1.24219	91.5	155	200	6.491342	40.03494243	0.33203263	60.5
DE2_S4	E13	1.83871	3.875	5.42857	4.59375	1.13953	1.34109	87.5	170	150	12.37221	134.6332327	-0.27725431	53.5
DE2_S4	G10	1.6	2.42424	3.97222	3.18182	1.17969	1.21538	31.5	170	150	3.741275	31.03600513	0.002729382	-2.5
DE2_S4	N7	1.66667	2.65625	4.23529	3.375	1.15625	1.22481	31	170	150	4.729554	33.35868232	-0.013874602	-3

**Figure 3.2:** Results of etching approximation, demonstrating the observed trends and approximations for the etching process across various samples.

## 3.2 Optical measurements

For the optical measurements we will proceed with 3 flakes chosen for the whole results part, we are going to name them M19, A1 and G6.

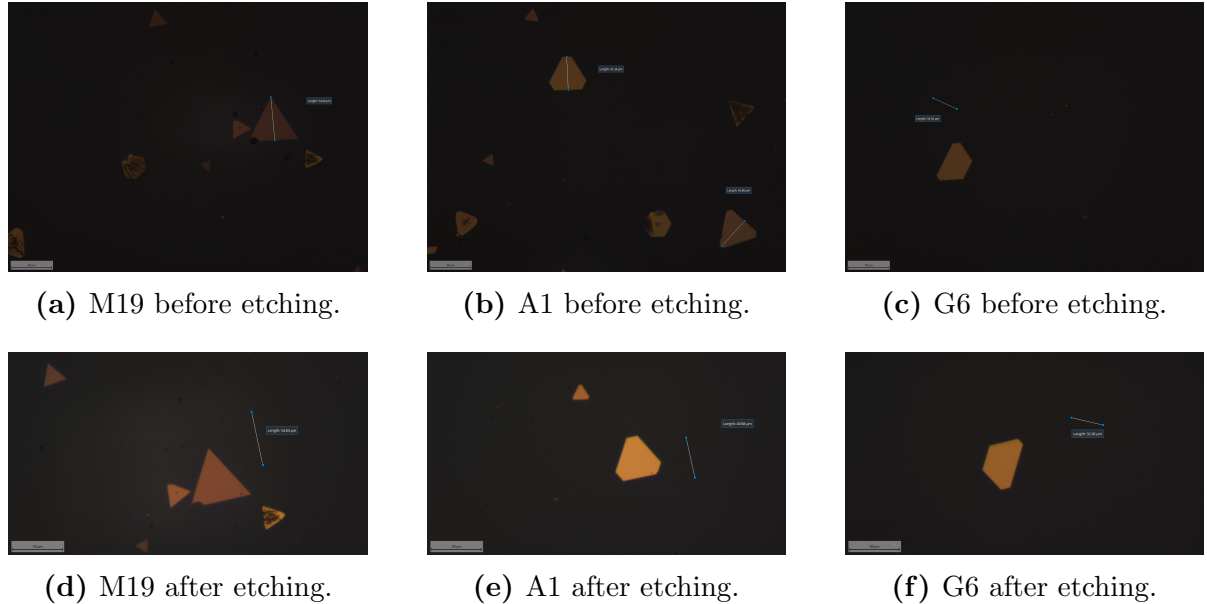


**Figure 3.3:** Comparison of samples before and after etching: Top row shows the pre-etching state, while the bottom row shows the post-etching results for samples M19, A1, and G6.

**Comparison with anti stokes thermometry:** In all spectra collected, there was no peak corresponding to the anti-stokes part, and since in our experiment with big 2D flakes, there is no plasmon resonance, the described theory and formula from paper [2] cannot be used as is. The seemingly apparent peak in the anti-stokes comes from the laser filtering attenuation near the cut-off window, which leads to assume there is no Raman peak. A ratio between  $I_{AS}$  and  $I_s$  was calculated, and seems very stable and precise, with an increase with increased laser power for the thin flake (M19) at 633, while for the same flake at 532 there is no trend. For the thick flak which has only onepower tested at the maximum of 14mW, an inverse result appears, a high ratio for the 532nm laser WL and a low one for the 633nm. According to the literature the thermometry that can be achieved by Raman AS scattering can give information about the temperature on the core matter instead of conventional methodes that gives info about the close environment temperature.

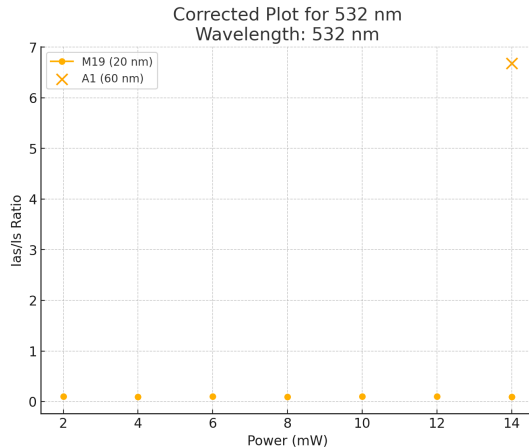


**Figure 3.4:** Integral values observed at 532 nm, for both samples.

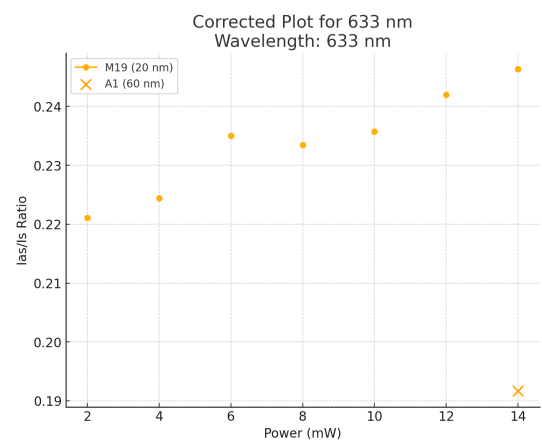


**Figure 3.5:** Integral values observed at 633 nm, for both samples

**Figure 3.6:** Comparison of integral values at two different wavelengths: (a) 532 nm (left) and (b) 633 nm (right).

### 3.2.1 532nm/633nm analysis

(Appendix B)

**Power intensity:** The ratio  $I_{AS}/I_S$  seems to increase for the thinner flake (M19) and an opposite trend could be for the thicker one (A1).

**Sample orientation:** From the analysis of Sample G6 it can be seen that parallel to the facets the response in higher than the background in contrast to the rotated response. while analyzing further it can be seen that this happens only for the cross polarized response, the co-polarized seems to be similar to the rotated flake. A possibility could be that some probing of the nuclei and thus the crystal lattice is achieved by the light matter interaction that leads to this correlation with crystal lattice. Further experiments are needed to investigate.

### 3.3 Computation of Transmitted Power in COMSOL

A COMSOL simulation modeling the optical experiment was made to test gold thickness and wavelength effects on light transmission and compare with theory and real measurements. Simulation assumes classical behavior, excluding quantum phenomena. The simulation consists of 3 zones, Air (on the left) Crystallin gold (in the middle) Appendix A and glass (on the right). A Gaussian beam focused on the gold surface interface is set as a scattering boundary condition from the air side, with incoming power set to 14 mW to match physical experiments.

In order to evaluate the power transmitted through a given boundary in our electromagnetic wave simulation, I integrated the normal component of the time-averaged Poynting vector over that boundary. In the frequency-domain formulation, the time-averaged Poynting vector is given by:

$$\mathbf{S} = \frac{1}{2} \operatorname{Re}(\mathbf{E} \times \mathbf{H}^*), \quad (3.1)$$

where  $\mathbf{E}$  is the electric field,  $\mathbf{H}$  is the magnetic field.

To compute the net power  $P$  crossing a boundary with outward unit normal  $\hat{\mathbf{n}}$ , we evaluate

$$P = \int_{\text{boundary}} \mathbf{S} \cdot \hat{\mathbf{n}} dA = \int_{\text{boundary}} \left[ \frac{1}{2} \operatorname{Re}(\mathbf{E} \times \mathbf{H}^*) \right] \cdot \hat{\mathbf{n}} dA. \quad (3.2)$$

In COMSOL's *Electromagnetic Waves, Frequency Domain* interface (`ewfd`), the built-in variable `ewfd.Poavn` represents the normal component of  $\mathbf{S}$  on a boundary, i.e.,

$$\text{ewfd.Poavn} = \left[ \frac{1}{2} \operatorname{Re}(\mathbf{E} \times \mathbf{H}^*) \right] \cdot \hat{\mathbf{n}},$$

which makes it straightforward to compute the total power by a surface integration of `ewfd.Poavn`:

$$P = \int_{\text{boundary}} \text{ewfd.Poavn} dA. \quad (3.3)$$

We use

```
intop2(ewfd.PoavnY)+intop2(ewfd.PoavnX)
```

on all 3 boundaries on the glass side, to account for all components.

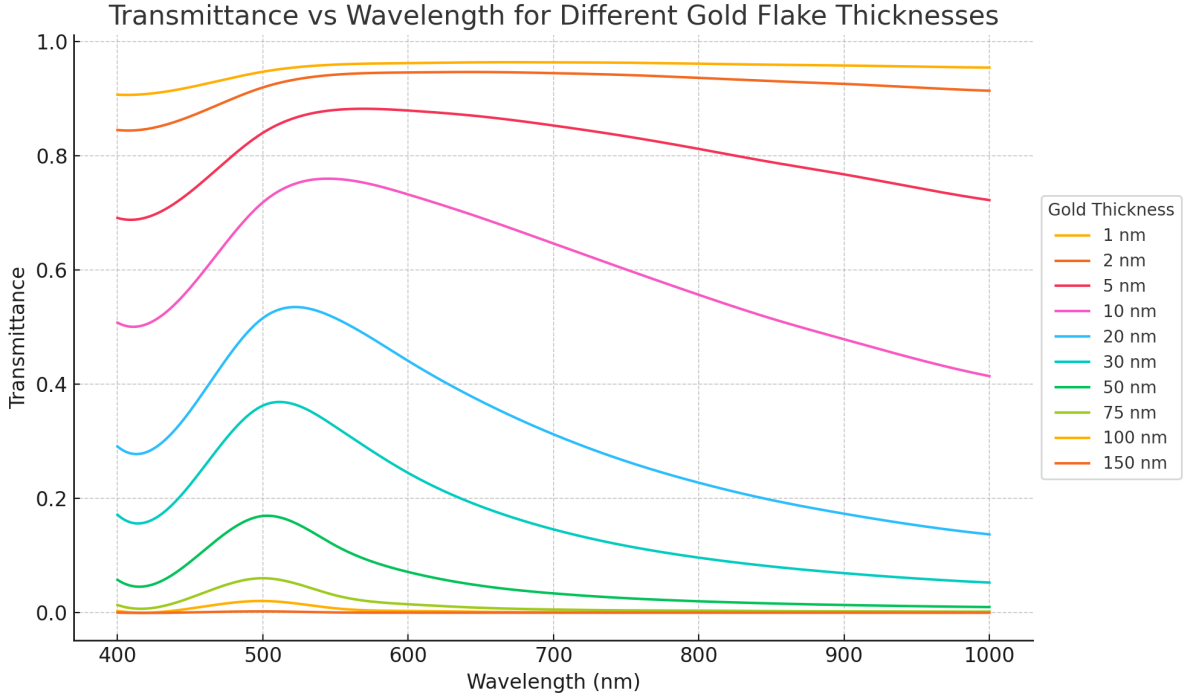


**Figure 3.7:** Transmission vs. Wavelength for all configurations, illustrating the spectral behavior across varying conditions.

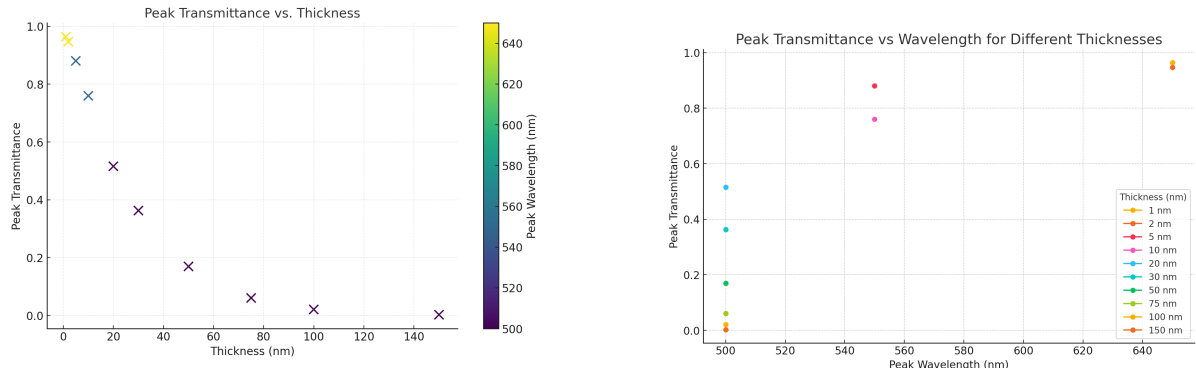


**Figure 3.8:** Peak transmission as a function of thickness, demonstrating the influence of material thickness on transmission properties.

**Figure 3.9:** Peak transmission as a function of peak wavelength, with color-coded variations representing different parameters.

**Figure 3.10:** Comparison of peak transmission dependencies: (a) as a function of thickness (left) and (b) as a function of wavelength with color-coded parameters (right).

By analyzing Figure 3.7 we can clearly see a decrease in the intensity of the transmitted light with increasing thicknesses, but also an increase in the relative peak Transmittance at the peak WL. Also the peak WL reduces with thickness. This can be better visualized in Figure 3.10. This can be explained by the fact that gold reflects most red and yellow and absorbs blue due to inter-band transition energy matching. When the

gold is very thin more red passes through, which shifts the spectrum to the right, while of course all light passes through more relatively.

A visualization of those results in 2D showing the E field absolute intensities is shown in Appendix A.

### 3.4 Atomic Force Microscopy (AFM) Analysis

The following figures present the Atomic Force Microscopy (AFM) characterization of gold flakes grown in the laboratory. The measurements were acquired using a Bruker Fast Scan AFM machine. The analysis highlights the structural and topographical features of the samples. This data was used to measure the flakes thickness.

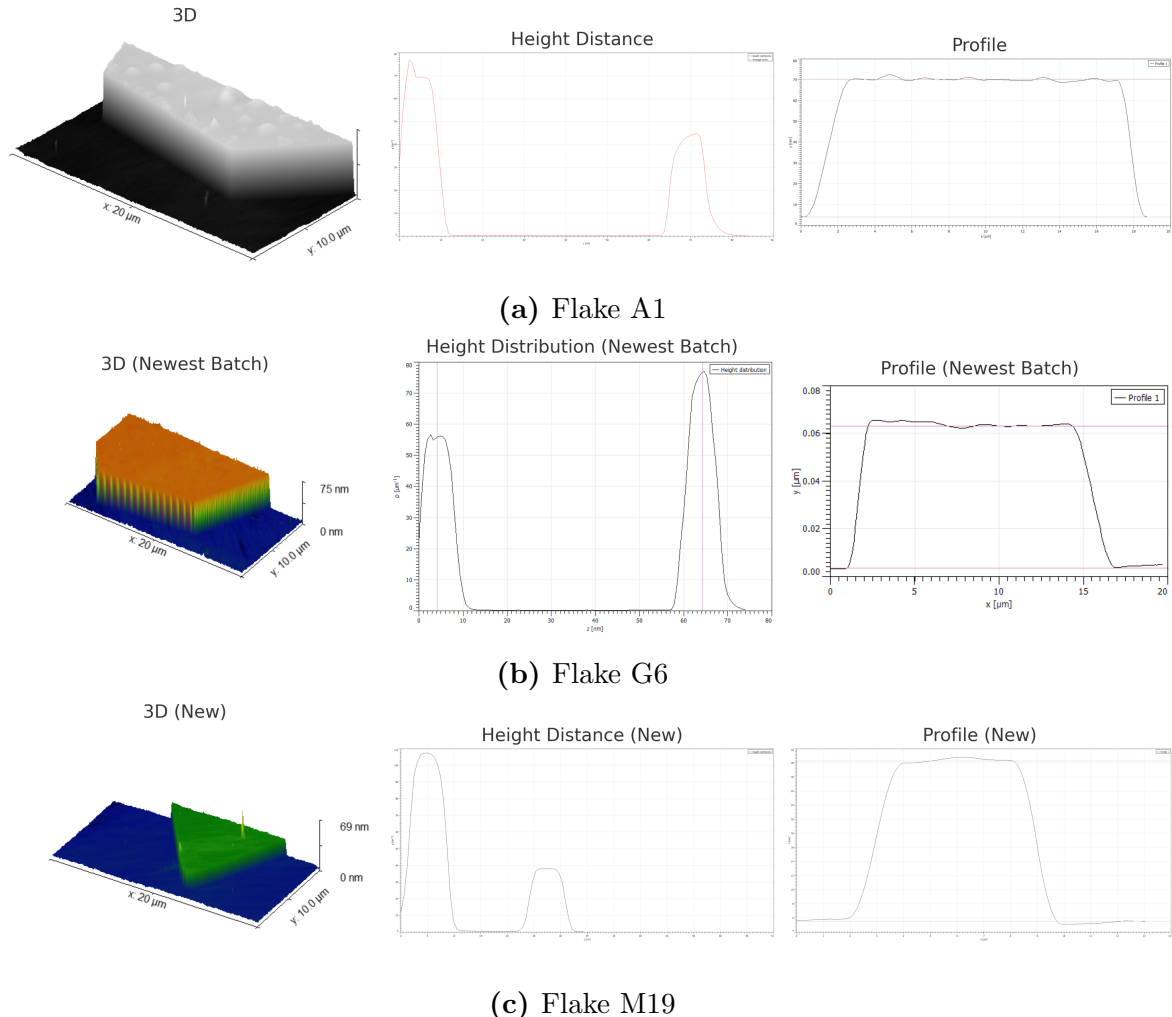


**Figure 3.11:** AFM characterization of the gold flakes using a Bruker Fast Scan AFM machine. The figures illustrate the 3D topography, height distribution, and profile of the samples.

## 4 Conclusion

This project, spanning almost six months, presented numerous challenges, both technical and personal. Throughout this journey, I gained significant experience across various domains, including chemical procedures, cleanroom operations, and laser measurements and manipulations as well as theoretical knowledge. One of the most valuable lessons was understanding the complexity and unpredictability of experimental work, where success is often the sole measure of progress.

While many of the project's objectives were not fully achieved, either in execution or results, the data acquired and the lessons learned provide a strong foundation for future work. The ratio of anti-Stokes to Stokes signal intensities in thin gold flakes may offer a simpler model that excludes localized or surface plasmon resonance effects. Furthermore, additional research is needed to explore quantum confinement effects in gold flakes thinner than 5 nm, an area with significant potential for discovery.

Despite its challenges, this project offers valuable insights and establishes a framework for more refined and focused studies in the future.

# Bibliography

- [1] Guillaume Baffou. Anti-Stokes Thermometry in Nanoplasmonics. *ACS Nano*, 15(4):5785–5792, April 2021.
- [2] Aquiles Carattino, Martín Calderola, and Michel Orrit. Gold Nanoparticles as Absolute Nanothermometers. *Nano Letters*, 18(2):874–880, February 2018.
- [3] Enno Krauss, René Kullock, Xiaofei Wu, Peter Geisler, Nils Lundt, Martin Kamp, and Bert Hecht. Controlled Growth of High-Aspect-Ratio Single-Crystalline Gold Platelets. *Crystal Growth & Design*, 18(3):1297–1302, March 2018.
- [4] Nicki Hogan, Shengxiang Wu, and Matthew Sheldon. Photothermalization and Hot Electron Dynamics in the Steady State. *The Journal of Physical Chemistry C*, 124(9):4931–4945, March 2020.
- [5] Alan R. Bowman, Alvaro Rodríguez Echarri, Fatemeh Kiani, Fadil Iyikanat, Ted V. Tsoulos, Joel D. Cox, Ravishankar Sundararaman, F. Javier García De Abajo, and Giulia Tagliabue. Quantum-mechanical effects in photoluminescence from thin crystalline gold films. *Light: Science & Applications*, 13(1):91, April 2024.
- [6] Fatemeh Kiani and Giulia Tagliabue. High Aspect Ratio Au Microflakes via Gap-Assisted Synthesis. *Chemistry of Materials*, 34(3):1278–1288, February 2022.
- [7] Shun Kashiwaya, Yuchen Shi, Jun Lu, Davide G. Sangiovanni, Grzegorz Greczynski, Martin Magnuson, Mike Andersson, Johanna Rosen, and Lars Hultman. Synthesis of goldene comprising single-atom layer gold. *Nature Synthesis*, 3(6):744–751, April 2024.
- [8] Daniel Abraham Elmaleh, 2024. Accessed: Jan. 3, 2025.
- [9] Daniel Abraham Elmaleh, 2024. Accessed: Jan. 3, 2025.

## A Appendix A (Figures)

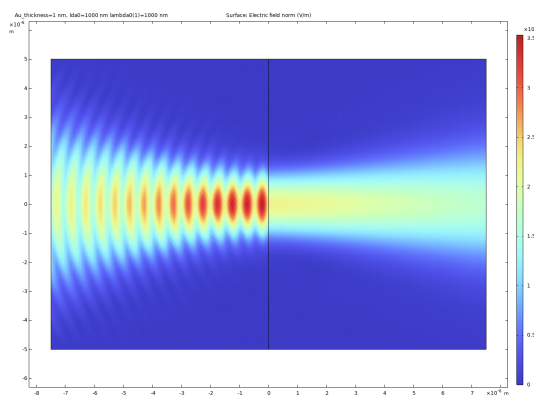


**Figure A.1:** COMSOL simulation for thickness 1 nm at 1000 nm wavelength.

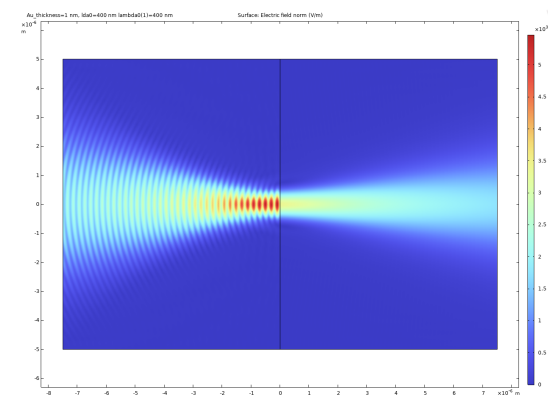


**Figure A.2:** COMSOL simulation for thickness 1 nm at 400 nm wavelength.

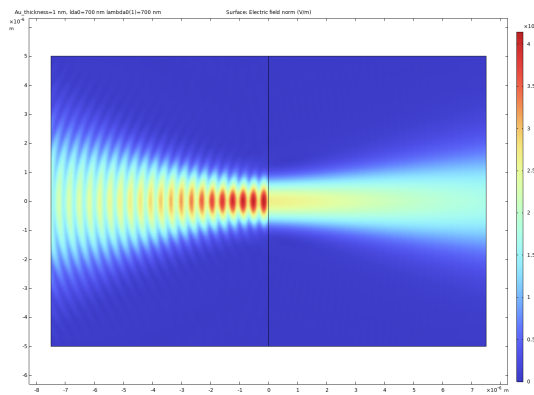


**Figure A.3:** COMSOL simulation for thickness 1 nm at 700 nm wavelength.

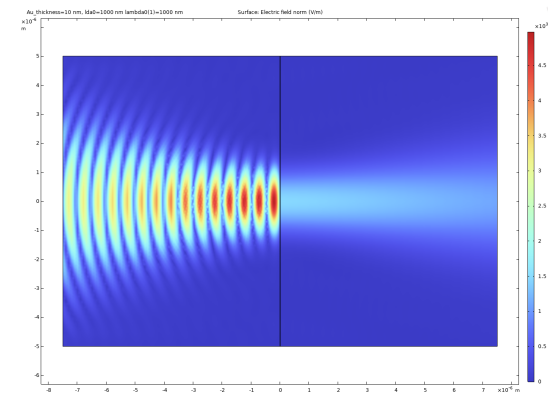


**Figure A.4:** COMSOL simulation for thickness 10 nm at 1000 nm wavelength.

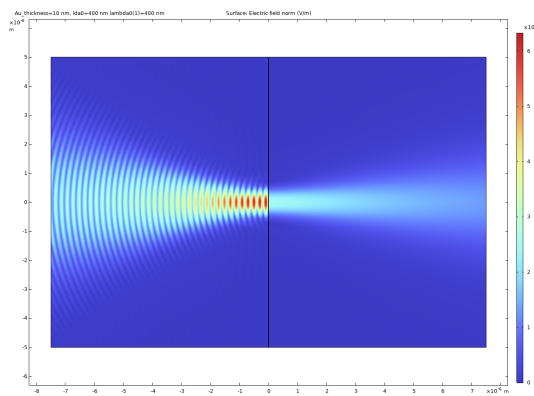


**Figure A.5:** COMSOL simulation for thickness 10 nm at 400 nm wavelength.

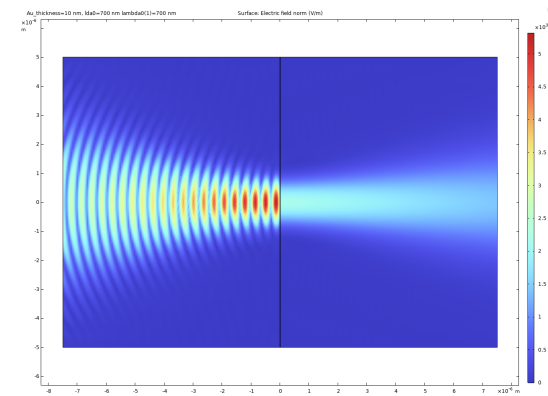


**Figure A.6:** COMSOL simulation for thickness 10 nm at 700 nm wavelength.

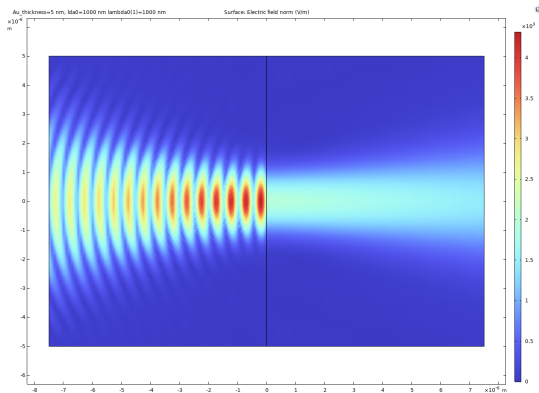


**Figure A.7:** COMSOL simulation for thickness 5 nm at 1000 nm wavelength.

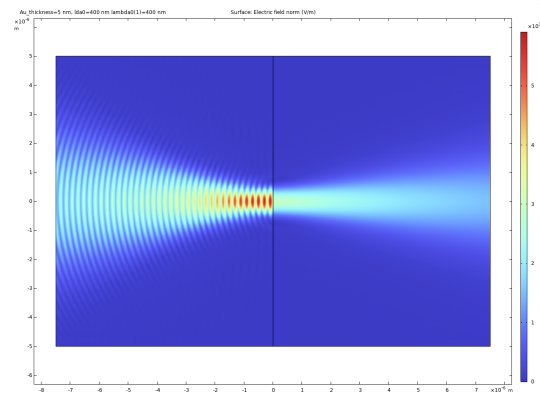


**Figure A.8:** COMSOL simulation for thickness 5 nm at 400 nm wavelength.

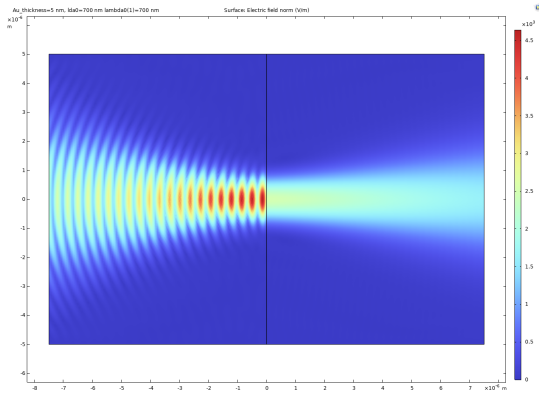


**Figure A.9:** COMSOL simulation for thickness 5 nm at 700 nm wavelength.

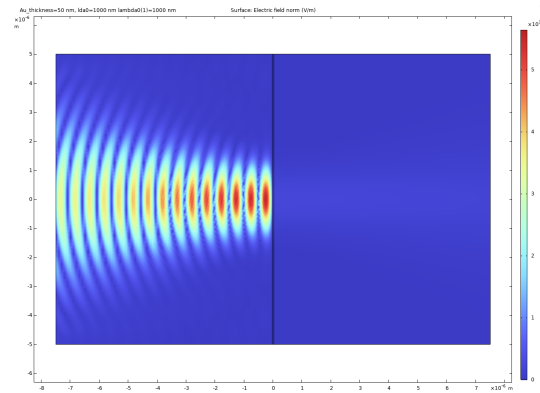


**Figure A.10:** COMSOL simulation for thickness 50 nm at 1000 nm wavelength.

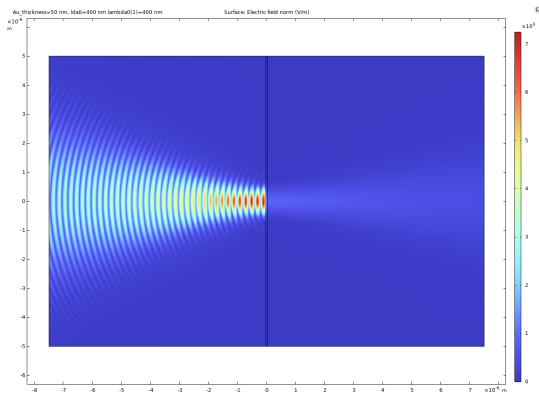


**Figure A.11:** COMSOL simulation for thickness 50 nm at 400 nm wavelength.

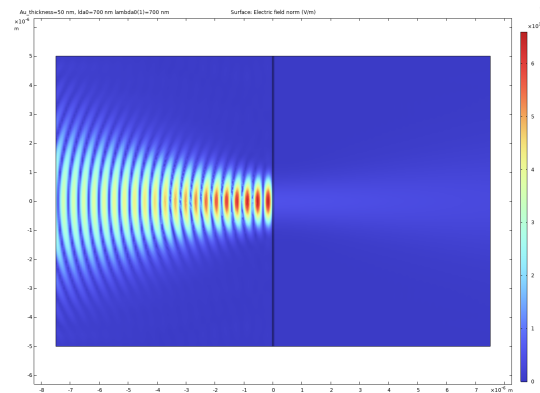


**Figure A.12:** COMSOL simulation for thickness 50 nm at 700 nm wavelength.

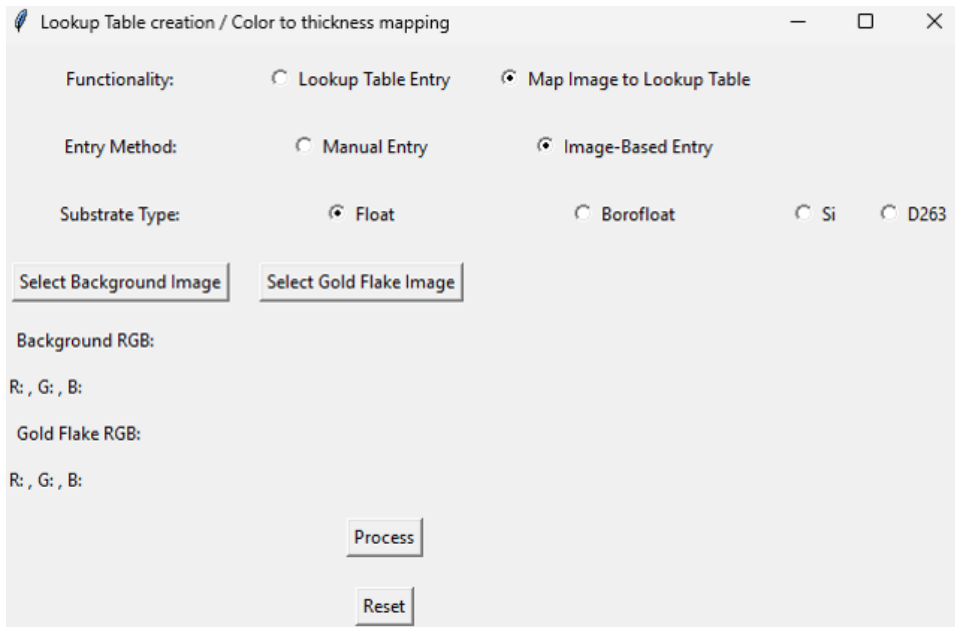


**Figure A.13:** Graphical User Interface (GUI) for color-to-thickness conversion. This tool maps colors to their respective thickness values for precise analysis.

Integral (Area)	Type	Power (mW)	I <sub>as</sub> /I <sub>s</sub>
105066.91	Stokes	2	0.105767
11112.58	Anti-Stokes	2	
190821.36	Stokes	4	0.096617
18436.68	Anti-Stokes	4	
281070.08	Stokes	6	0.100719
28309.04	Anti-Stokes	6	
354438.59	Stokes	8	0.096058
34046.67	Anti-Stokes	8	
411172.81	Stokes	10	0.10009
41154.33	Anti-Stokes	10	
490297.45	Stokes	12	0.100012
49035.68	Anti-Stokes	12	
628524.71	Stokes	14	0.093561
58805.66	Anti-Stokes	14	

**Figure A.14:** Ratio  $(I_{as})/(I_s)$  for flake M19 at 532 nm.

Integral (Area)	Type	Power (mW)	I <sub>as</sub> /I <sub>s</sub>
186038.68	Stokes	2	0.221077
41128.95	Anti-Stokes	2	
312141.74	Stokes	4	0.22444
70057.13	Anti-Stokes	4	
464894.53	Stokes	6	0.235051
109273.78	Anti-Stokes	6	
613917.92	Stokes	8	0.233494
143345.9	Anti-Stokes	8	
743936.12	Stokes	10	0.235758
175388.86	Anti-Stokes	10	
877826.93	Stokes	12	0.241975
212412.49	Anti-Stokes	12	
968822.77	Stokes	14	0.246331
238651.01	Anti-Stokes	14	

**Figure A.15:** Ratio  $(I_{as})/(I_s)$  for flake M19 at 633 nm.

Integral (Area)	Type	Power (mW)	I <sub>as</sub> /I <sub>s</sub>
385468.78	Stokes	14	6.678953
57713.95	Anti-Stokes	14	

**Figure A.16:** Ratio  $(I_{as})/(I_s)$  for flake A1 at 532 nm.

Integral (Area)	Type	Power (mW)	I <sub>as</sub> /I <sub>s</sub>
414325.5	Stokes	14	0.19169
79421.91	Anti-Stokes	14	

**Figure A.17:** Ratio  $(I_{as})/(I_s)$  for flake A1 at 633 nm.

**Figure A.18:** Comparison of the  $(I_{as})/(I_s)$  ratios for flakes M19 and A1 at two wavelengths (532 nm and 633 nm). Top row: Flake M19; Bottom row: Flake A1.

## B Appendix B (Reports)

### Look-up tables

R	G	B	L	a	b	Thickness [nm]
1.32143	3.10345	4.78125	4.07143	1.16406	1.3125	43
1.48	2.45833	3.96154	3.45455	1.12403	1.17323	28.75
1.42308	2.48	4.07407	3.47826	1.13178	1.19685	32.2
1.07407	1.07407	1.2	1.11538	1.0155	1.00781	21.2
1.47368	2.33333	3.33333	3.71429	1.07752	1.11811	33.7
1.5	1.94444	2.7619	2.8	1.06977	1.07031	22.5
1.58824	2.94444	4	4.5	1.07031	1.16406	66.7
1.42105	1.94737	2.90909	3.06667	1.07752	1.09375	39
1.26316	1.72222	2.52381	2.64286	1.06202	1.07874	24.74
1.42105	2.89474	4.09524	4.46667	1.07812	1.17188	70
1.47059	2.9375	3.68421	4.23077	1.04651	1.14961	174
1.42105	2.05556	3	3	1.07752	1.08594	26.5
1.47368	2.68421	3.7619	4.13333	1.07031	1.14844	171
1.47368	2.44444	3.38095	3.6	1.06977	1.11719	39.4
1.35	2.4	3.54545	3.6875	1.07752	1.14062	40.2
1.47368	2.1	3.08696	3.05882	1.07752	1.10078	38.5

R	G	B	L	a	b	Thickness [nm]
1.52632	2.36842	3.36364	3.4375	1.08594	1.10853	91.5
1.35	1.94737	3.09524	3.06667	1.07752	1.10236	25.5
1.4	2.73684	3.66667	4.06667	1.05426	1.15748	47.1
1.26316	1.6	2.5	2.375	1.07812	1.07031	31.5
1.45	2	2.90476	3	1.06202	1.08661	31
1.42105	2.64706	3.45	3.85714	1.05426	1.13386	87.5

**Optical measurements analysis reports**

# Spectrometry Analysis Report

Sample: A1

Laser Wavelength (after shift): 532.13 nm

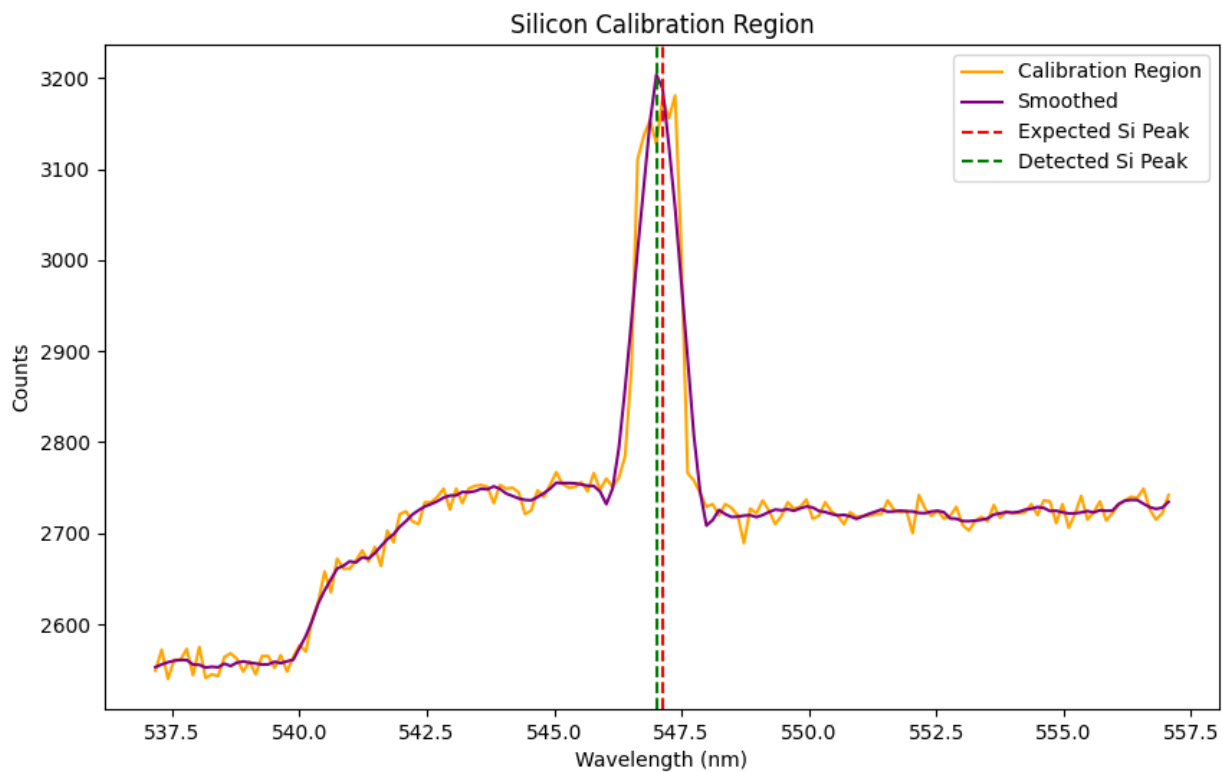
Power Levels: 14.0 mW

Thickness: 65.0 nm

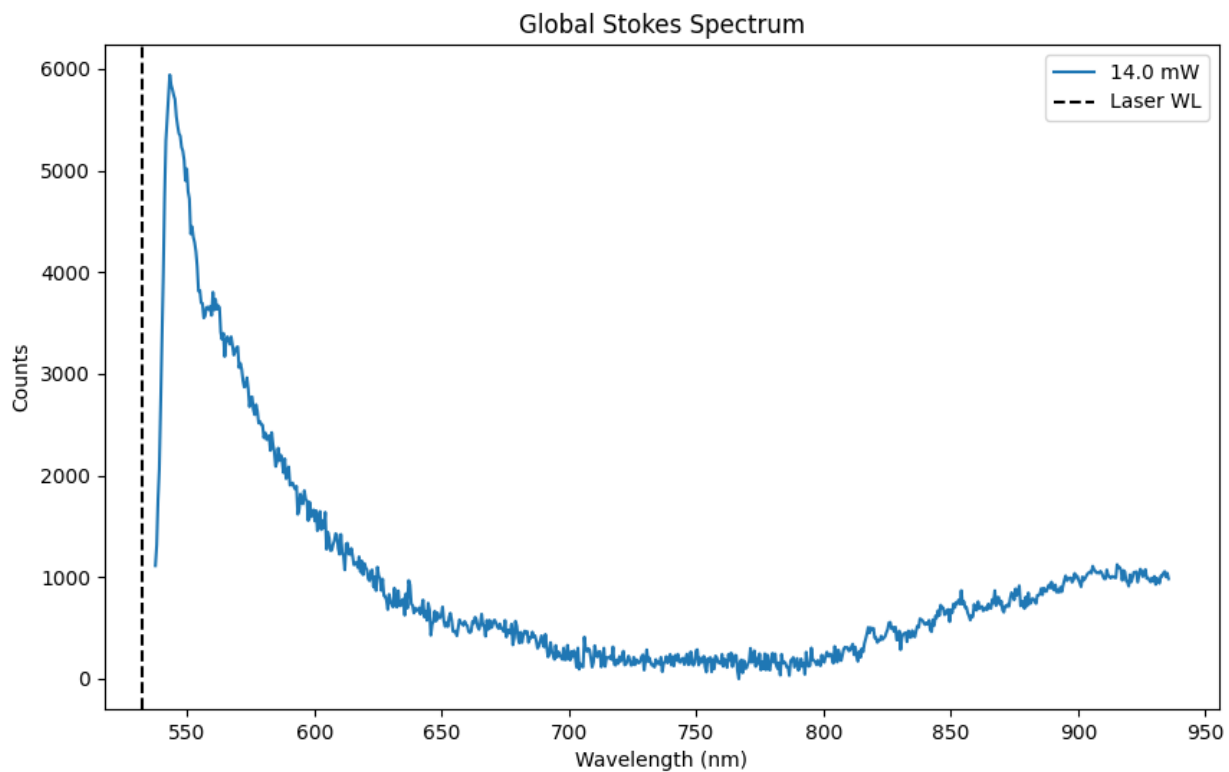
Laser Filter Window:  $\pm 5.0$  nm

Calibration Shift: 0.13 nm

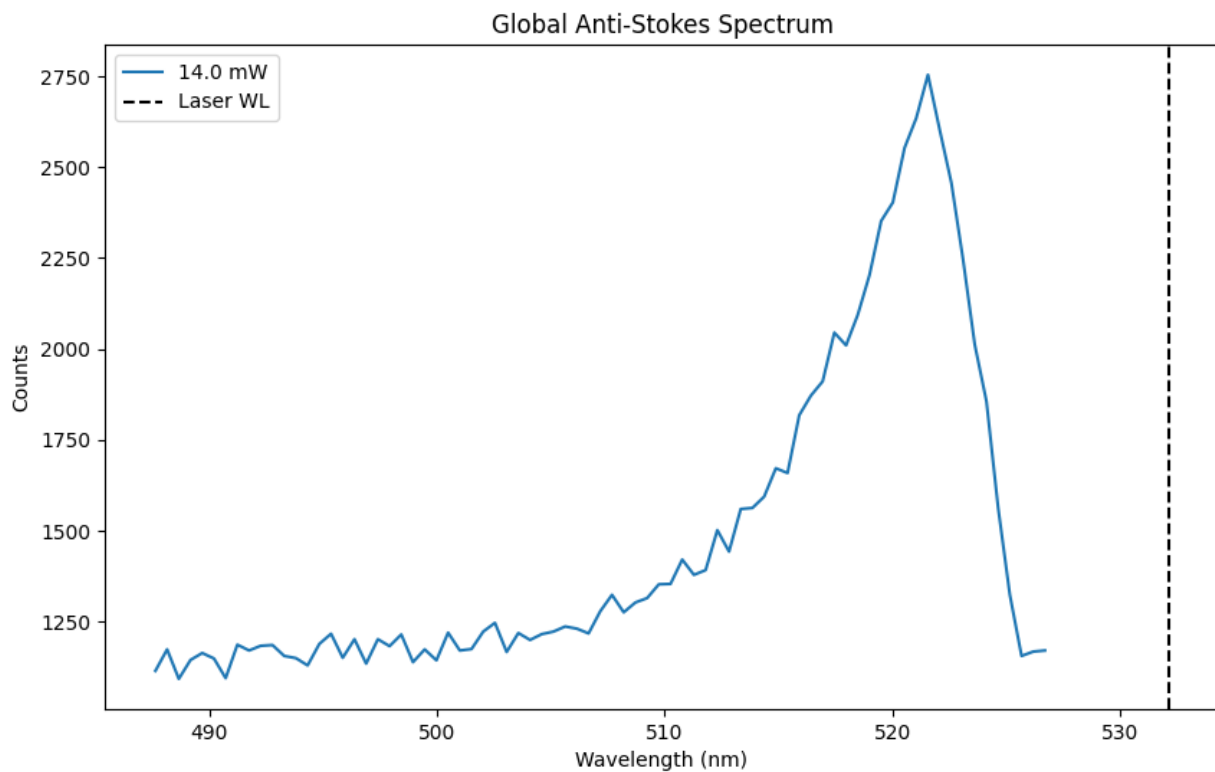
## Calibration Region



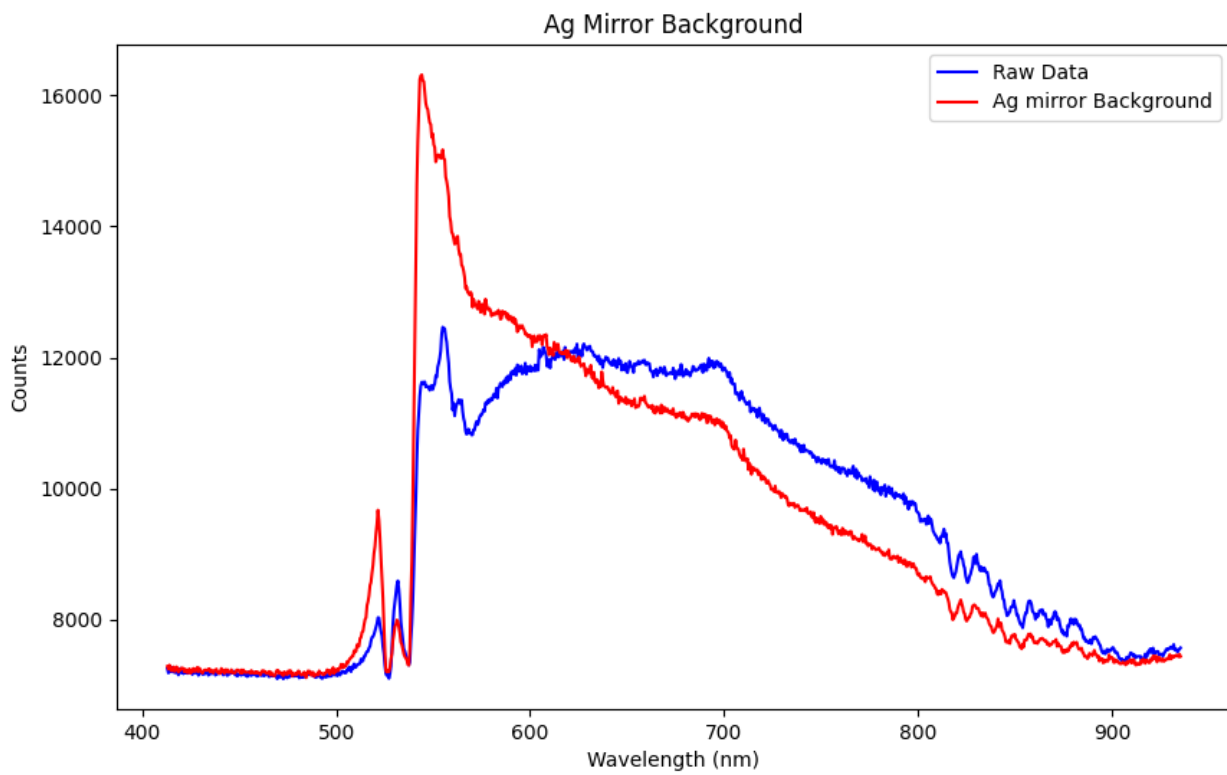
## Global Stokes Spectrum



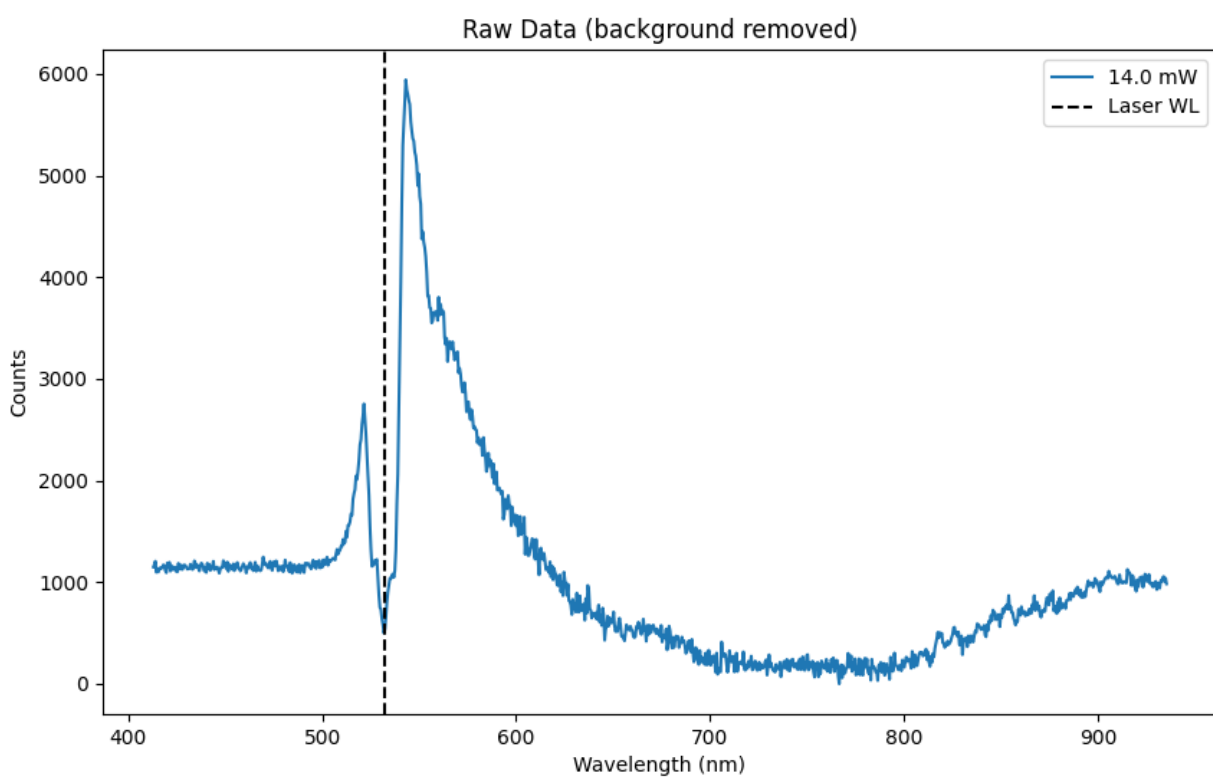
## Global Anti-Stokes Spectrum



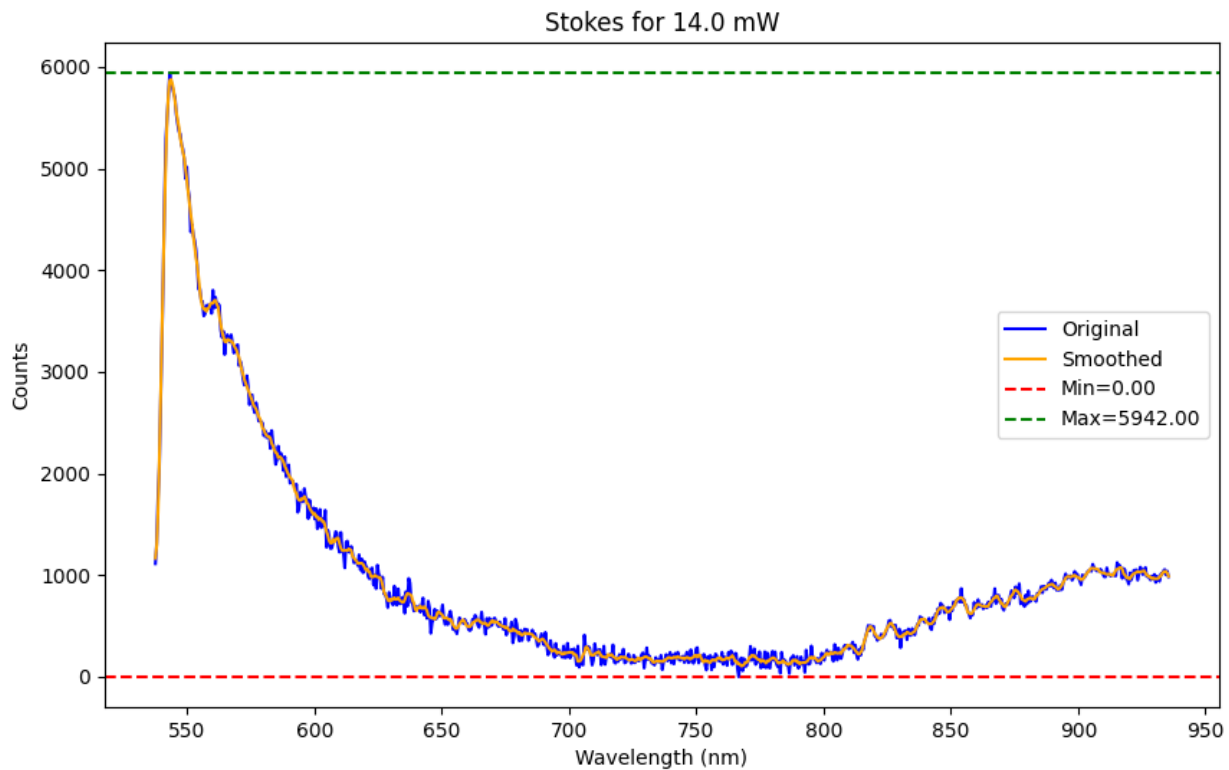
## Ag Mirror Background



## Raw Data



### Stokes for 14.0 mW



Integral (Area) = 385468.78

Peak Info (Stokes):

WL=543.14, Cnt=5942.00

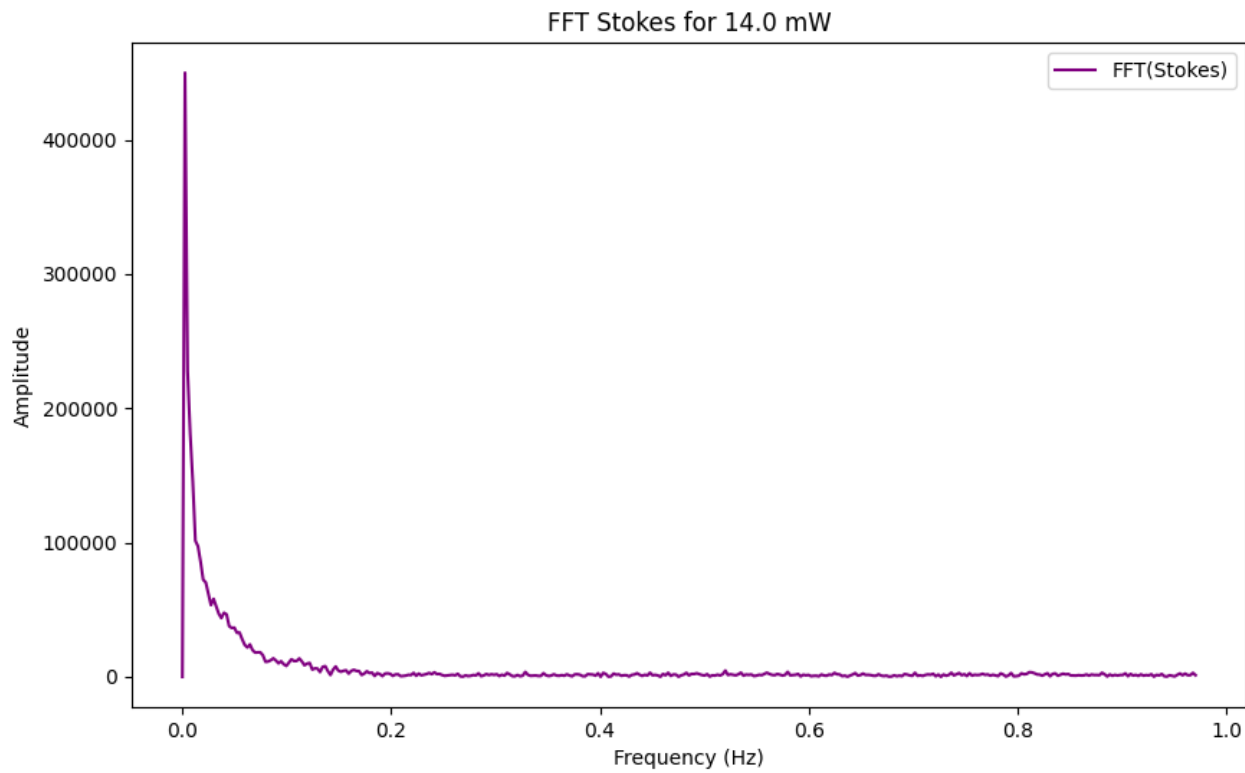
WL=549.82, Cnt=5016.00

WL=551.87, Cnt=4447.00

WL=554.95, Cnt=3820.00

WL=560.09, Cnt=3803.00

## FFT Stokes for 14.0 mW



Peak Info (FFT Stokes):

Freq=0.00, Amp=449964.28

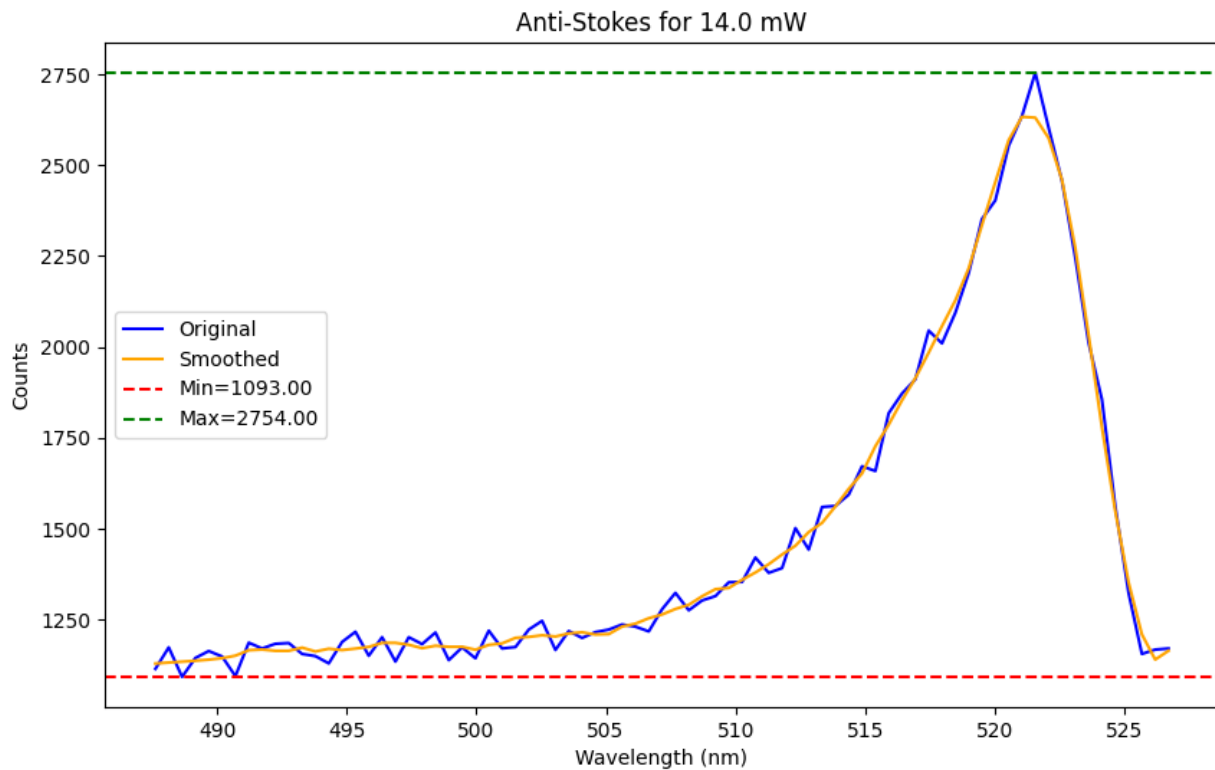
Freq=0.03, Amp=58087.76

Freq=0.04, Amp=47733.15

Freq=0.05, Amp=36657.34

Freq=0.05, Amp=33025.41

## Anti-Stokes for 14.0 mW



Integral (Area) = 57713.95

Peak Info (Anti-Stokes):

WL=521.56, Cnt=2754.00

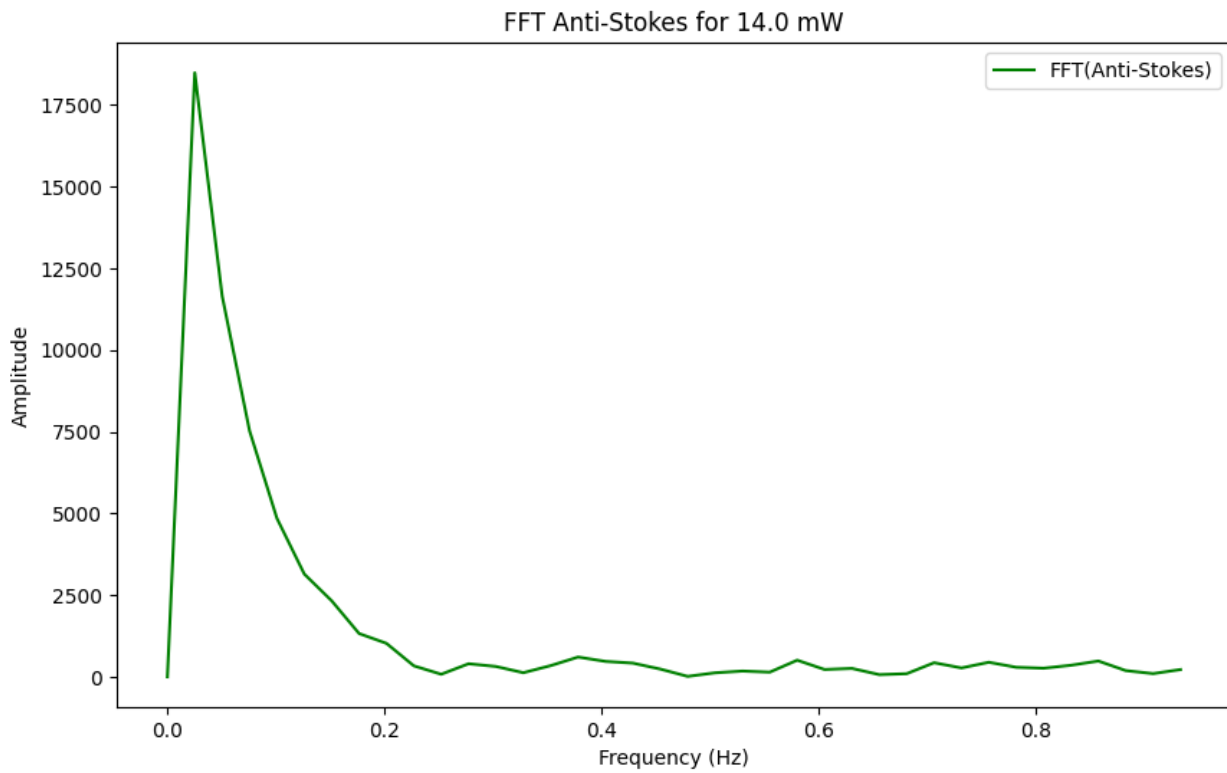
WL=517.45, Cnt=2045.00

WL=514.88, Cnt=1672.00

WL=512.31, Cnt=1502.00

WL=510.77, Cnt=1421.00

### FFT Anti-Stokes for 14.0 mW



Peak Info (FFT Anti-Stokes):

Freq=0.03, Amp=18486.84

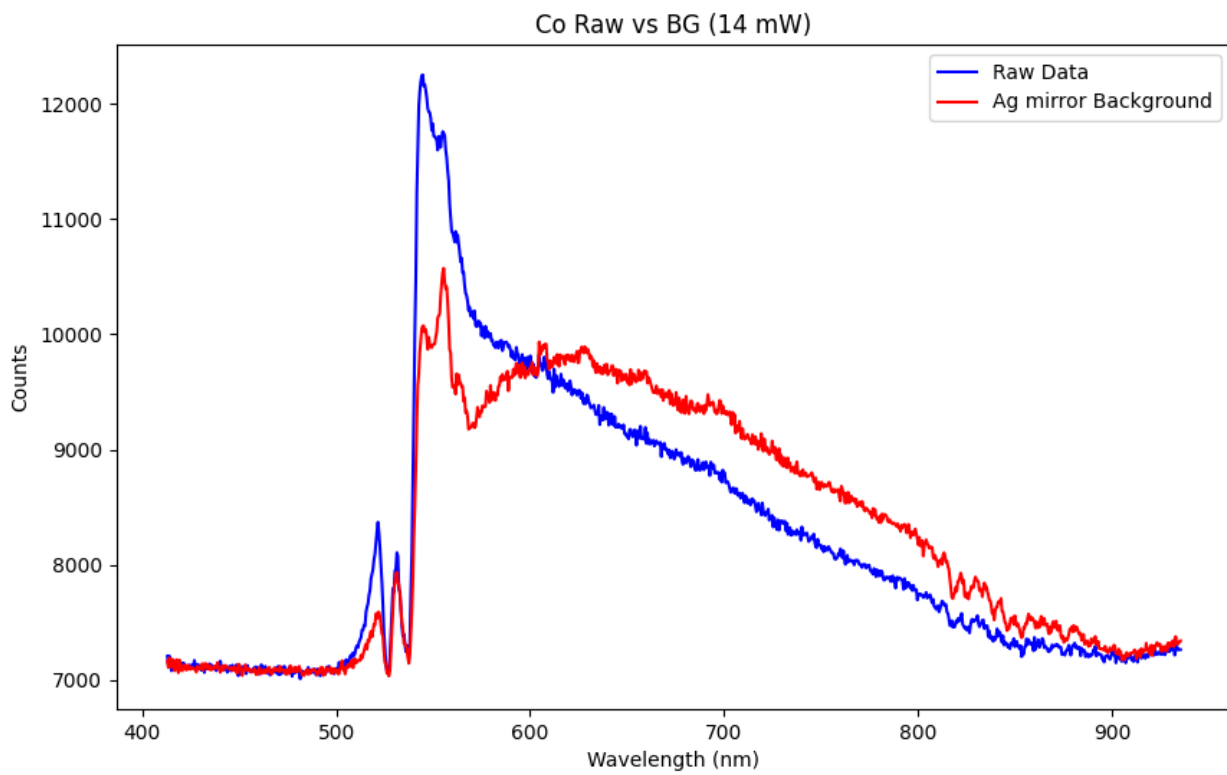
Freq=0.38, Amp=606.18

Freq=0.58, Amp=509.78

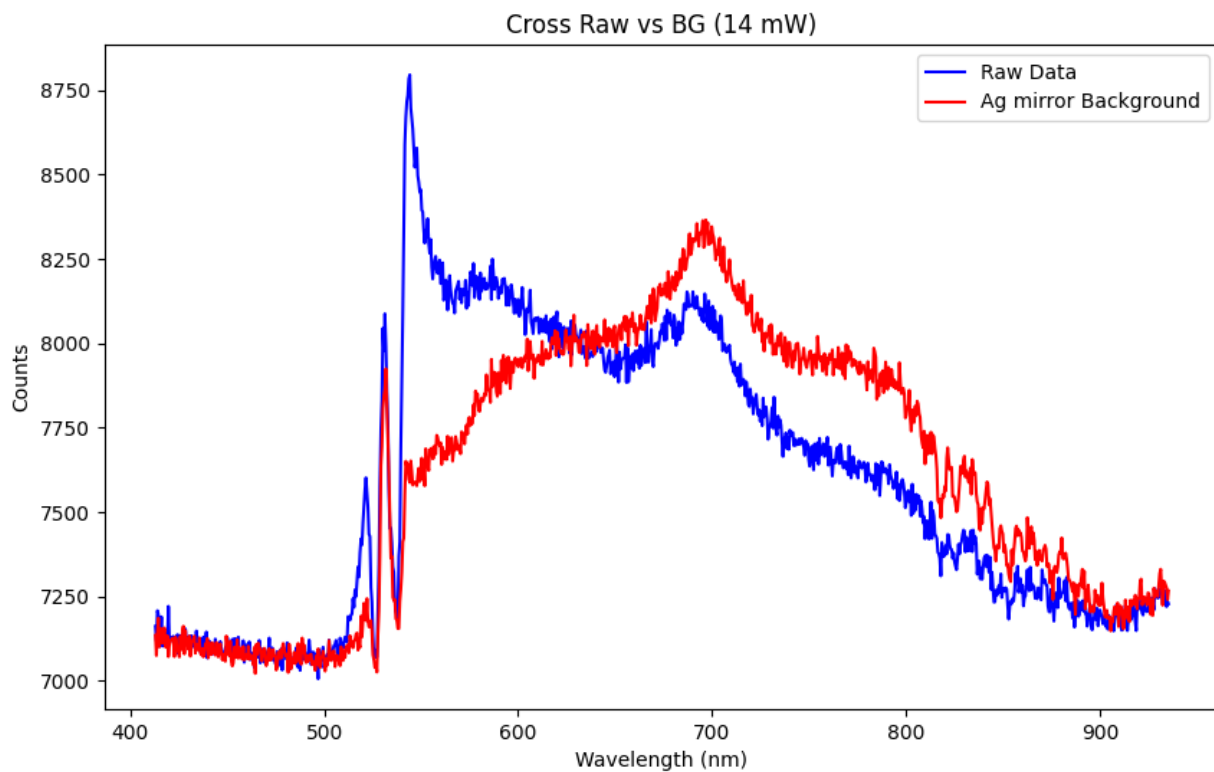
Freq=0.86, Amp=484.51

Freq=0.76, Amp=446.12

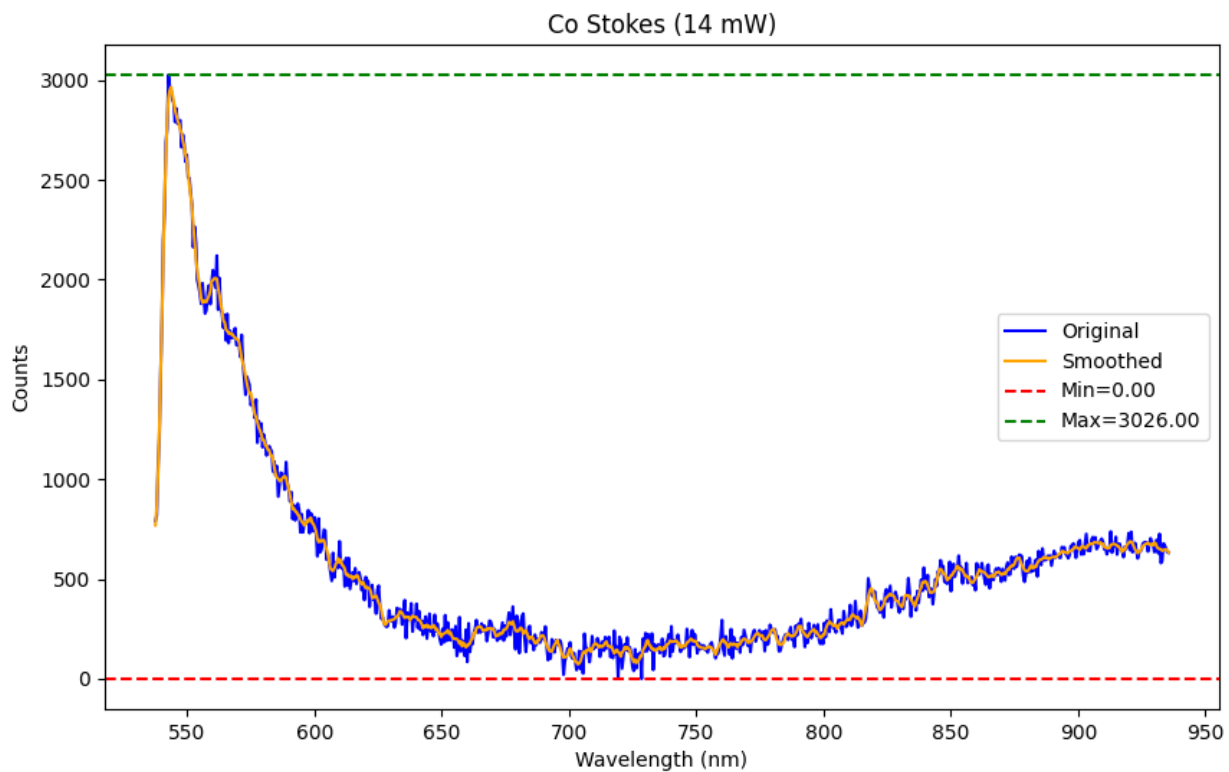
### Co Raw vs BG (14 mW)



### Cross Raw vs BG (14 mW)



### Co Stokes (14 mW)



#### Peak Info:

WL=542.63, Cnt=3026.00

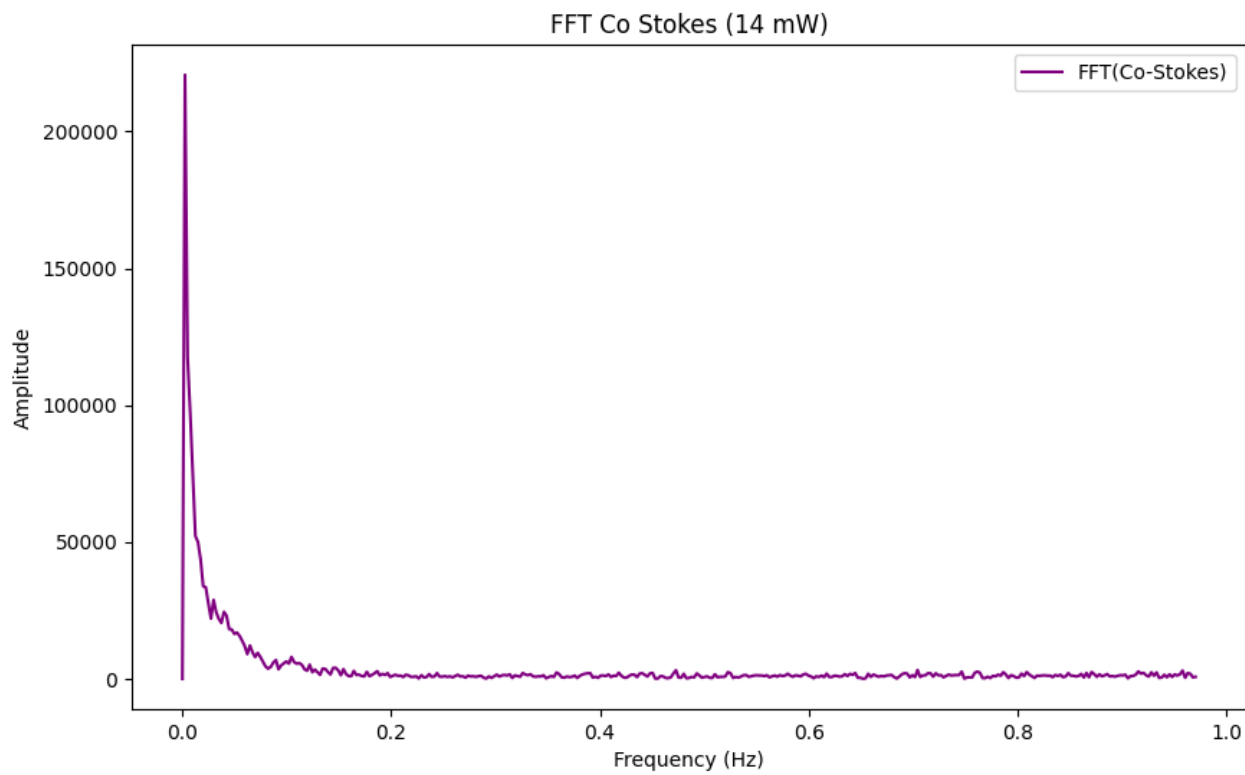
WL=545.71, Cnt=2857.00

WL=547.25, Cnt=2798.00

WL=548.28, Cnt=2726.00

WL=549.82, Cnt=2625.00

### FFT Co Stokes (14 mW)



#### FFT Peak Info:

Freq=0.00, Amp=220717.25

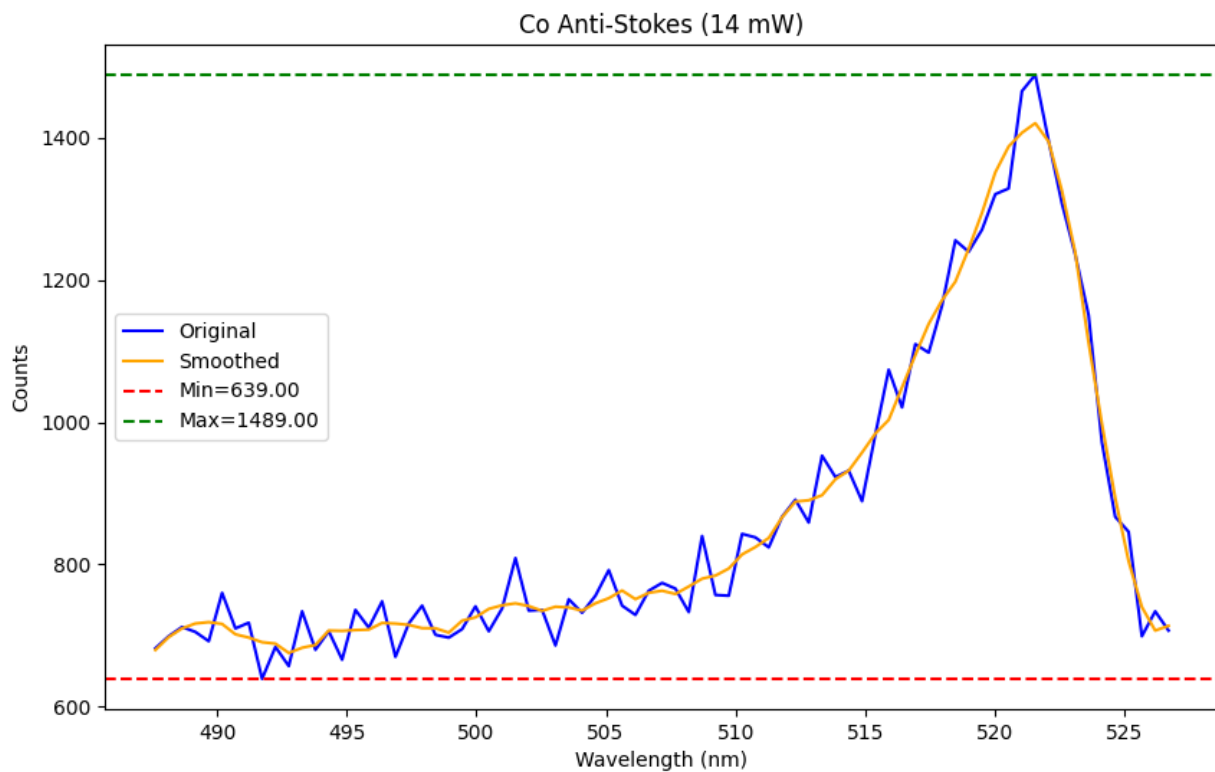
Freq=0.03, Amp=28868.10

Freq=0.04, Amp=24474.39

Freq=0.05, Amp=16918.54

Freq=0.06, Amp=12182.41

### Co Anti-Stokes (14 mW)



Peak Info:

WL=521.56, Cnt=1489.00

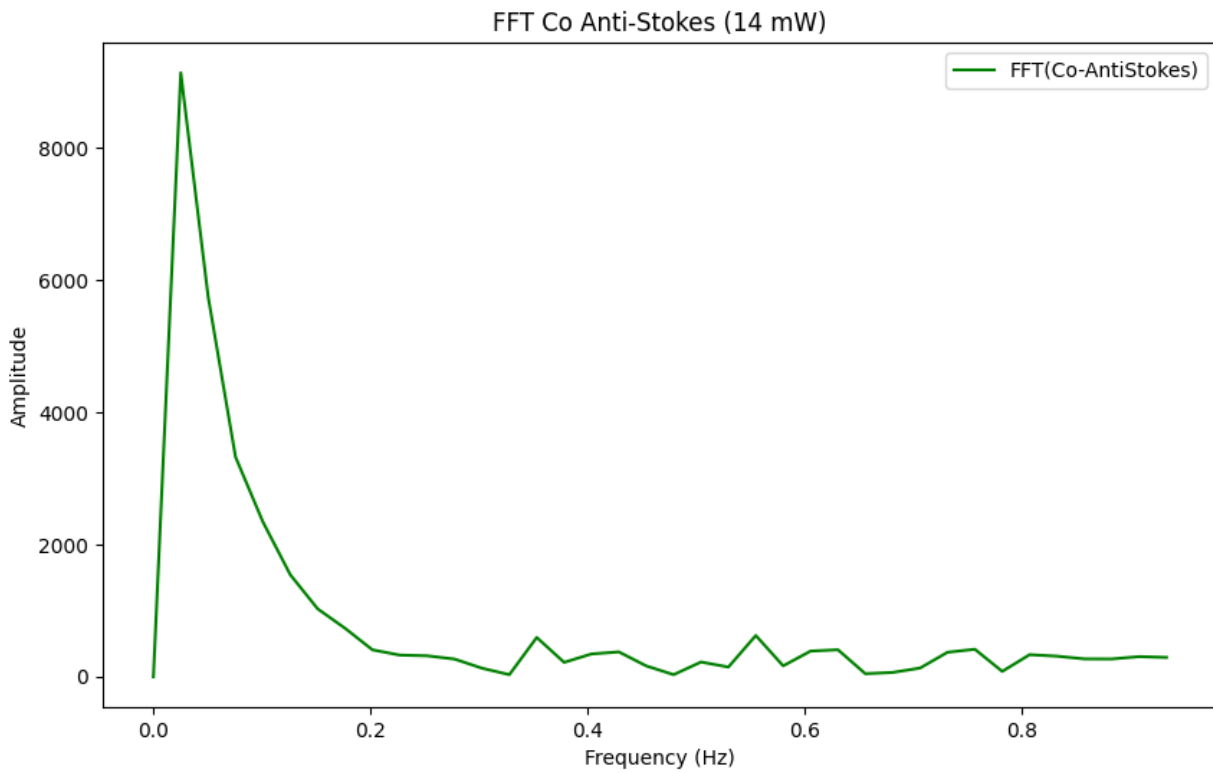
WL=518.48, Cnt=1256.00

WL=516.93, Cnt=1110.00

WL=515.91, Cnt=1074.00

WL=513.34, Cnt=953.00

### FFT Co Anti-Stokes (14 mW)



### FFT Peak Info:

Freq=0.03, Amp=9142.33

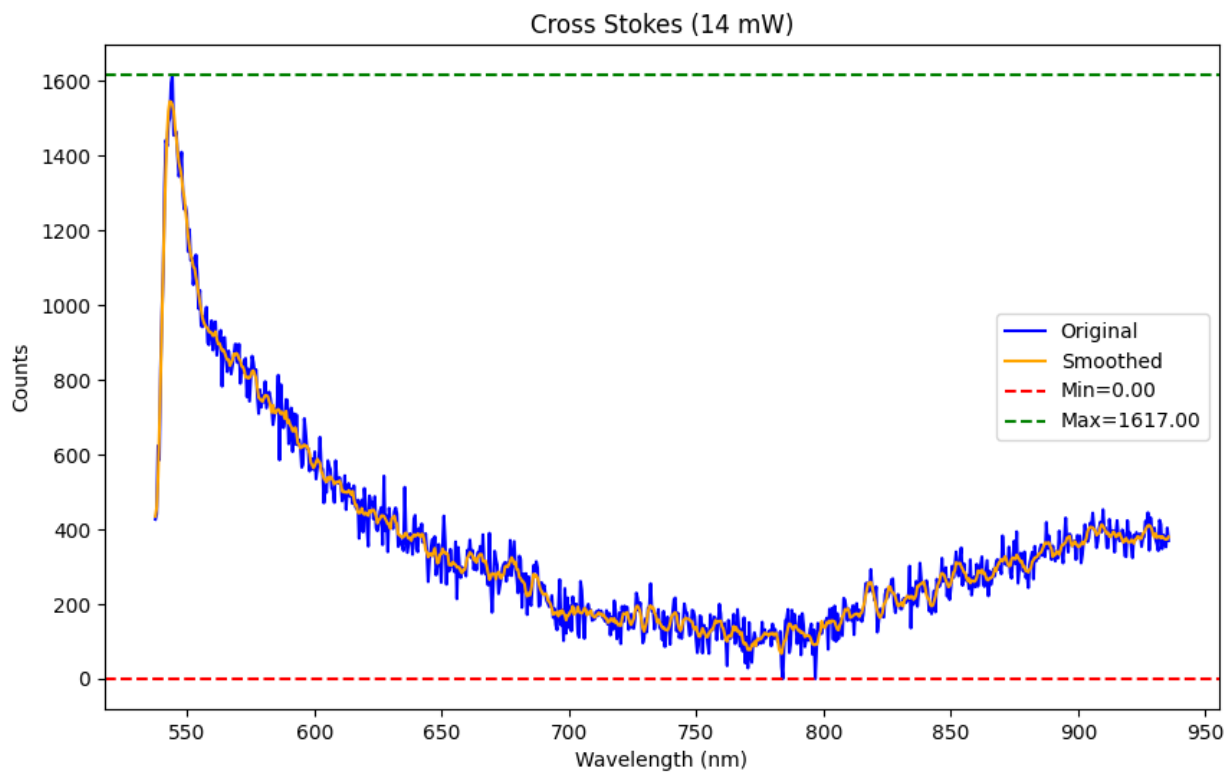
Freq=0.56, Amp=626.26

Freq=0.35, Amp=596.56

Freq=0.76, Amp=417.78

Freq=0.63, Amp=410.36

### Cross Stokes (14 mW)



#### Peak Info:

WL=544.17, Cnt=1617.00

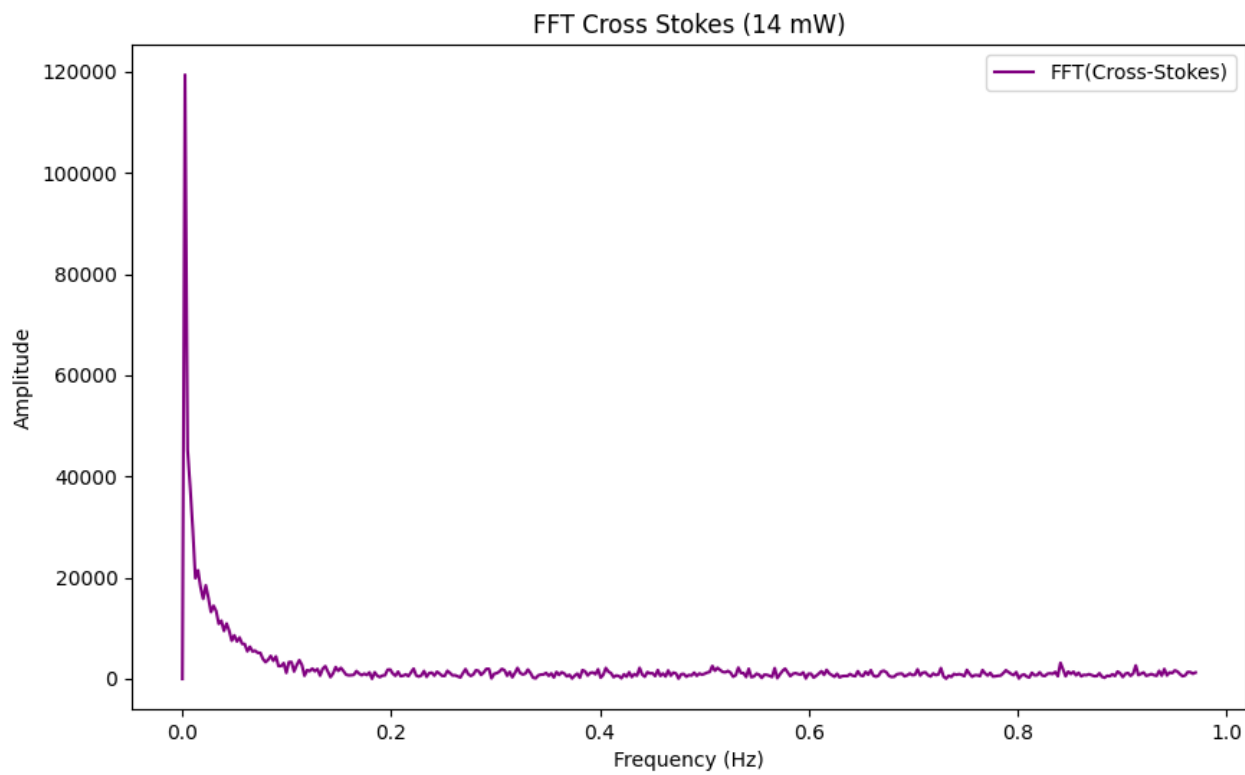
WL=545.71, Cnt=1464.00

WL=541.60, Cnt=1442.00

WL=547.76, Cnt=1410.00

WL=549.30, Cnt=1266.00

## FFT Cross Stokes (14 mW)



### FFT Peak Info:

Freq=0.00, Amp=119400.11

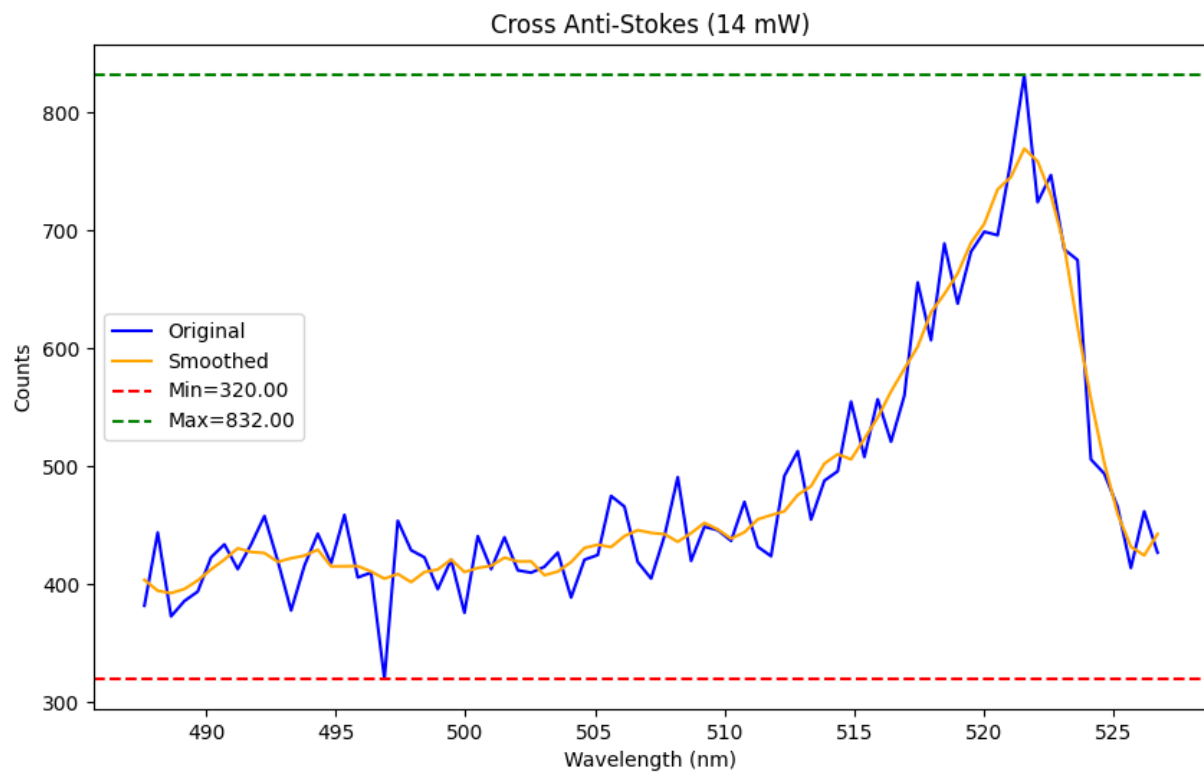
Freq=0.01, Amp=21462.36

Freq=0.02, Amp=18494.86

Freq=0.03, Amp=14438.85

Freq=0.04, Amp=11487.06

### Cross Anti-Stokes (14 mW)



Peak Info:

WL=521.56, Cnt=832.00

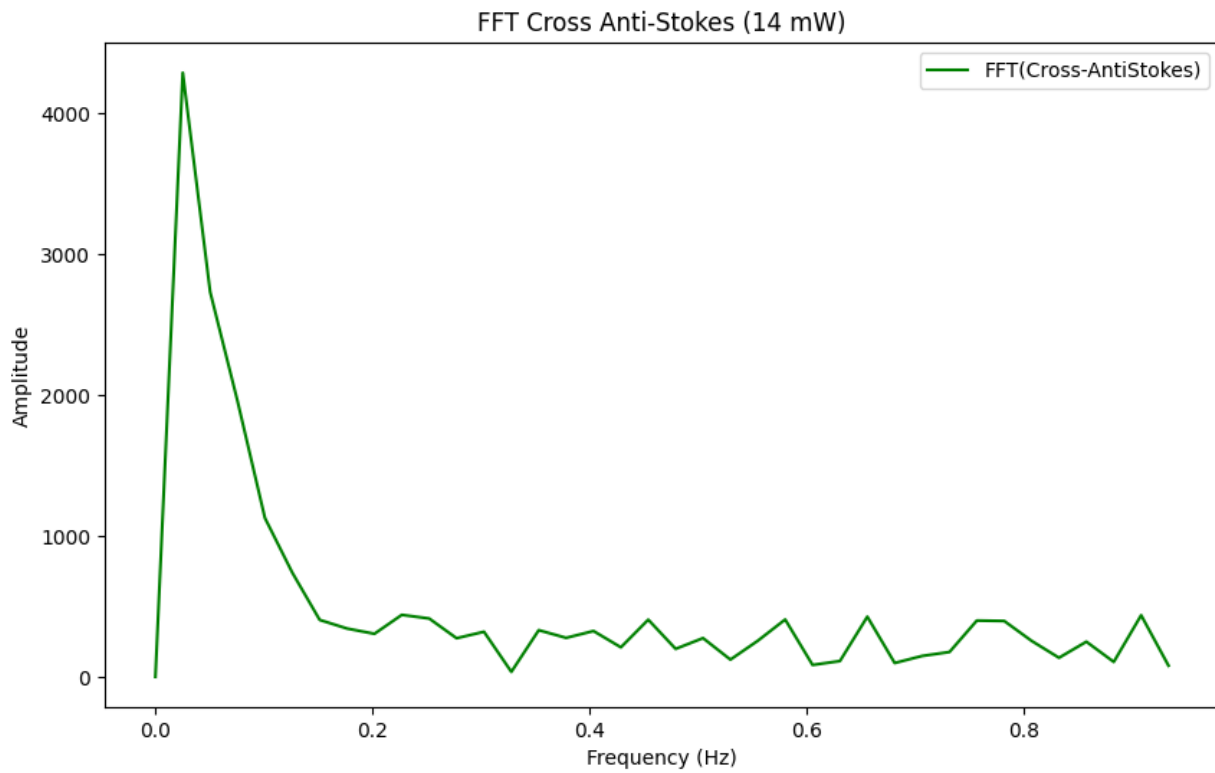
WL=522.59, Cnt=747.00

WL=520.02, Cnt=699.00

WL=518.48, Cnt=689.00

WL=517.45, Cnt=656.00

### FFT Cross Anti-Stokes (14 mW)



#### FFT Peak Info:

Freq=0.03, Amp=4288.26

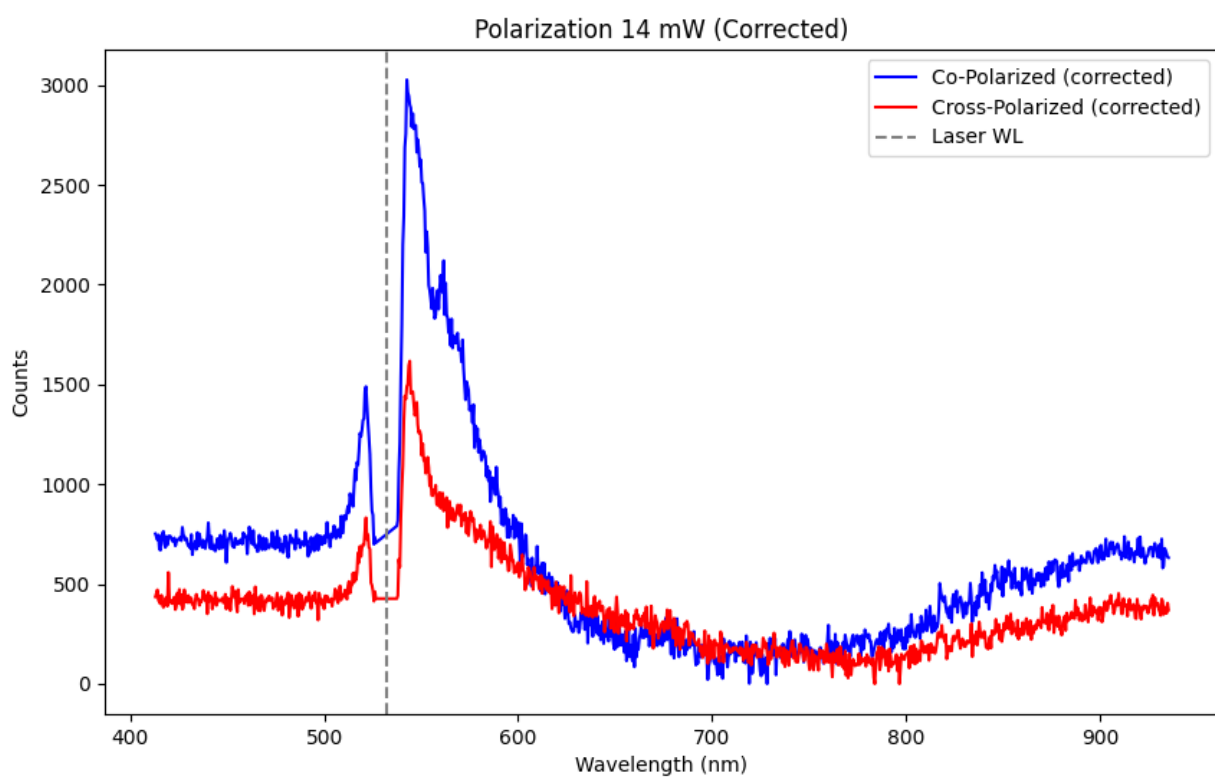
Freq=0.23, Amp=440.10

Freq=0.91, Amp=437.36

Freq=0.66, Amp=427.21

Freq=0.58, Amp=407.15

Polarization 14 mW



# Spectrometry Analysis Report

Sample: A1

Laser Wavelength (after shift): 633.27 nm

Power Levels: 14.0 mW

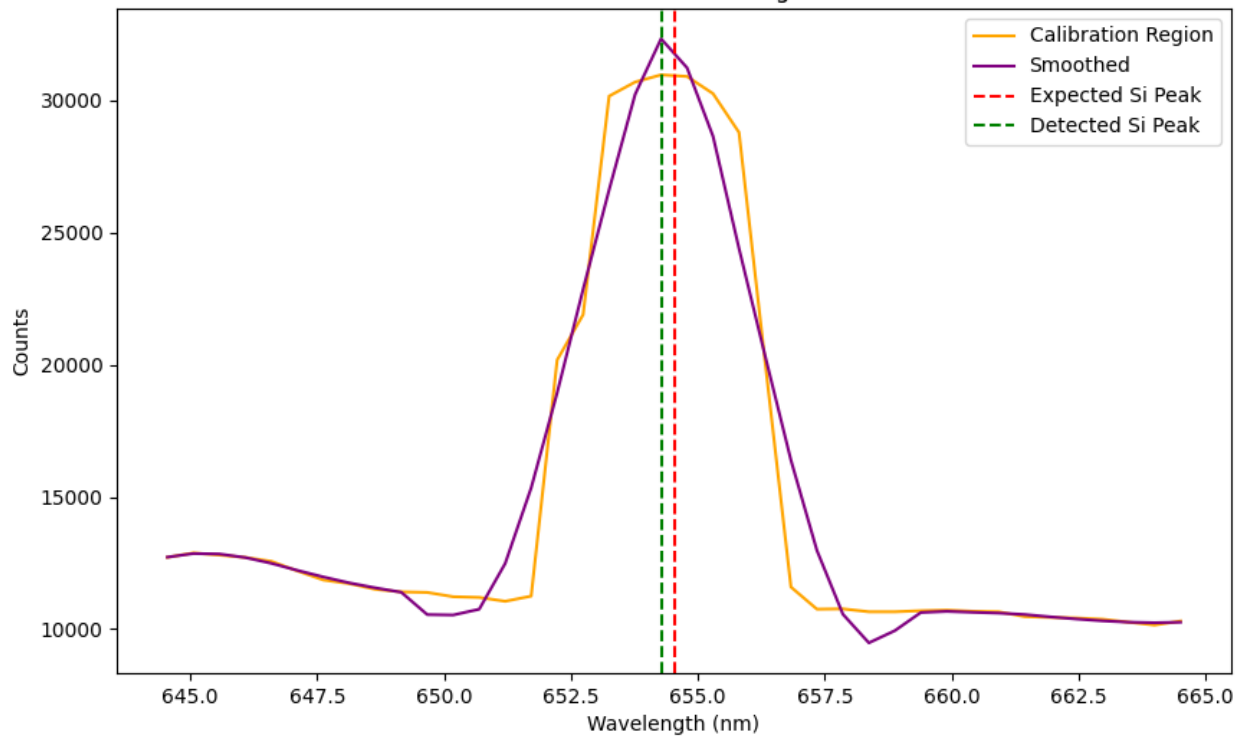
Thickness: 60.0 nm

Laser Filter Window:  $\pm 5.0$  nm

Calibration Shift: 0.27 nm

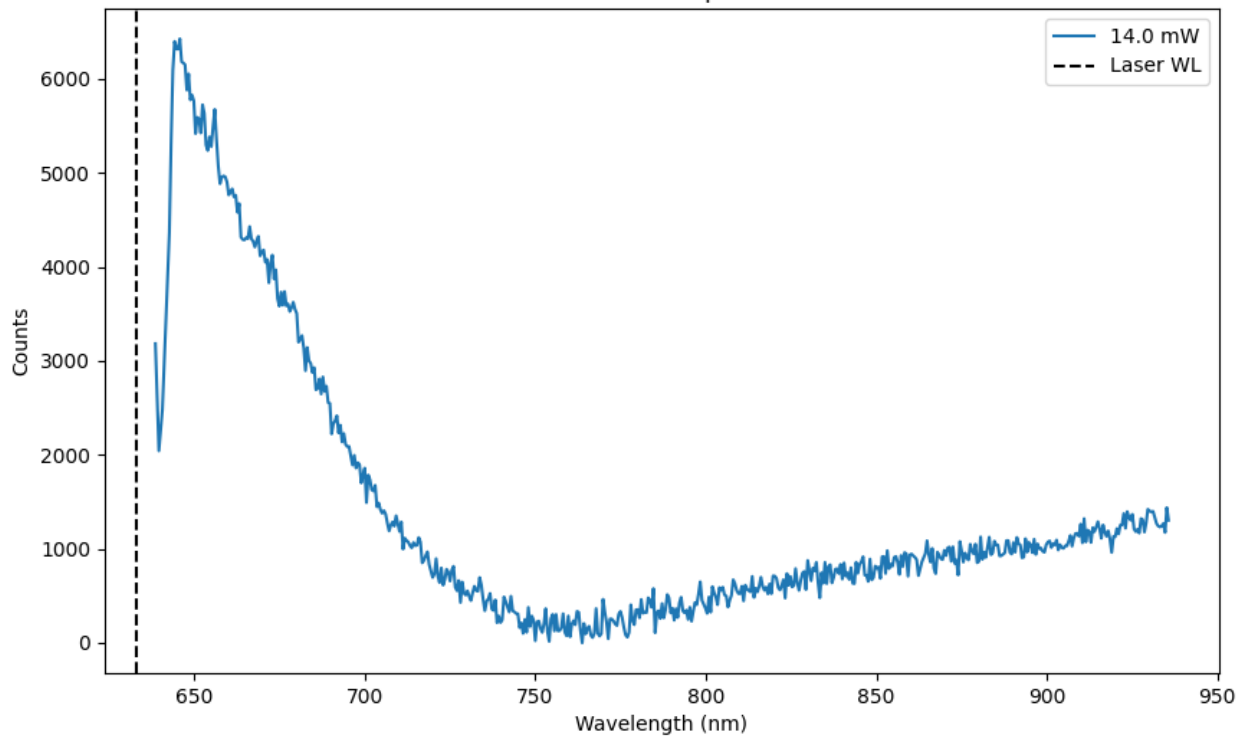
## Calibration Region

### Silicon Calibration Region

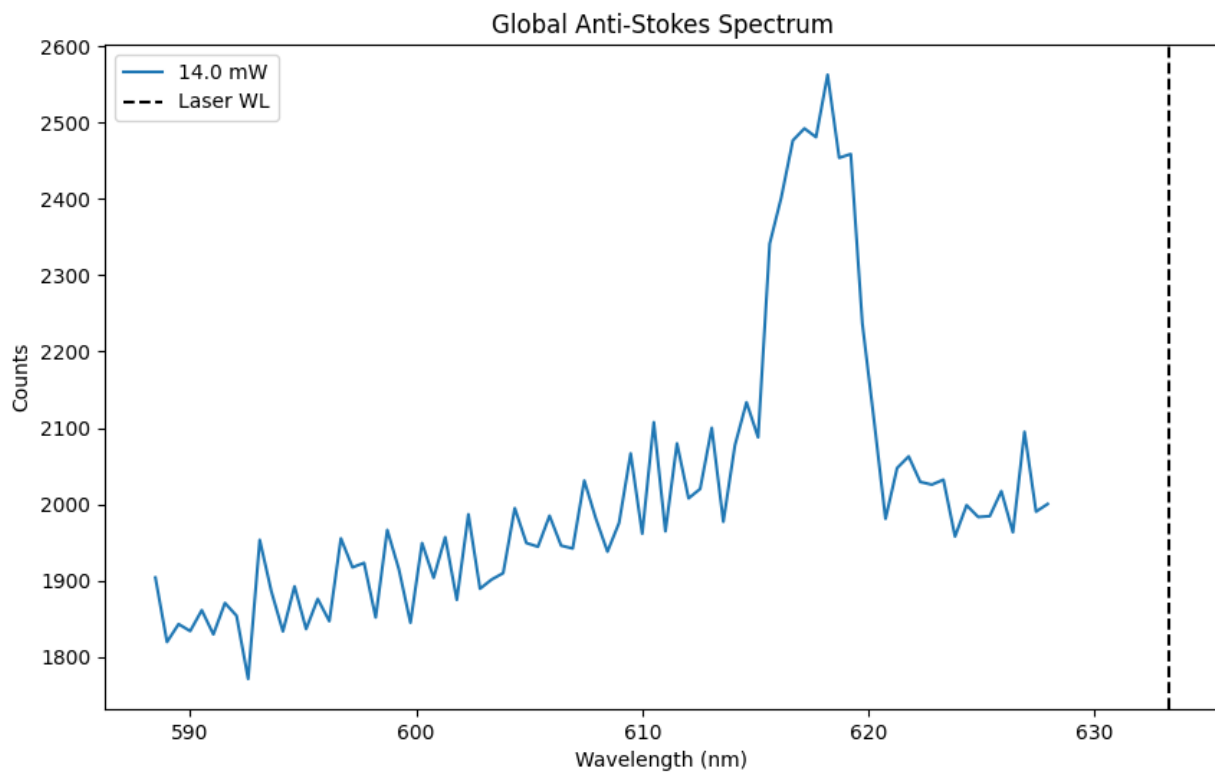


## Global Stokes Spectrum

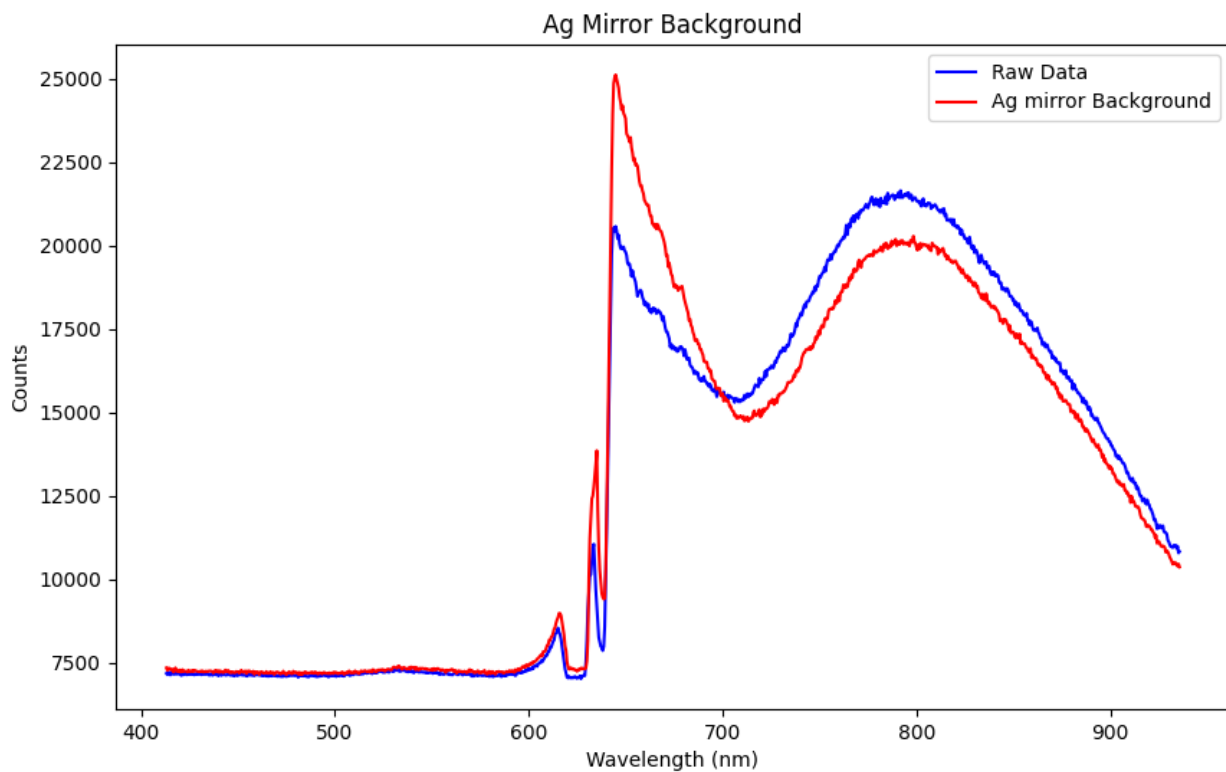
Global Stokes Spectrum



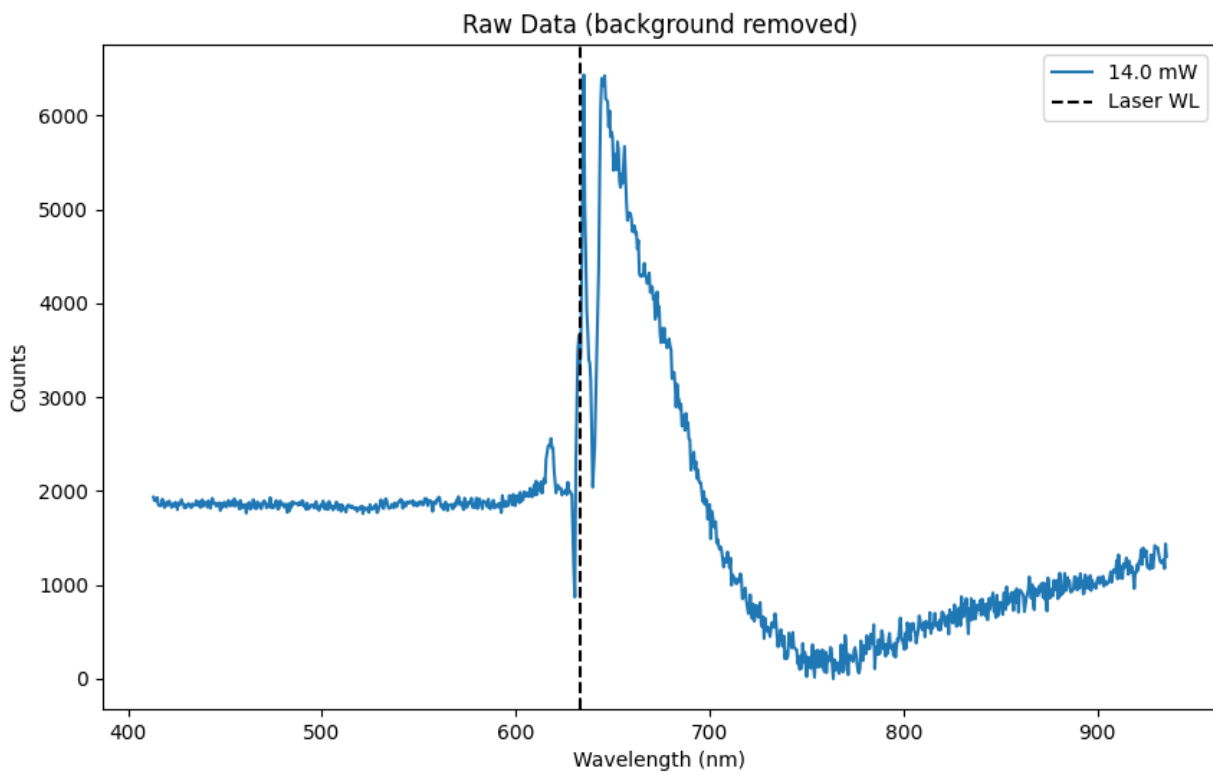
## Global Anti-Stokes Spectrum



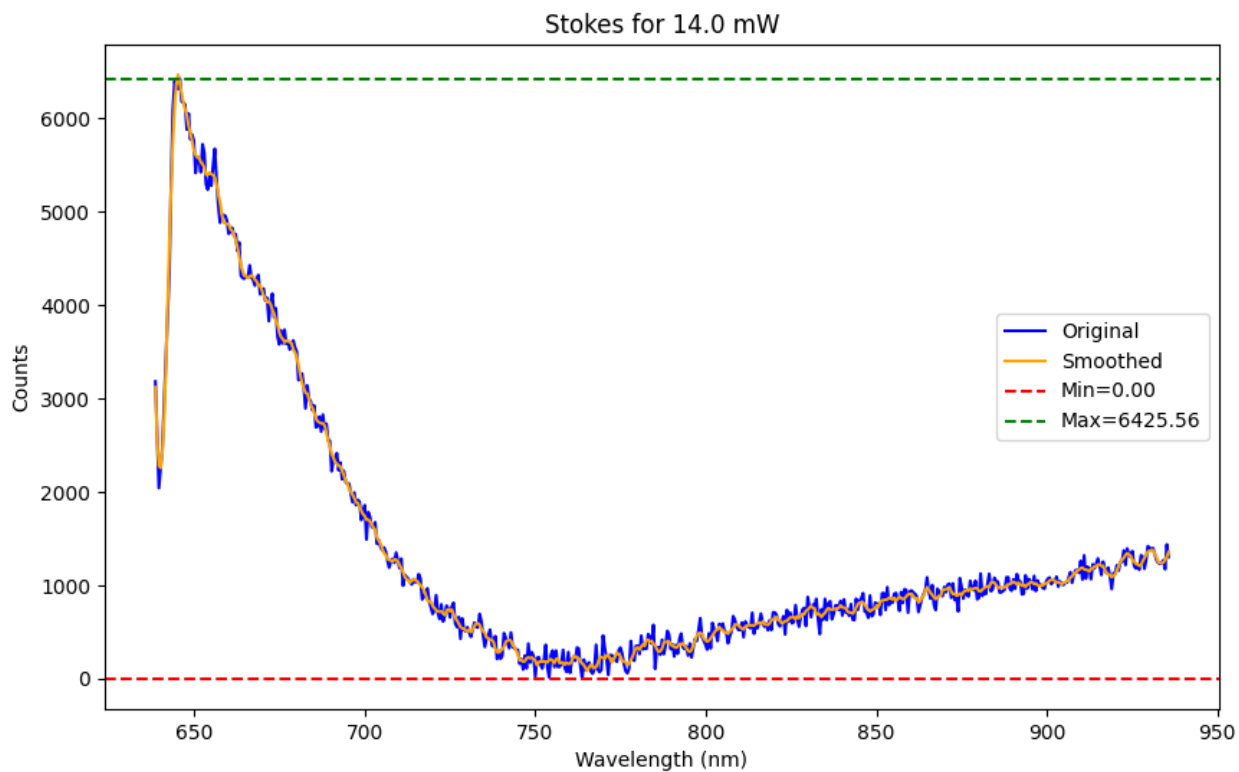
## Ag Mirror Background



## Raw Data



## Stokes for 14.0 mW



Integral (Area) = 414325.50

Peak Info (Stokes):

WL=645.85, Cnt=6425.56

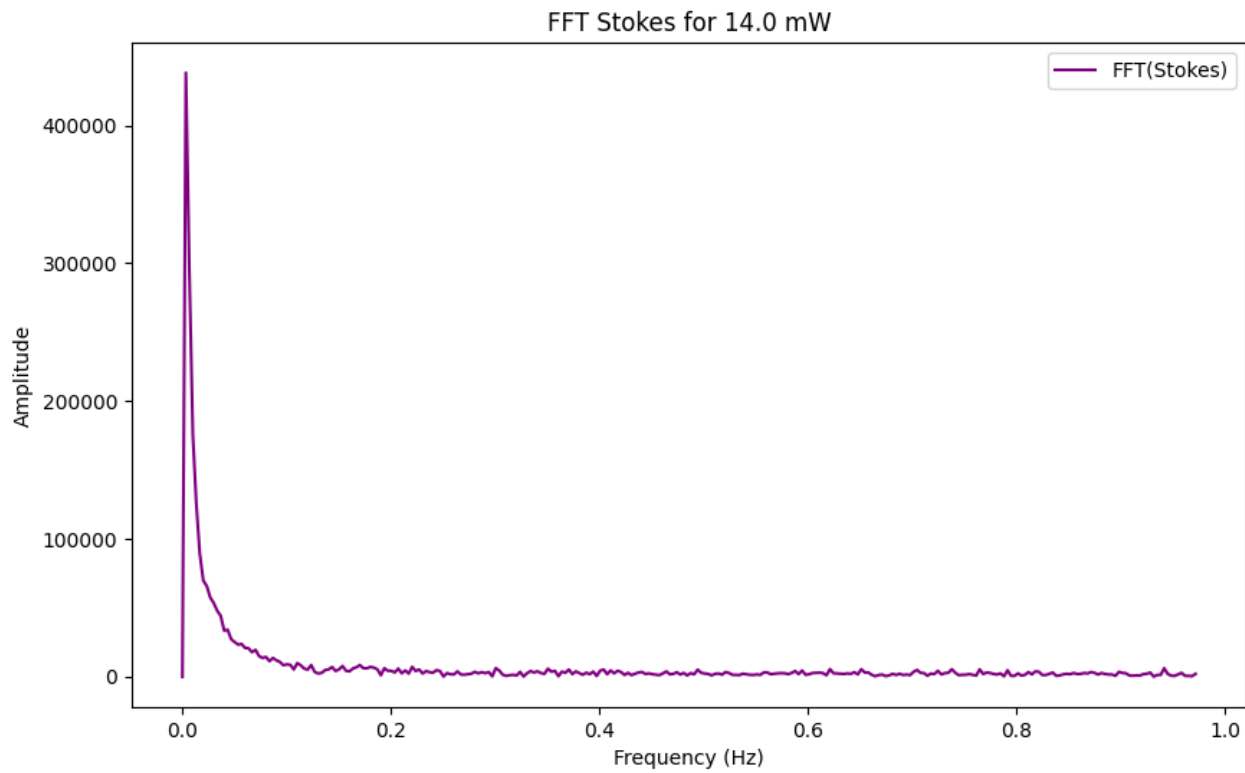
WL=644.31, Cnt=6398.08

WL=648.40, Cnt=6052.07

WL=649.43, Cnt=5825.77

WL=652.50, Cnt=5723.34

## FFT Stokes for 14.0 mW



Peak Info (FFT Stokes):

Freq=0.00, Amp=438149.07

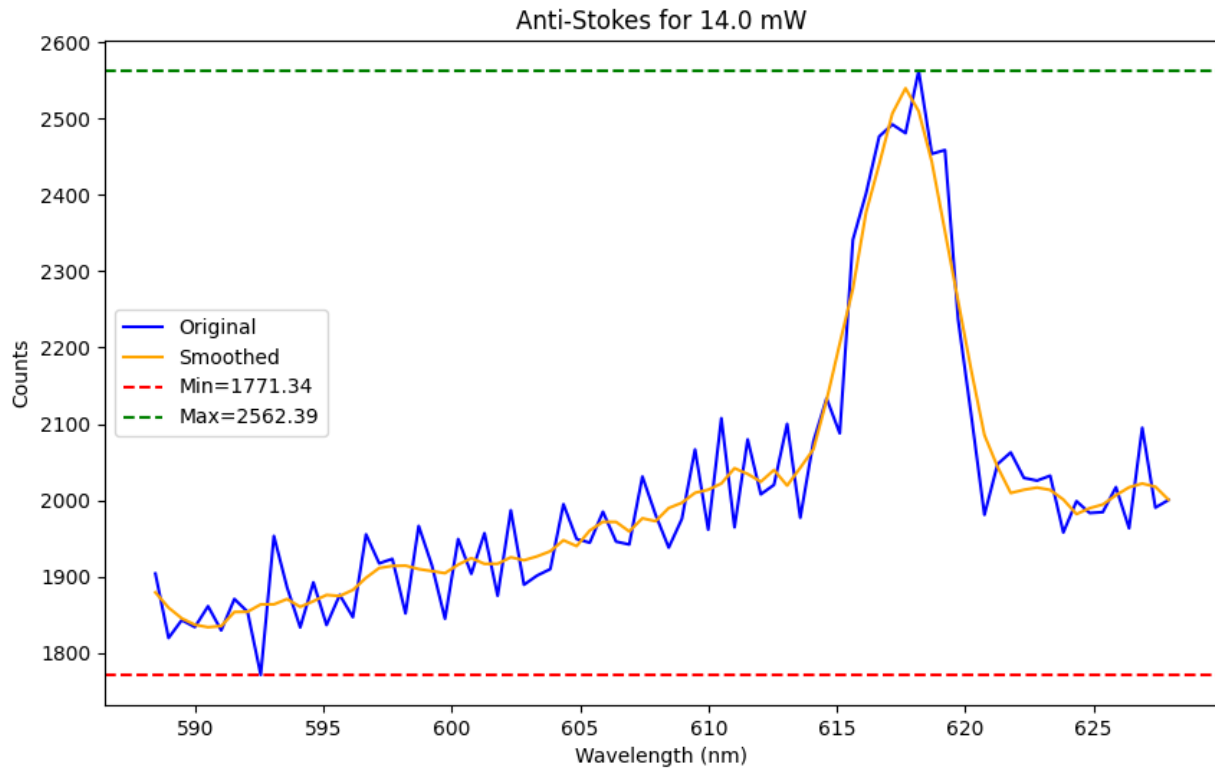
Freq=0.04, Amp=34168.66

Freq=0.06, Amp=23854.76

Freq=0.07, Amp=19590.29

Freq=0.08, Amp=14419.75

## Anti-Stokes for 14.0 mW



Integral (Area) = 79421.91

Peak Info (Anti-Stokes):

WL=618.19, Cnt=2562.39

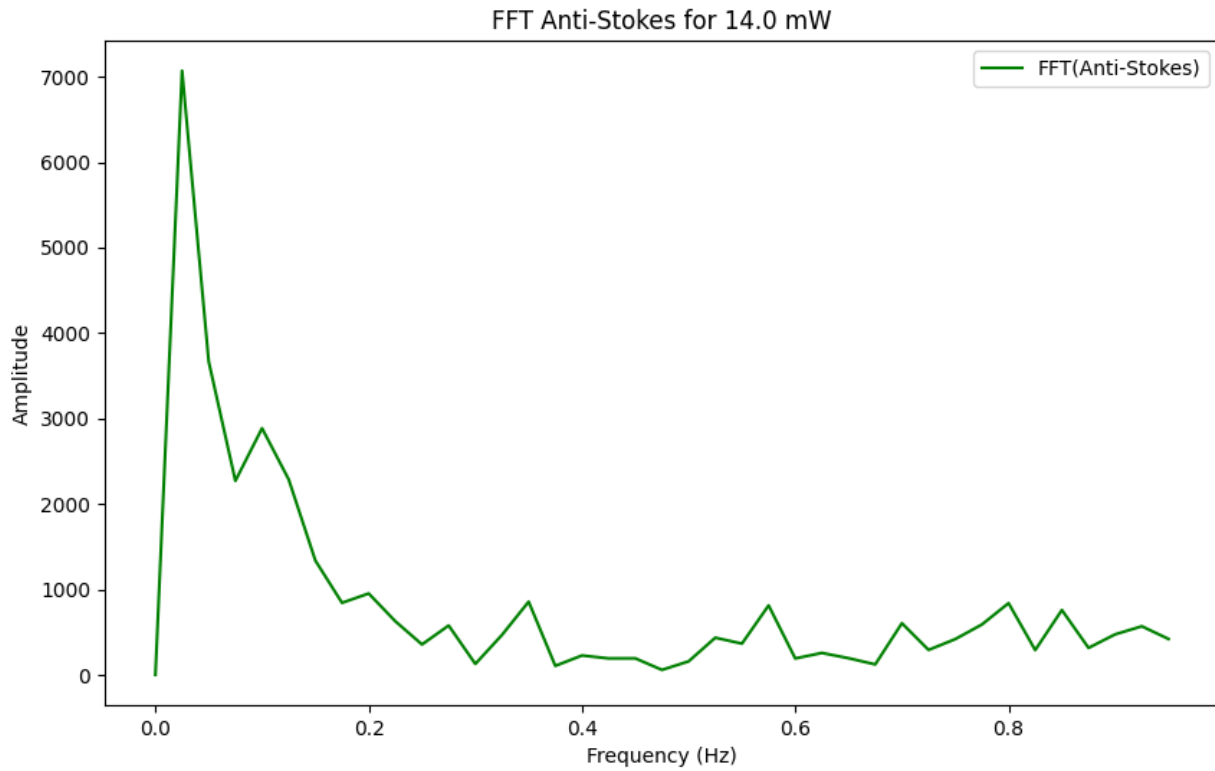
WL=617.17, Cnt=2492.06

WL=619.22, Cnt=2458.55

WL=614.60, Cnt=2133.50

WL=610.50, Cnt=2107.39

## FFT Anti-Stokes for 14.0 mW



Peak Info (FFT Anti-Stokes):

Freq=0.02, Amp=7070.37

Freq=0.10, Amp=2886.31

Freq=0.20, Amp=952.26

Freq=0.35, Amp=856.30

Freq=0.80, Amp=839.09

# Spectrometry Analysis Report

Sample: G6

Laser Wavelength (after shift): 532.13 nm

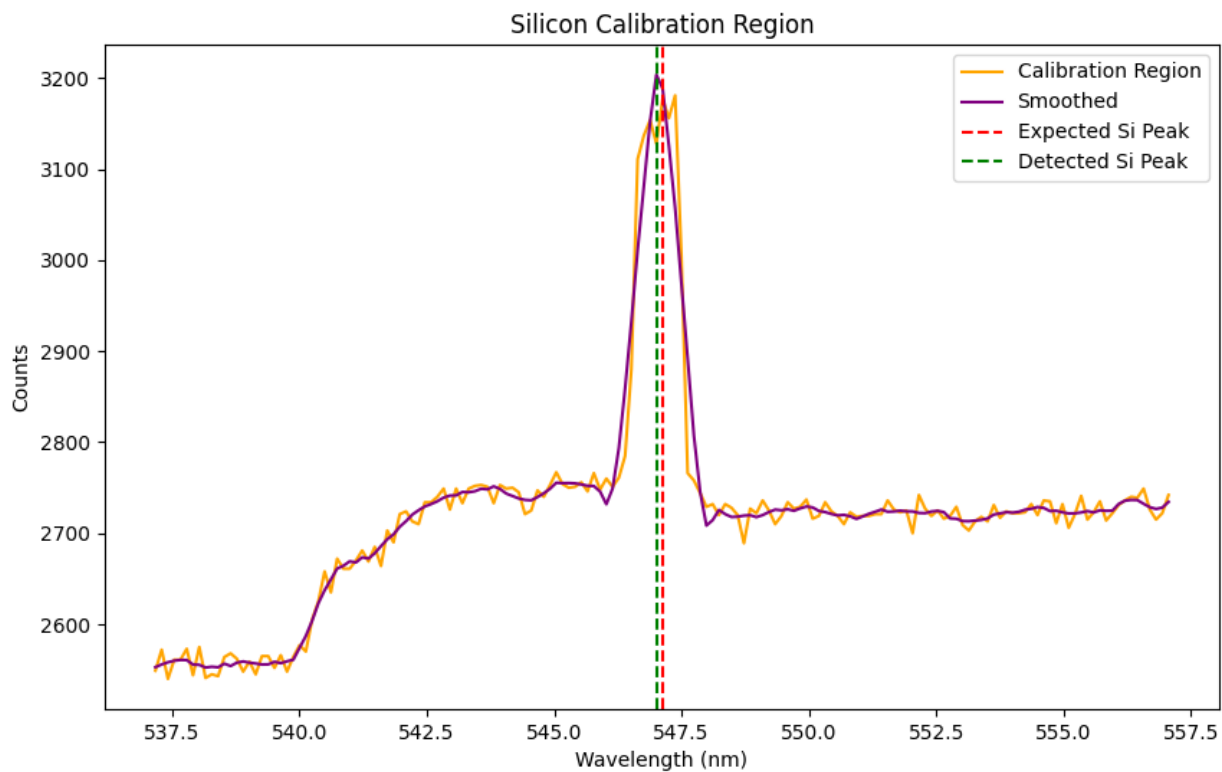
Power Levels: 14.0 mW

Thickness: 160.0 nm

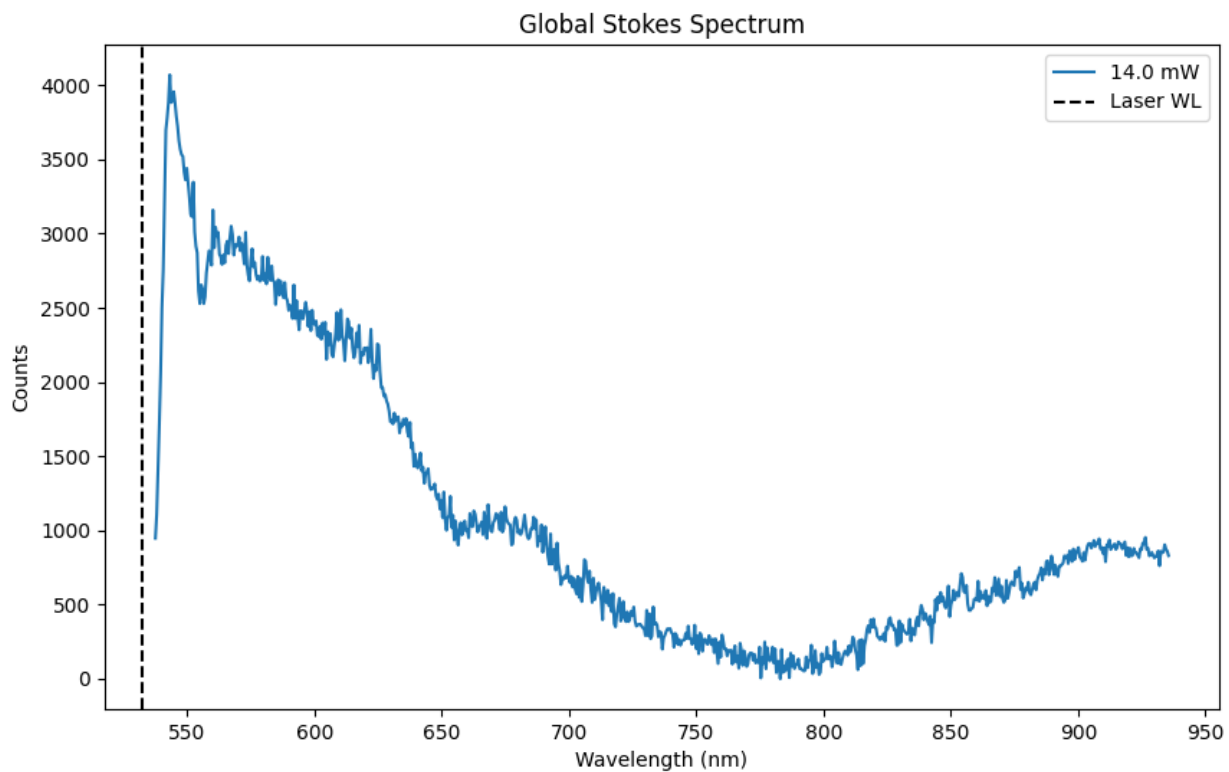
Laser Filter Window:  $\pm 5.0$  nm

Calibration Shift: 0.13 nm

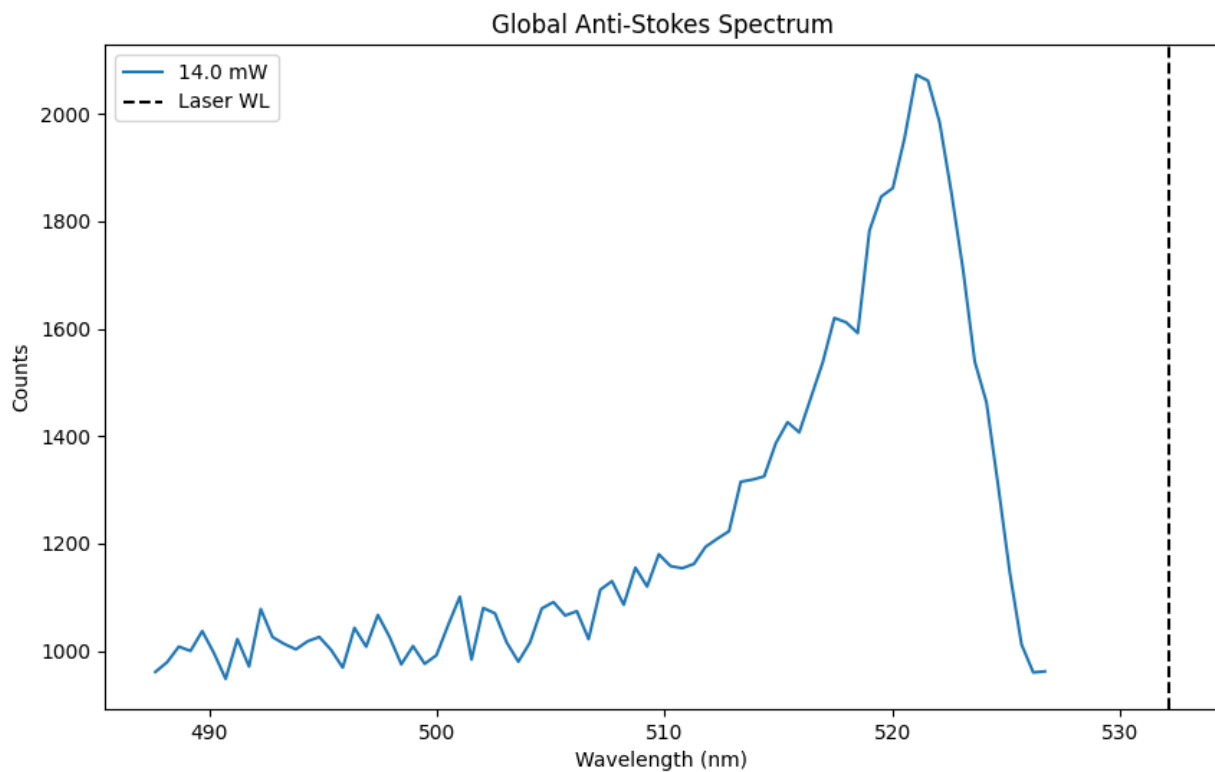
## Calibration Region



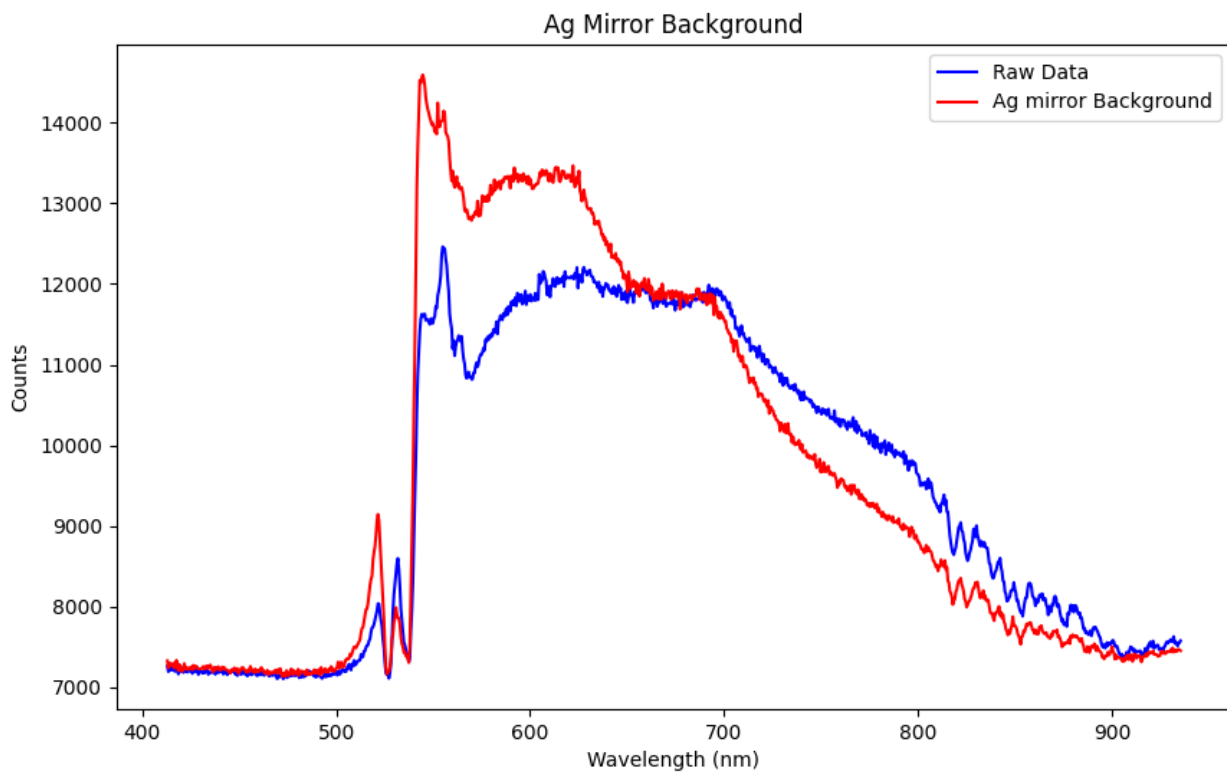
## Global Stokes Spectrum



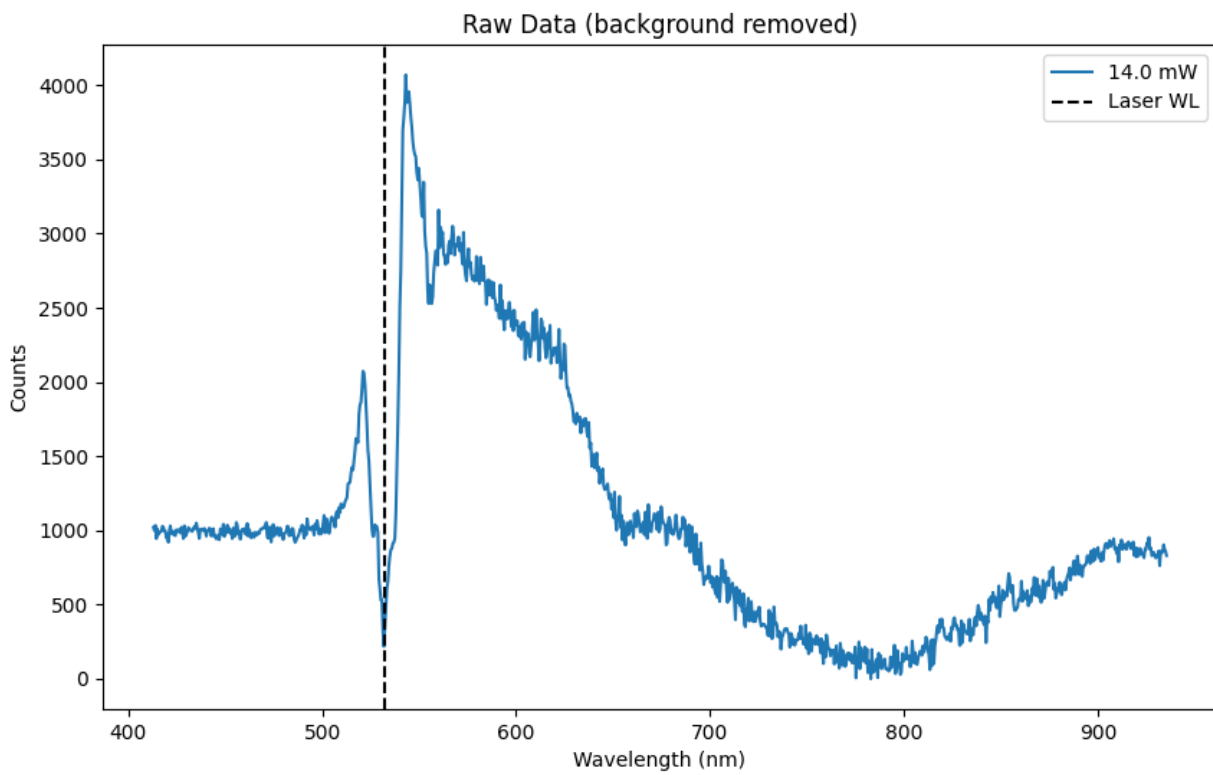
## Global Anti-Stokes Spectrum



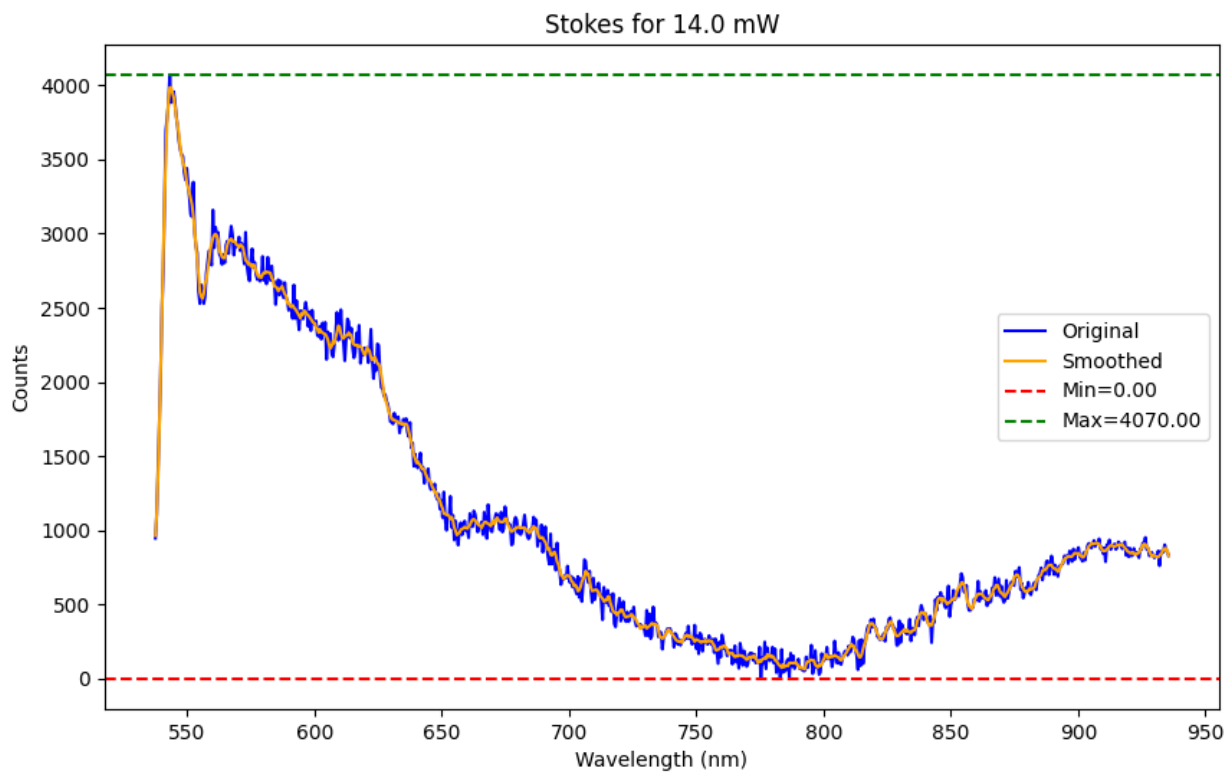
## Ag Mirror Background



## Raw Data



### Stokes for 14.0 mW



Integral (Area) = 430983.65

Peak Info (Stokes):

WL=543.14, Cnt=4070.00

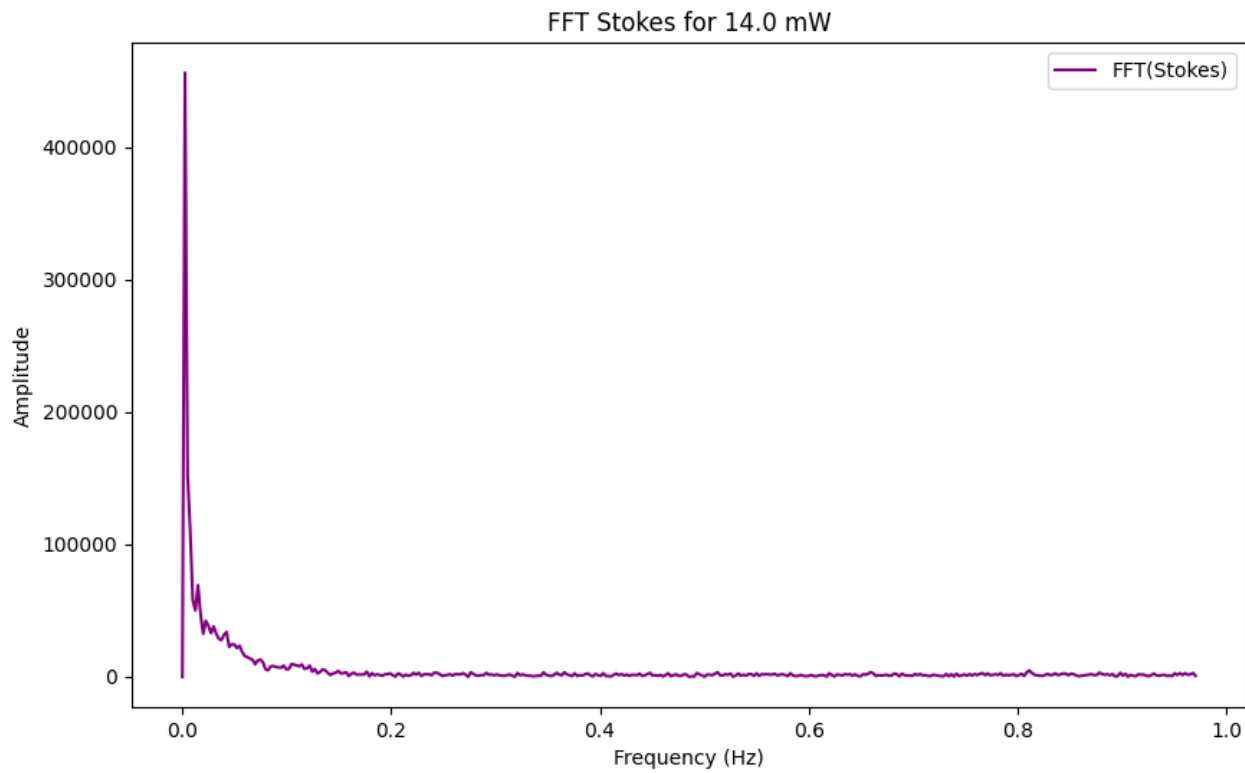
WL=544.68, Cnt=3956.00

WL=549.82, Cnt=3440.00

WL=552.39, Cnt=3347.00

WL=560.09, Cnt=3159.00

## FFT Stokes for 14.0 mW



Peak Info (FFT Stokes):

Freq=0.00, Amp=456040.06

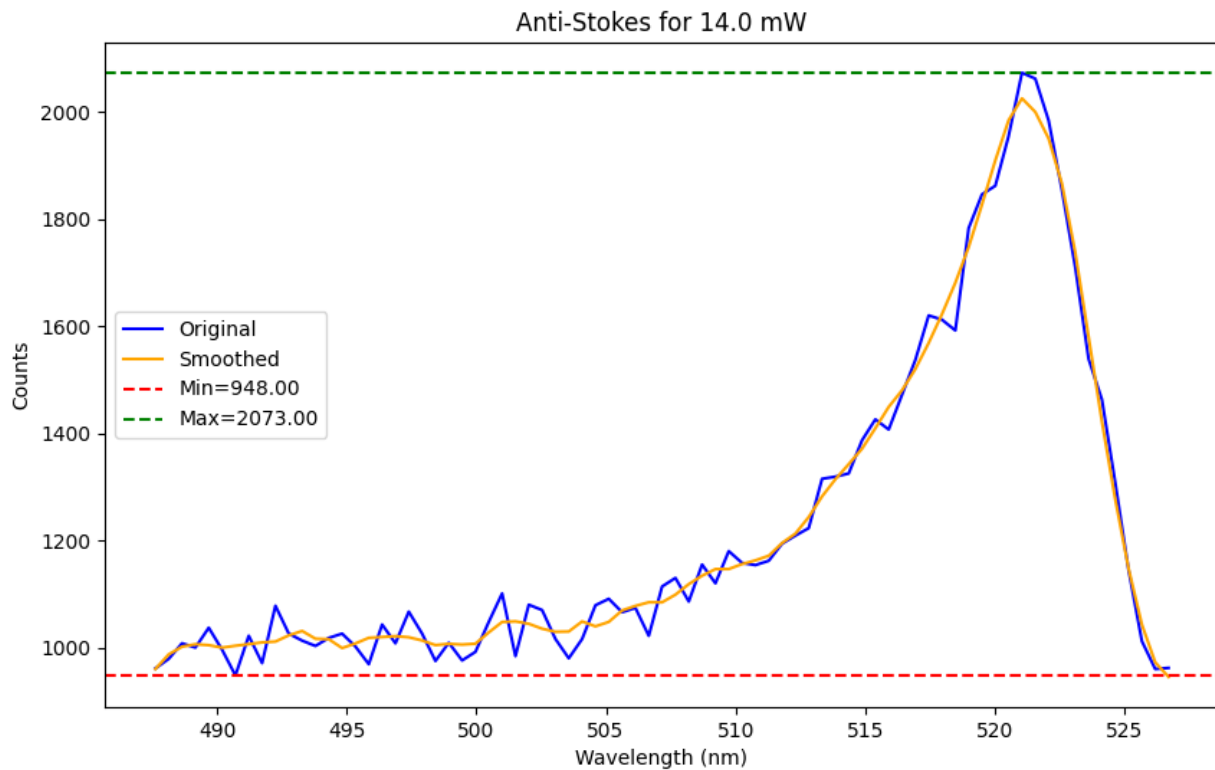
Freq=0.01, Amp=69250.35

Freq=0.02, Amp=42312.76

Freq=0.03, Amp=38094.54

Freq=0.04, Amp=33836.31

### Anti-Stokes for 14.0 mW



Integral (Area) = 47937.53

Peak Info (Anti-Stokes):

WL=521.05, Cnt=2073.00

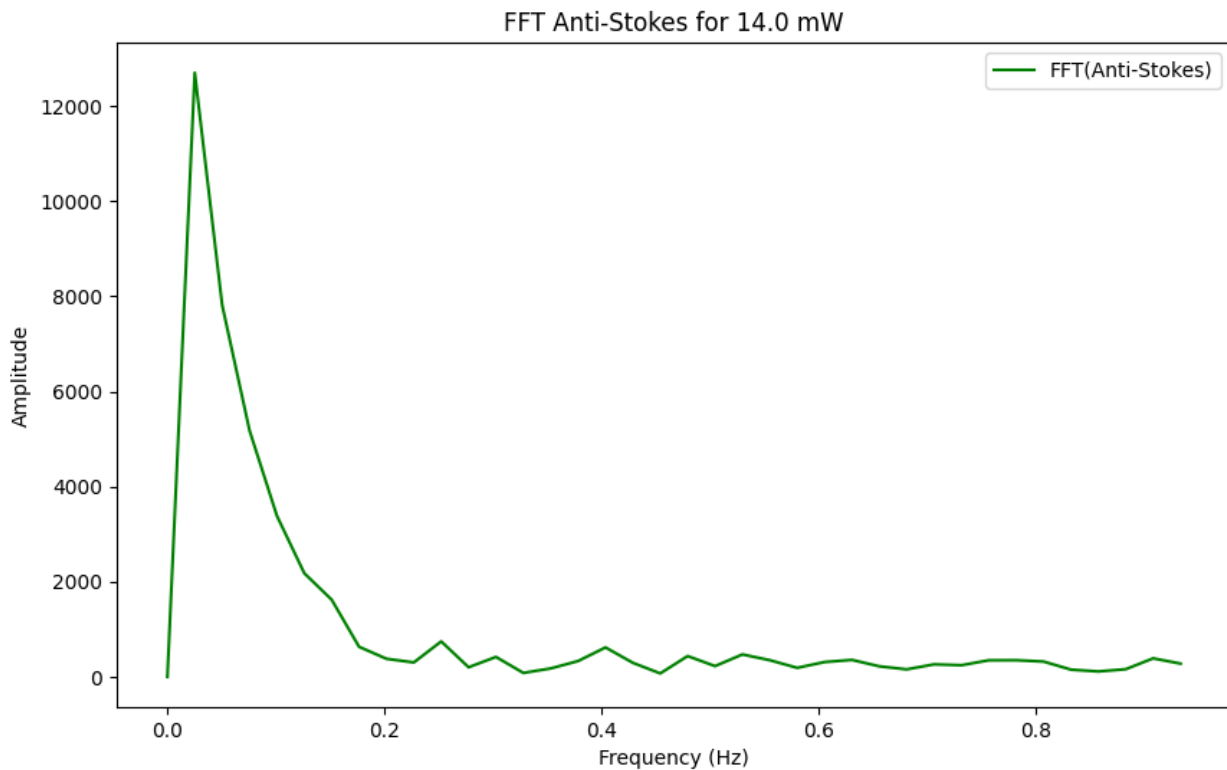
WL=517.45, Cnt=1620.00

WL=515.39, Cnt=1426.00

WL=509.74, Cnt=1180.00

WL=508.71, Cnt=1155.00

### FFT Anti-Stokes for 14.0 mW



Peak Info (FFT Anti-Stokes):

Freq=0.03, Amp=12702.09

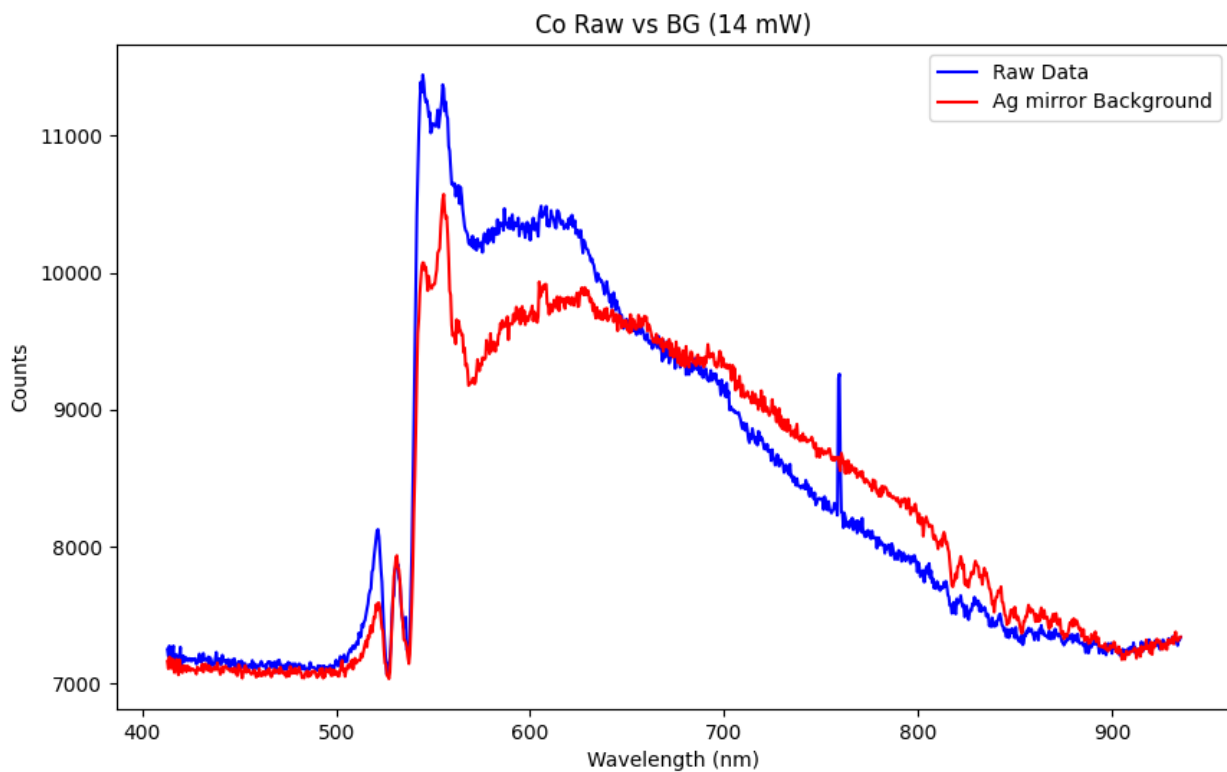
Freq=0.25, Amp=745.20

Freq=0.40, Amp=618.80

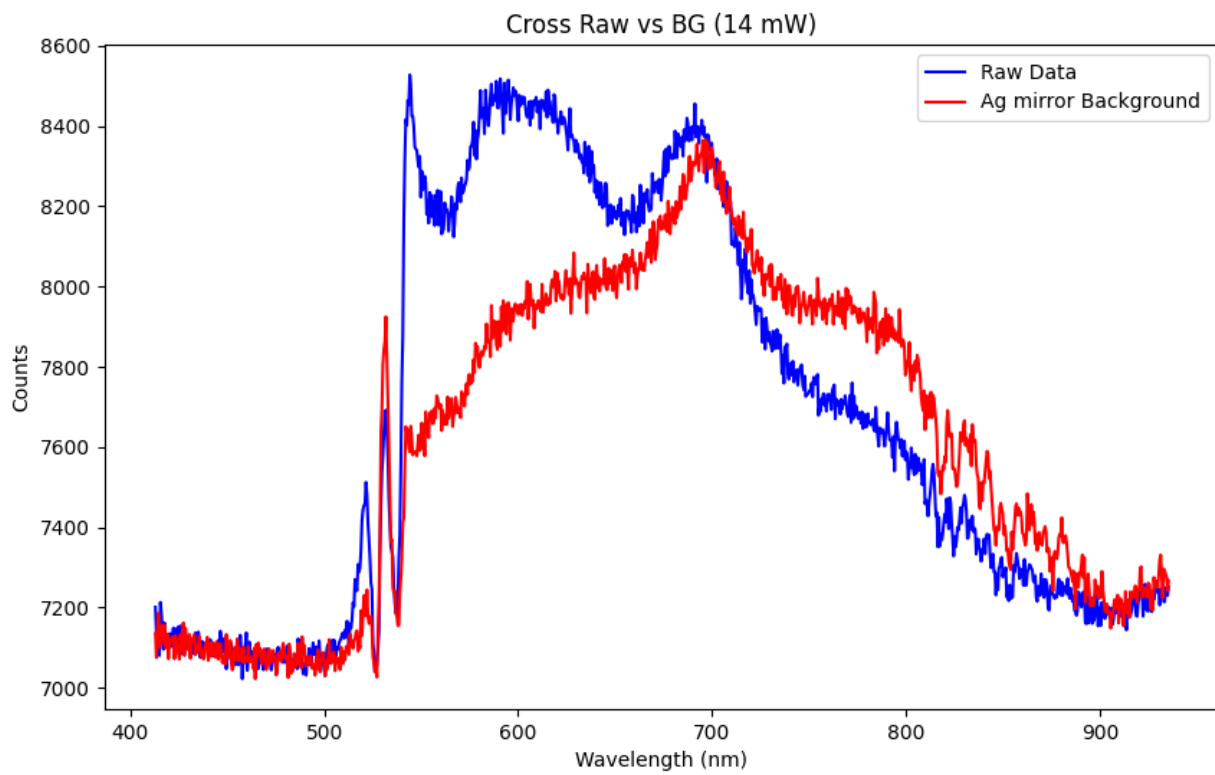
Freq=0.53, Amp=471.53

Freq=0.48, Amp=437.56

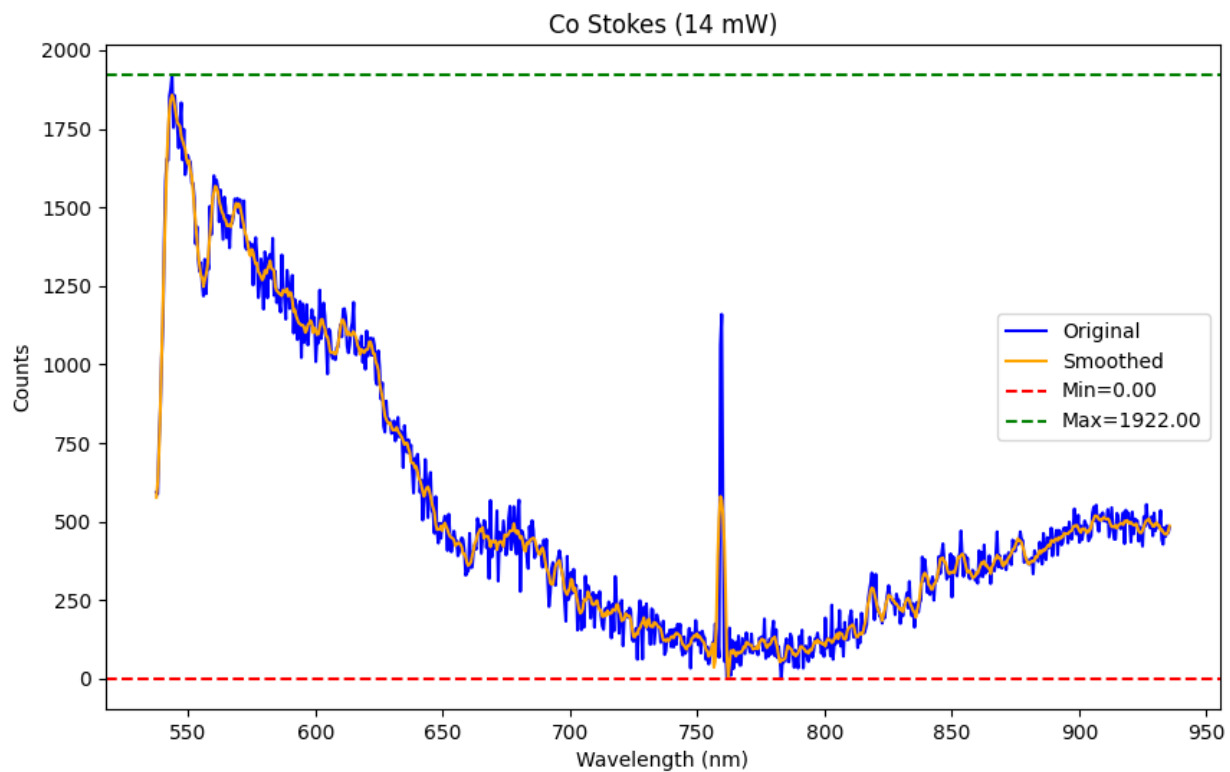
### Co Raw vs BG (14 mW)



### Cross Raw vs BG (14 mW)



### Co Stokes (14 mW)



#### Peak Info:

WL=543.66, Cnt=1922.00

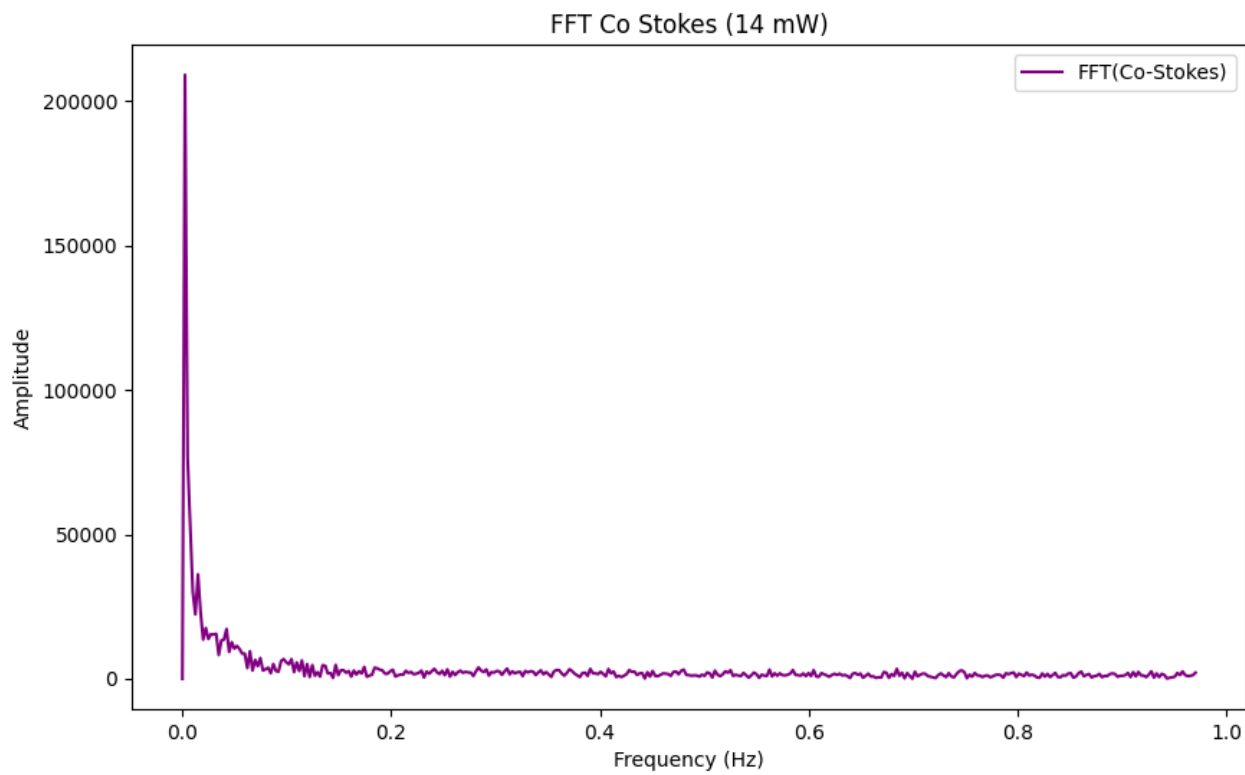
WL=544.68, Cnt=1856.00

WL=547.25, Cnt=1833.00

WL=548.28, Cnt=1749.00

WL=549.82, Cnt=1666.00

### FFT Co Stokes (14 mW)



#### FFT Peak Info:

Freq=0.00, Amp=209013.55

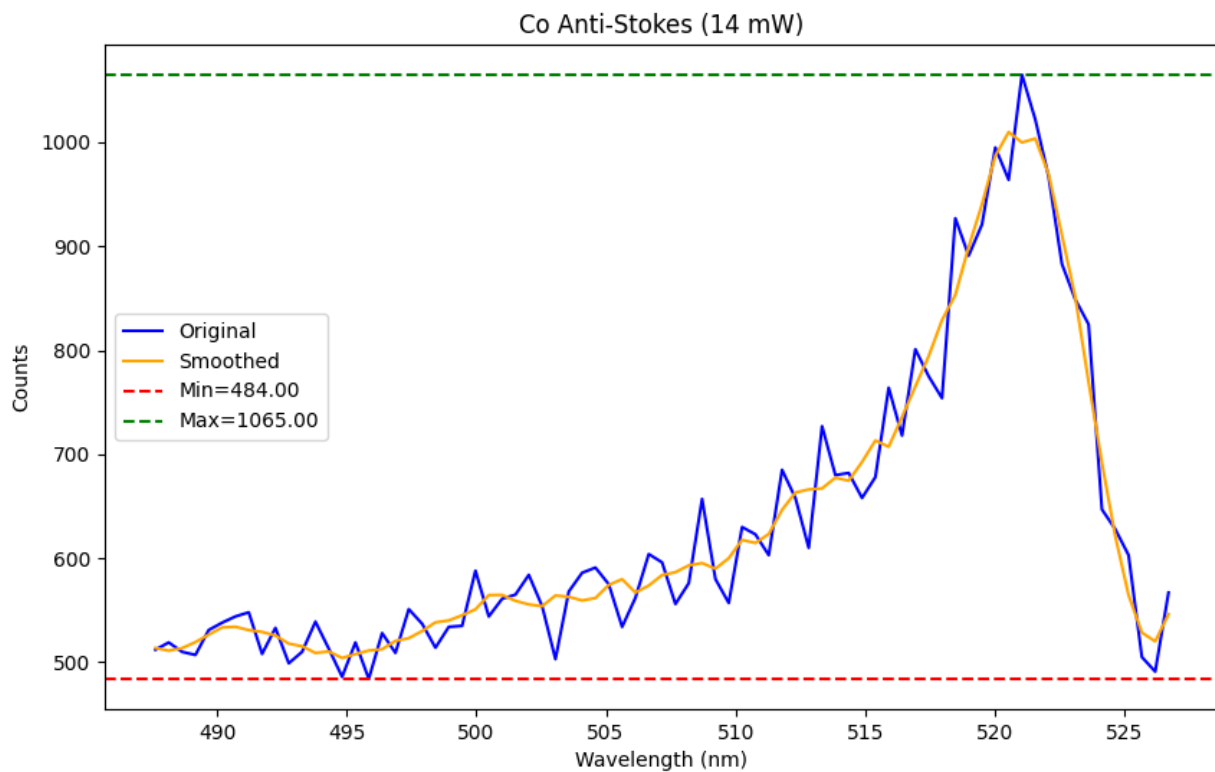
Freq=0.01, Amp=36155.76

Freq=0.02, Amp=17613.95

Freq=0.04, Amp=17276.17

Freq=0.03, Amp=15570.17

## Co Anti-Stokes (14 mW)



Peak Info:

WL=521.05, Cnt=1065.00

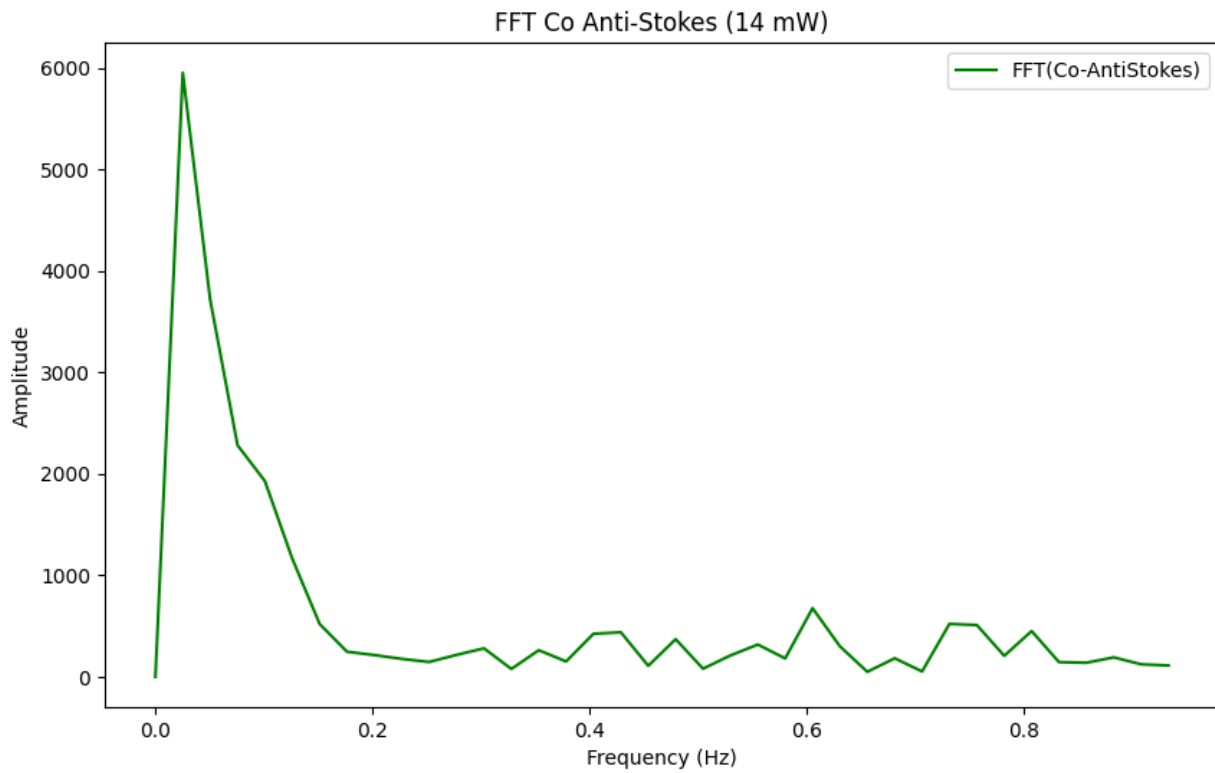
WL=520.02, Cnt=995.00

WL=518.48, Cnt=927.00

WL=516.93, Cnt=801.00

WL=515.91, Cnt=764.00

### FFT Co Anti-Stokes (14 mW)



#### FFT Peak Info:

Freq=0.03, Amp=5956.57

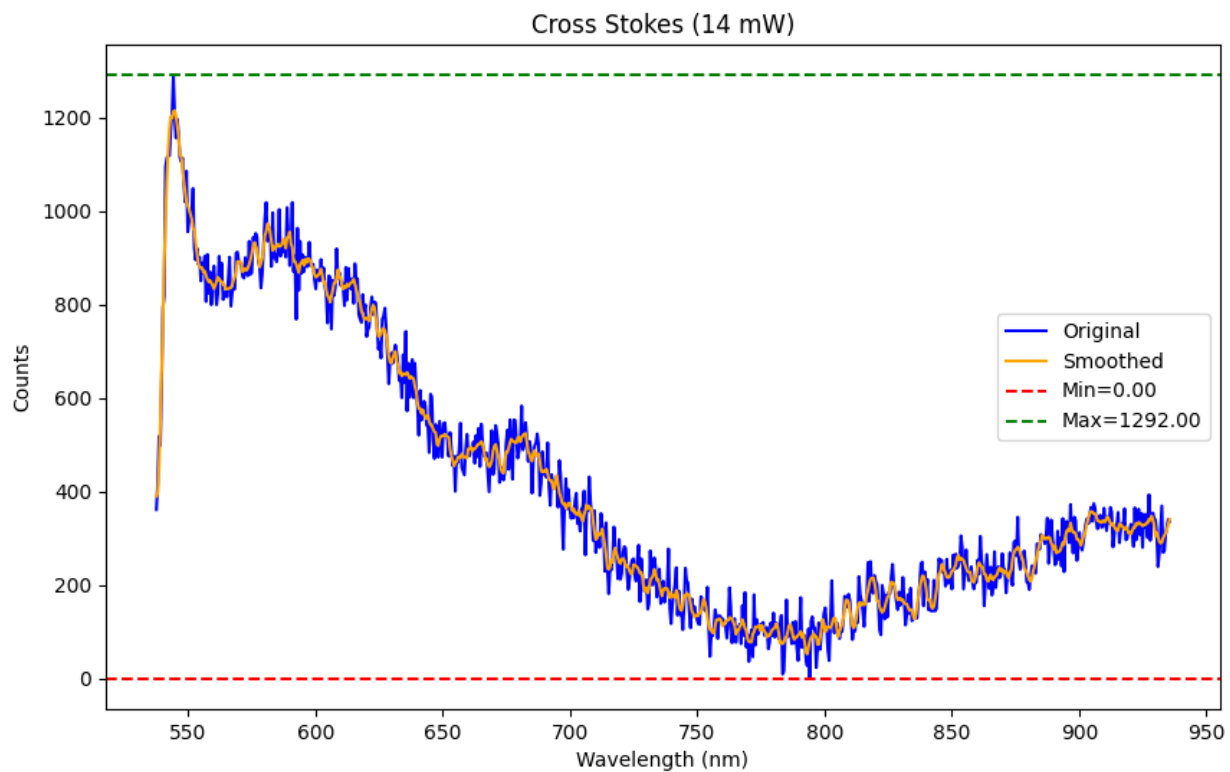
Freq=0.61, Amp=676.84

Freq=0.73, Amp=522.70

Freq=0.81, Amp=451.35

Freq=0.43, Amp=439.11

### Cross Stokes (14 mW)



#### Peak Info:

WL=544.17, Cnt=1292.00

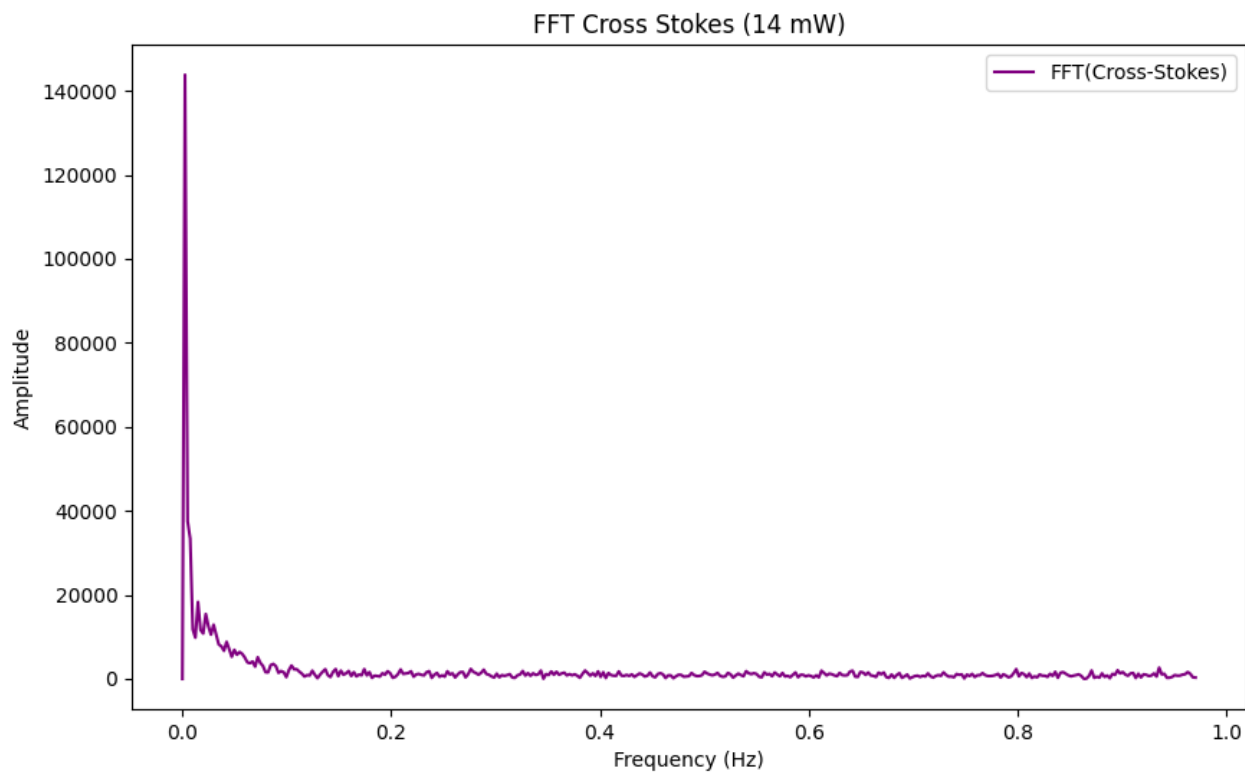
WL=545.71, Cnt=1197.00

WL=547.76, Cnt=1114.00

WL=549.30, Cnt=1086.00

WL=551.87, Cnt=1049.00

## FFT Cross Stokes (14 mW)



### FFT Peak Info:

Freq=0.00, Amp=143820.00

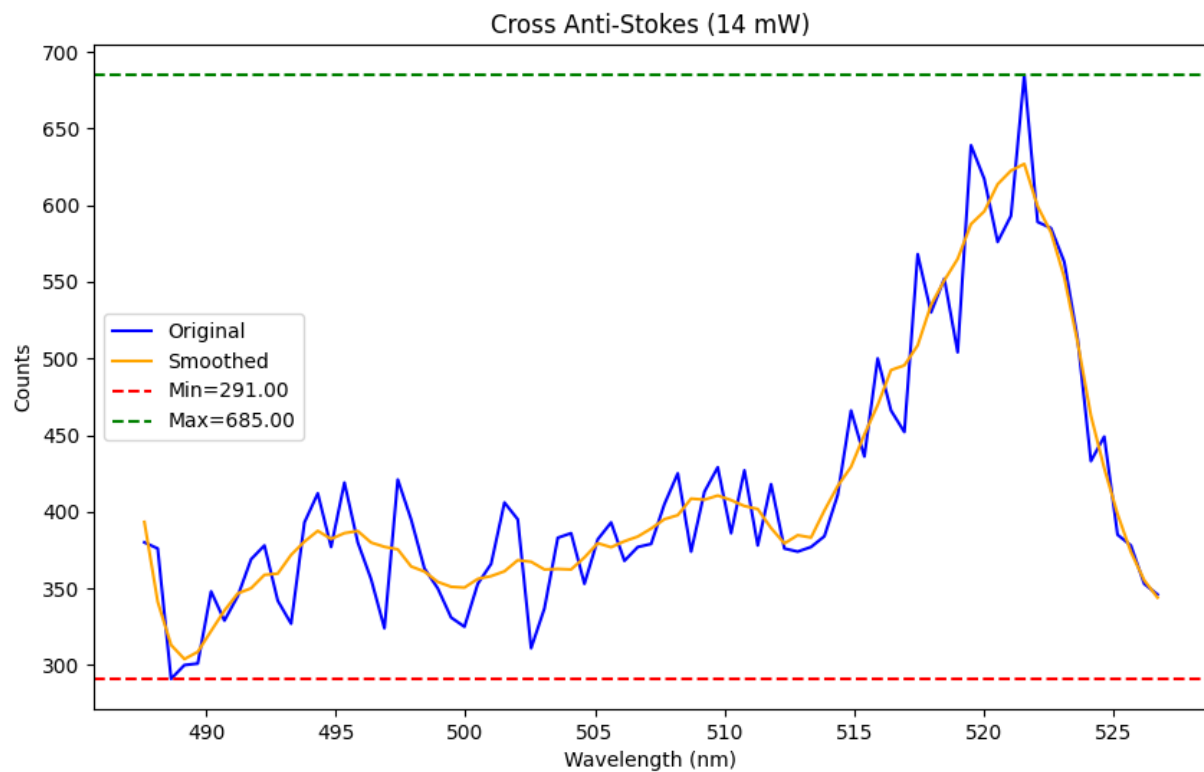
Freq=0.01, Amp=18312.40

Freq=0.02, Amp=15445.06

Freq=0.03, Amp=12890.90

Freq=0.04, Amp=8819.83

### Cross Anti-Stokes (14 mW)



Peak Info:

WL=521.56, Cnt=685.00

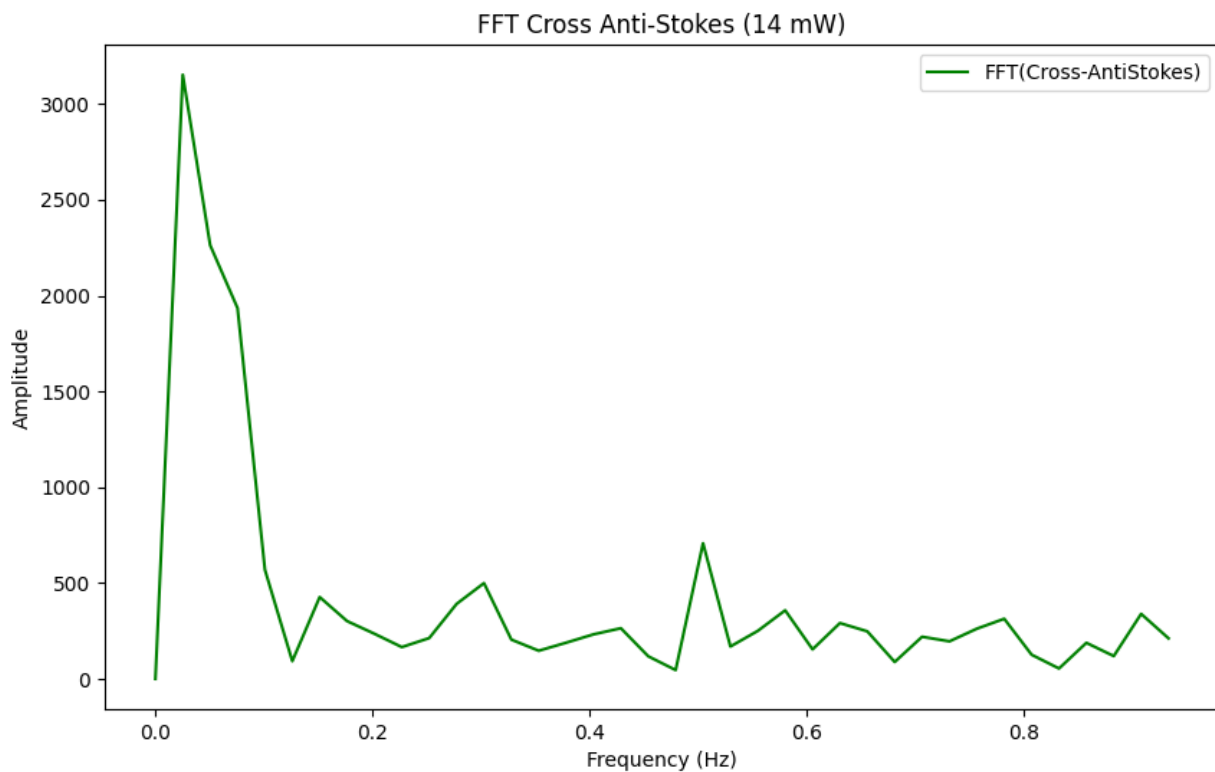
WL=519.50, Cnt=639.00

WL=517.45, Cnt=568.00

WL=518.48, Cnt=552.00

WL=515.91, Cnt=500.00

### FFT Cross Anti-Stokes (14 mW)



#### FFT Peak Info:

Freq=0.03, Amp=3153.12

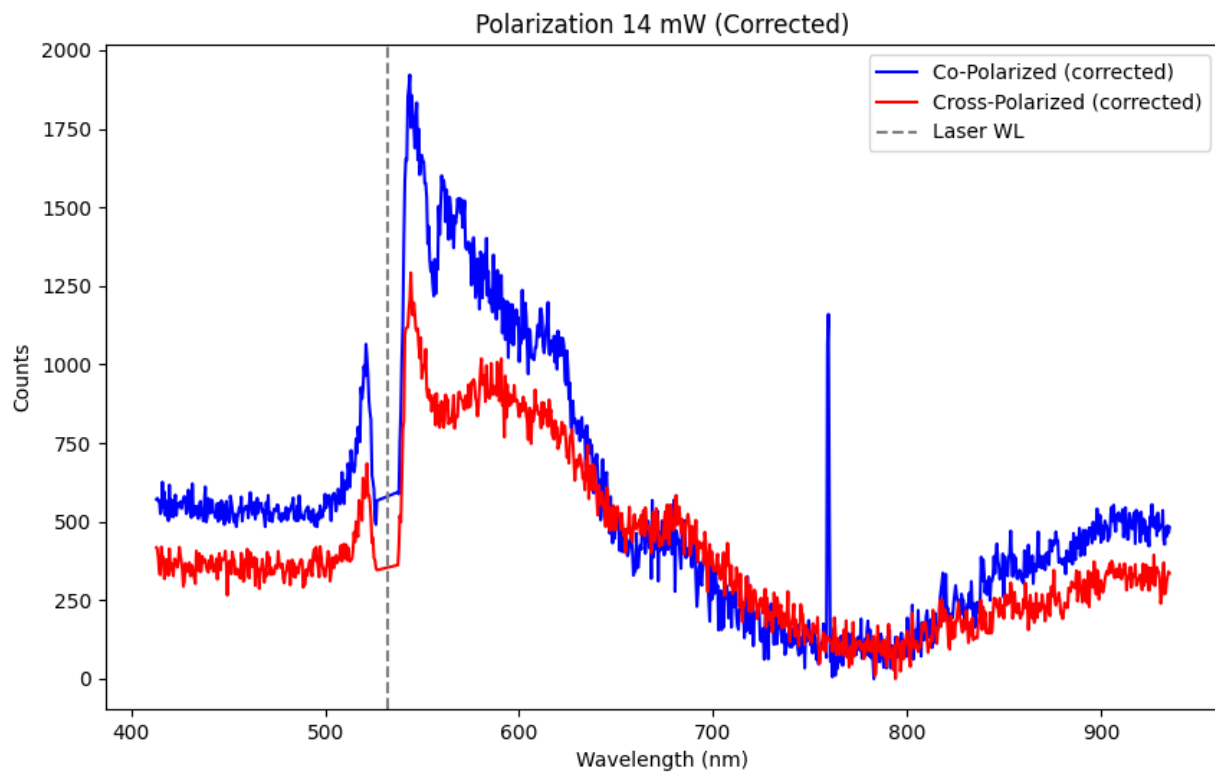
Freq=0.50, Amp=708.02

Freq=0.30, Amp=499.73

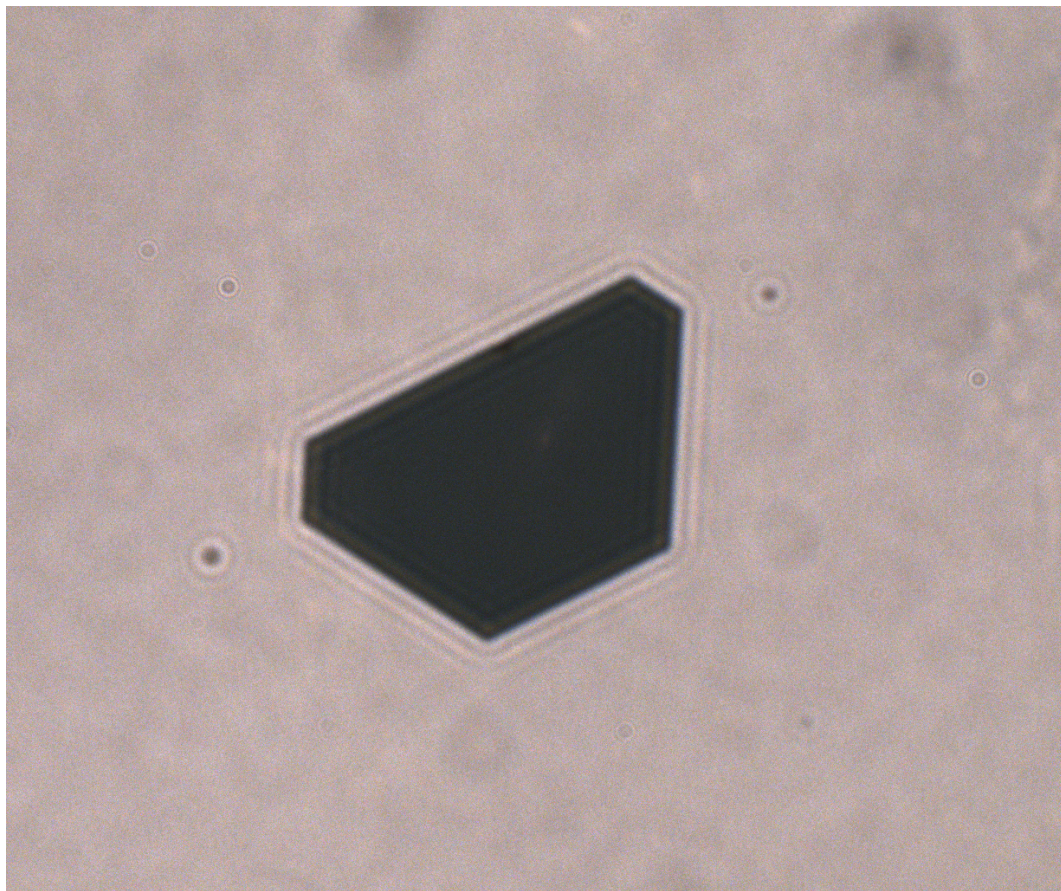
Freq=0.15, Amp=426.85

Freq=0.58, Amp=357.59

Polarization 14 mW



## Sample Image



# Spectrometry Analysis Report

Sample: G6 rotated

Laser Wavelength (after shift): 532.13 nm

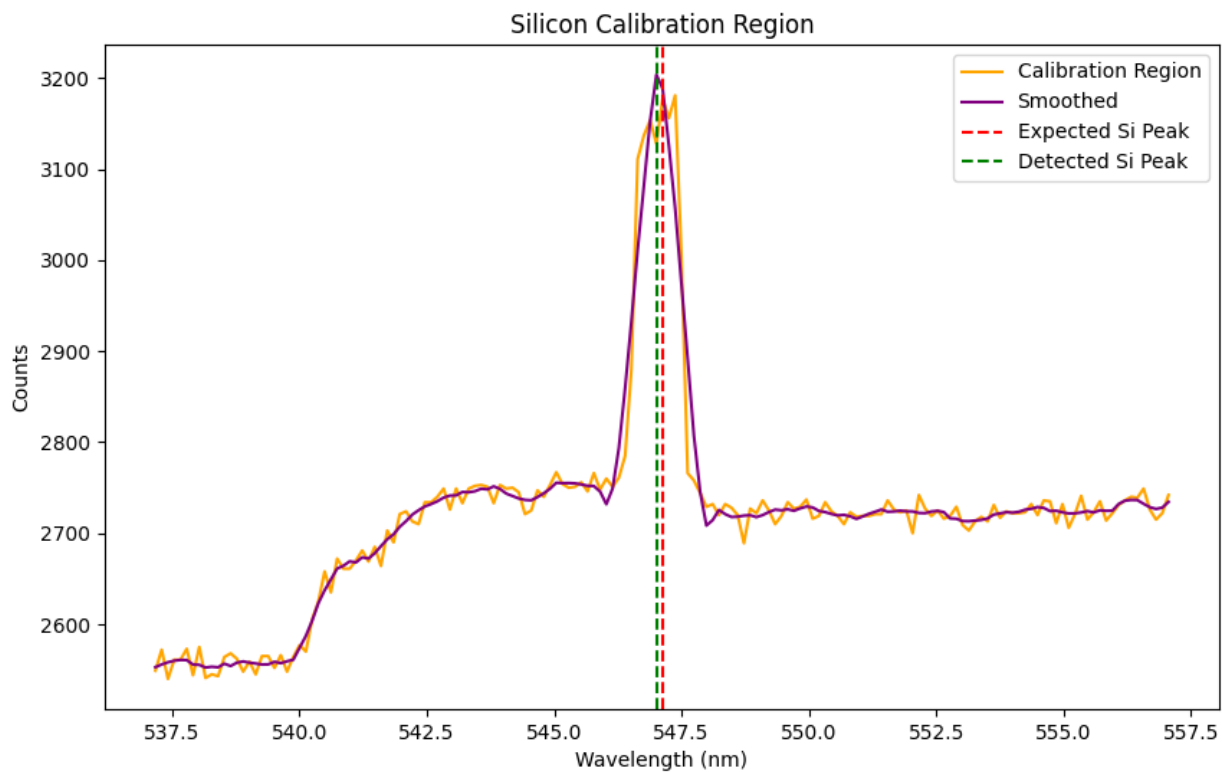
Power Levels: 14.0 mW

Thickness: 160.0 nm

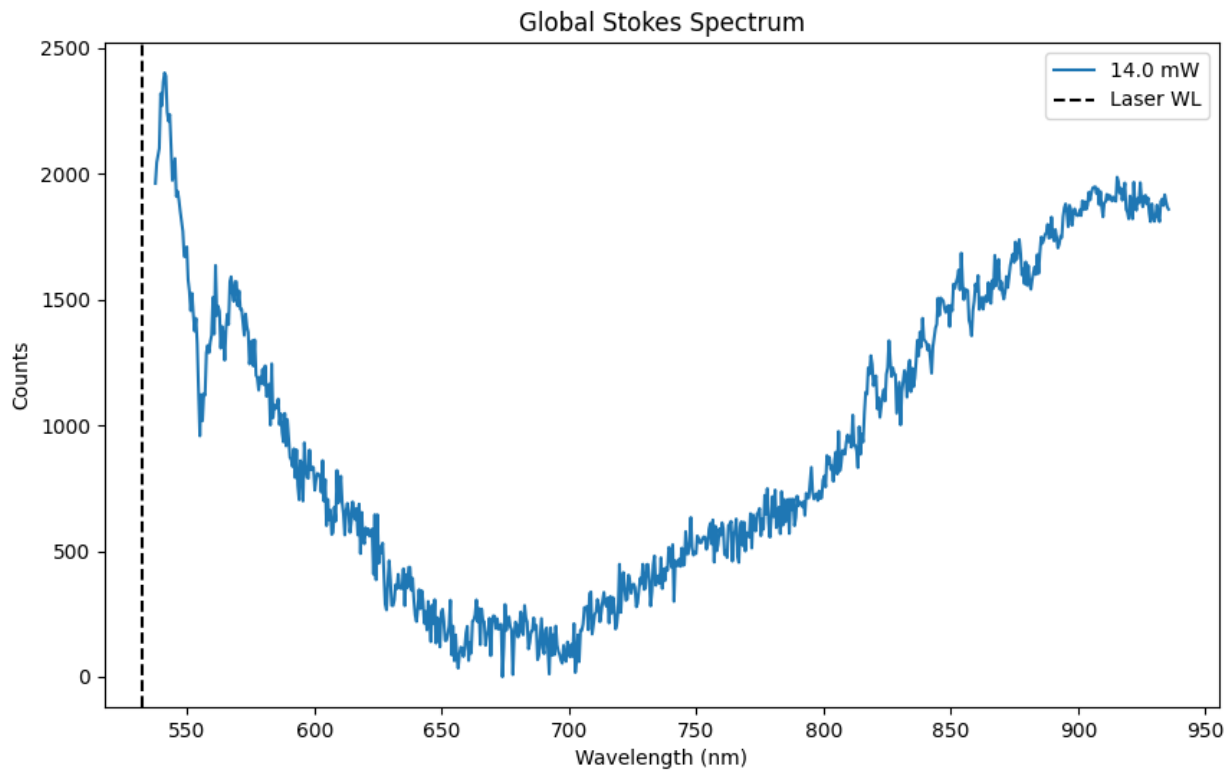
Laser Filter Window:  $\pm 5.0$  nm

Calibration Shift: 0.13 nm

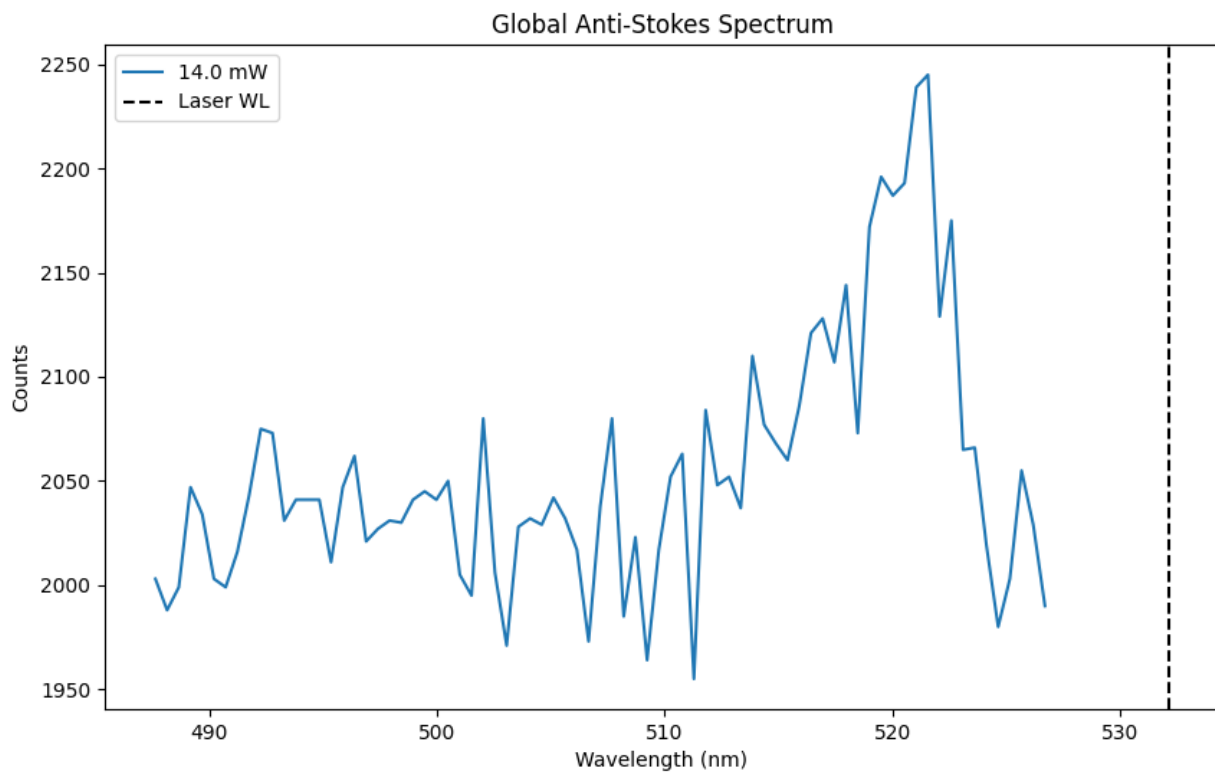
## Calibration Region



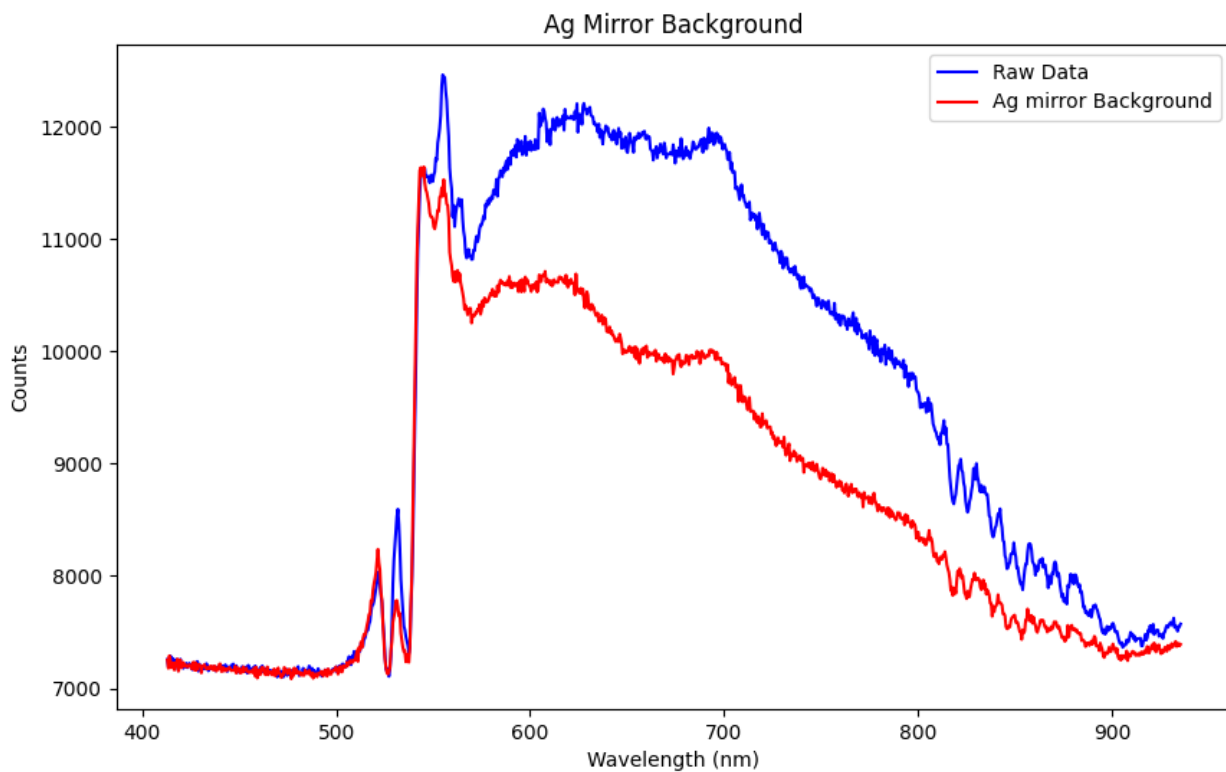
## Global Stokes Spectrum



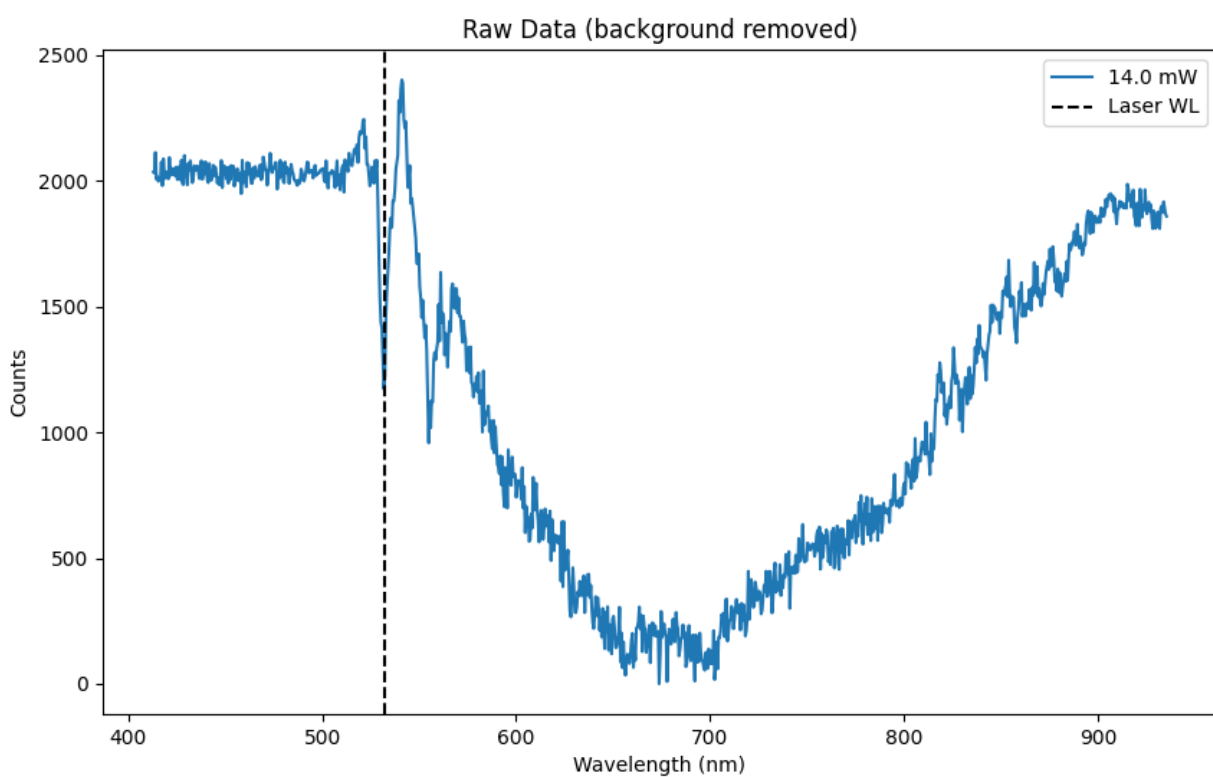
## Global Anti-Stokes Spectrum



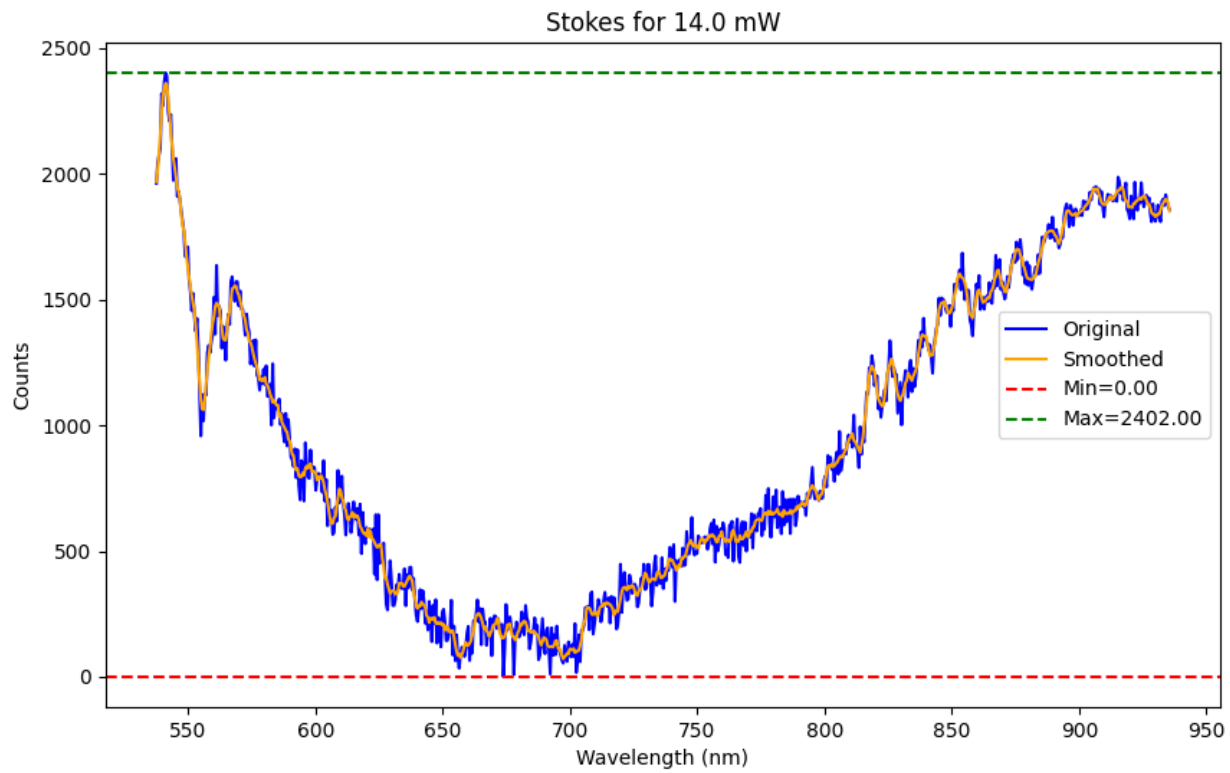
## Ag Mirror Background



## Raw Data



### Stokes for 14.0 mW



Integral (Area) = 371652.94

Peak Info (Stokes):

WL=541.09, Cnt=2402.00

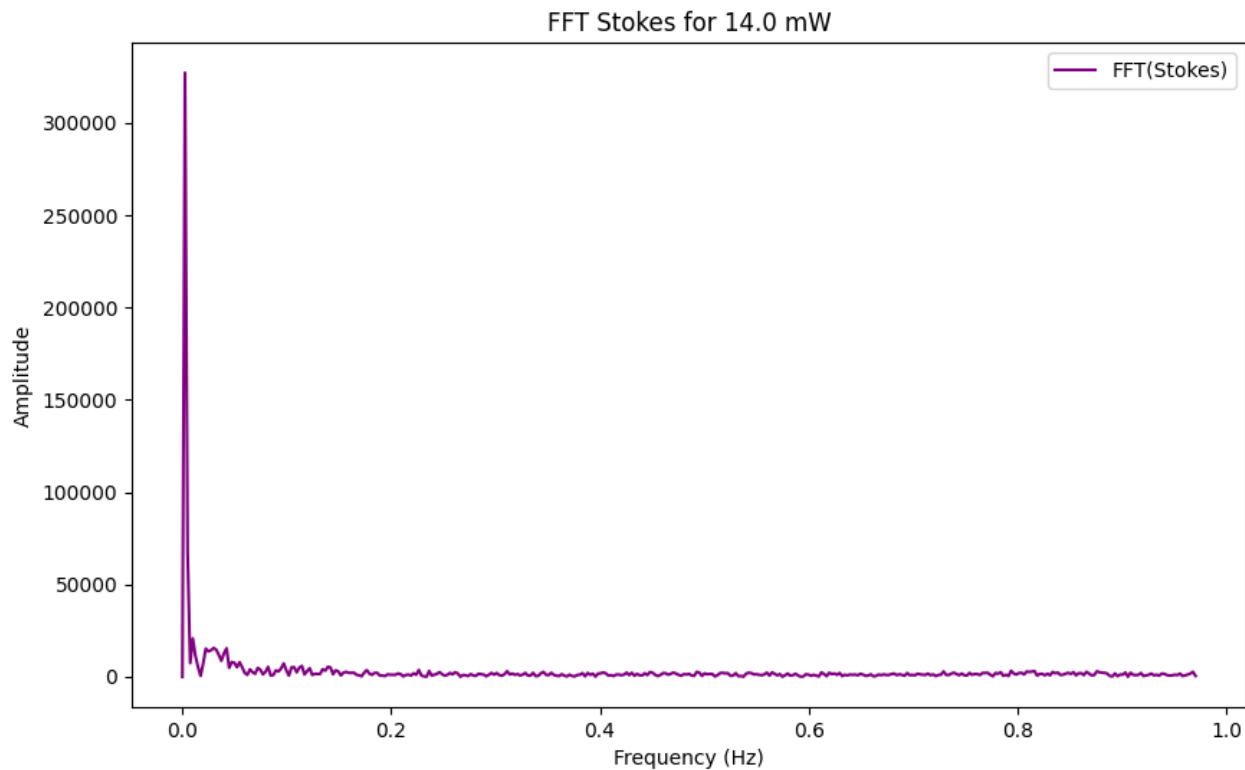
WL=539.55, Cnt=2319.00

WL=543.14, Cnt=2236.00

WL=545.20, Cnt=2061.00

WL=915.32, Cnt=1987.00

## FFT Stokes for 14.0 mW



Peak Info (FFT Stokes):

Freq=0.00, Amp=327190.24

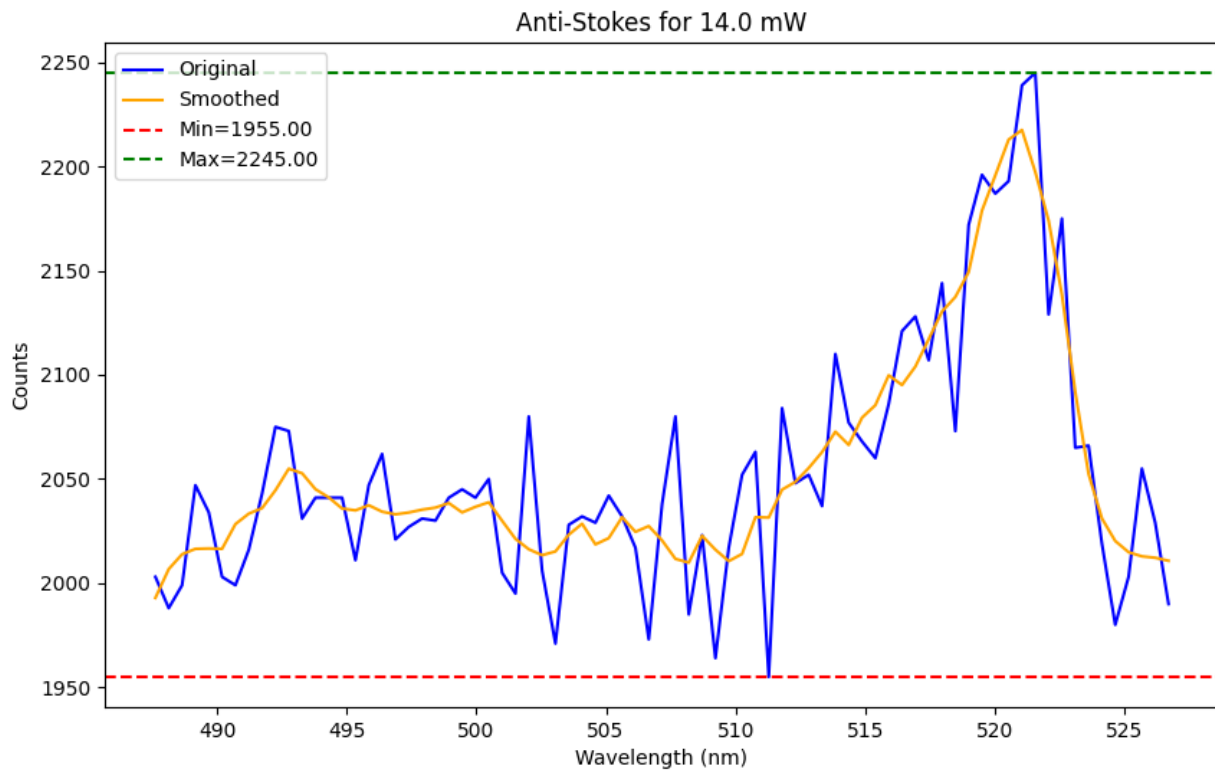
Freq=0.01, Amp=20767.96

Freq=0.03, Amp=15578.51

Freq=0.04, Amp=15465.65

Freq=0.02, Amp=15307.70

### Anti-Stokes for 14.0 mW



Integral (Area) = 80300.73

Peak Info (Anti-Stokes):

WL=521.56, Cnt=2245.00

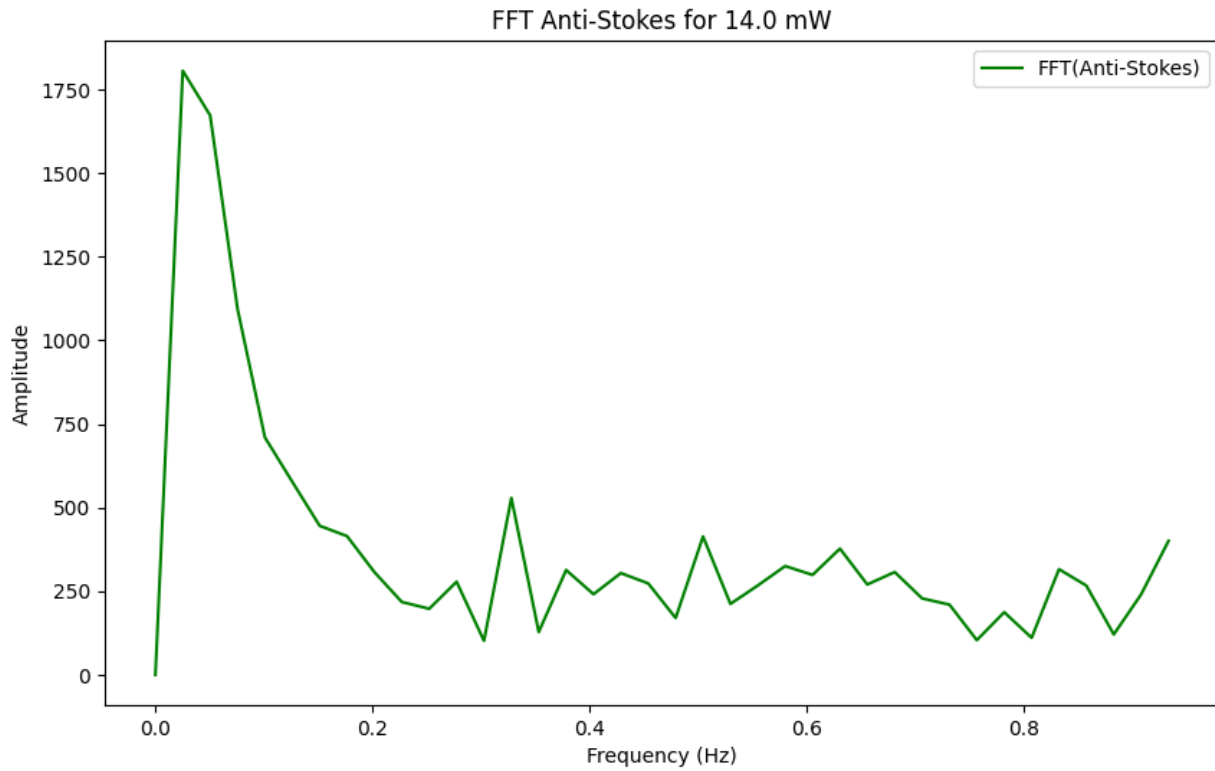
WL=519.50, Cnt=2196.00

WL=522.59, Cnt=2175.00

WL=517.96, Cnt=2144.00

WL=516.93, Cnt=2128.00

### FFT Anti-Stokes for 14.0 mW



Peak Info (FFT Anti-Stokes):

Freq=0.03, Amp=1806.43

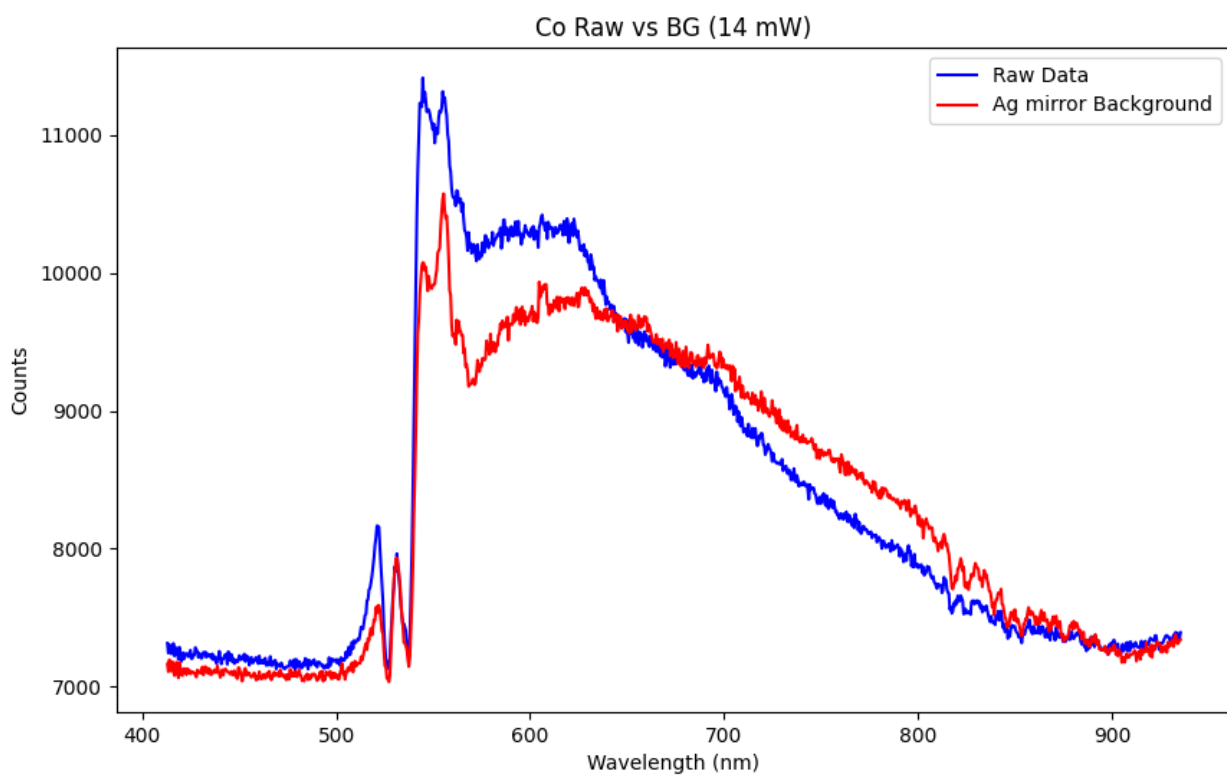
Freq=0.33, Amp=529.03

Freq=0.50, Amp=413.78

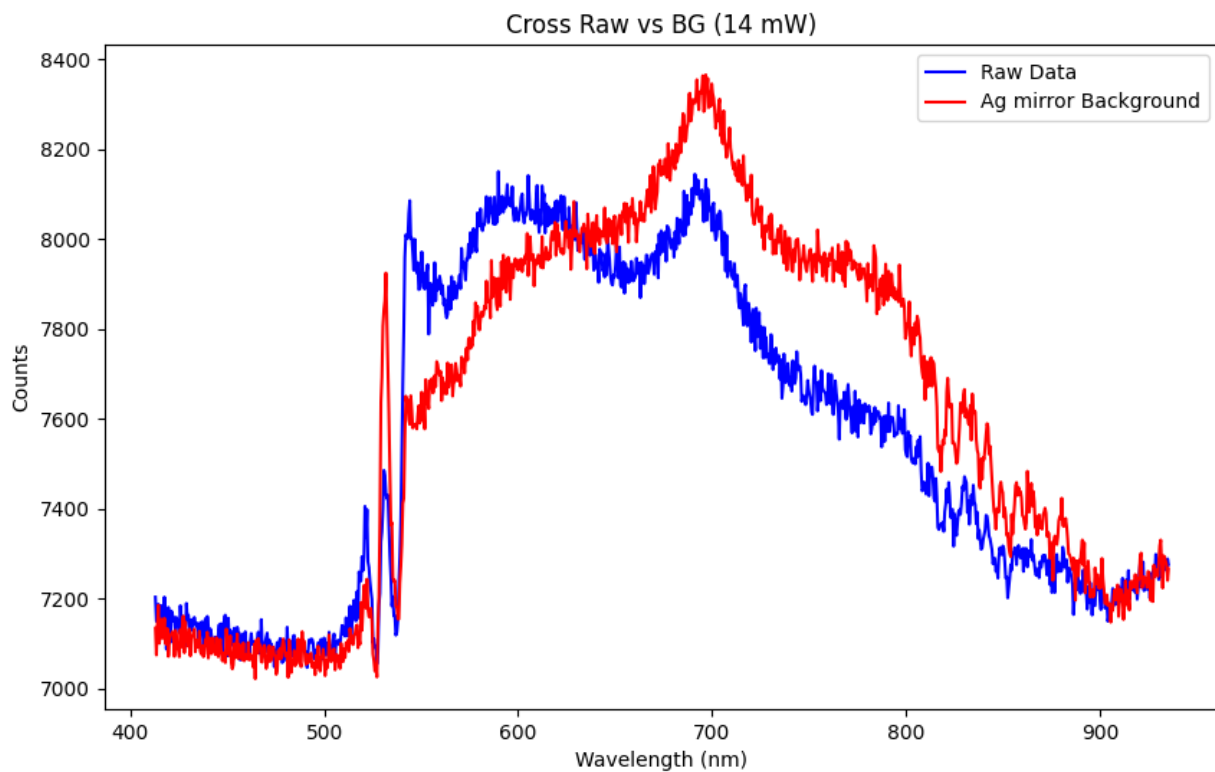
Freq=0.63, Amp=377.41

Freq=0.58, Amp=325.29

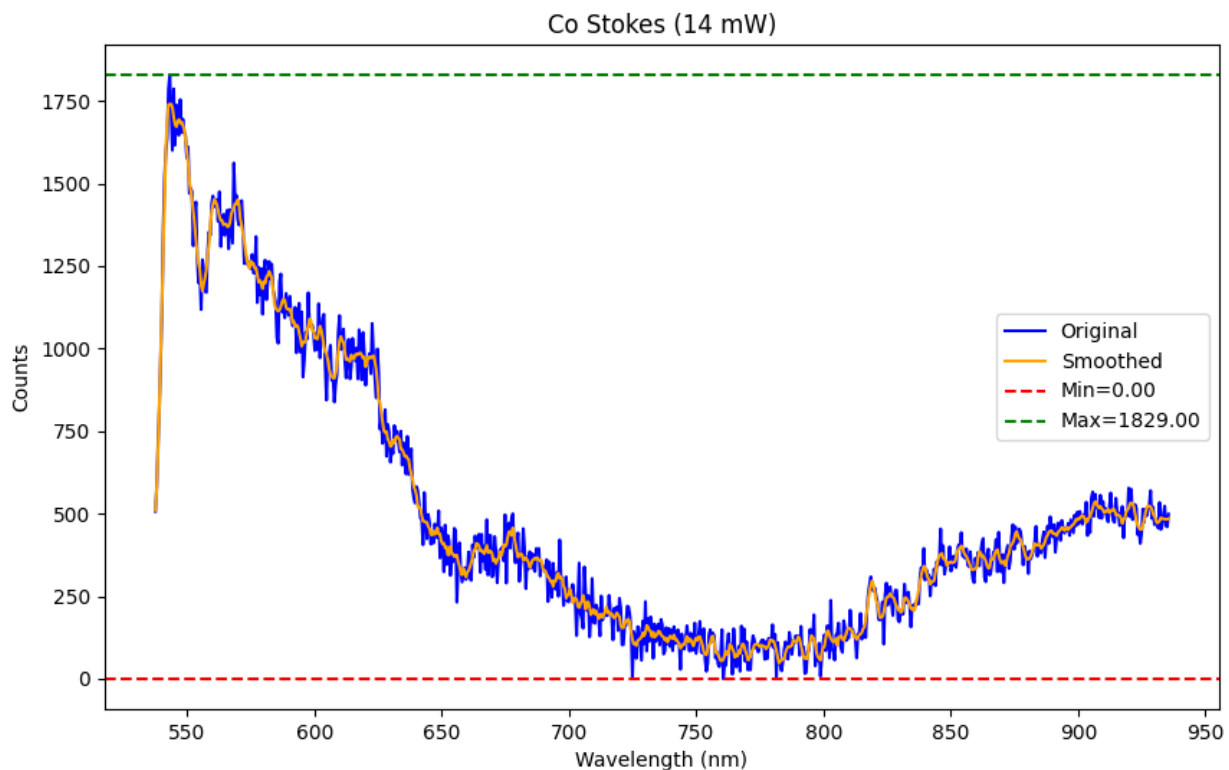
### Co Raw vs BG (14 mW)



### Cross Raw vs BG (14 mW)



### Co Stokes (14 mW)



#### Peak Info:

WL=543.14, Cnt=1829.00

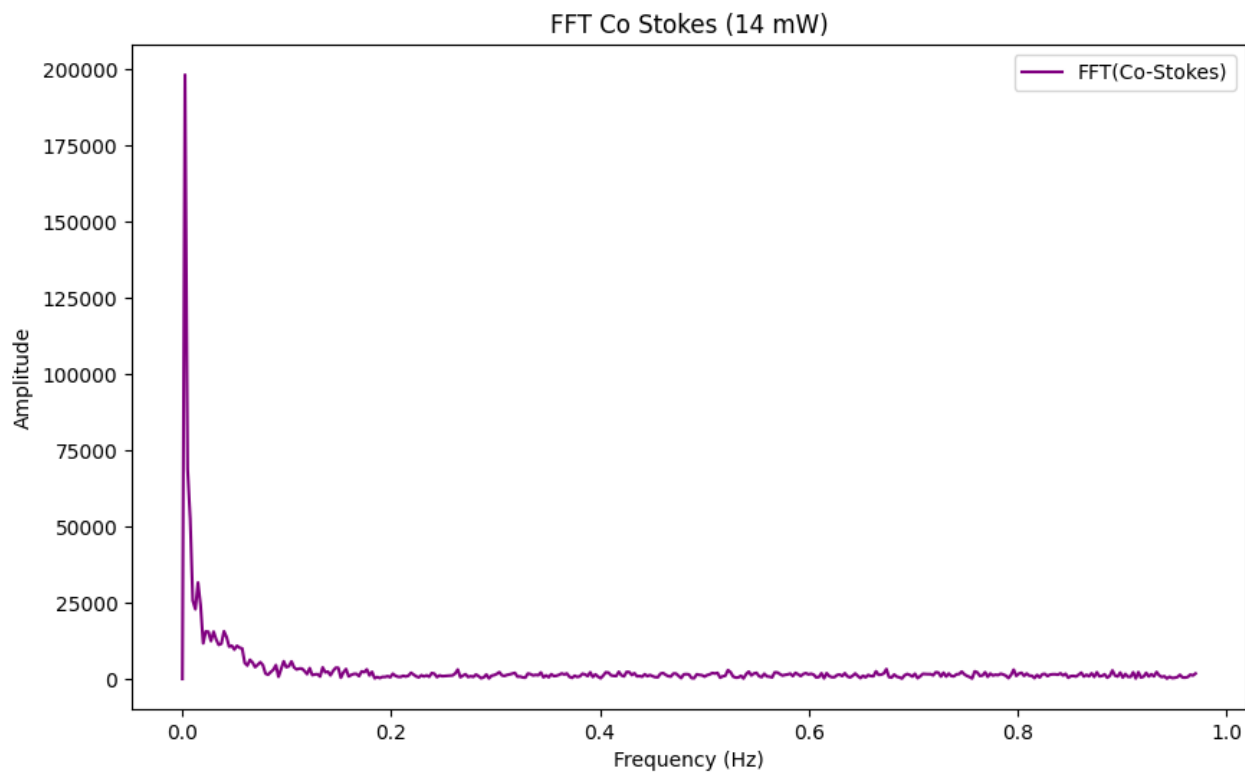
WL=544.68, Cnt=1786.00

WL=547.25, Cnt=1754.00

WL=545.71, Cnt=1738.00

WL=548.28, Cnt=1695.00

### FFT Co Stokes (14 mW)



#### FFT Peak Info:

Freq=0.00, Amp=198287.00

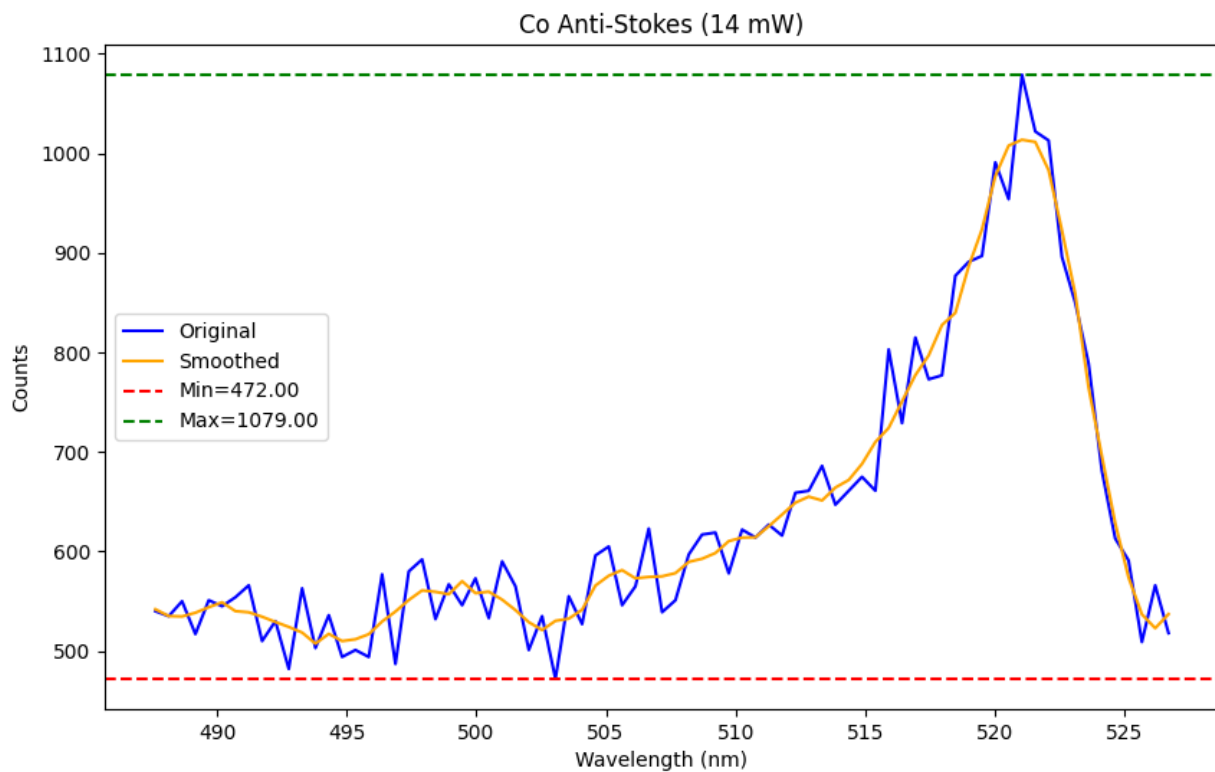
Freq=0.01, Amp=31609.74

Freq=0.04, Amp=15619.03

Freq=0.02, Amp=15576.61

Freq=0.03, Amp=15495.92

## Co Anti-Stokes (14 mW)



### Peak Info:

WL=521.05, Cnt=1079.00

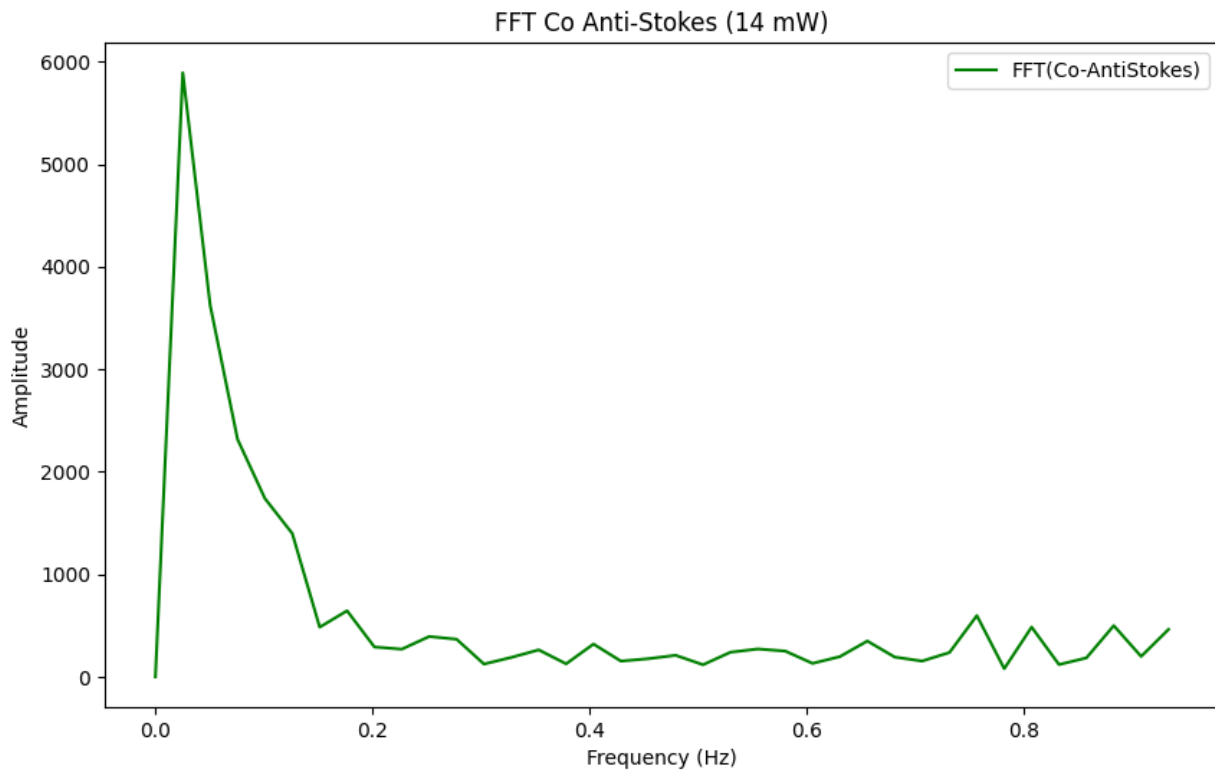
WL=520.02, Cnt=991.00

WL=516.93, Cnt=815.00

WL=515.91, Cnt=803.00

WL=513.34, Cnt=686.00

### FFT Co Anti-Stokes (14 mW)



#### FFT Peak Info:

Freq=0.03, Amp=5891.81

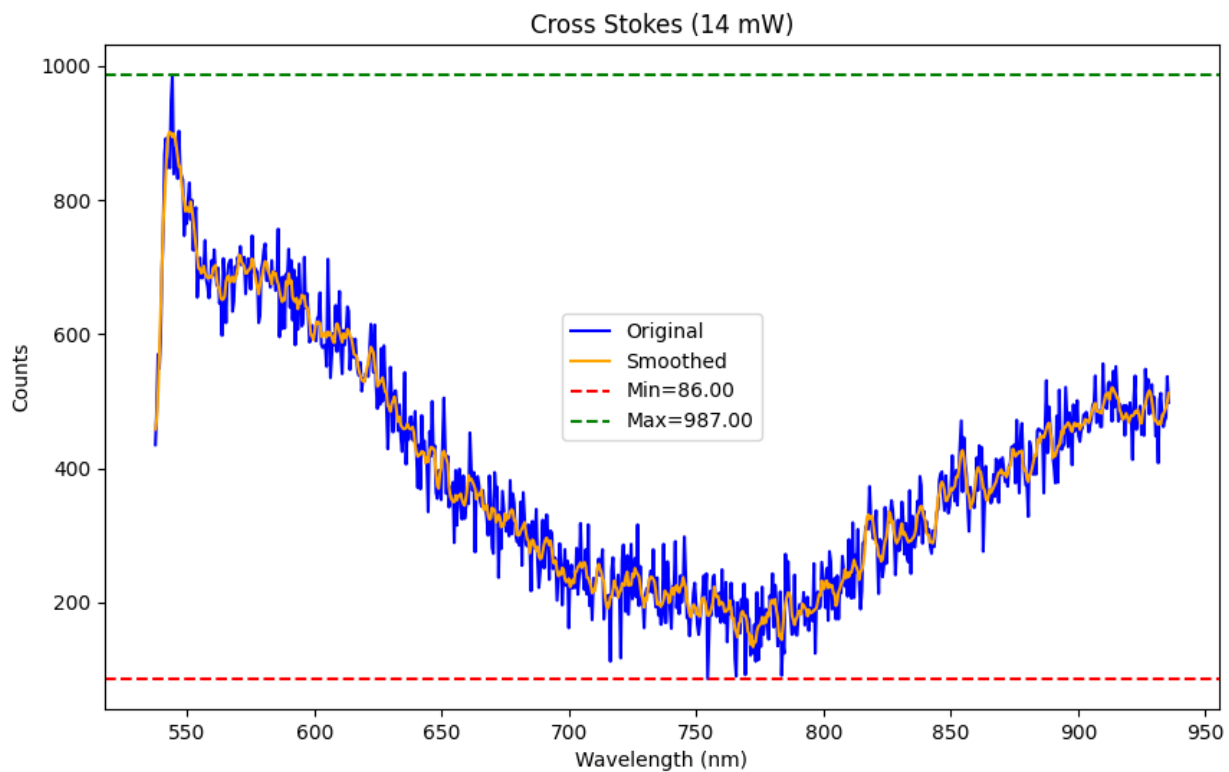
Freq=0.18, Amp=644.54

Freq=0.76, Amp=597.53

Freq=0.88, Amp=499.64

Freq=0.81, Amp=485.18

## Cross Stokes (14 mW)



### Peak Info:

WL=544.17, Cnt=987.00

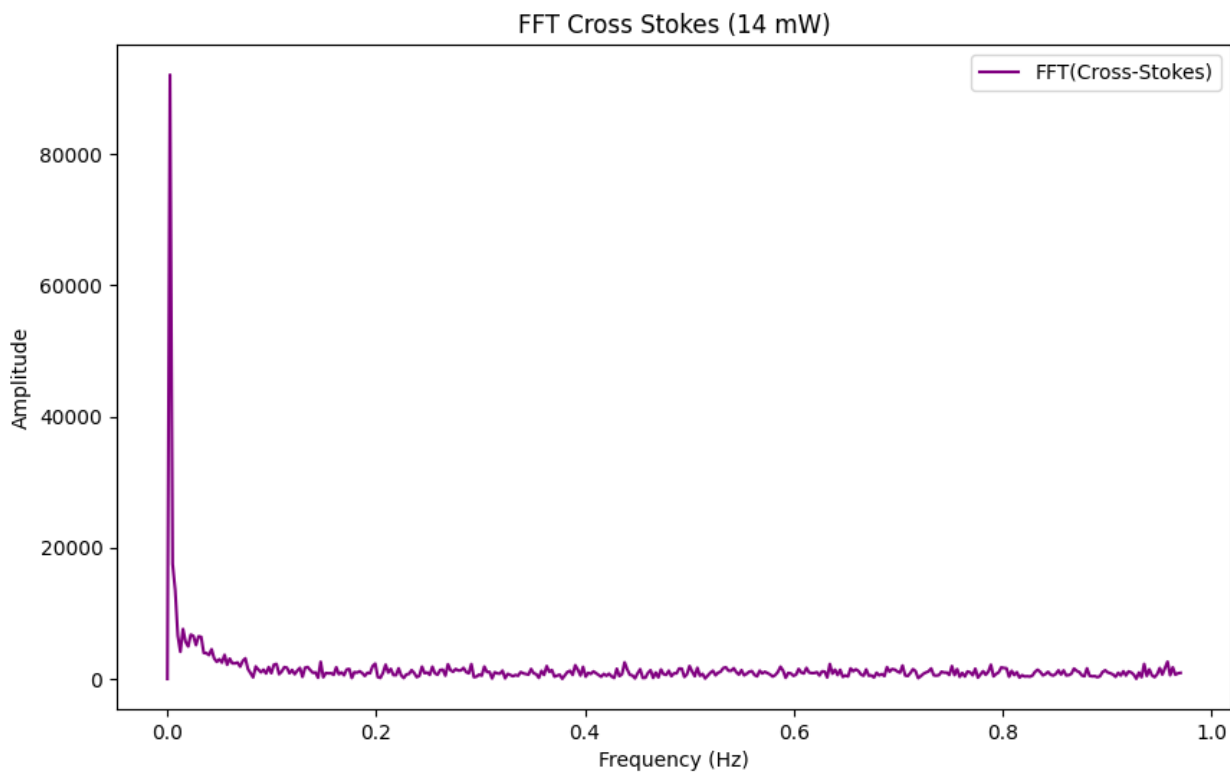
WL=546.74, Cnt=903.00

WL=541.60, Cnt=892.00

WL=545.71, Cnt=879.00

WL=542.63, Cnt=858.00

## FFT Cross Stokes (14 mW)



### FFT Peak Info:

Freq=0.00, Amp=92124.47

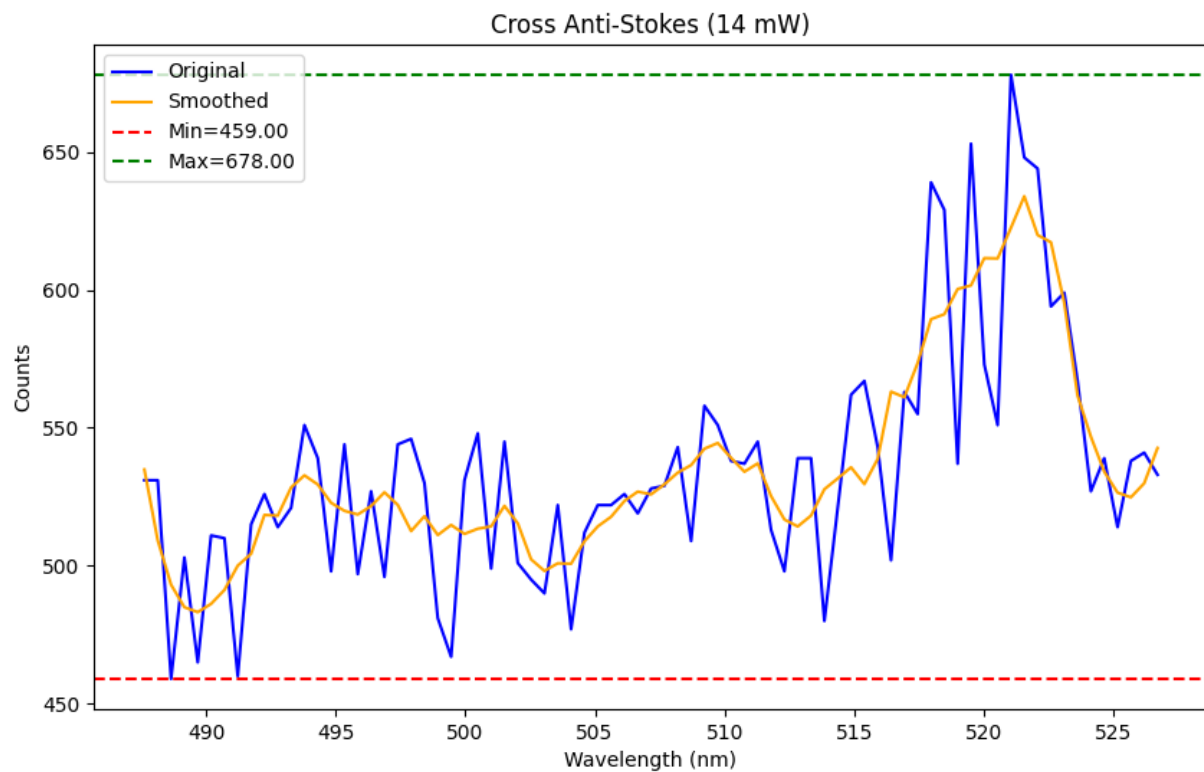
Freq=0.01, Amp=7595.11

Freq=0.02, Amp=6745.35

Freq=0.03, Amp=6484.51

Freq=0.04, Amp=4516.28

### Cross Anti-Stokes (14 mW)



#### Peak Info:

WL=521.05, Cnt=678.00

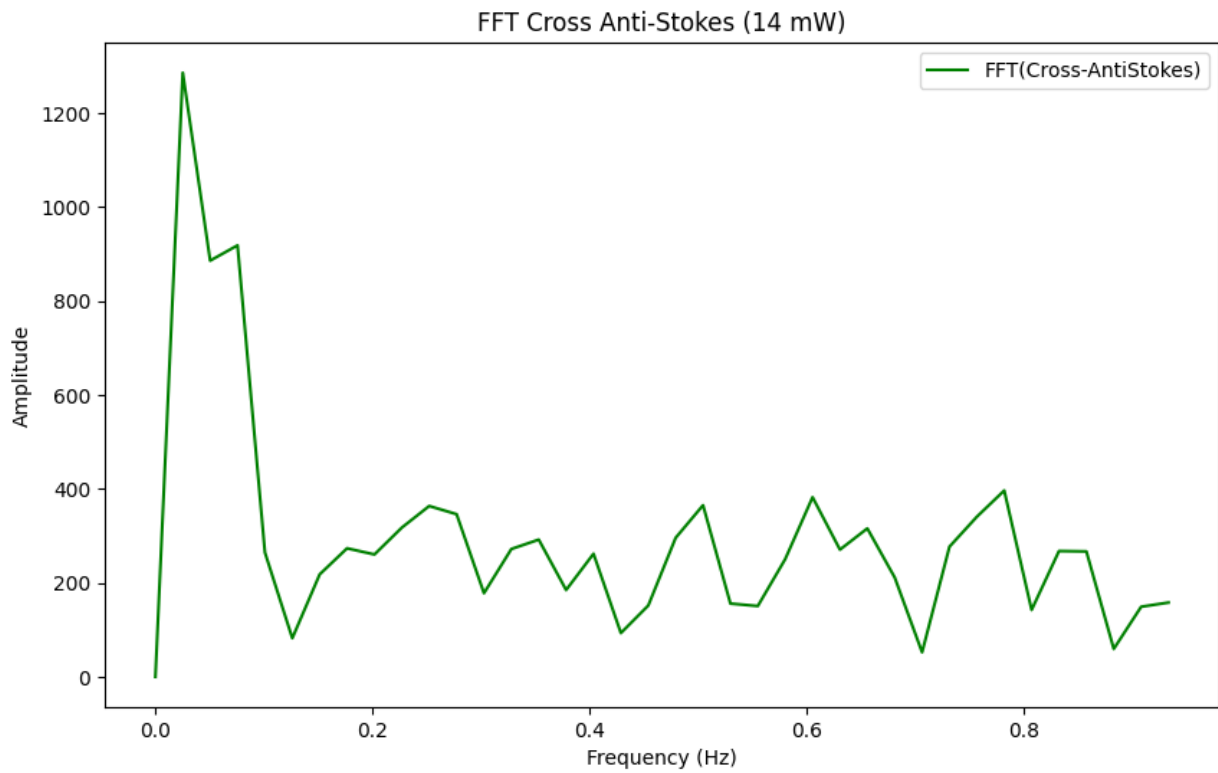
WL=519.50, Cnt=653.00

WL=517.96, Cnt=639.00

WL=523.10, Cnt=599.00

WL=515.39, Cnt=567.00

### FFT Cross Anti-Stokes (14 mW)



#### FFT Peak Info:

Freq=0.03, Amp=1286.10

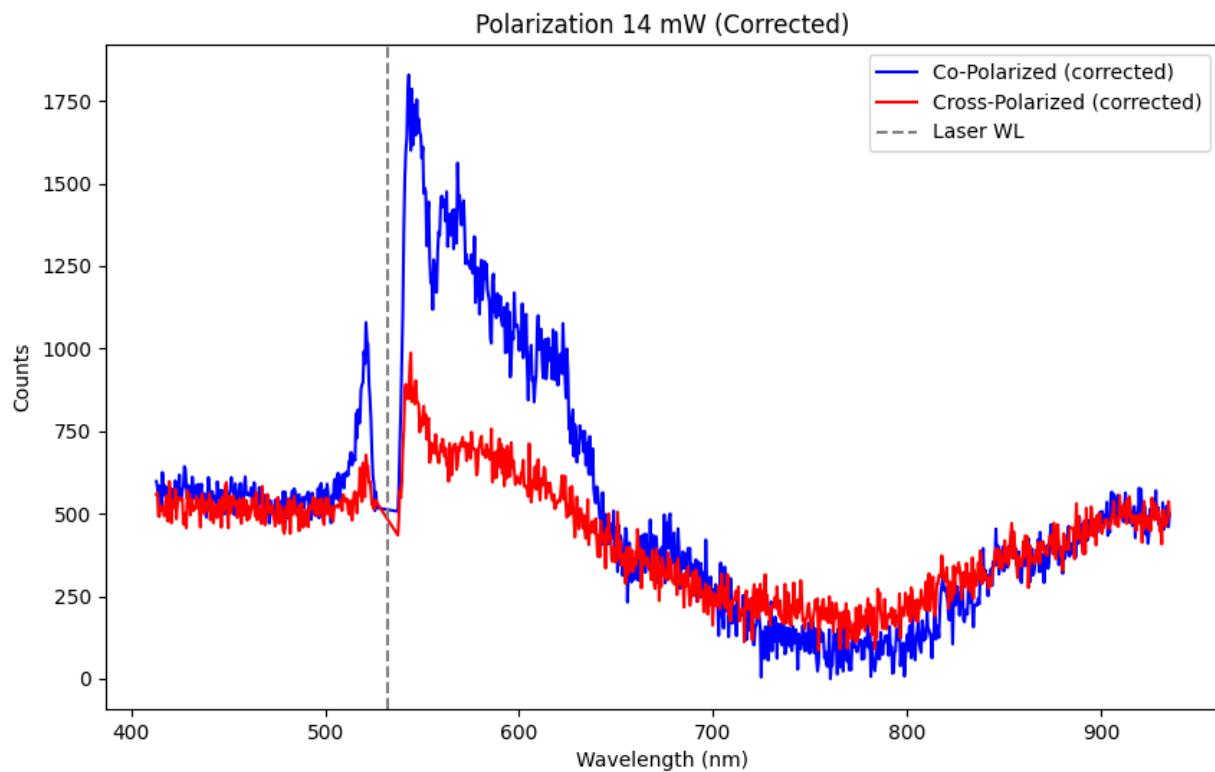
Freq=0.08, Amp=918.64

Freq=0.78, Amp=396.68

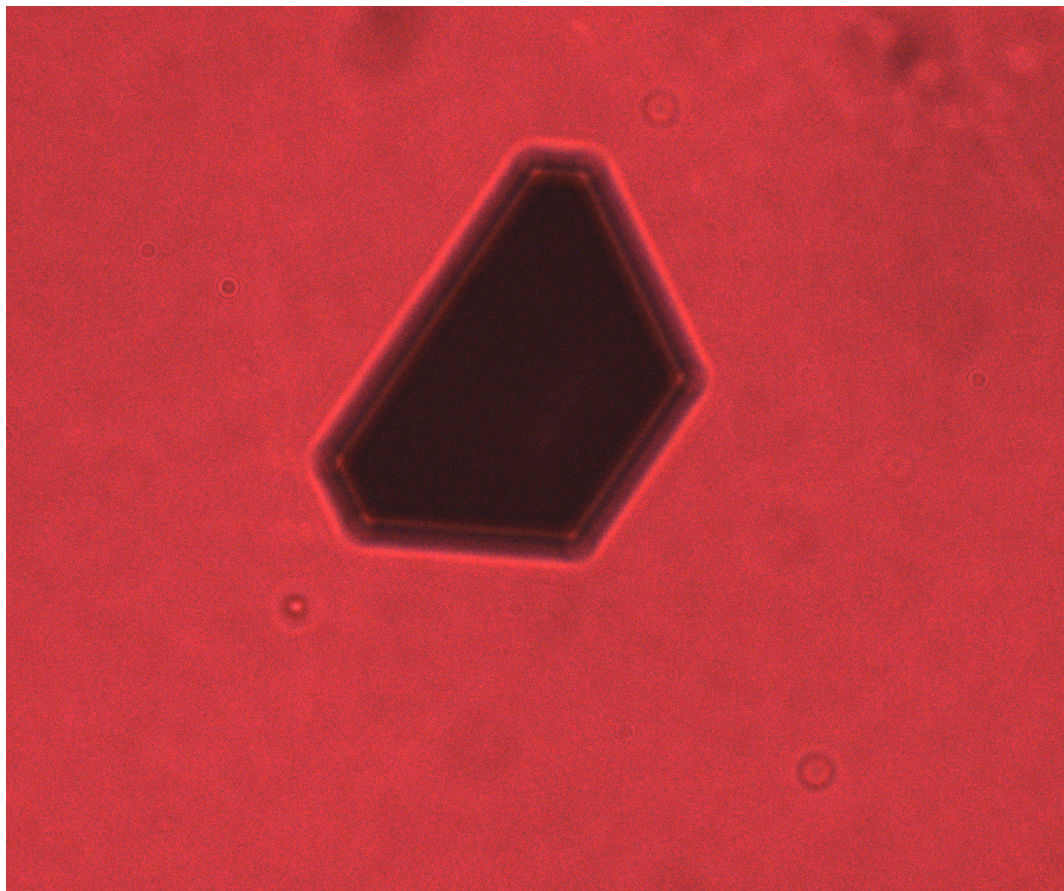
Freq=0.61, Amp=382.43

Freq=0.50, Amp=365.40

Polarization 14 mW



## Sample Image



# Spectrometry Analysis Report

Sample: M19

Laser Wavelength (after shift): 532.13 nm

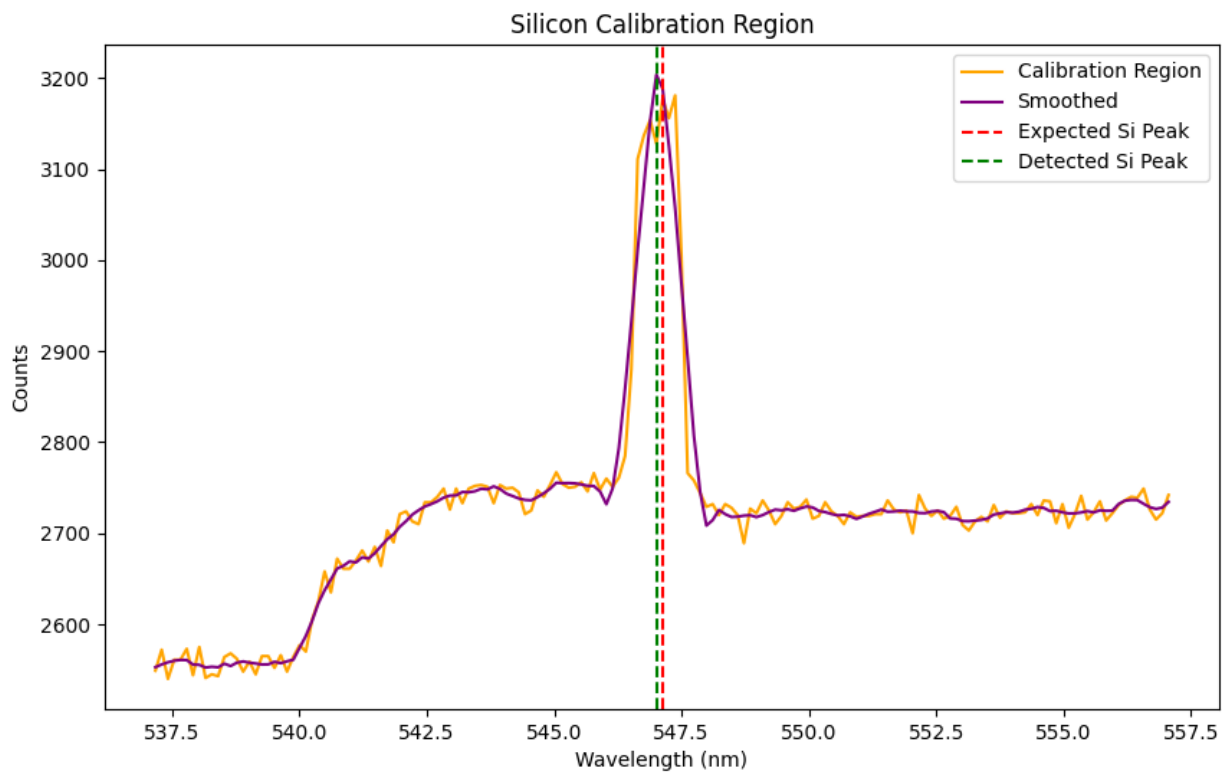
Power Levels: 2.0, 4.0, 6.0, 8.0, 10.0, 12.0, 14.0 mW

Thickness: 20.0 nm

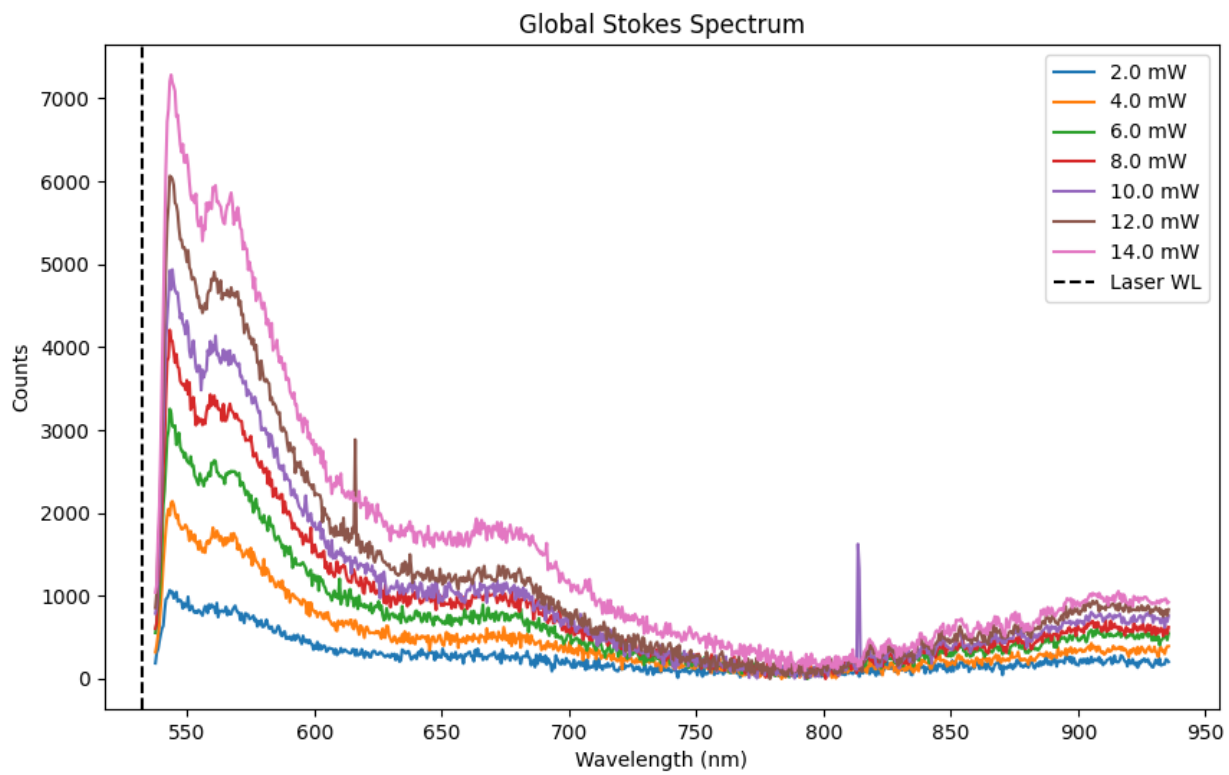
Laser Filter Window:  $\pm 5.0$  nm

Calibration Shift: 0.13 nm

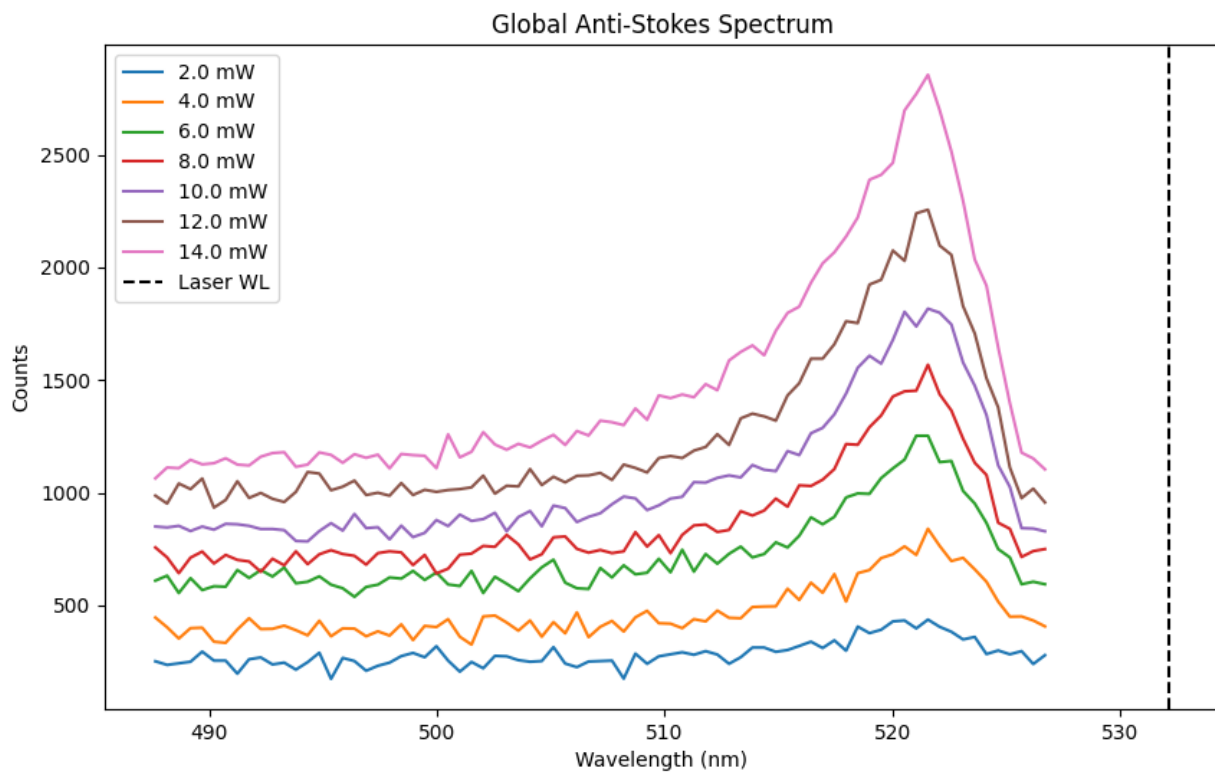
## Calibration Region



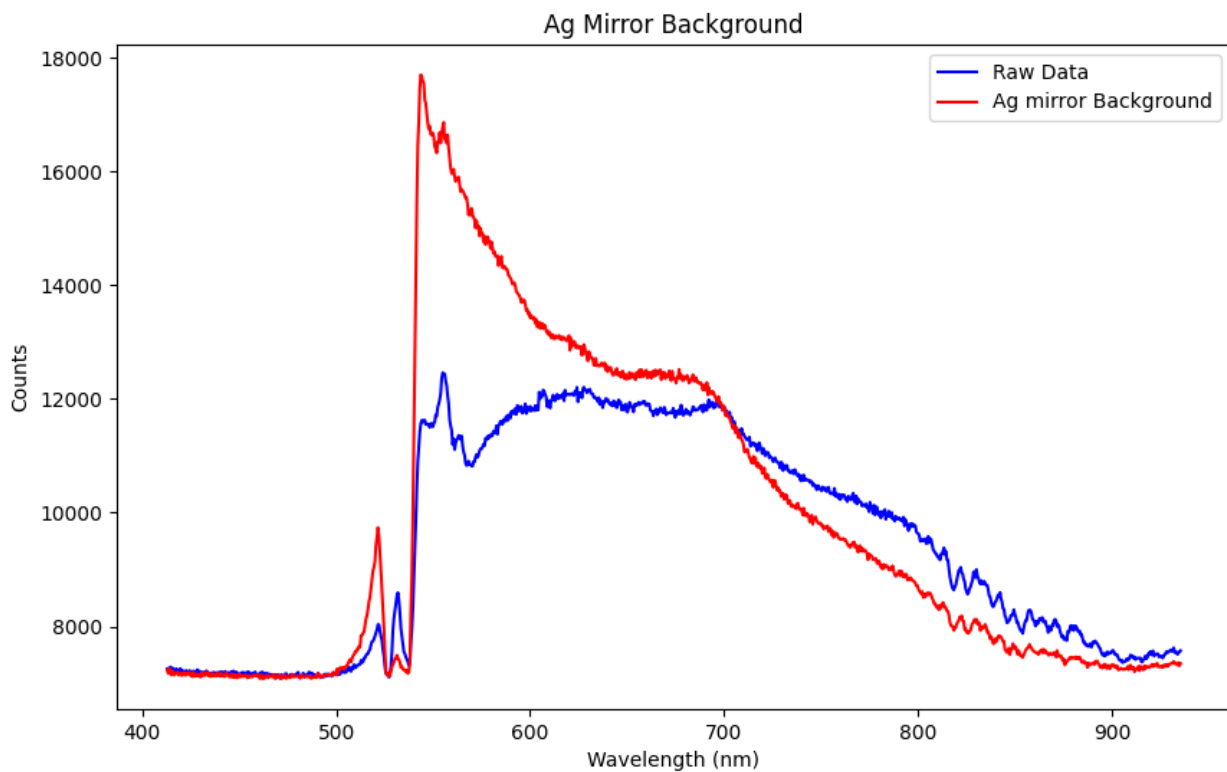
## Global Stokes Spectrum



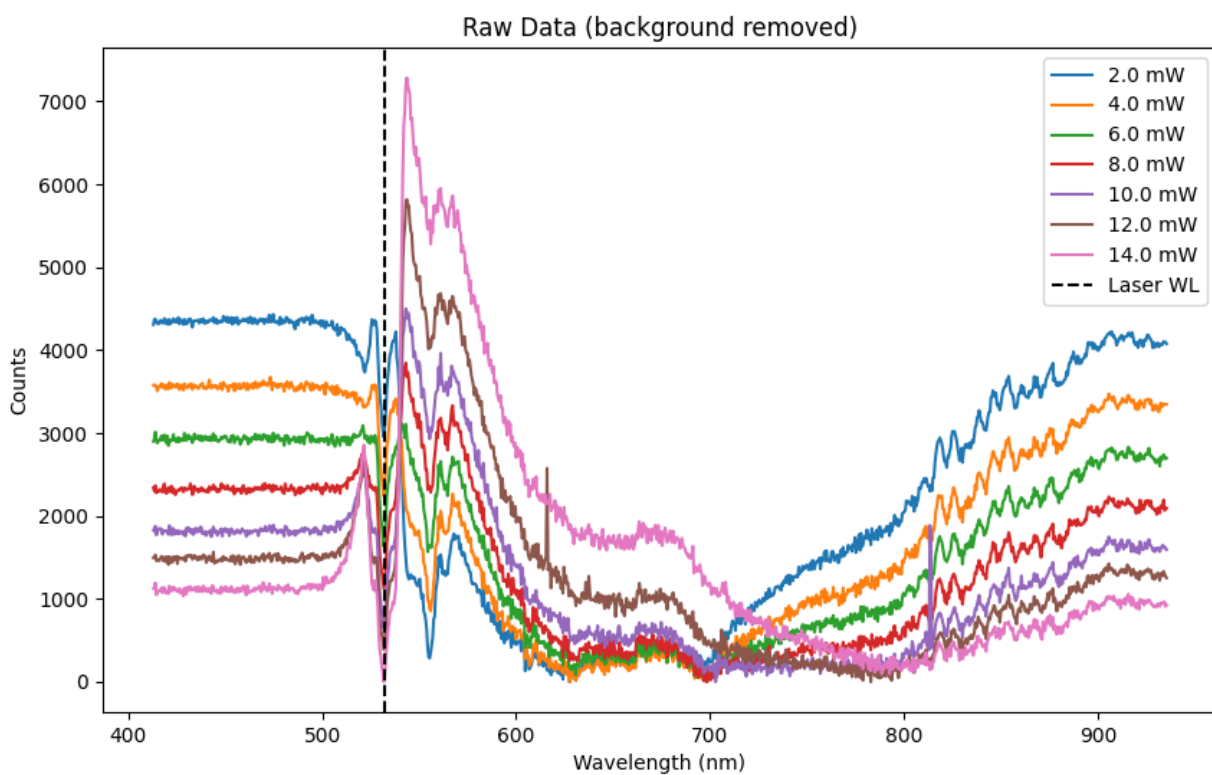
## Global Anti-Stokes Spectrum



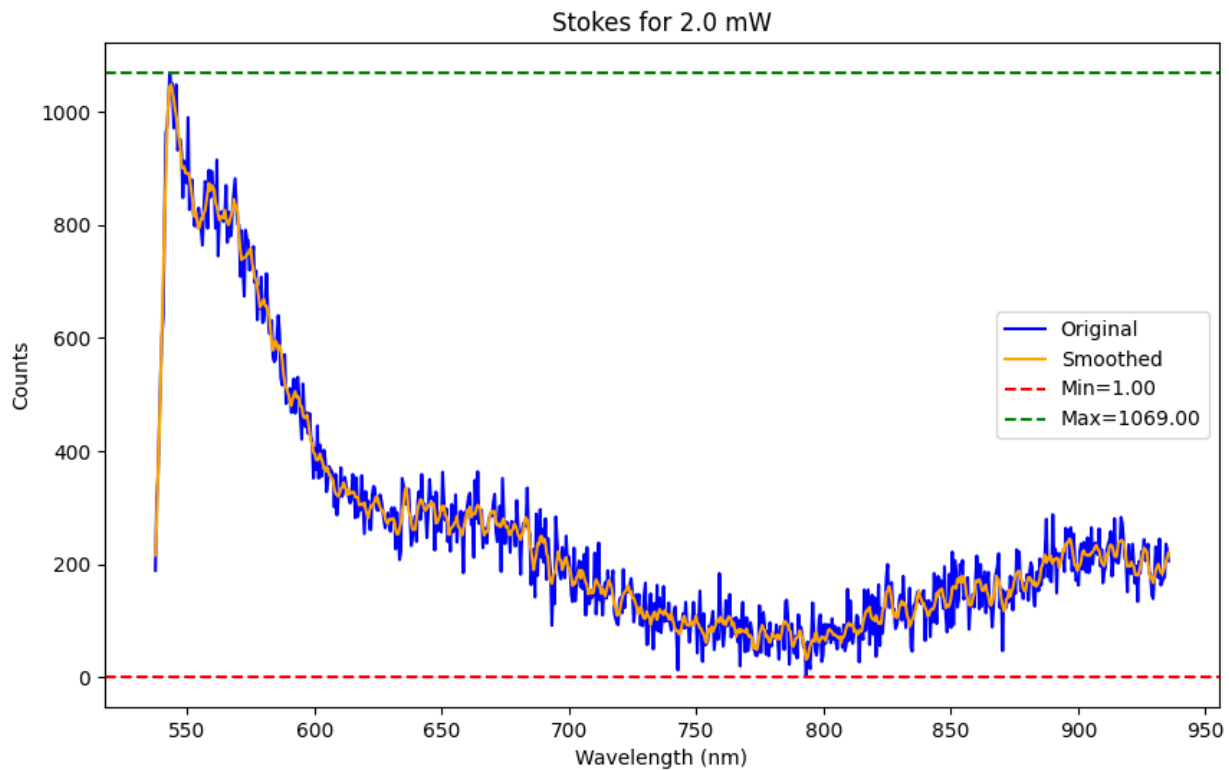
## Ag Mirror Background



## Raw Data



### Stokes for 2.0 mW



Integral (Area) = 105066.91

Peak Info (Stokes):

WL=543.14, Cnt=1069.00

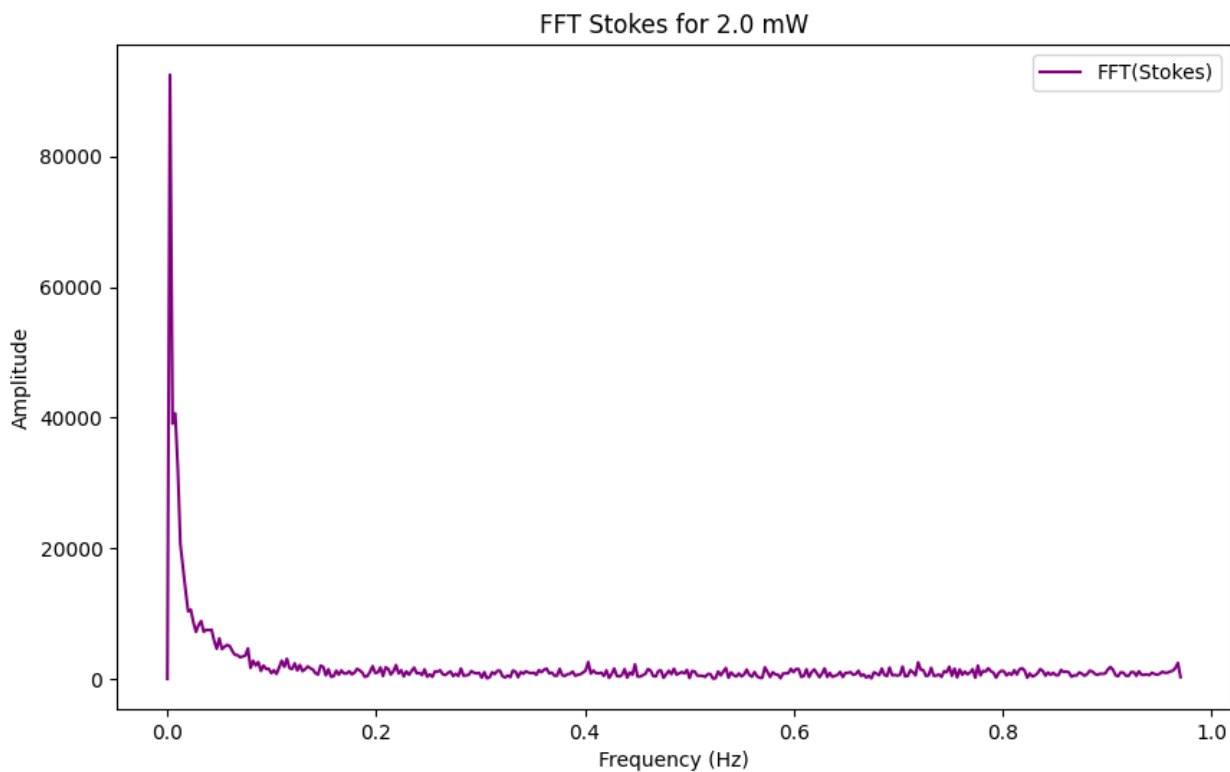
WL=544.17, Cnt=1050.00

WL=545.71, Cnt=1048.00

WL=550.33, Cnt=990.00

WL=547.25, Cnt=951.00

### FFT Stokes for 2.0 mW



Peak Info (FFT Stokes):

Freq=0.00, Amp=92533.96

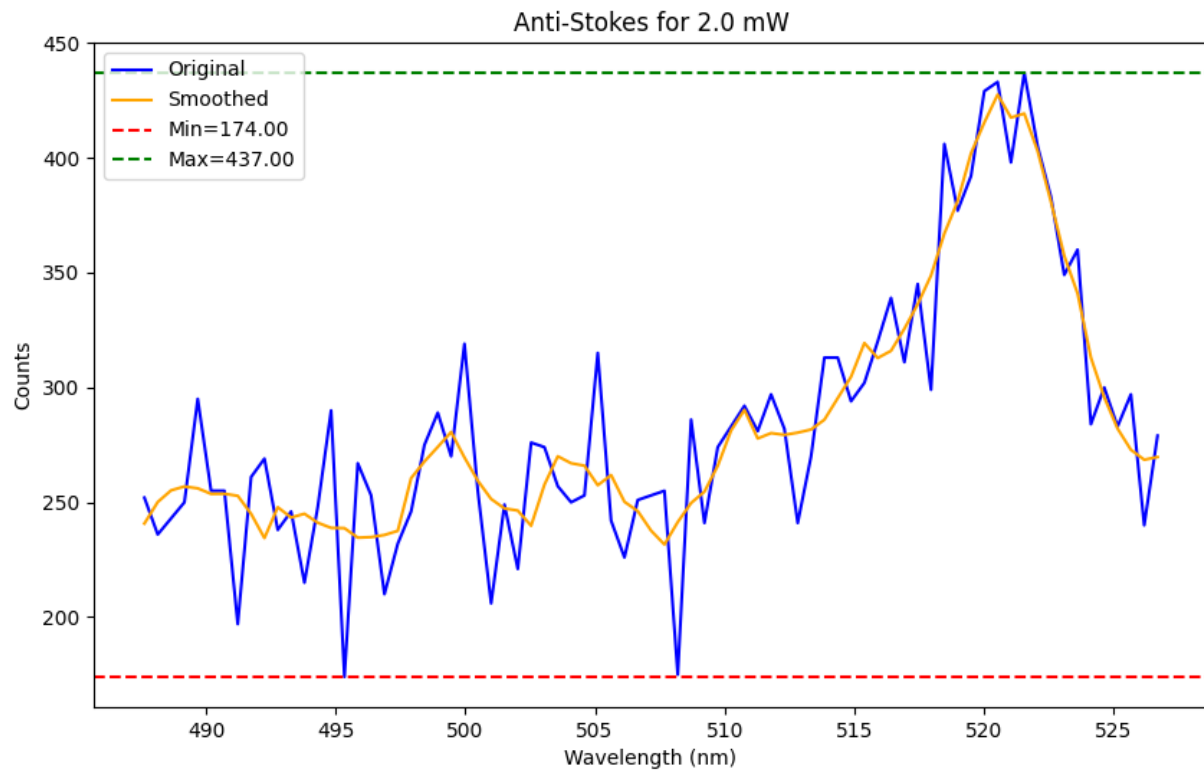
Freq=0.01, Amp=40652.96

Freq=0.02, Amp=10608.77

Freq=0.03, Amp=8843.31

Freq=0.04, Amp=7525.64

### Anti-Stokes for 2.0 mW



Integral (Area) = 11112.58

Peak Info (Anti-Stokes):

WL=521.56, Cnt=437.00

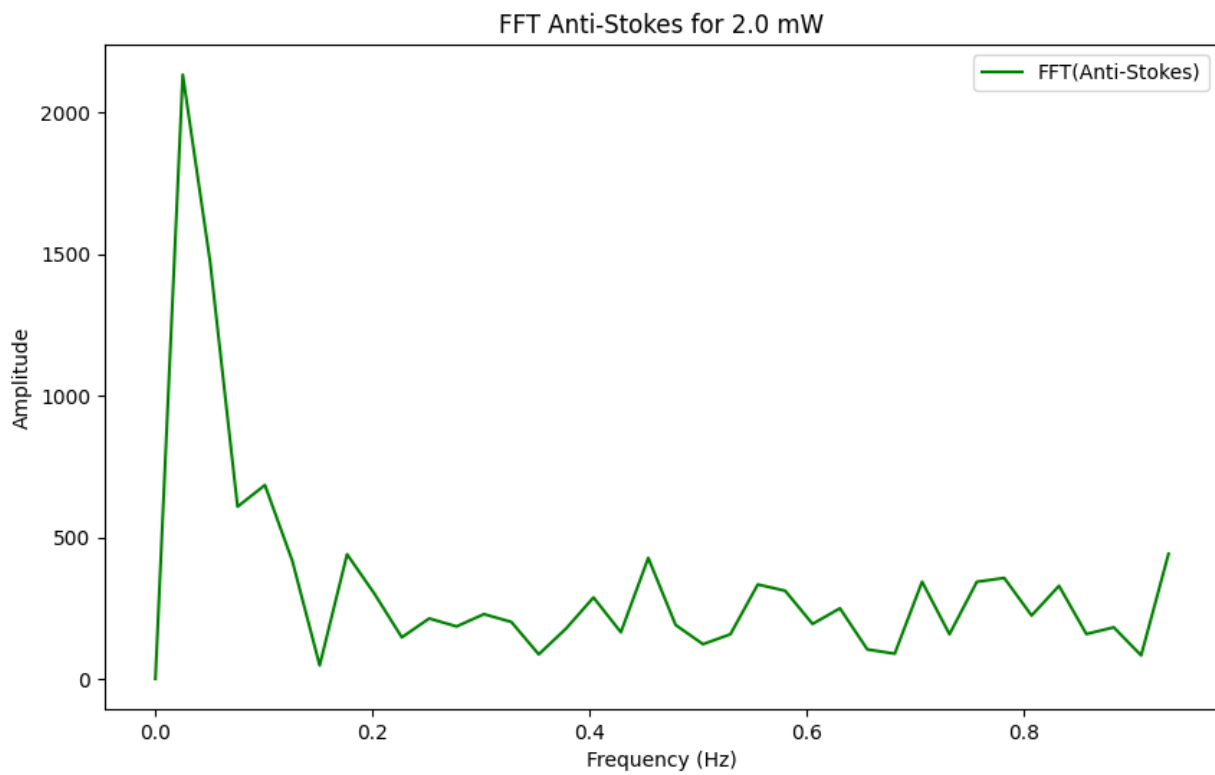
WL=520.53, Cnt=433.00

WL=518.48, Cnt=406.00

WL=523.62, Cnt=360.00

WL=517.45, Cnt=345.00

### FFT Anti-Stokes for 2.0 mW



Peak Info (FFT Anti-Stokes):

Freq=0.03, Amp=2132.55

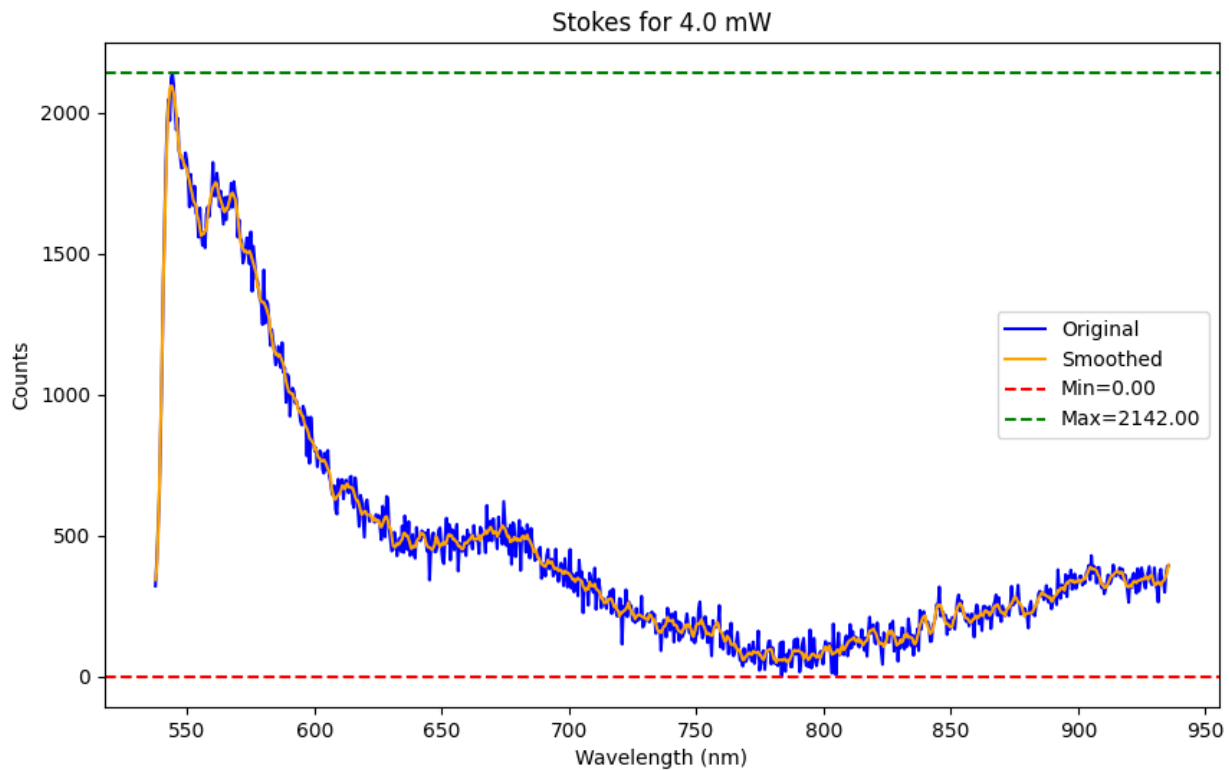
Freq=0.10, Amp=684.02

Freq=0.18, Amp=439.77

Freq=0.45, Amp=426.84

Freq=0.78, Amp=356.12

### Stokes for 4.0 mW



Integral (Area) = 190821.36

Peak Info (Stokes):

WL=544.17, Cnt=2142.00

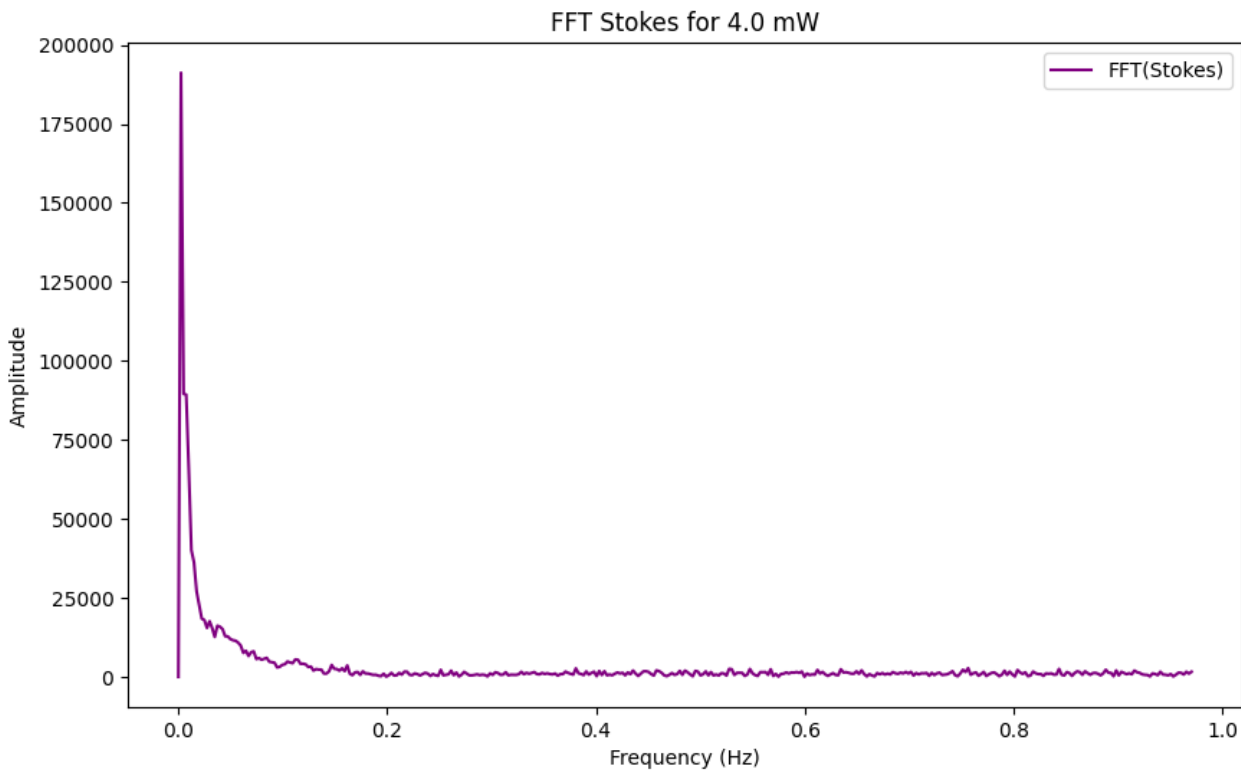
WL=542.63, Cnt=2047.00

WL=546.22, Cnt=1981.00

WL=549.30, Cnt=1858.00

WL=560.09, Cnt=1824.00

### FFT Stokes for 4.0 mW



Peak Info (FFT Stokes):

Freq=0.00, Amp=191164.42

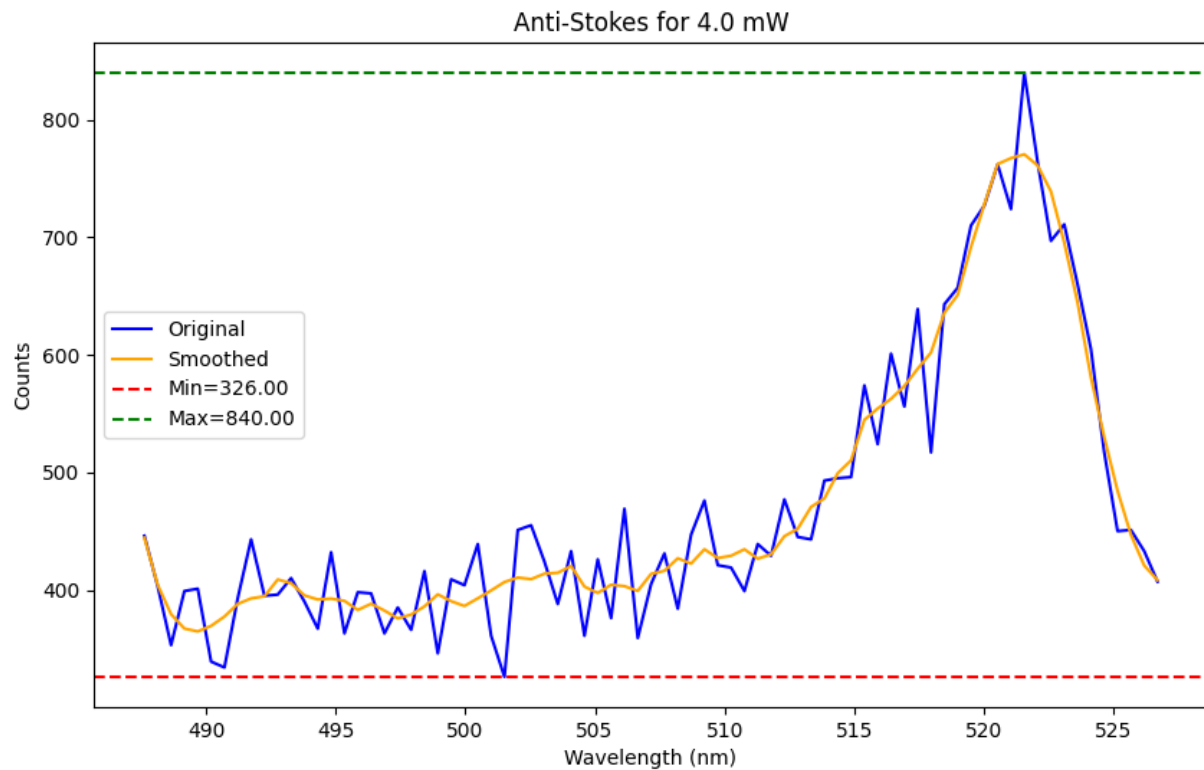
Freq=0.03, Amp=17593.46

Freq=0.04, Amp=16183.23

Freq=0.06, Amp=8260.24

Freq=0.07, Amp=8059.81

### Anti-Stokes for 4.0 mW



Integral (Area) = 18436.68

Peak Info (Anti-Stokes):

WL=521.56, Cnt=840.00

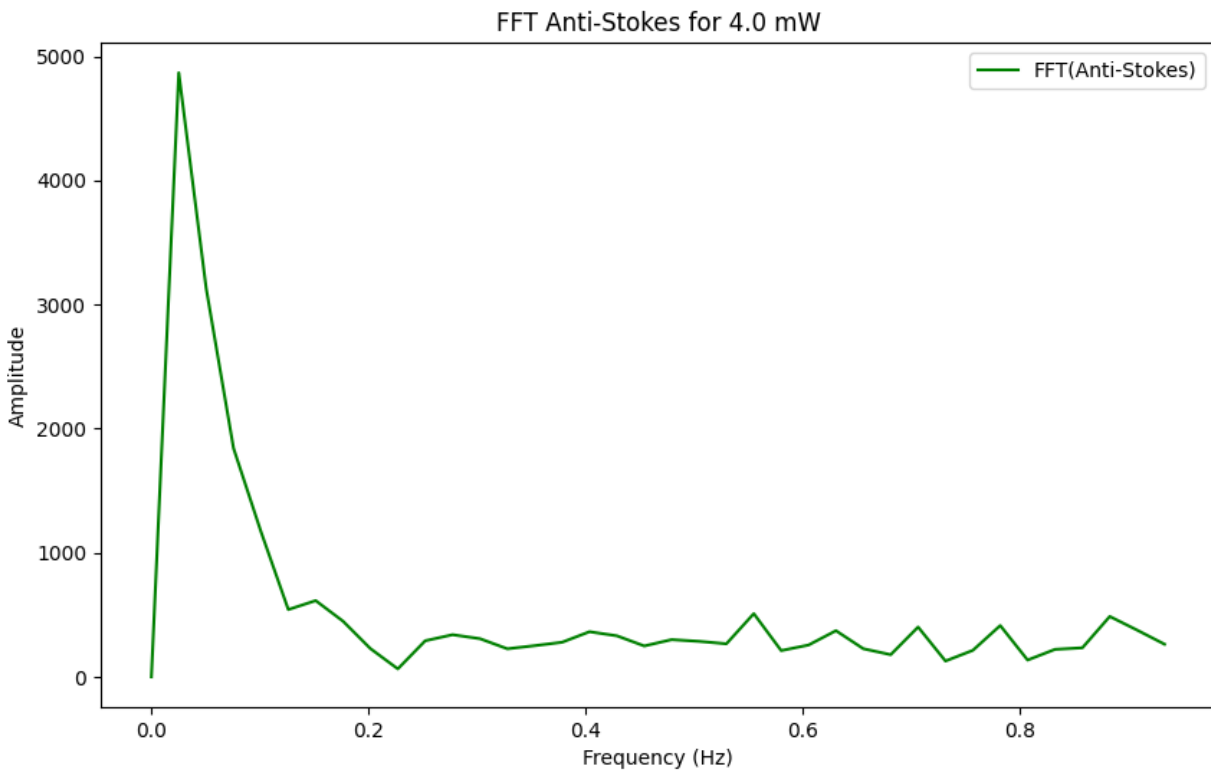
WL=520.53, Cnt=762.00

WL=523.10, Cnt=711.00

WL=517.45, Cnt=639.00

WL=516.42, Cnt=601.00

## FFT Anti-Stokes for 4.0 mW



Peak Info (FFT Anti-Stokes):

Freq=0.03, Amp=4868.88

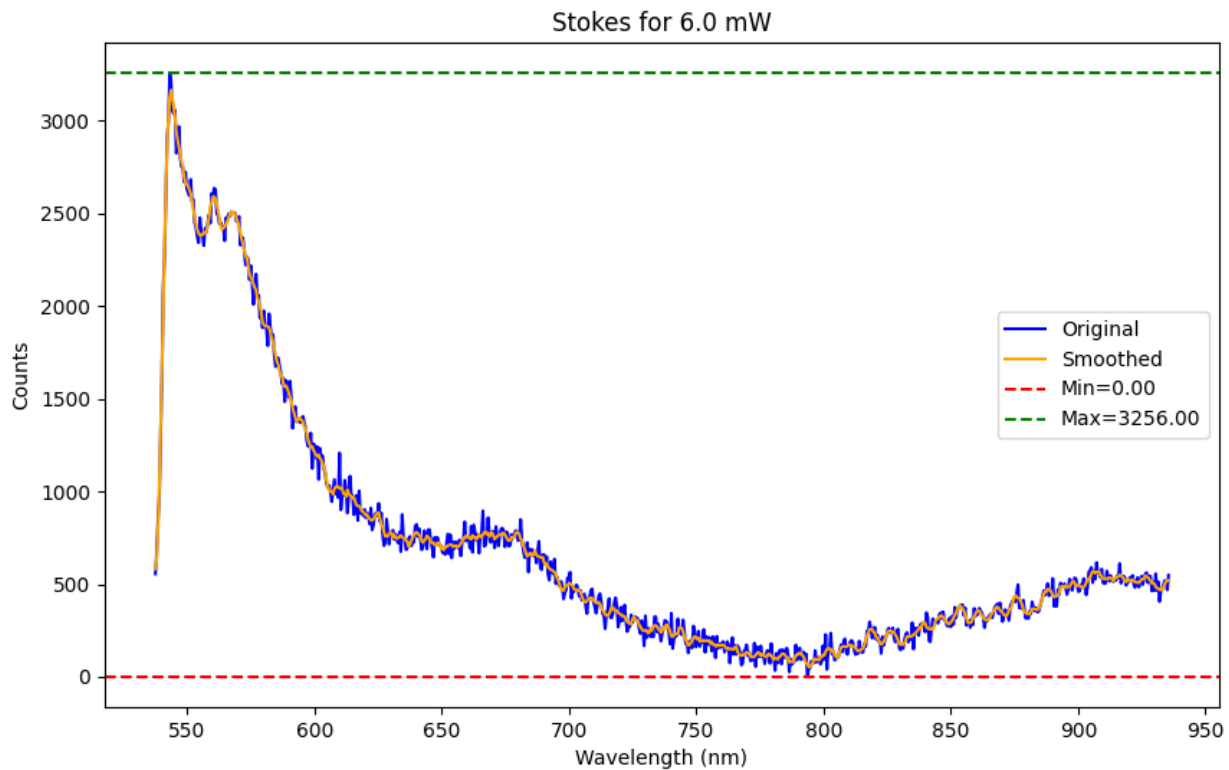
Freq=0.15, Amp=614.55

Freq=0.56, Amp=509.60

Freq=0.88, Amp=486.92

Freq=0.78, Amp=413.61

### Stokes for 6.0 mW



Integral (Area) = 281070.08

Peak Info (Stokes):

WL=543.14, Cnt=3256.00

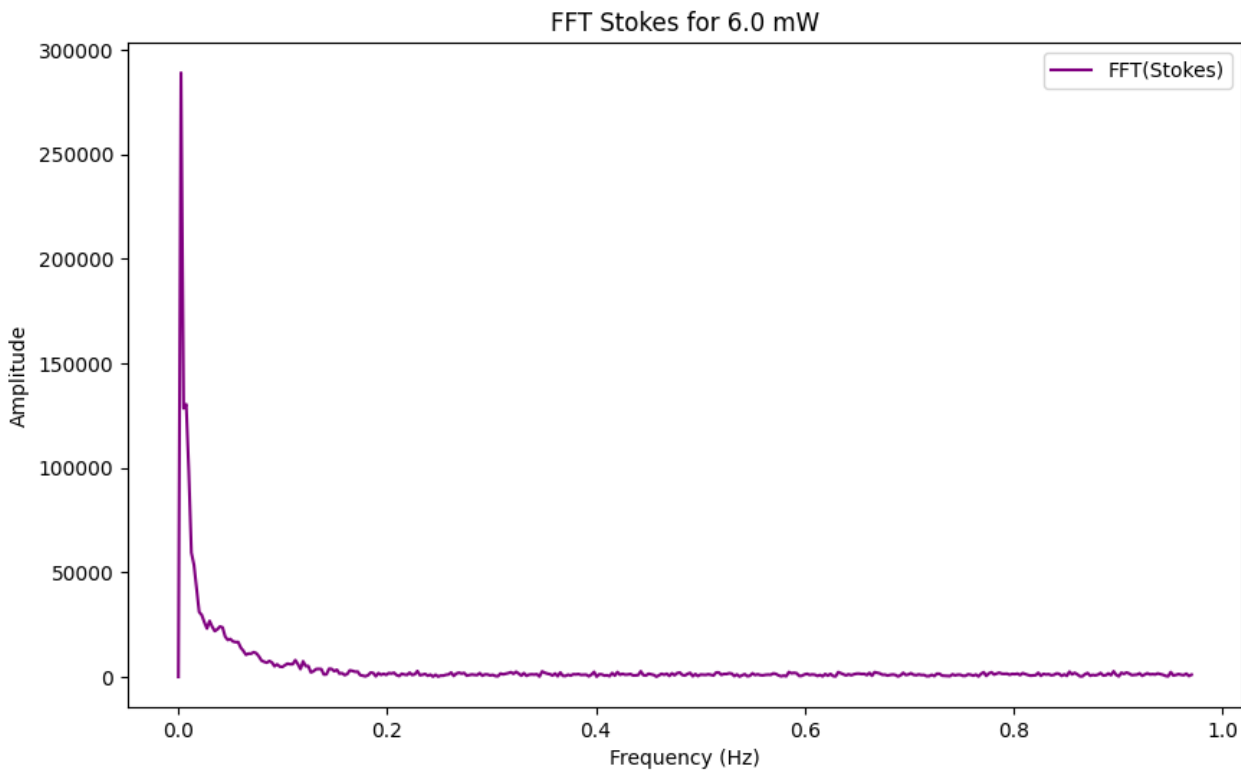
WL=545.20, Cnt=3056.00

WL=546.74, Cnt=2966.00

WL=549.30, Cnt=2721.00

WL=551.36, Cnt=2681.00

### FFT Stokes for 6.0 mW



Peak Info (FFT Stokes):

Freq=0.00, Amp=289144.27

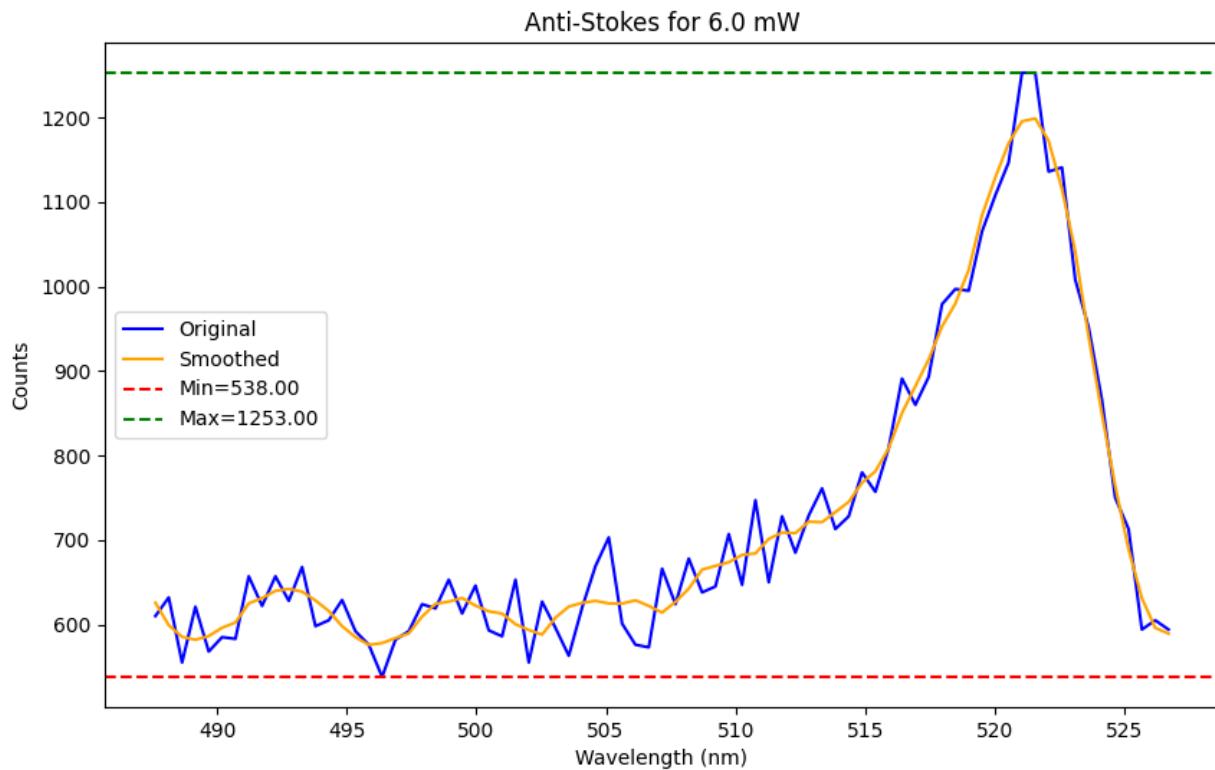
Freq=0.01, Amp=130493.14

Freq=0.03, Amp=26757.11

Freq=0.04, Amp=24088.44

Freq=0.05, Amp=18094.81

### Anti-Stokes for 6.0 mW



Integral (Area) = 28309.04

Peak Info (Anti-Stokes):

WL=521.05, Cnt=1253.00

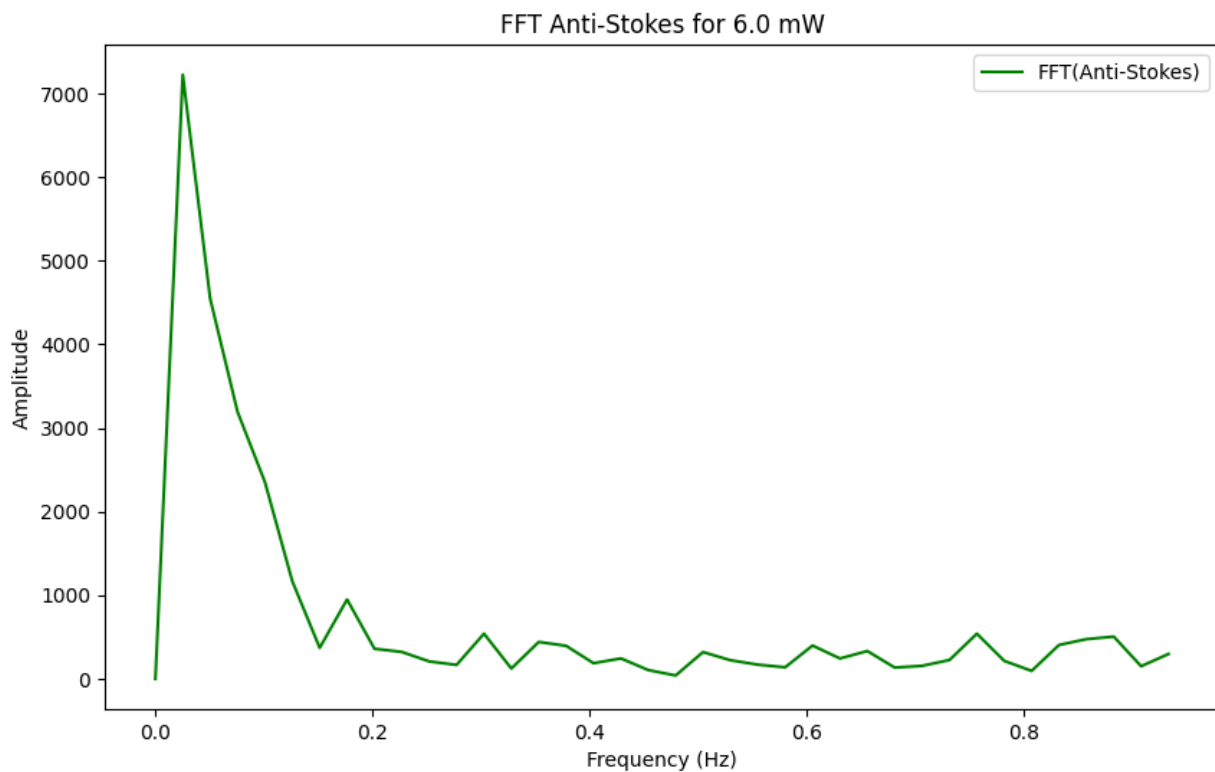
WL=522.59, Cnt=1141.00

WL=518.48, Cnt=997.00

WL=516.42, Cnt=891.00

WL=514.88, Cnt=780.00

### FFT Anti-Stokes for 6.0 mW



Peak Info (FFT Anti-Stokes):

Freq=0.03, Amp=7225.16

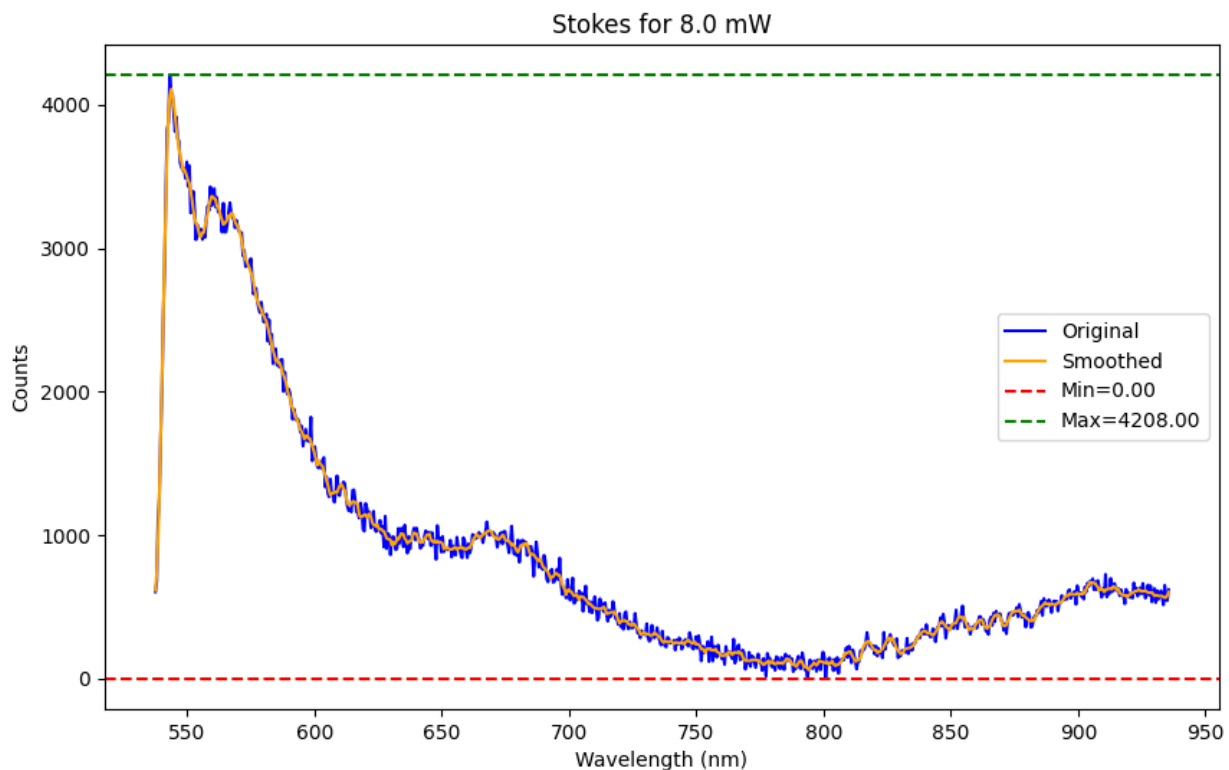
Freq=0.18, Amp=949.62

Freq=0.30, Amp=540.57

Freq=0.76, Amp=540.33

Freq=0.88, Amp=505.12

### Stokes for 8.0 mW



Integral (Area) = 354438.59

Peak Info (Stokes):

WL=543.14, Cnt=4208.00

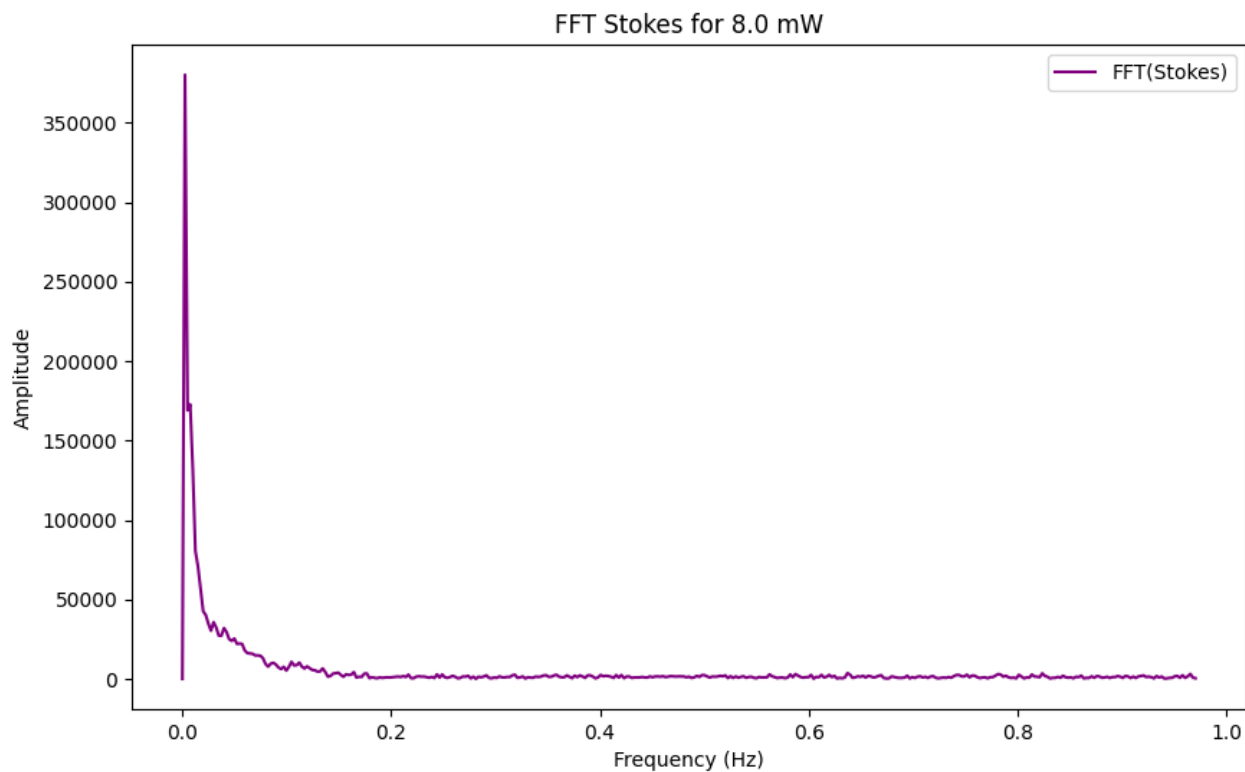
WL=545.71, Cnt=3915.00

WL=549.82, Cnt=3601.00

WL=550.85, Cnt=3575.00

WL=548.79, Cnt=3551.00

### FFT Stokes for 8.0 mW



Peak Info (FFT Stokes):

Freq=0.00, Amp=380333.19

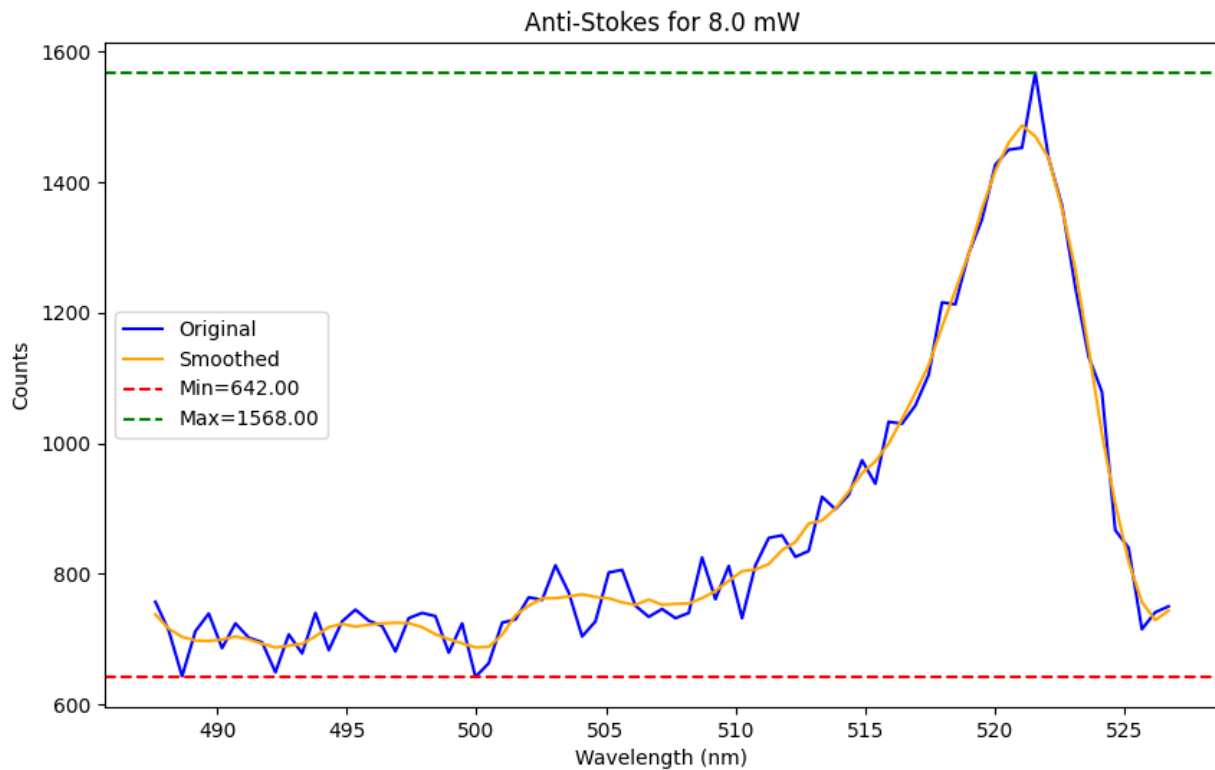
Freq=0.01, Amp=172790.48

Freq=0.03, Amp=35716.64

Freq=0.04, Amp=31968.00

Freq=0.05, Amp=25406.91

### Anti-Stokes for 8.0 mW



Integral (Area) = 34046.67

Peak Info (Anti-Stokes):

WL=521.56, Cnt=1568.00

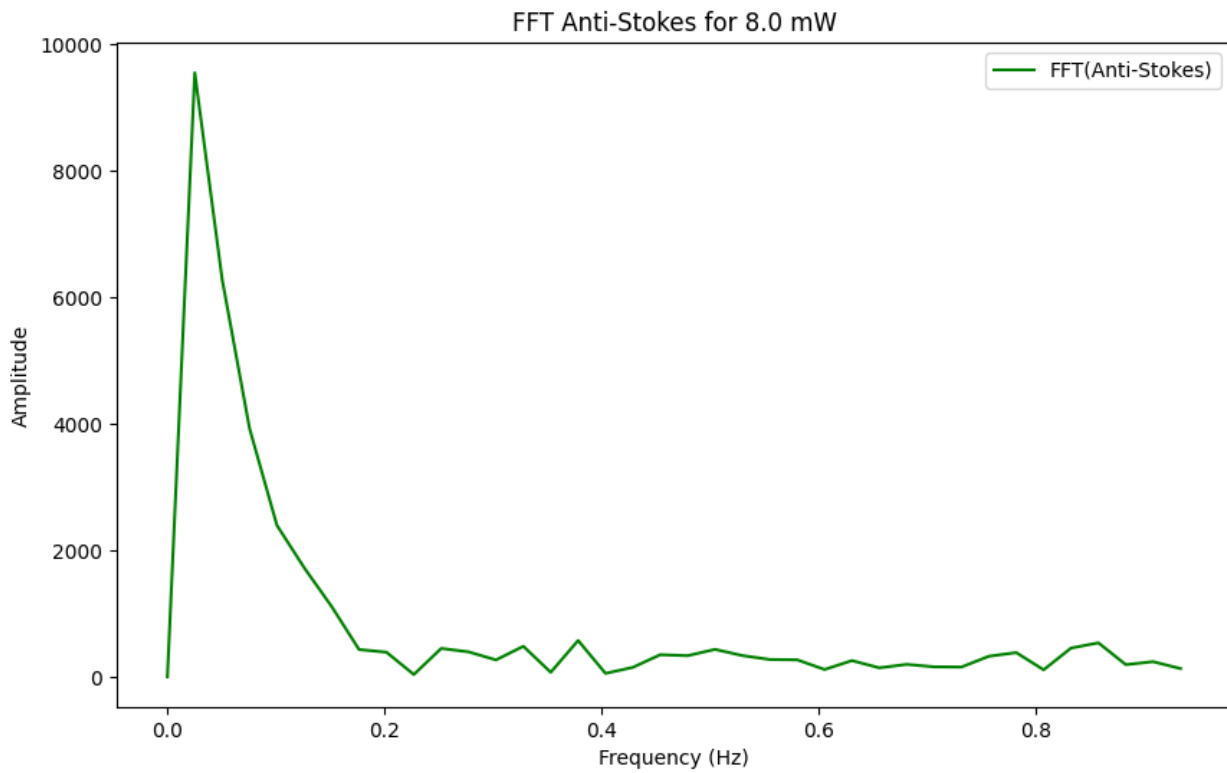
WL=517.96, Cnt=1216.00

WL=515.91, Cnt=1033.00

WL=514.88, Cnt=974.00

WL=513.34, Cnt=918.00

### FFT Anti-Stokes for 8.0 mW



Peak Info (FFT Anti-Stokes):

Freq=0.03, Amp=9552.62

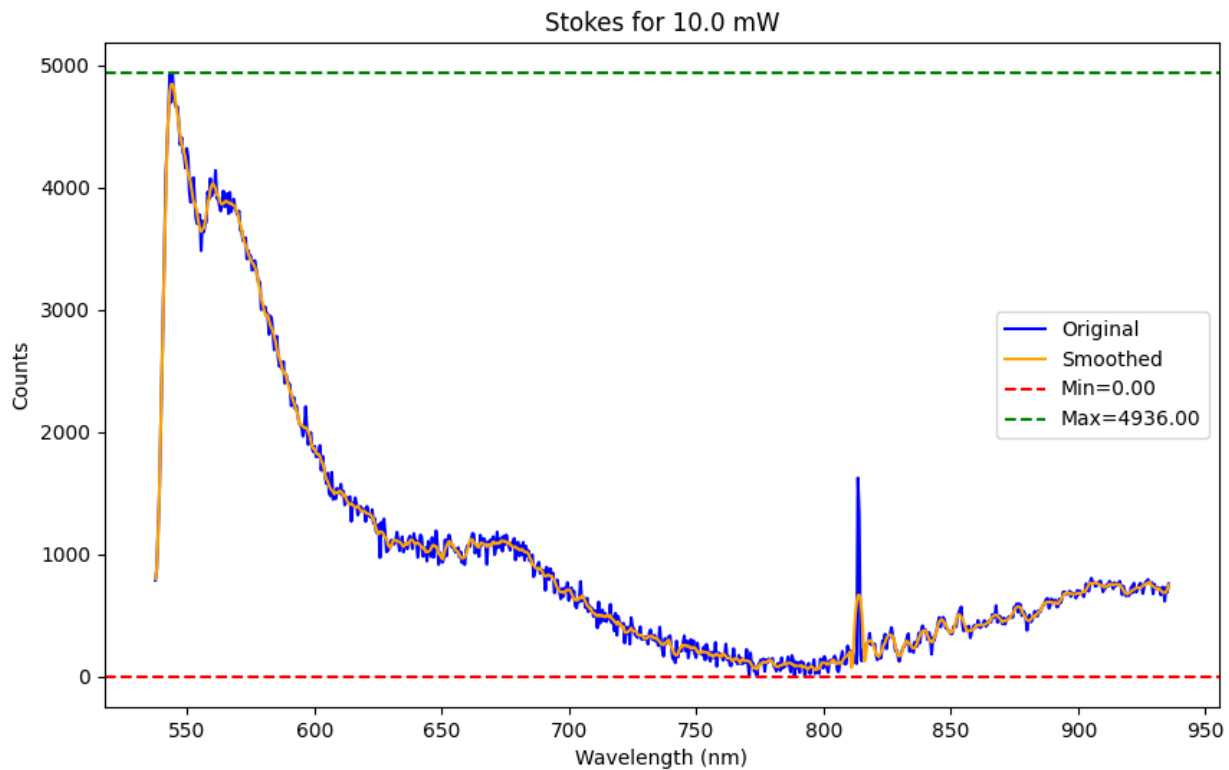
Freq=0.38, Amp=575.31

Freq=0.86, Amp=538.43

Freq=0.33, Amp=483.79

Freq=0.25, Amp=449.83

### Stokes for 10.0 mW



Integral (Area) = 411172.81

Peak Info (Stokes):

WL=544.17, Cnt=4936.00

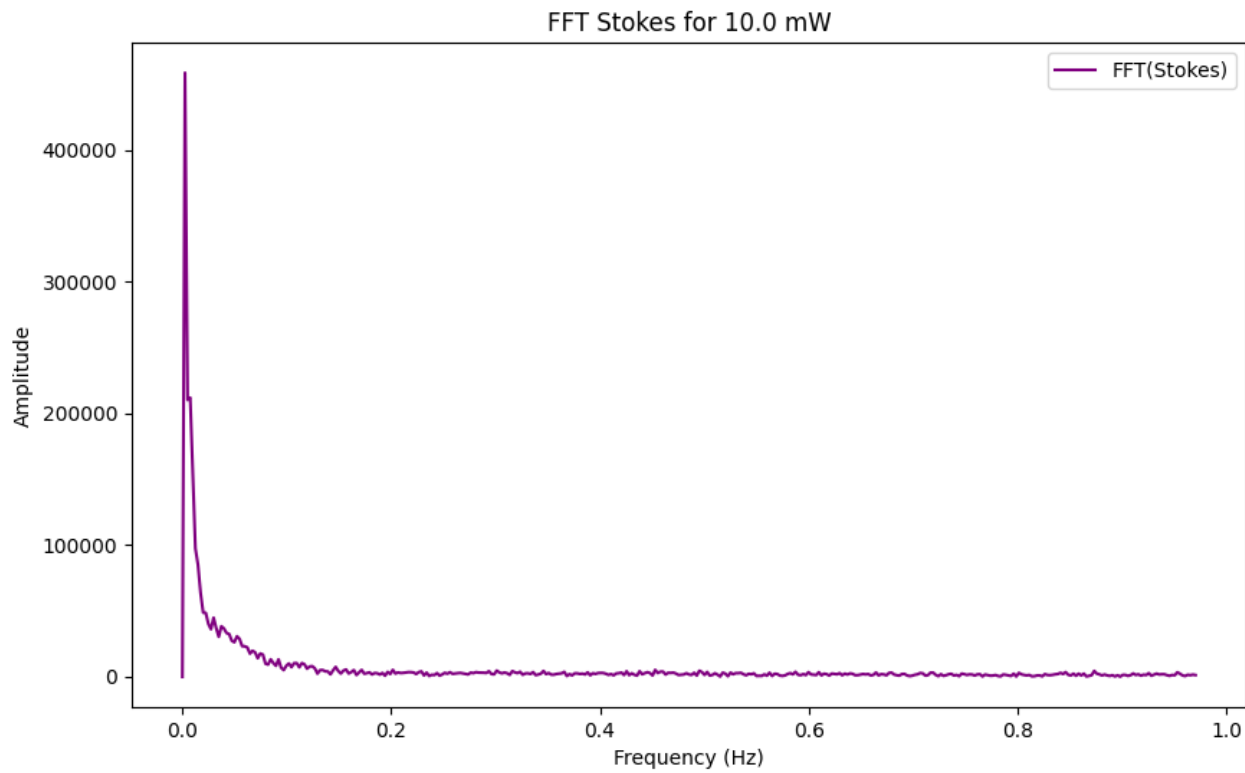
WL=543.14, Cnt=4924.00

WL=546.22, Cnt=4657.00

WL=547.76, Cnt=4408.00

WL=549.82, Cnt=4317.00

## FFT Stokes for 10.0 mW



Peak Info (FFT Stokes):

Freq=0.00, Amp=459008.70

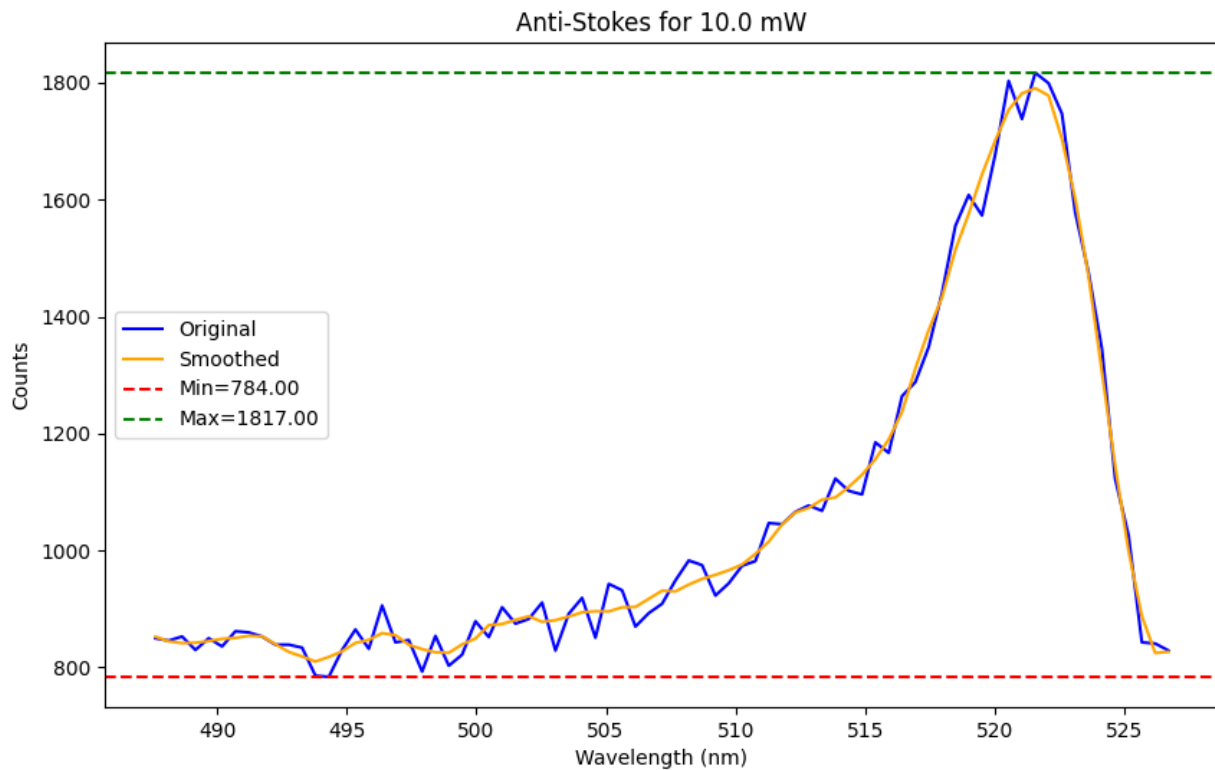
Freq=0.01, Amp=212134.54

Freq=0.03, Amp=44945.58

Freq=0.04, Amp=38425.05

Freq=0.05, Amp=30849.16

### Anti-Stokes for 10.0 mW



Integral (Area) = 41154.33

Peak Info (Anti-Stokes):

WL=521.56, Cnt=1817.00

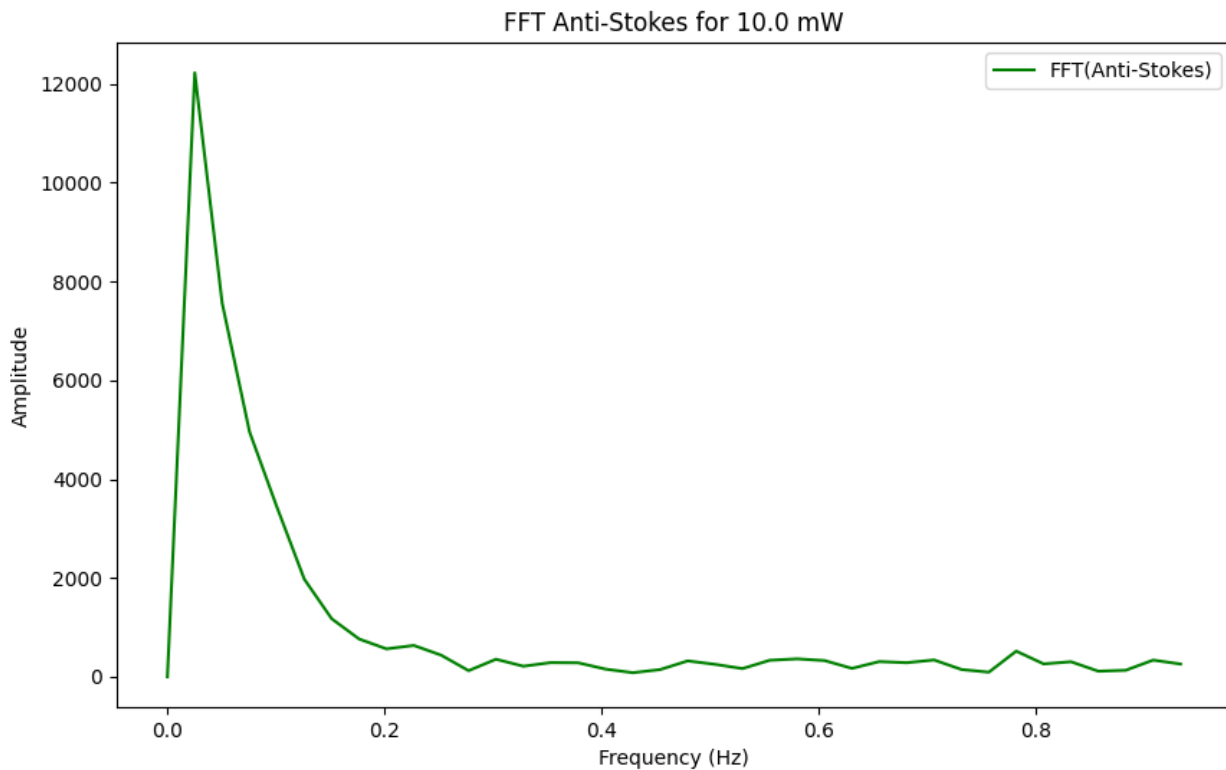
WL=520.53, Cnt=1803.00

WL=518.99, Cnt=1608.00

WL=515.39, Cnt=1185.00

WL=513.85, Cnt=1123.00

### FFT Anti-Stokes for 10.0 mW



Peak Info (FFT Anti-Stokes):

Freq=0.03, Amp=12220.29

Freq=0.23, Amp=635.65

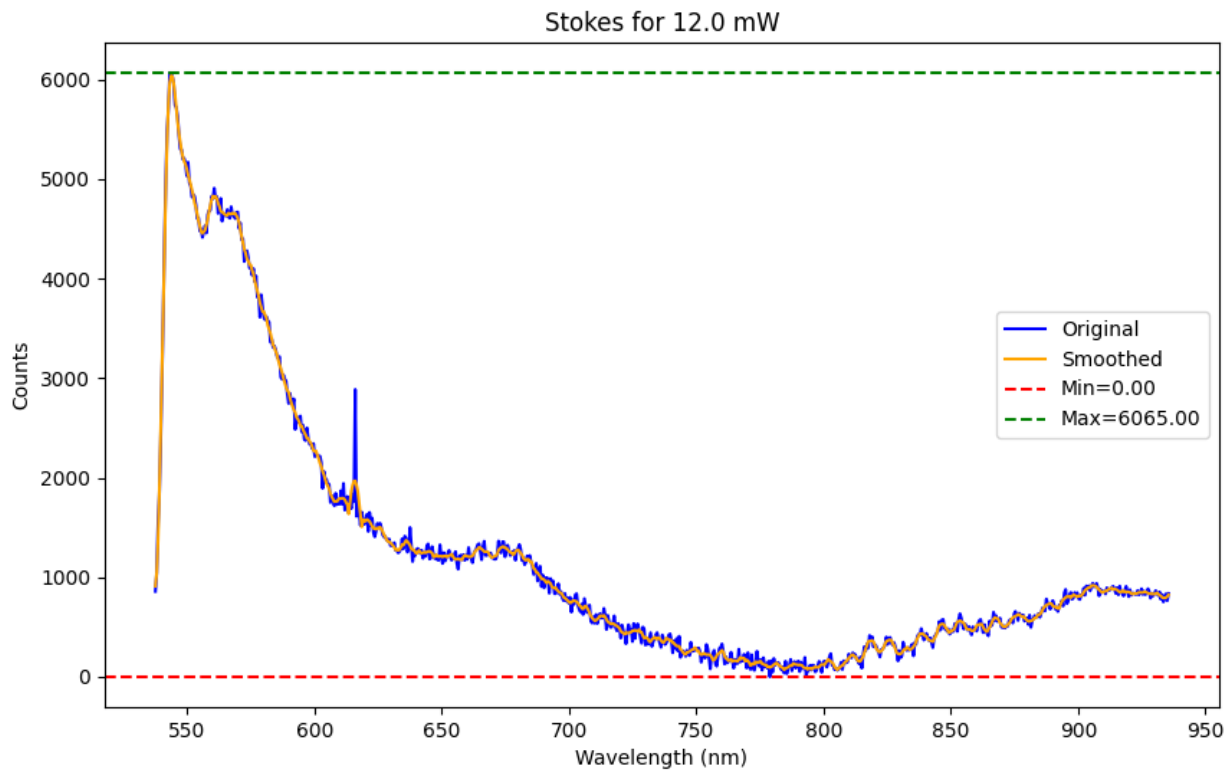
Freq=0.30, Amp=356.62

Freq=0.43, Amp=364.26

Freq=0.58, Amp=520.27

Freq=0.78, Amp=520.27

## Stokes for 12.0 mW



Integral (Area) = 490297.45

Peak Info (Stokes):

WL=543.14, Cnt=6065.00

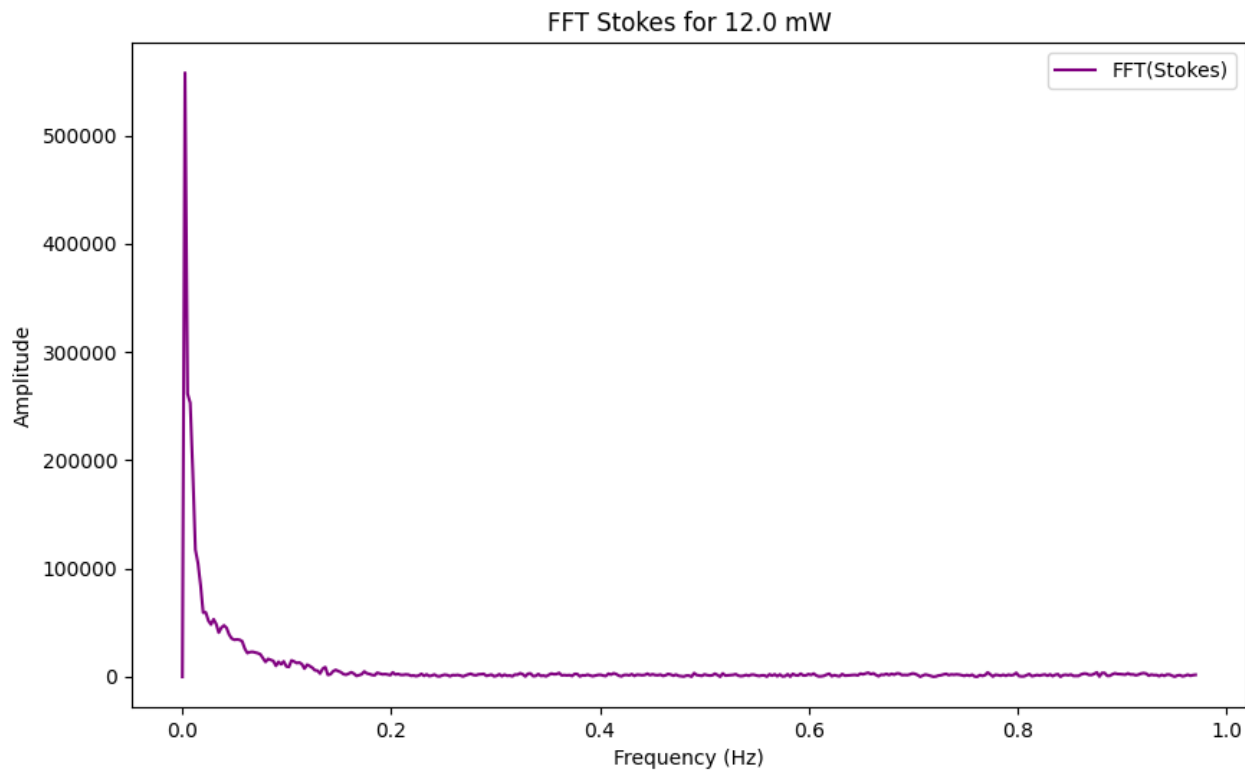
WL=548.79, Cnt=5205.00

WL=550.33, Cnt=5167.00

WL=560.60, Cnt=4906.00

WL=552.39, Cnt=4842.00

## FFT Stokes for 12.0 mW



Peak Info (FFT Stokes):

Freq=0.00, Amp=558002.83

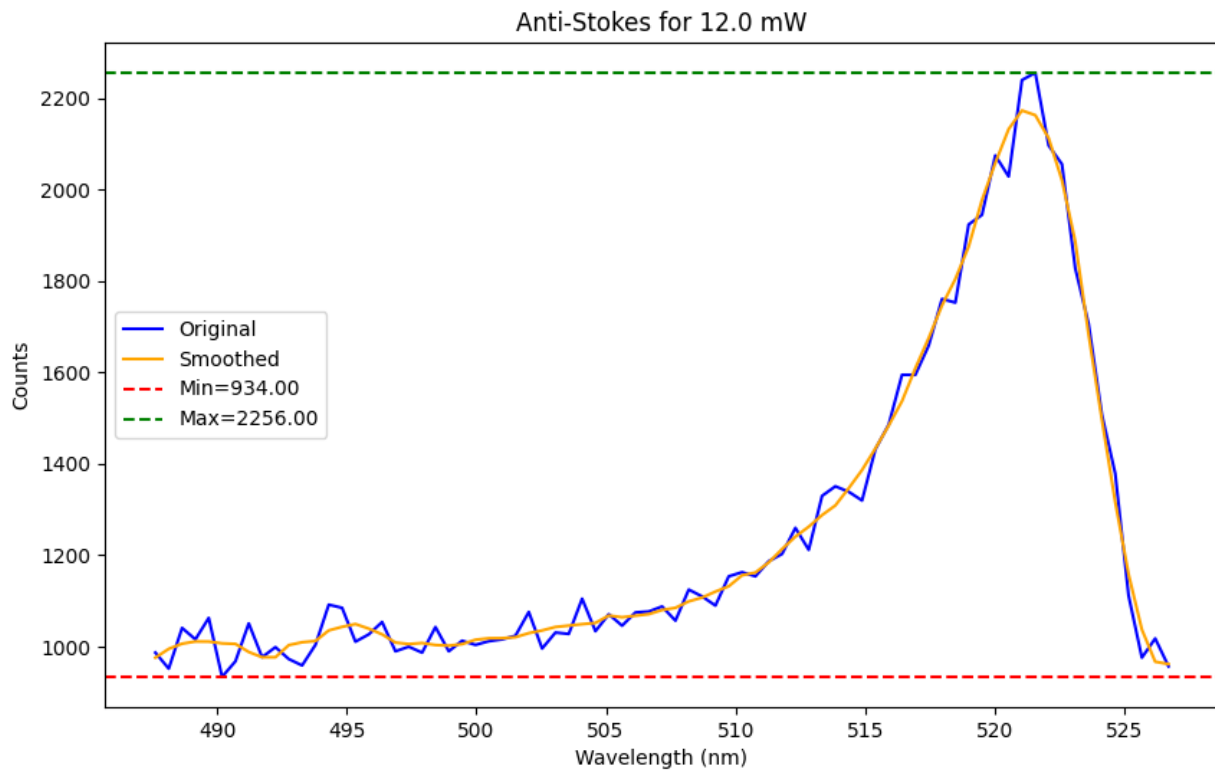
Freq=0.02, Amp=59565.02

Freq=0.03, Amp=53188.30

Freq=0.04, Amp=47505.36

Freq=0.05, Amp=34552.91

## Anti-Stokes for 12.0 mW



Integral (Area) = 49035.68

Peak Info (Anti-Stokes):

WL=521.56, Cnt=2256.00

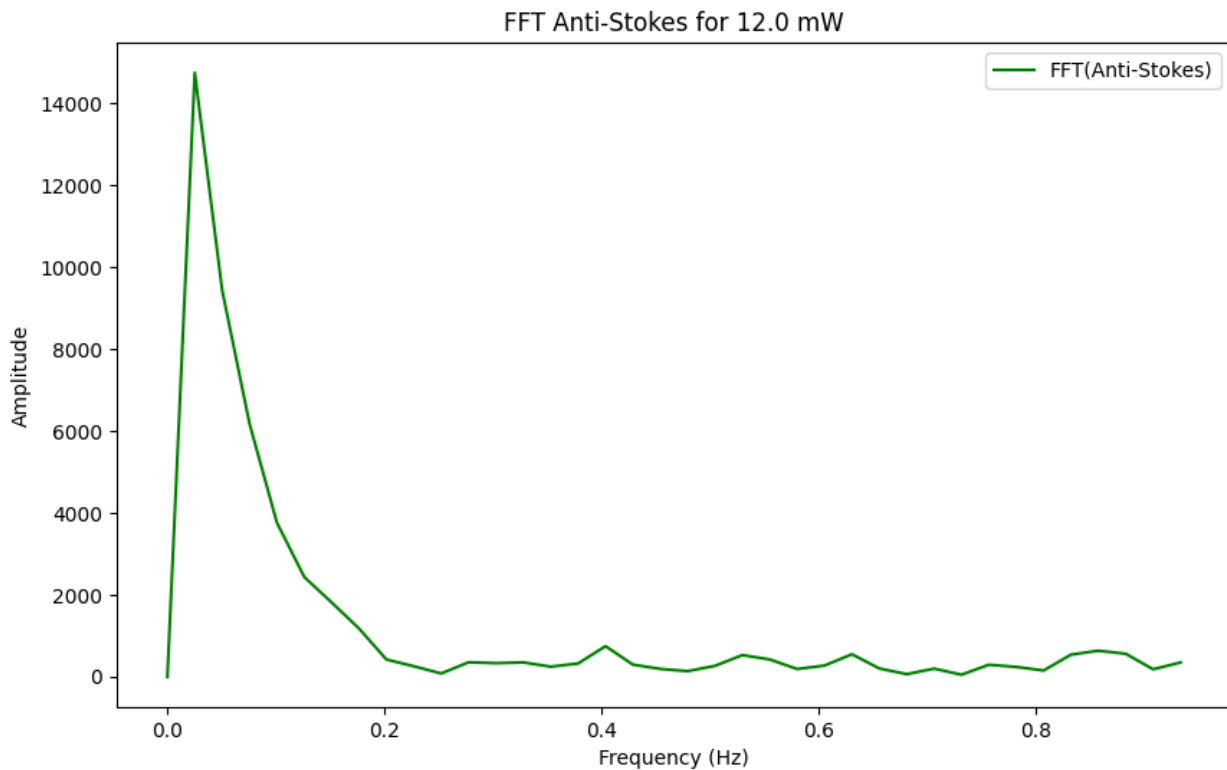
WL=520.02, Cnt=2075.00

WL=517.96, Cnt=1761.00

WL=513.85, Cnt=1351.00

WL=512.31, Cnt=1260.00

### FFT Anti-Stokes for 12.0 mW



Peak Info (FFT Anti-Stokes):

Freq=0.03, Amp=14738.29

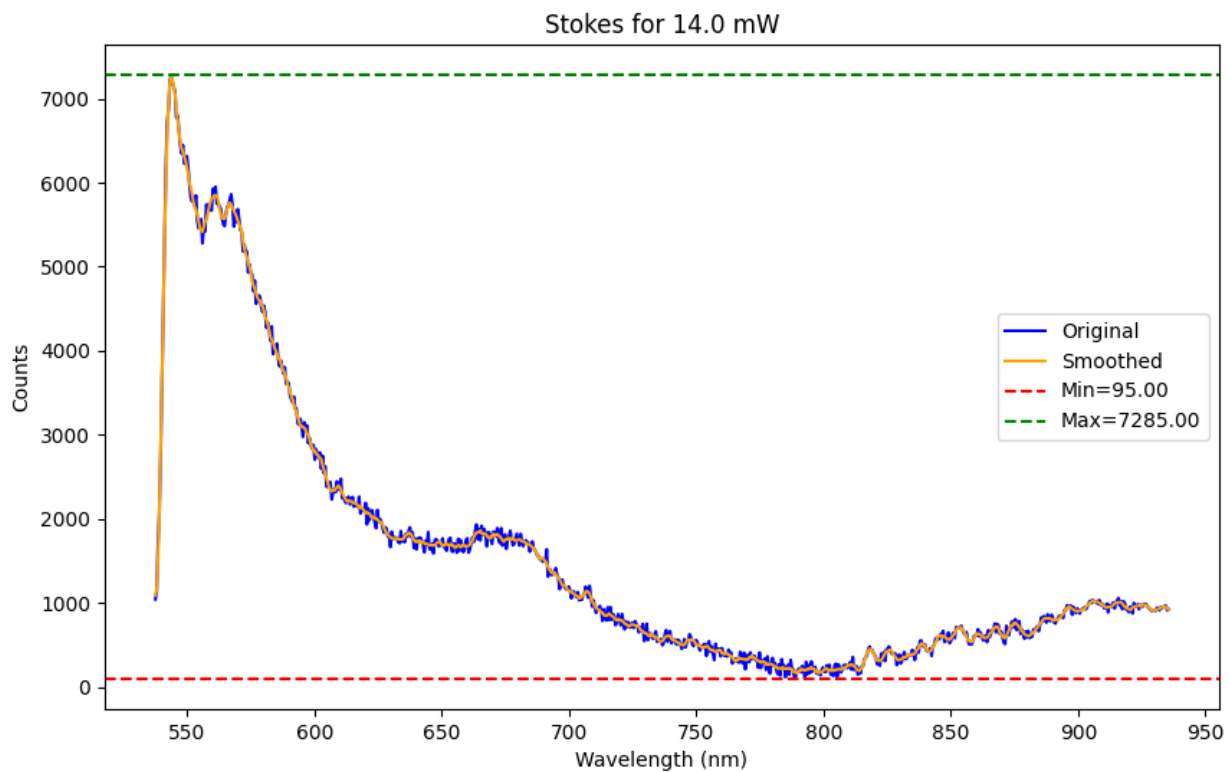
Freq=0.40, Amp=749.18

Freq=0.86, Amp=637.98

Freq=0.63, Amp=551.82

Freq=0.53, Amp=531.03

### Stokes for 14.0 mW



Integral (Area) = 628524.71

Peak Info (Stokes):

WL=543.66, Cnt=7285.00

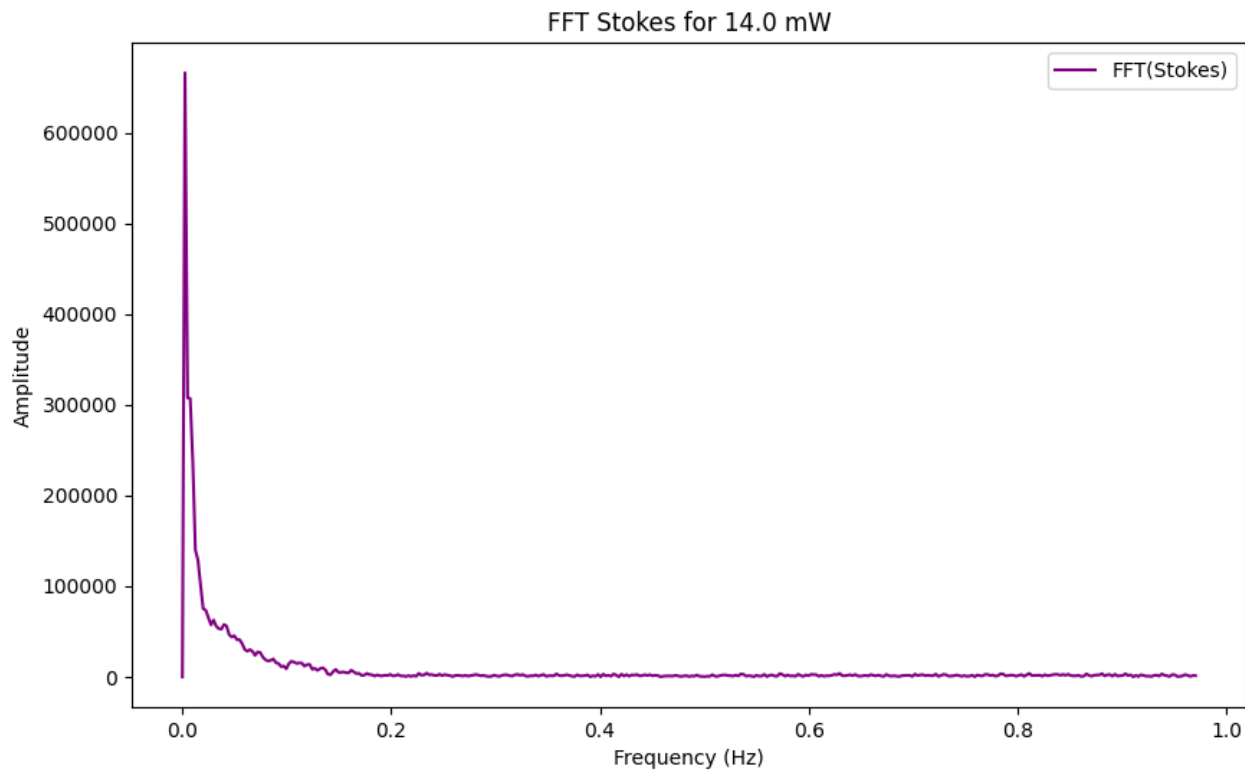
WL=546.22, Cnt=6802.00

WL=548.28, Cnt=6449.00

WL=549.82, Cnt=6318.00

WL=561.11, Cnt=5952.00

## FFT Stokes for 14.0 mW



Peak Info (FFT Stokes):

Freq=0.00, Amp=666303.83

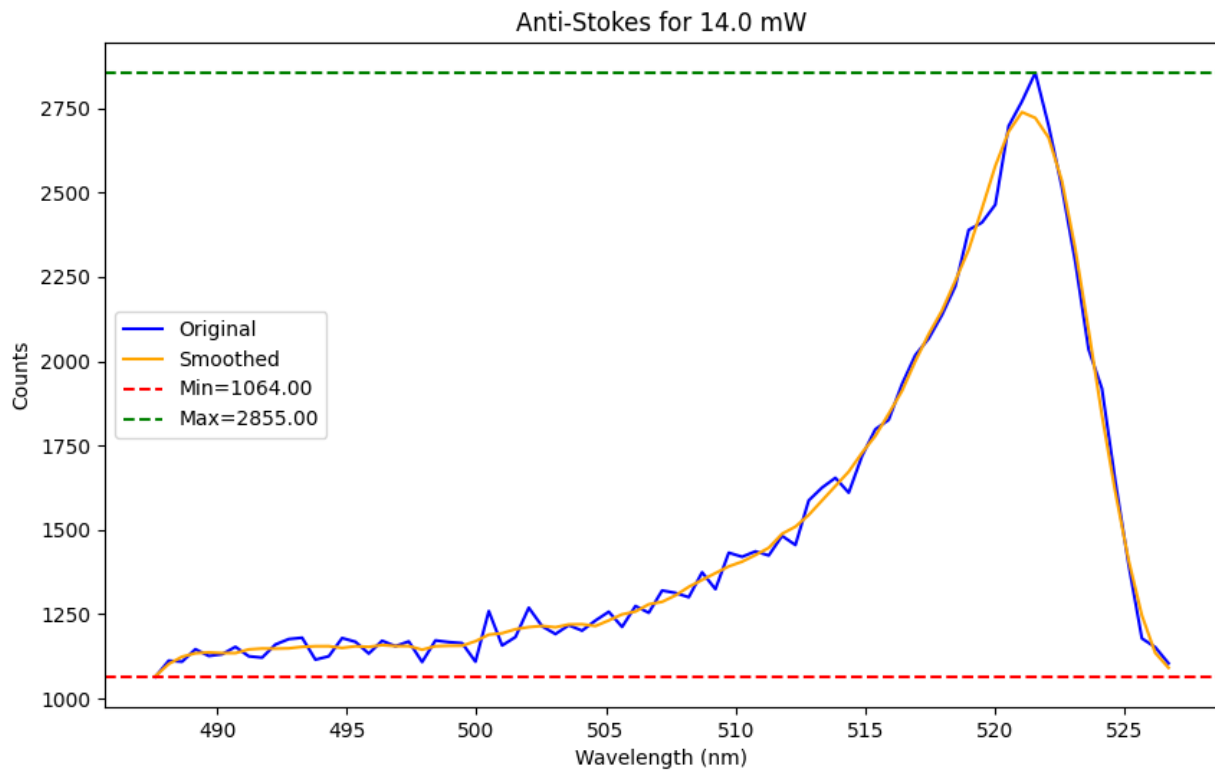
Freq=0.03, Amp=62767.92

Freq=0.04, Amp=57746.96

Freq=0.05, Amp=45330.39

Freq=0.06, Amp=30036.84

### Anti-Stokes for 14.0 mW



Integral (Area) = 58805.66

Peak Info (Anti-Stokes):

WL=521.56, Cnt=2855.00

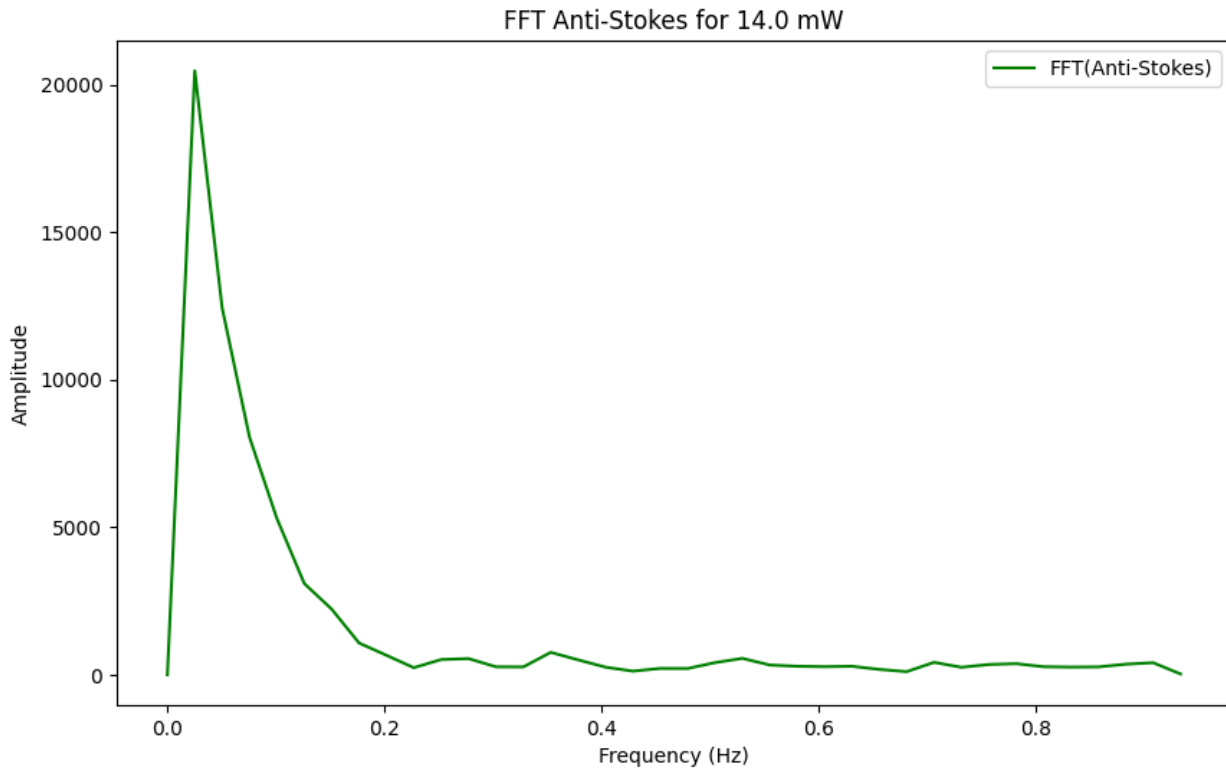
WL=513.85, Cnt=1654.00

WL=511.79, Cnt=1482.00

WL=510.77, Cnt=1436.00

WL=509.74, Cnt=1432.00

### FFT Anti-Stokes for 14.0 mW



Peak Info (FFT Anti-Stokes):

Freq=0.03, Amp=20467.04

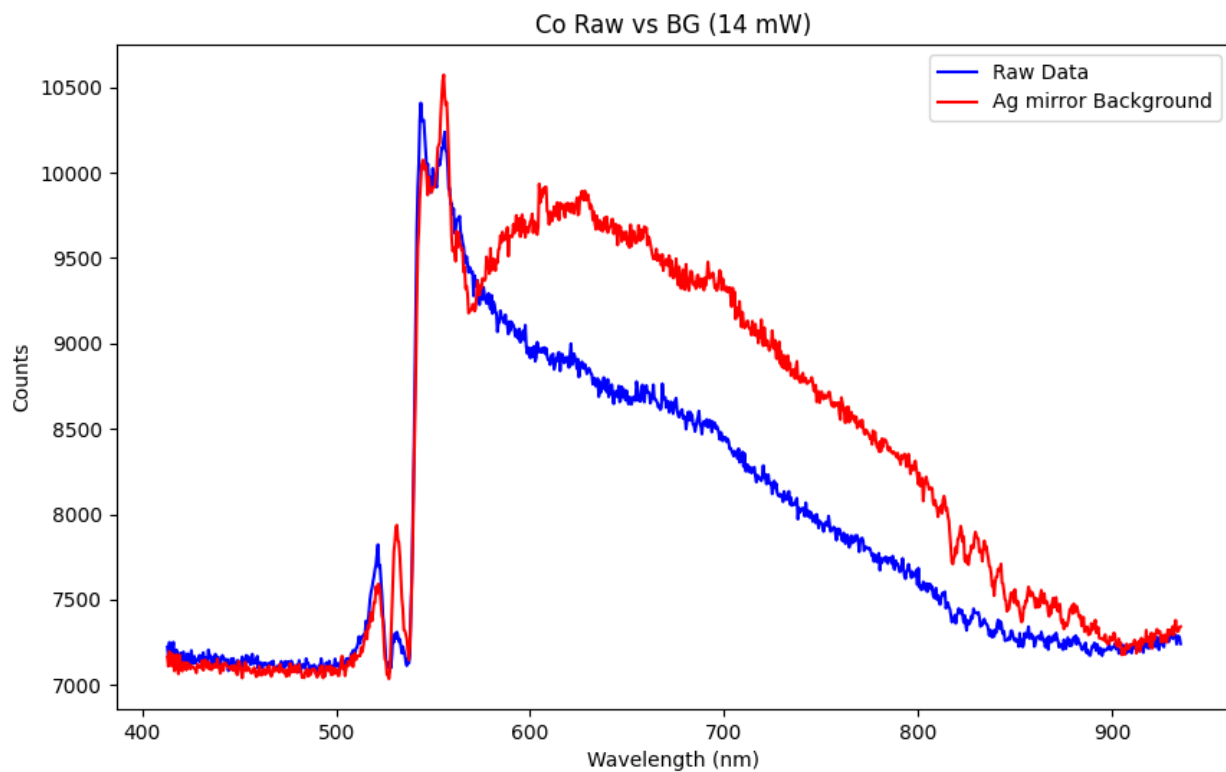
Freq=0.35, Amp=761.73

Freq=0.53, Amp=558.35

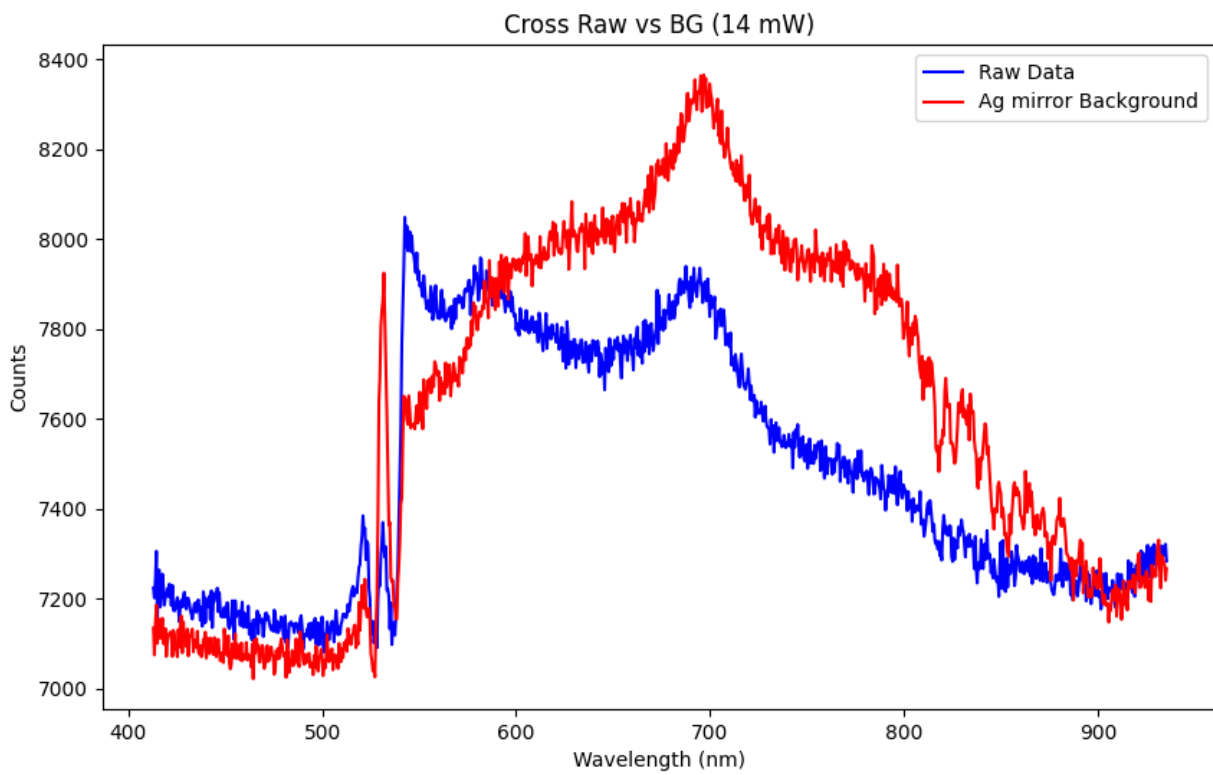
Freq=0.28, Amp=550.38

Freq=0.71, Amp=423.87

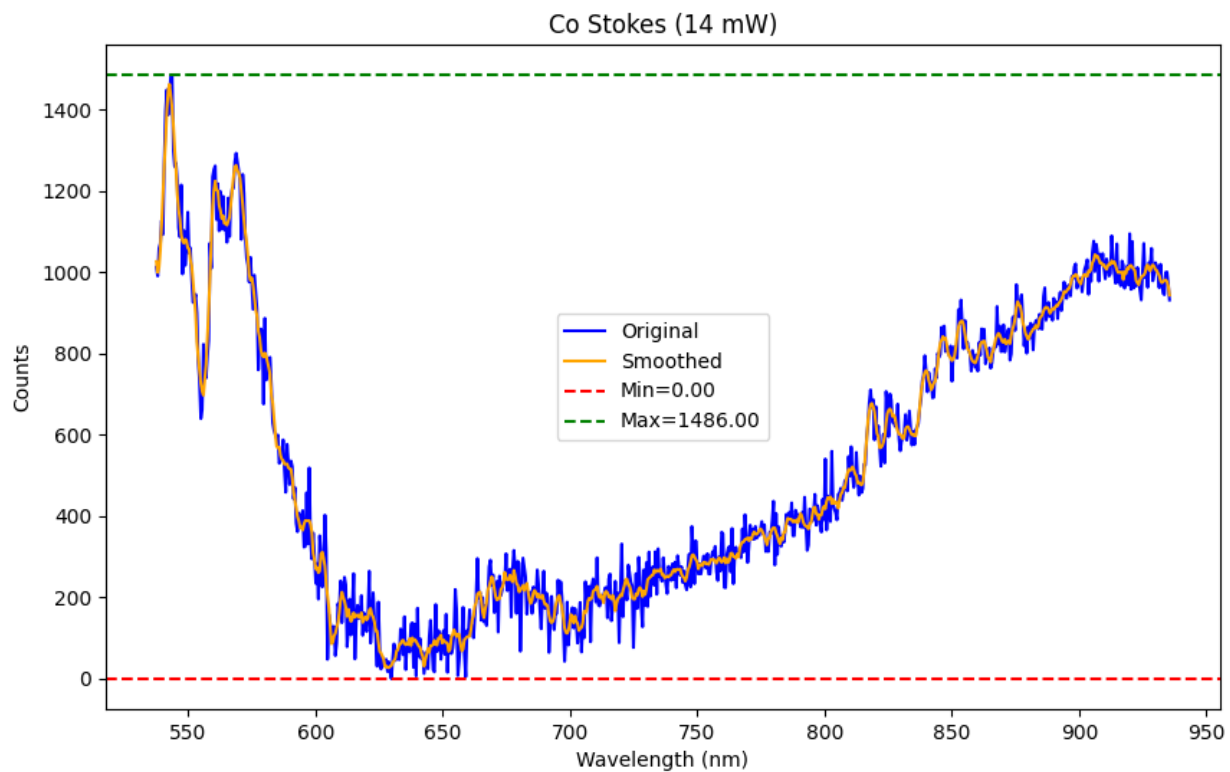
### Co Raw vs BG (14 mW)



### Cross Raw vs BG (14 mW)



### Co Stokes (14 mW)



#### Peak Info:

WL=543.66, Cnt=1486.00

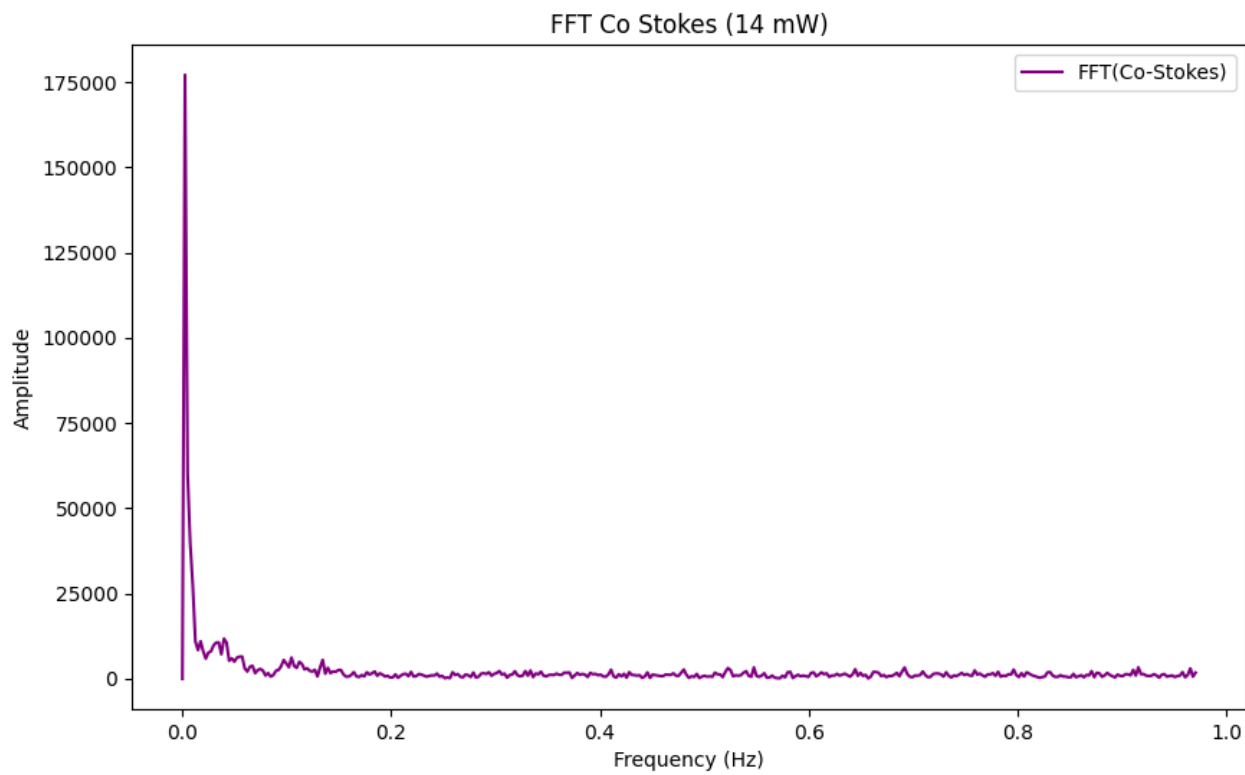
WL=541.60, Cnt=1449.00

WL=568.81, Cnt=1293.00

WL=545.20, Cnt=1269.00

WL=560.60, Cnt=1262.00

### FFT Co Stokes (14 mW)



#### FFT Peak Info:

Freq=0.00, Amp=177145.72

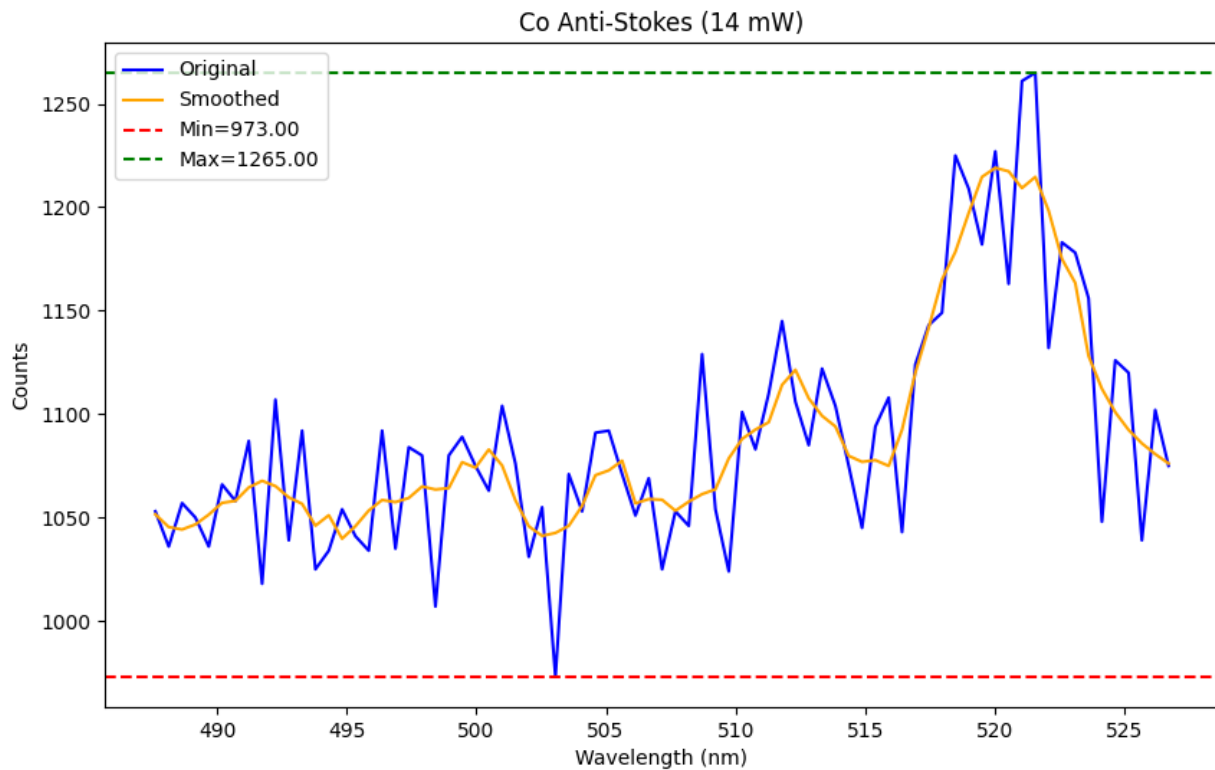
Freq=0.04, Amp=11783.78

Freq=0.02, Amp=11025.52

Freq=0.03, Amp=10668.93

Freq=0.06, Amp=6527.47

### Co Anti-Stokes (14 mW)



#### Peak Info:

WL=521.56, Cnt=1265.00

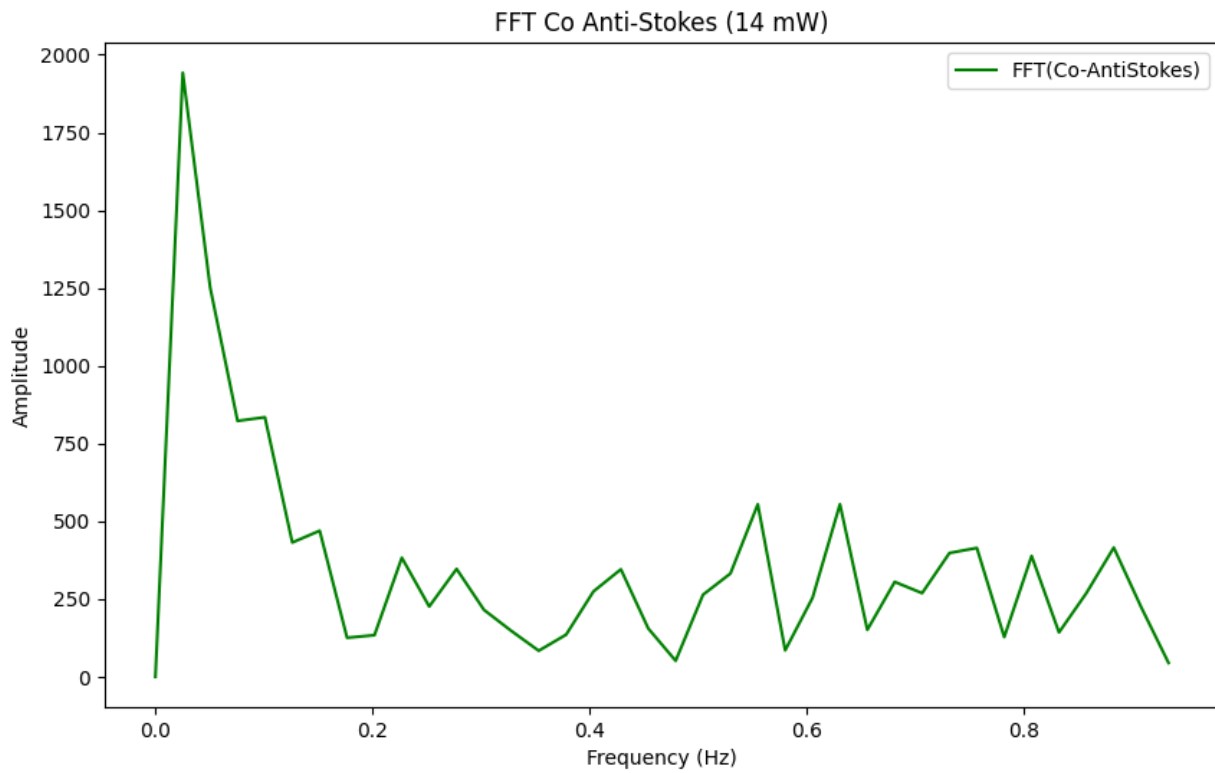
WL=520.02, Cnt=1227.00

WL=518.48, Cnt=1225.00

WL=522.59, Cnt=1183.00

WL=511.79, Cnt=1145.00

### FFT Co Anti-Stokes (14 mW)



#### FFT Peak Info:

Freq=0.03, Amp=1941.98

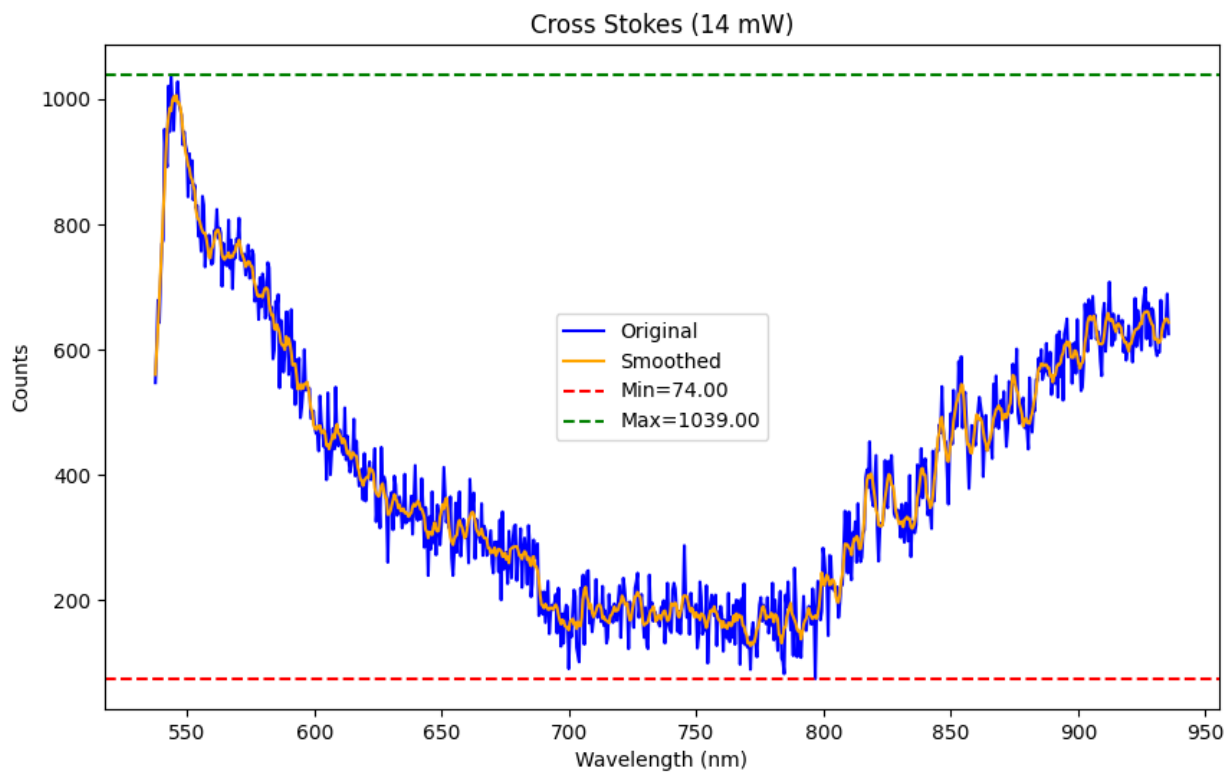
Freq=0.10, Amp=834.54

Freq=0.63, Amp=554.86

Freq=0.56, Amp=554.63

Freq=0.15, Amp=469.78

## Cross Stokes (14 mW)



### Peak Info:

WL=543.66, Cnt=1039.00

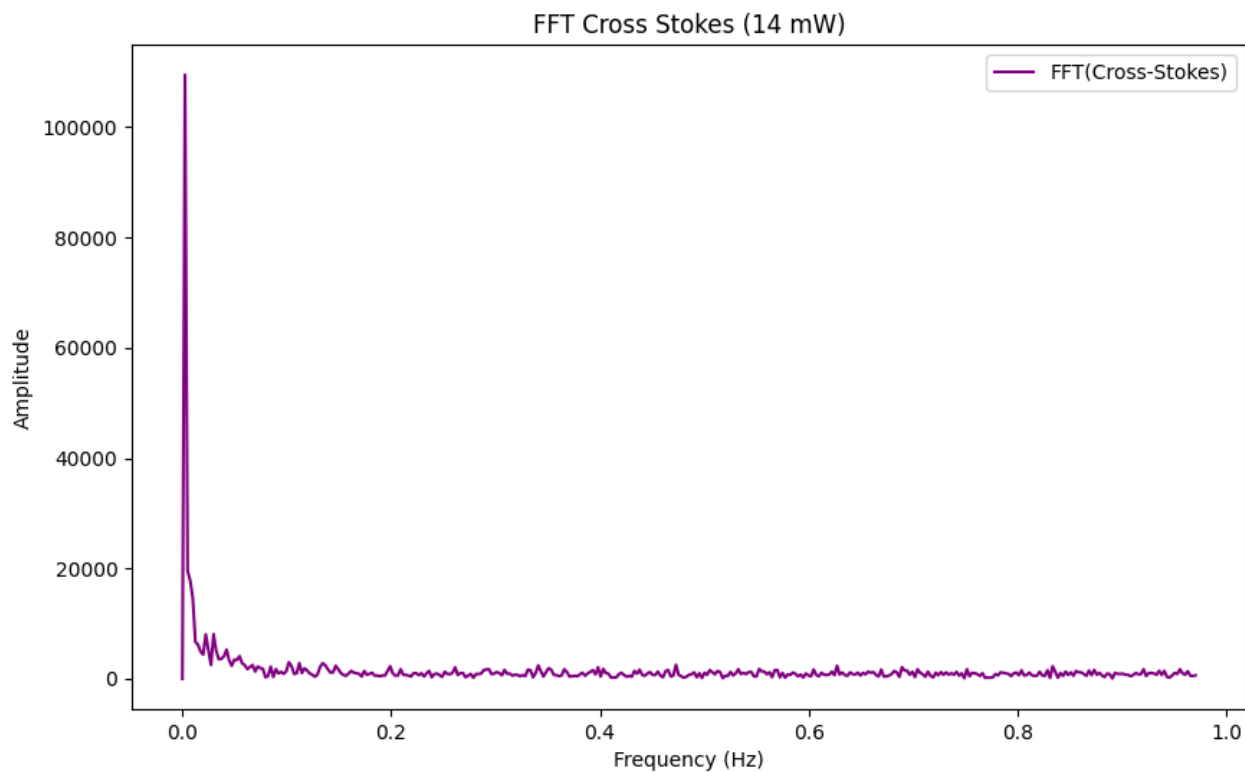
WL=546.22, Cnt=1028.00

WL=542.63, Cnt=1021.00

WL=545.20, Cnt=1005.00

WL=541.09, Cnt=952.00

## FFT Cross Stokes (14 mW)



### FFT Peak Info:

Freq=0.00, Amp=109505.09

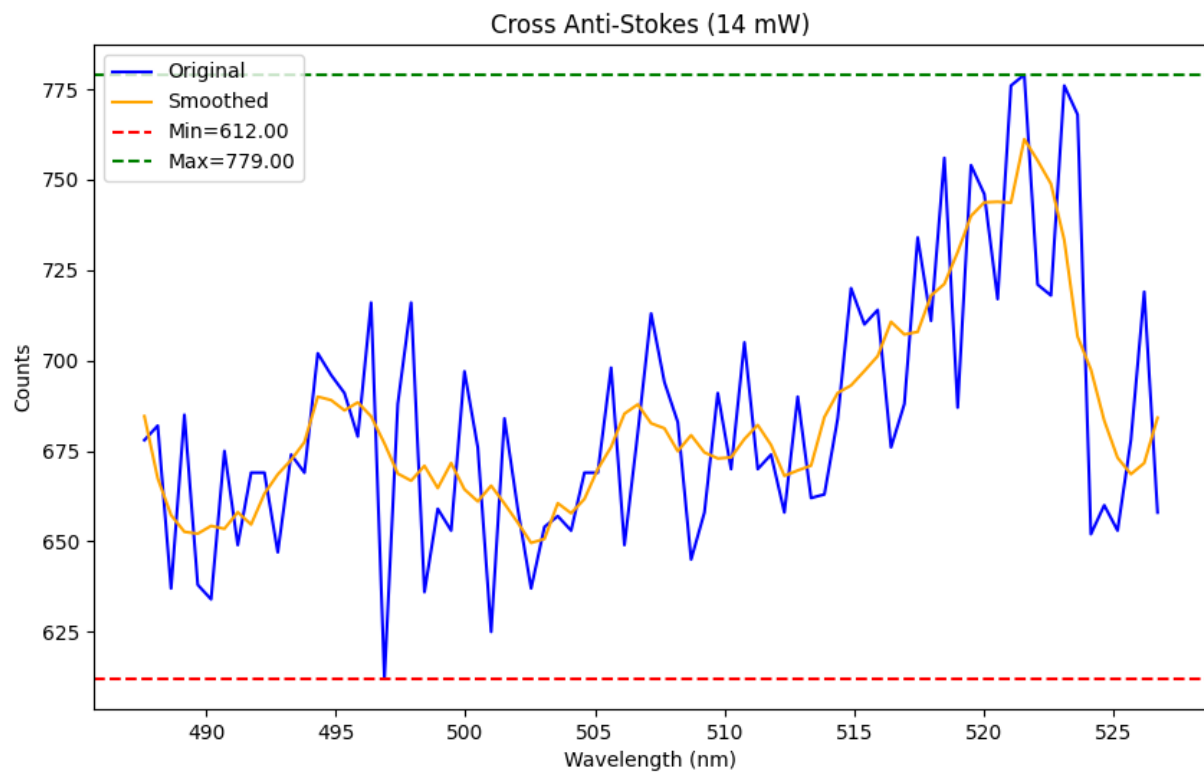
Freq=0.03, Amp=8092.41

Freq=0.02, Amp=8056.13

Freq=0.04, Amp=5301.08

Freq=0.05, Amp=4117.61

### Cross Anti-Stokes (14 mW)



Peak Info:

WL=521.56, Cnt=779.00

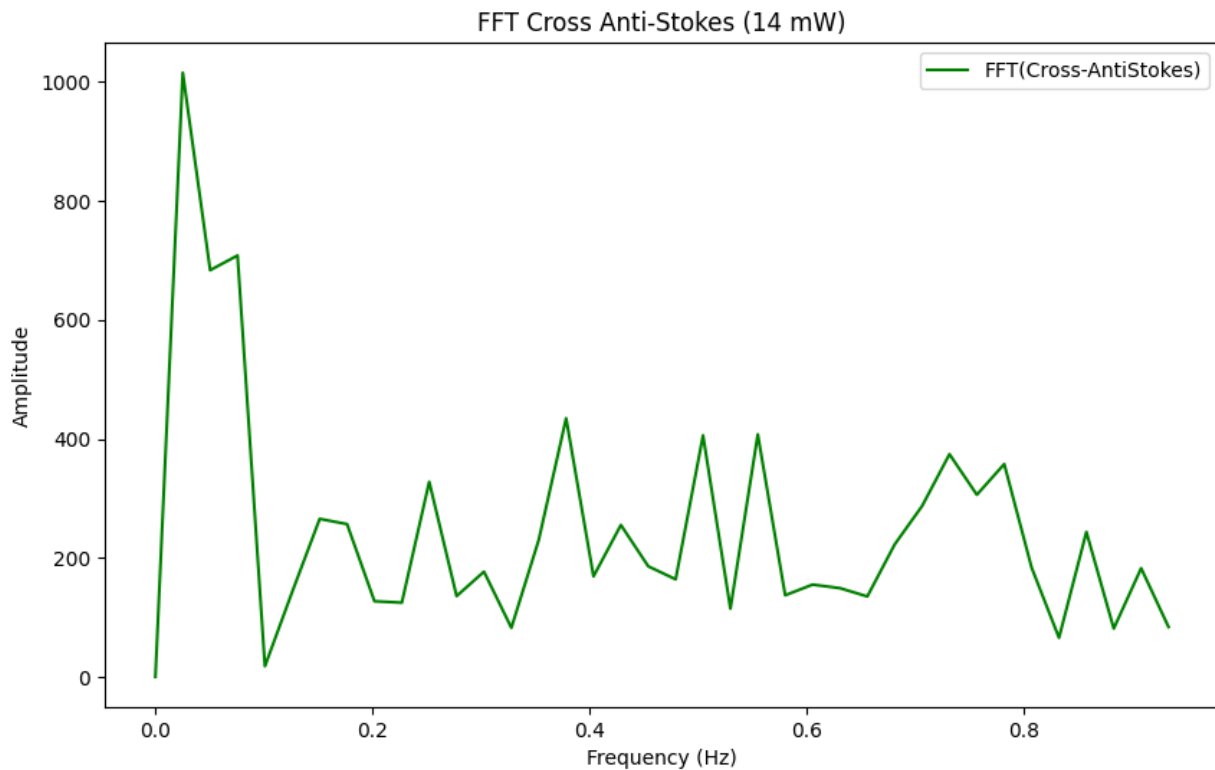
WL=523.10, Cnt=776.00

WL=518.48, Cnt=756.00

WL=519.50, Cnt=754.00

WL=517.45, Cnt=734.00

### FFT Cross Anti-Stokes (14 mW)



#### FFT Peak Info:

Freq=0.03, Amp=1015.31

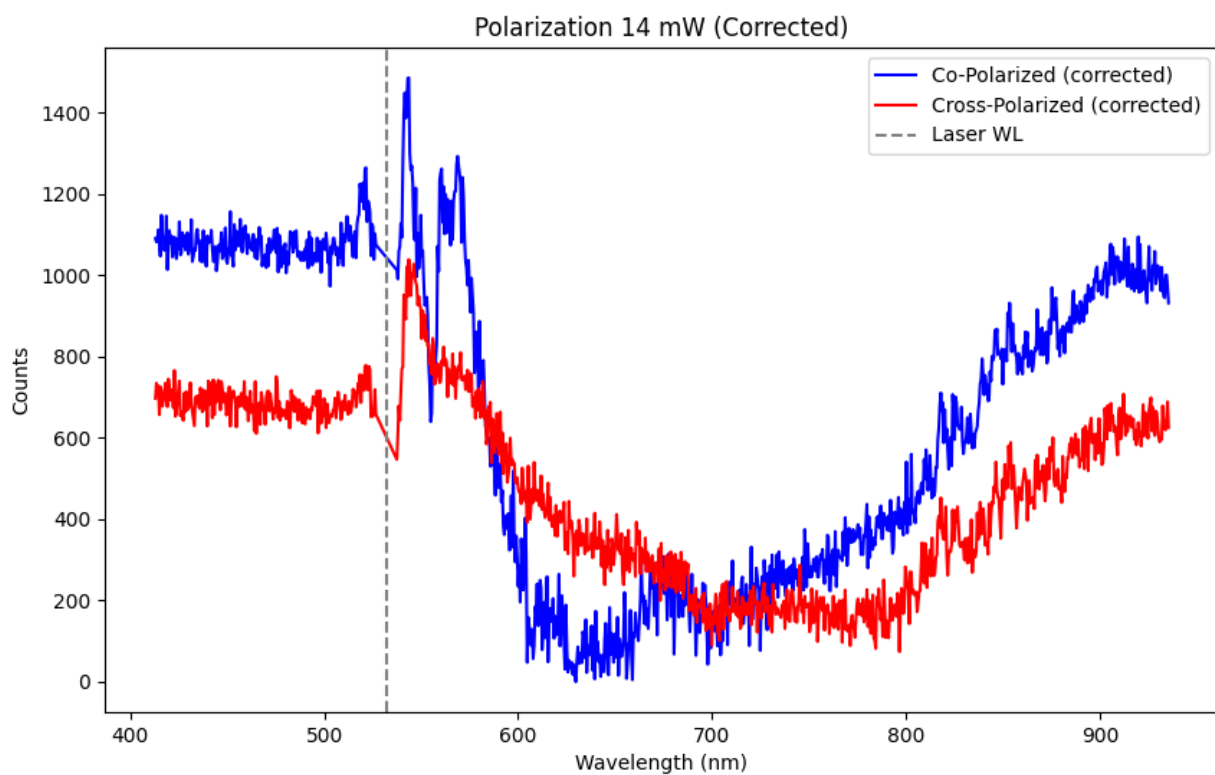
Freq=0.08, Amp=708.19

Freq=0.38, Amp=434.54

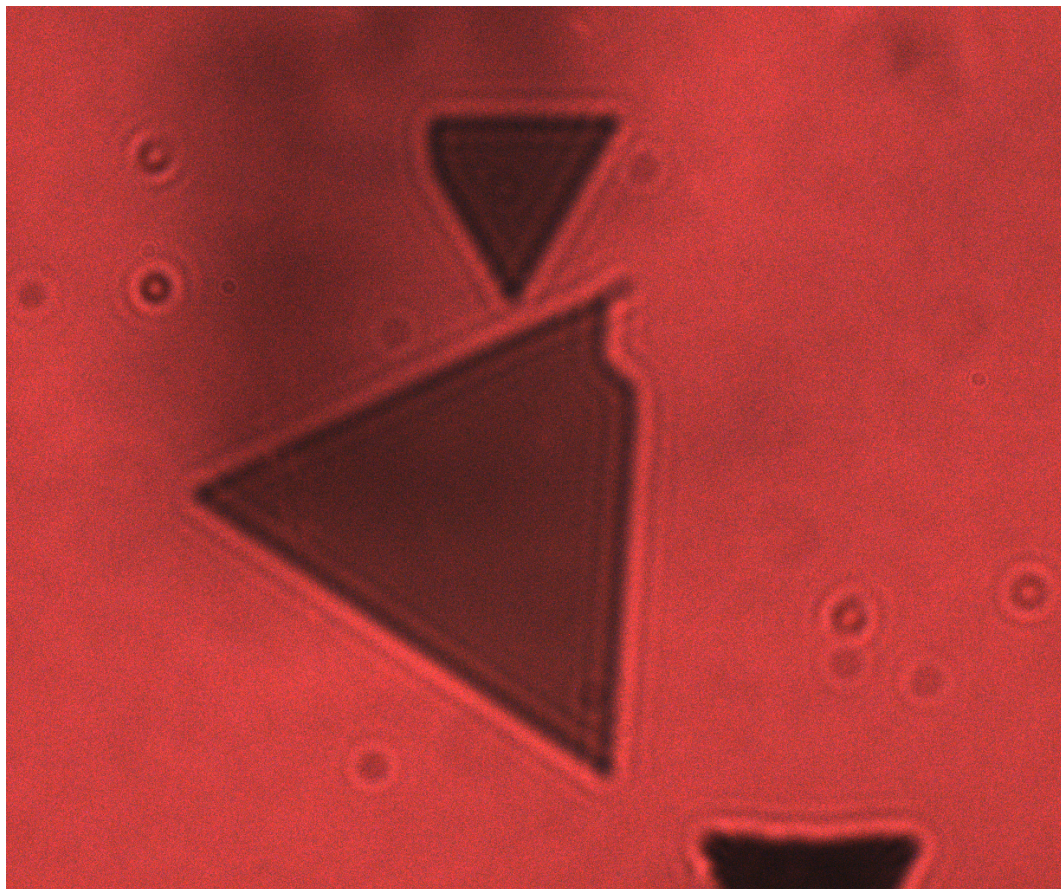
Freq=0.56, Amp=407.46

Freq=0.50, Amp=405.84

Polarization 14 mW



## Sample Image



# Spectrometry Analysis Report

Sample: M19

Laser Wavelength (after shift): 633.27 nm

Power Levels: 2.0, 4.0, 6.0, 8.0, 10.0, 12.0, 14.0 mW

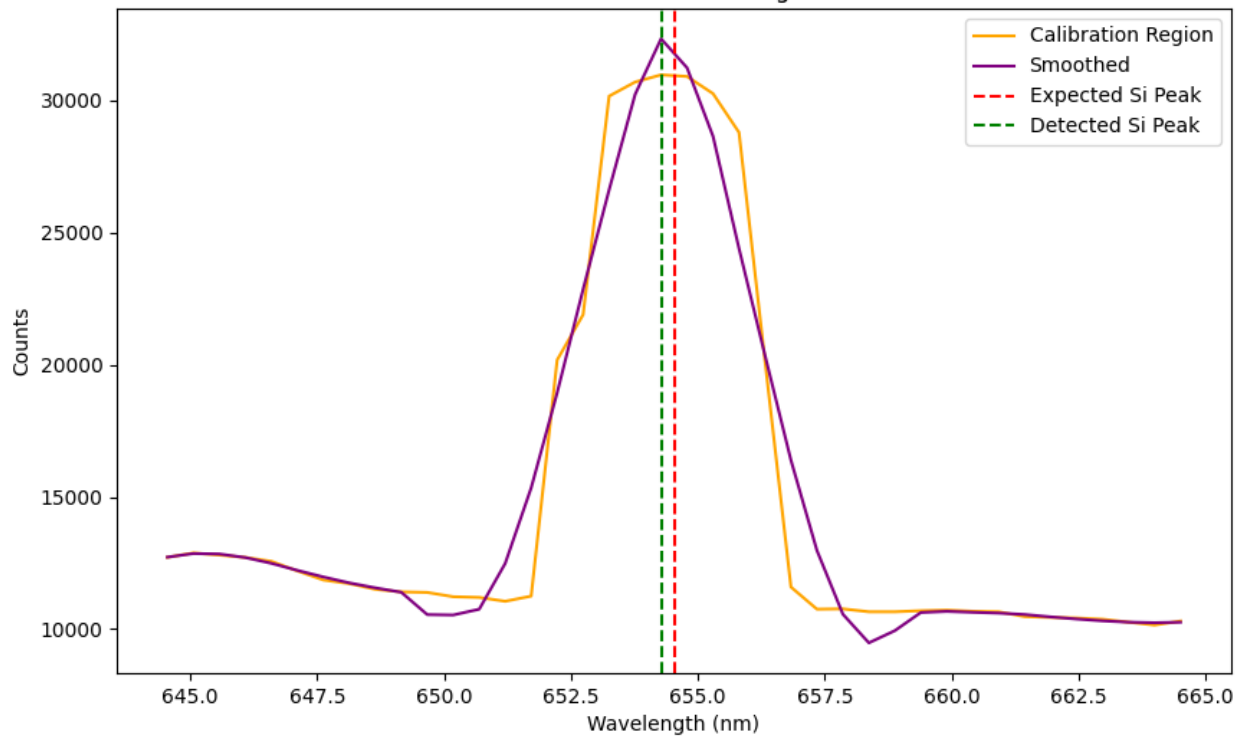
Thickness: 20.0 nm

Laser Filter Window:  $\pm 5.0$  nm

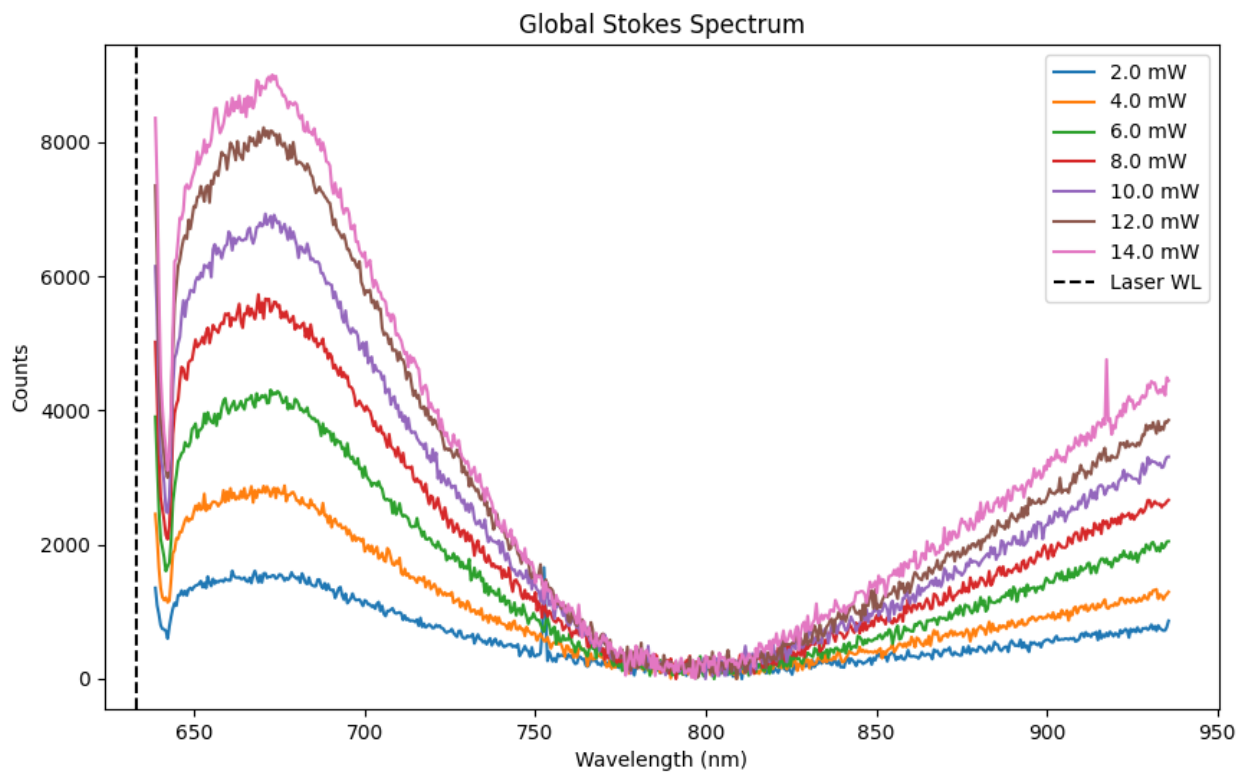
Calibration Shift: 0.27 nm

## Calibration Region

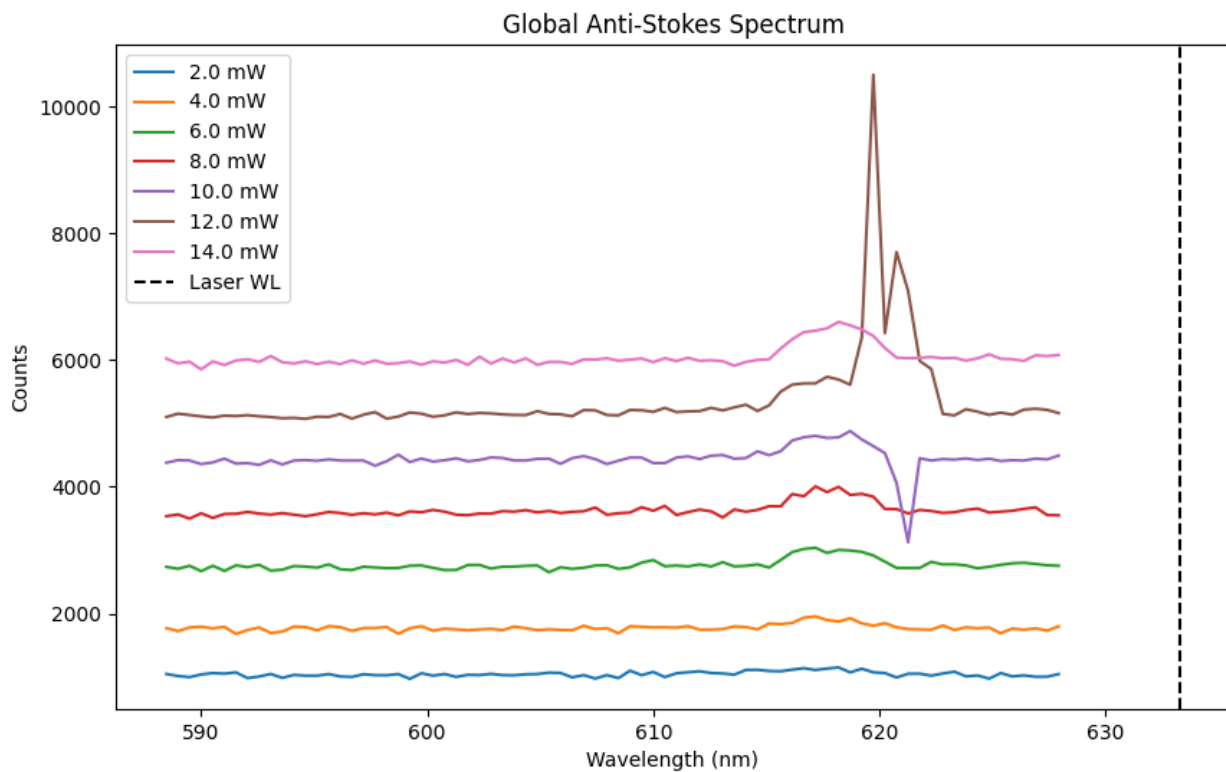
### Silicon Calibration Region



## Global Stokes Spectrum

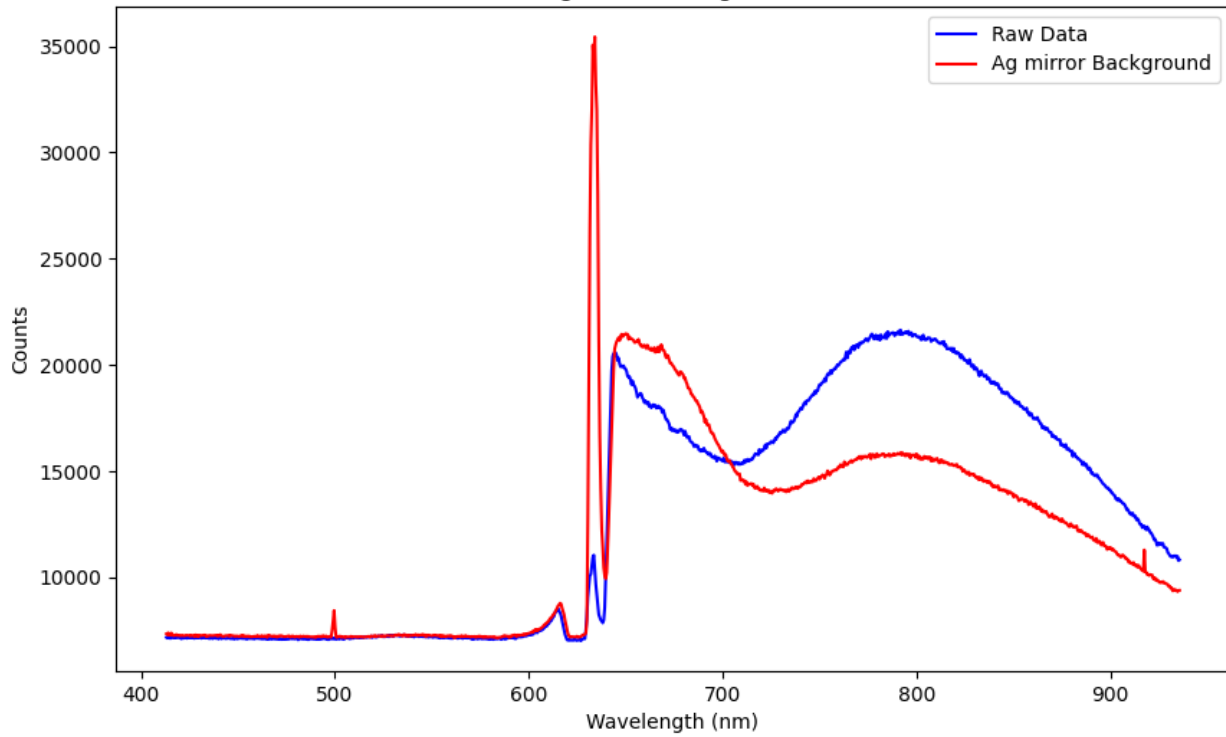


## Global Anti-Stokes Spectrum

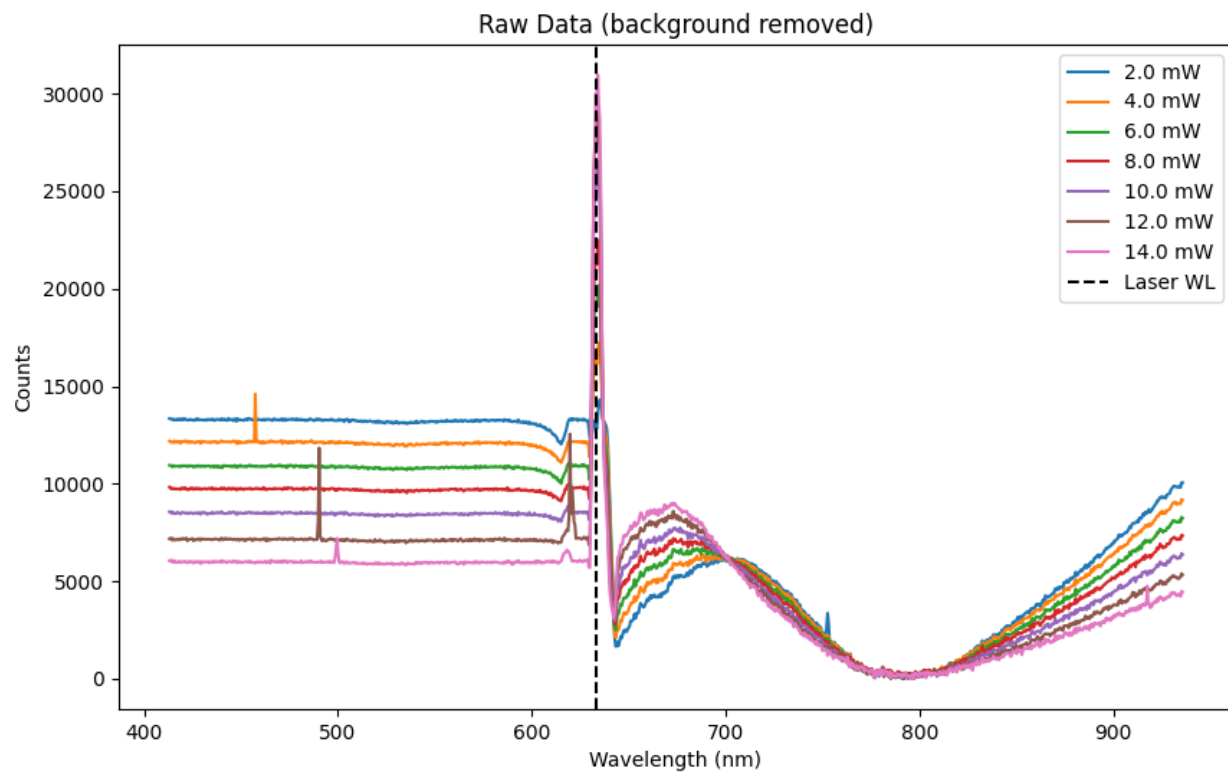


## Ag Mirror Background

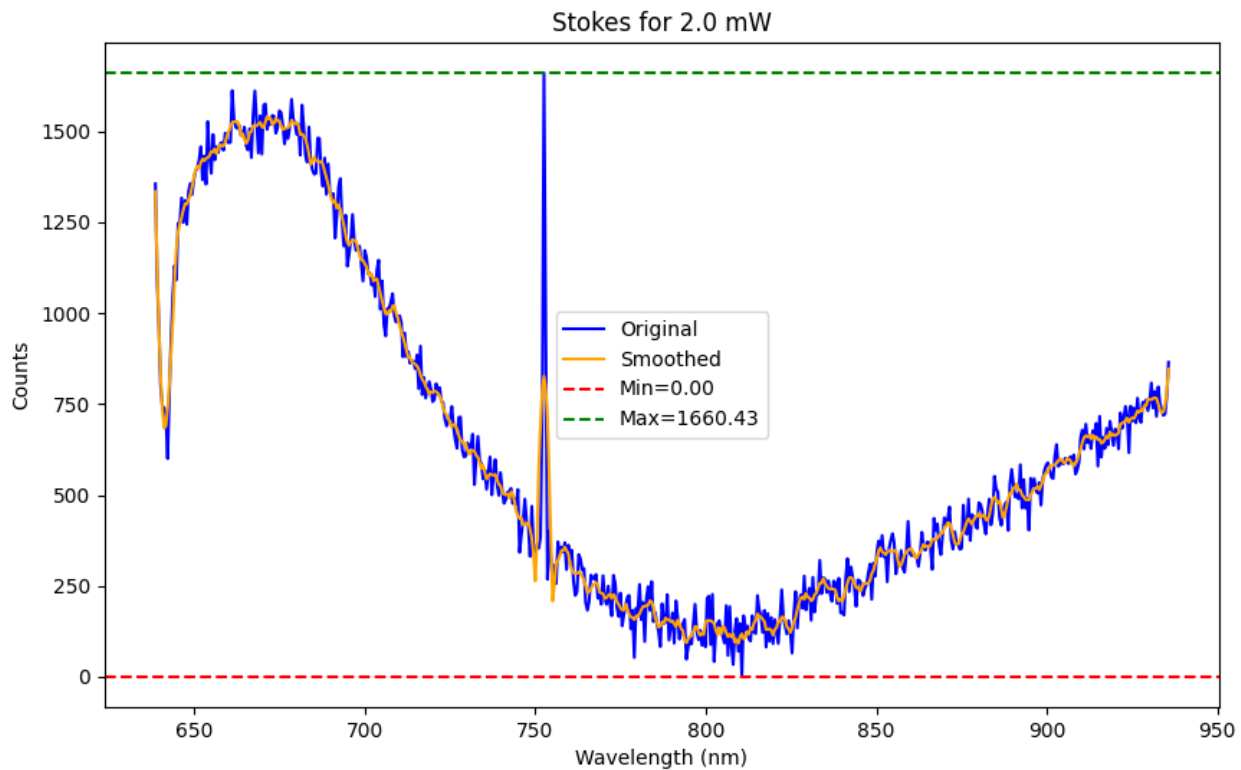
Ag Mirror Background



## Raw Data



## Stokes for 2.0 mW



Integral (Area) = 186038.68

Peak Info (Stokes):

WL=752.59, Cnt=1660.43

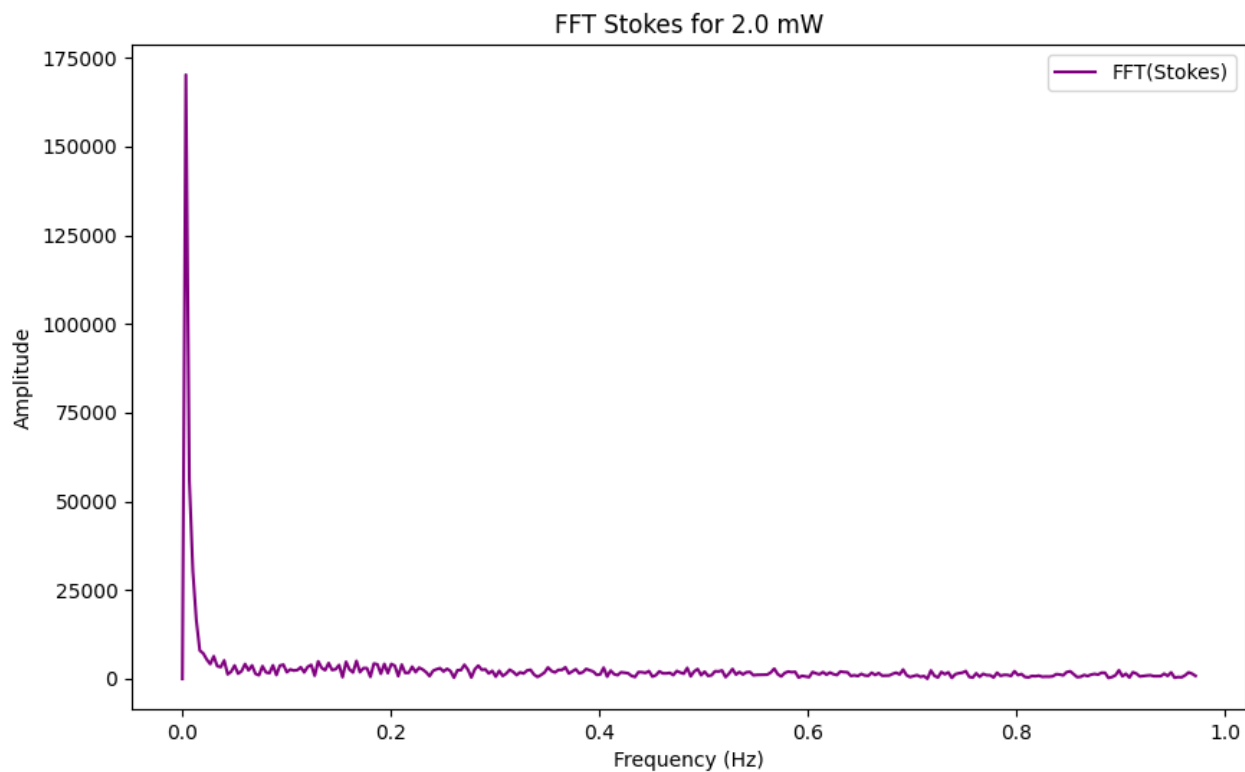
WL=661.20, Cnt=1611.41

WL=667.84, Cnt=1610.58

WL=678.58, Cnt=1587.49

WL=670.91, Cnt=1574.88

### FFT Stokes for 2.0 mW



Peak Info (FFT Stokes):

Freq=0.00, Amp=170260.99

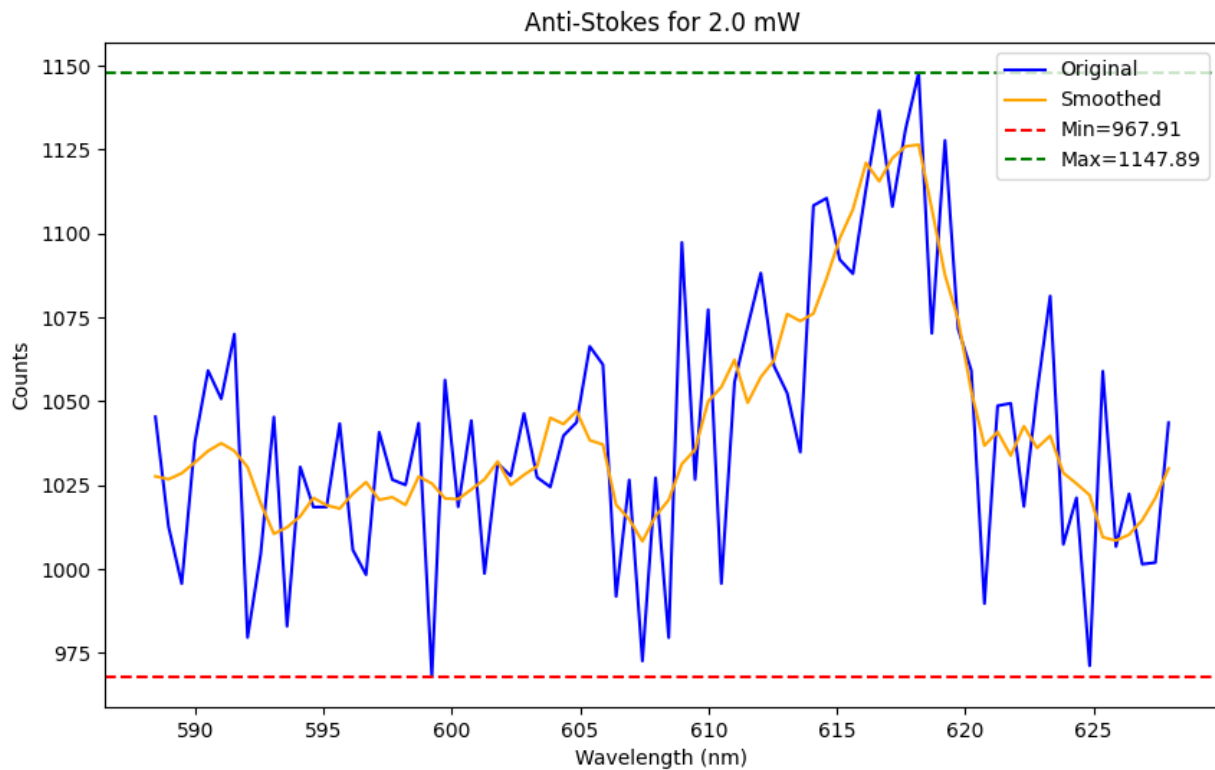
Freq=0.03, Amp=6373.67

Freq=0.04, Amp=5187.06

Freq=0.17, Amp=5056.82

Freq=0.13, Amp=4943.88

## Anti-Stokes for 2.0 mW



Integral (Area) = 41128.95

Peak Info (Anti-Stokes):

WL=618.19, Cnt=1147.89

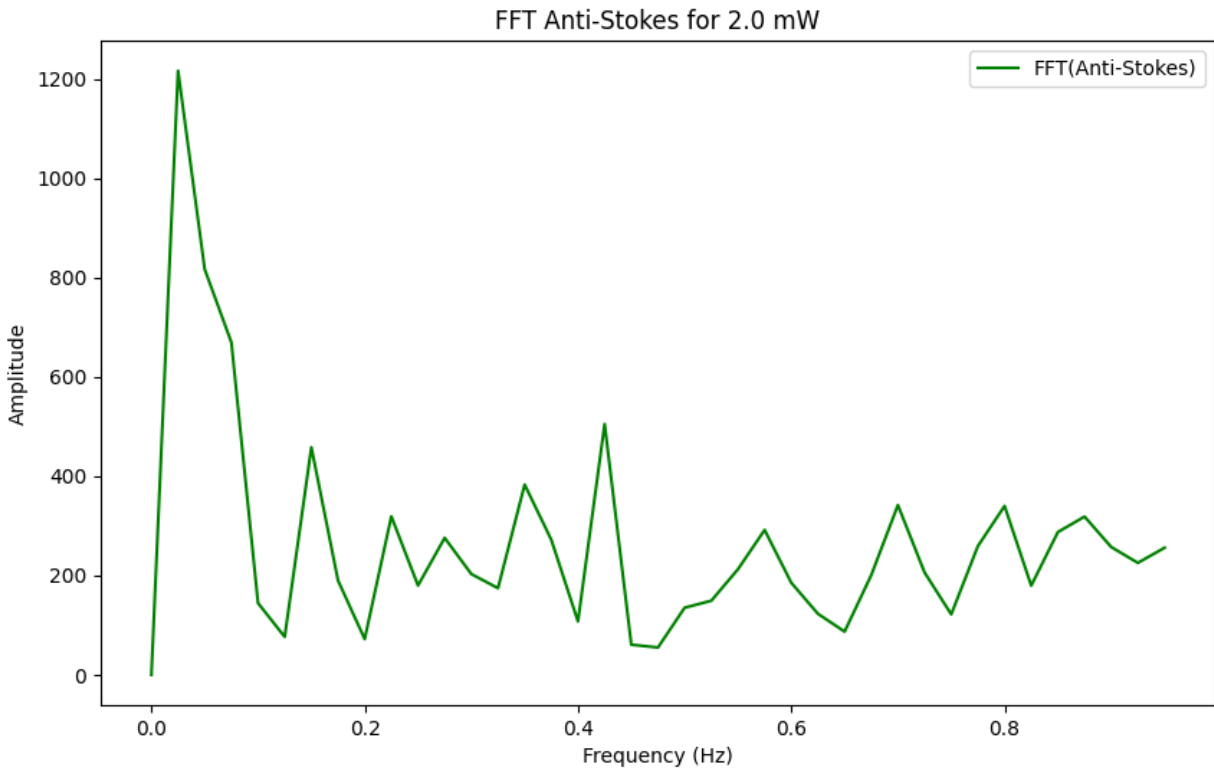
WL=616.65, Cnt=1136.63

WL=619.22, Cnt=1127.72

WL=614.60, Cnt=1110.52

WL=608.97, Cnt=1097.34

## FFT Anti-Stokes for 2.0 mW



Peak Info (FFT Anti-Stokes):

Freq=0.02, Amp=1216.16

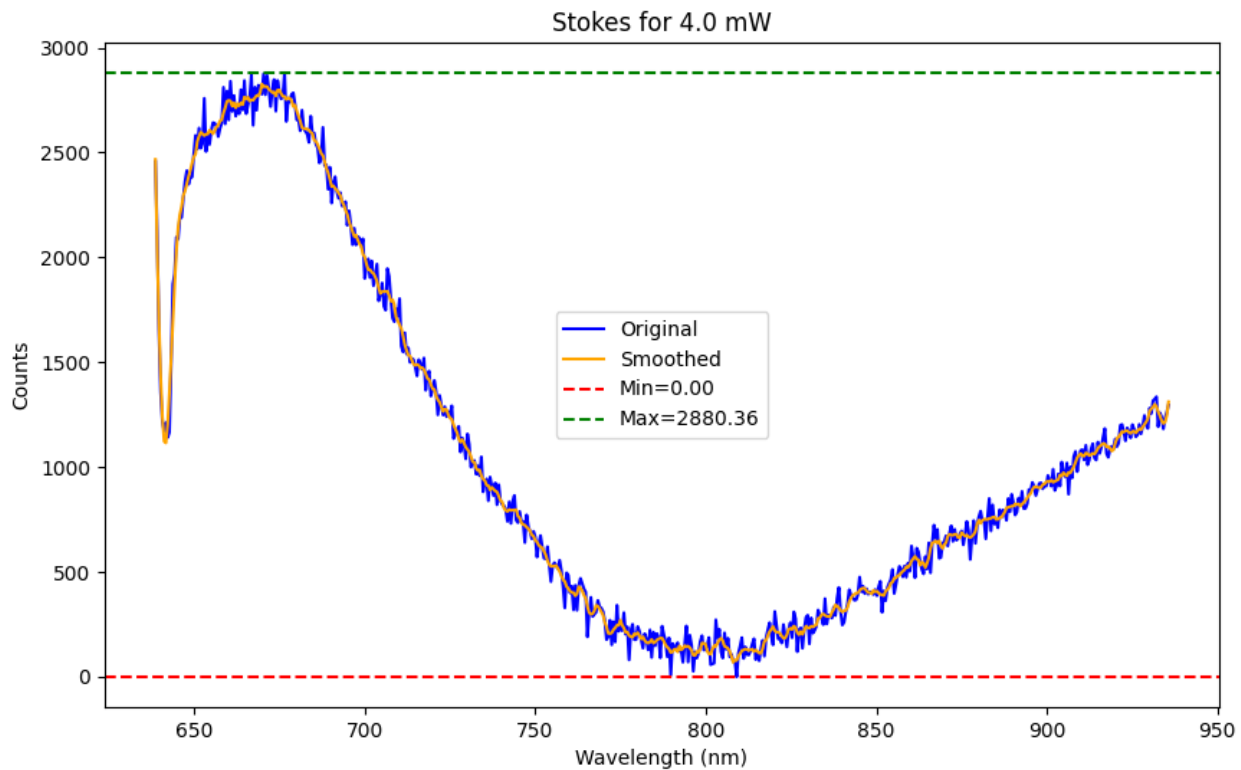
Freq=0.42, Amp=505.05

Freq=0.15, Amp=458.21

Freq=0.35, Amp=382.98

Freq=0.70, Amp=341.78

## Stokes for 4.0 mW



Integral (Area) = 312141.74

Peak Info (Stokes):

WL=676.54, Cnt=2880.36

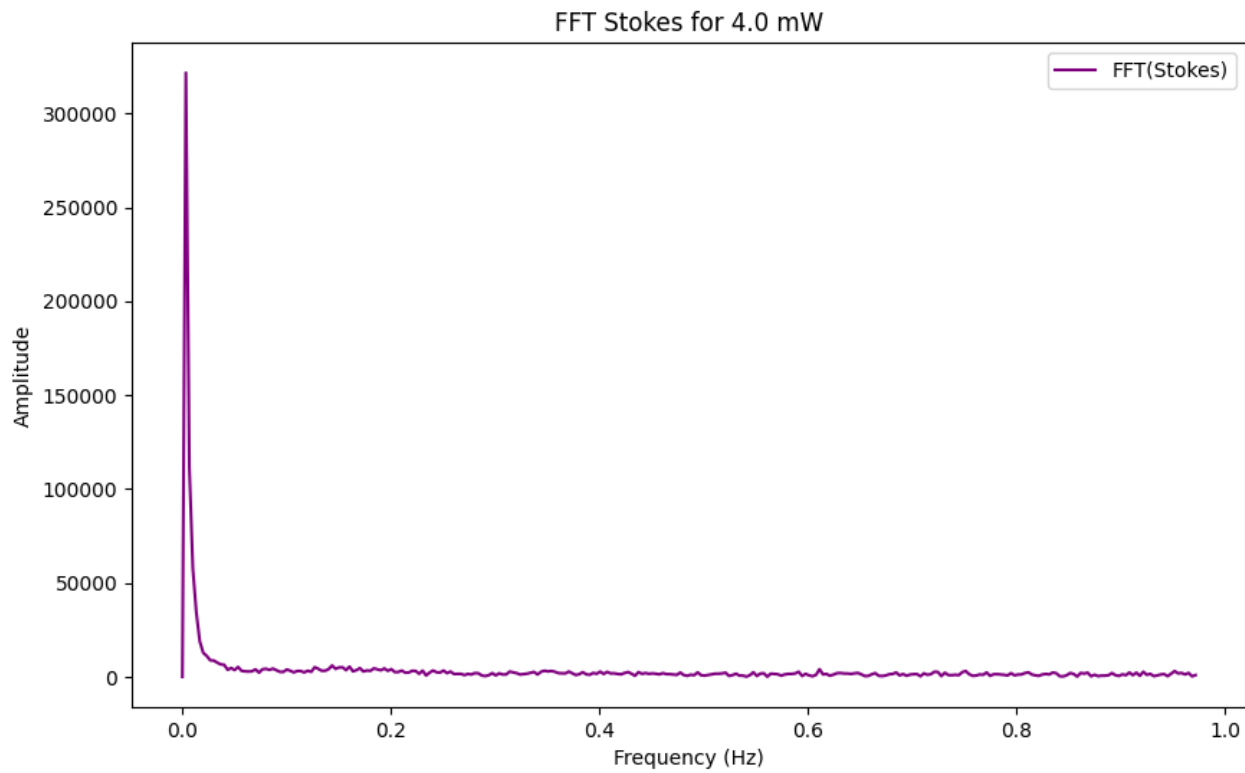
WL=670.40, Cnt=2874.63

WL=666.82, Cnt=2869.90

WL=671.42, Cnt=2866.74

WL=673.47, Cnt=2847.96

### FFT Stokes for 4.0 mW



Peak Info (FFT Stokes):

Freq=0.00, Amp=321647.17

Freq=0.14, Amp=6064.38

Freq=0.16, Amp=5464.07

Freq=0.05, Amp=5256.45

Freq=0.13, Amp=5132.59

### Anti-Stokes for 4.0 mW



Integral (Area) = 70057.13

Peak Info (Anti-Stokes):

WL=617.17, Cnt=1954.65

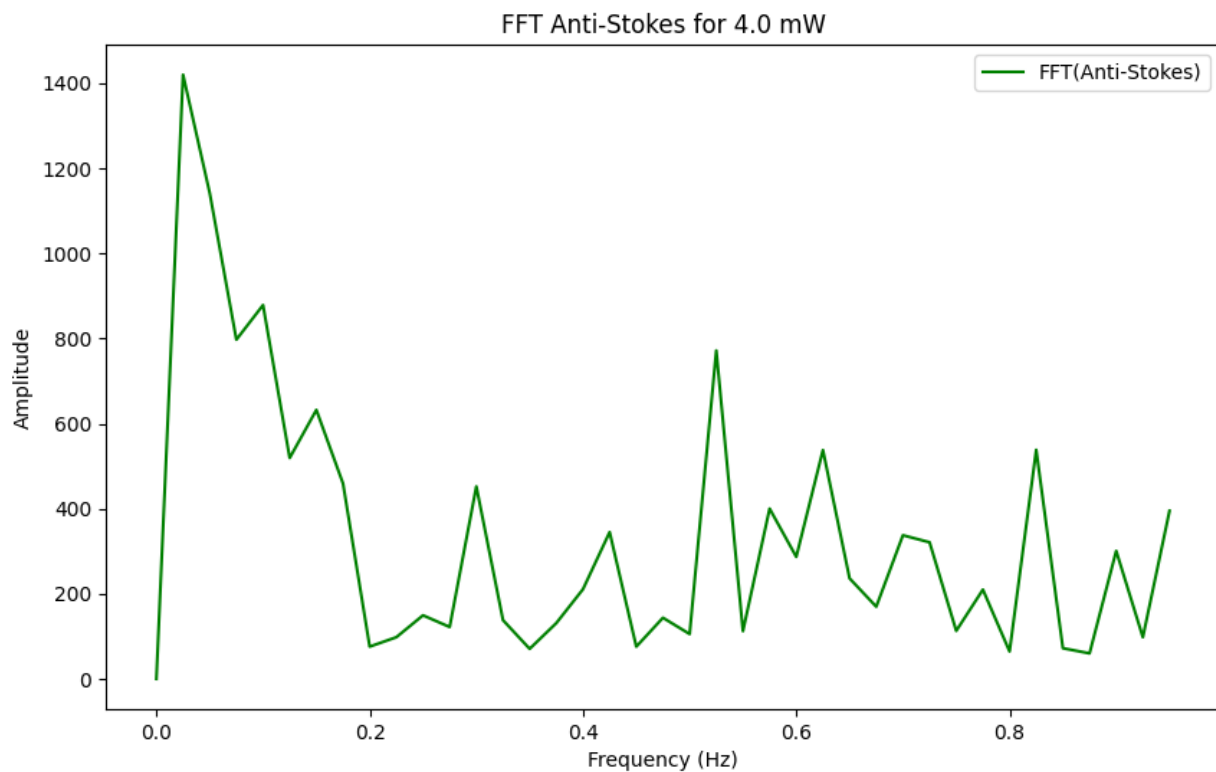
WL=618.70, Cnt=1925.59

WL=620.24, Cnt=1846.02

WL=615.12, Cnt=1840.28

WL=622.80, Cnt=1809.92

### FFT Anti-Stokes for 4.0 mW



Peak Info (FFT Anti-Stokes):

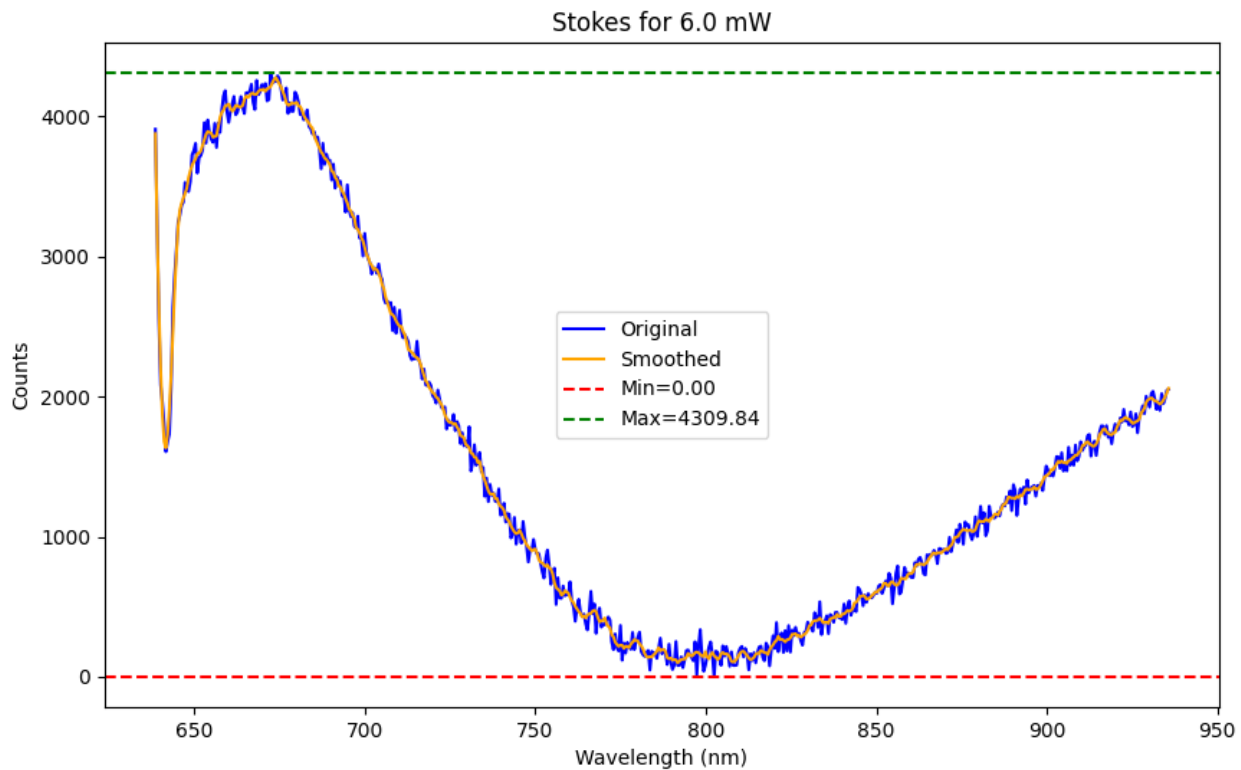
Freq=0.02, Amp=1419.98

Freq=0.10, Amp=878.65

Freq=0.15, Amp=632.19

Freq=0.82, Amp=538.28

## Stokes for 6.0 mW



Integral (Area) = 464894.53

Peak Info (Stokes):

WL=672.45, Cnt=4309.84

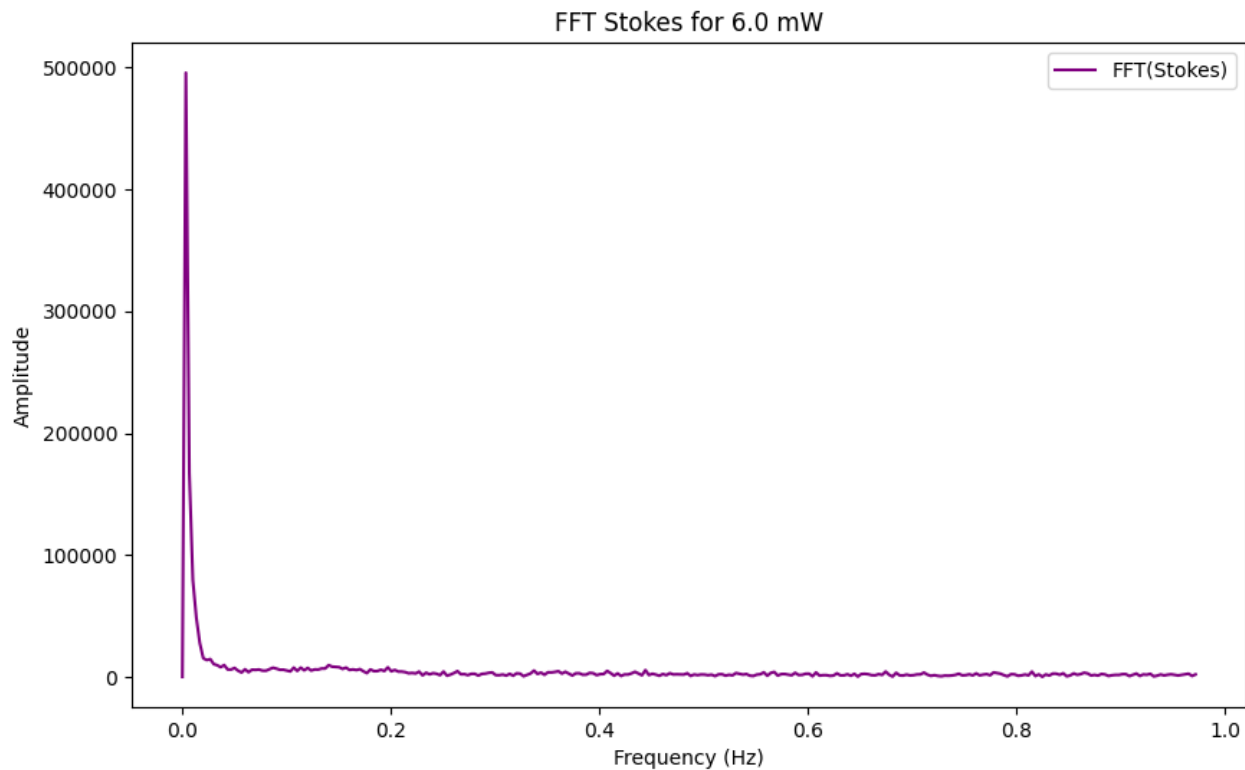
WL=674.49, Cnt=4288.11

WL=673.47, Cnt=4264.31

WL=668.36, Cnt=4254.85

WL=670.91, Cnt=4233.17

### FFT Stokes for 6.0 mW



Peak Info (FFT Stokes):

Freq=0.00, Amp=495717.99

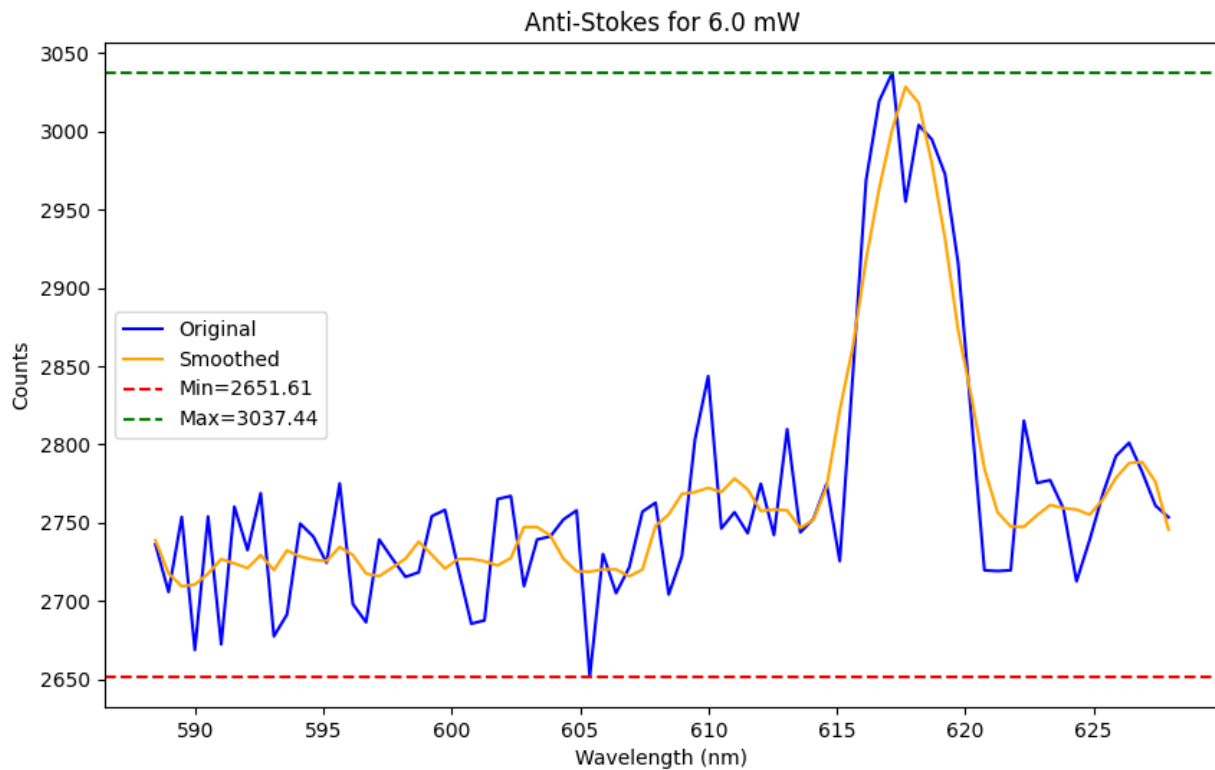
Freq=0.03, Amp=14580.32

Freq=0.04, Amp=9672.10

Freq=0.14, Amp=9613.62

Freq=0.20, Amp=7804.14

### Anti-Stokes for 6.0 mW



Integral (Area) = 109273.78

Peak Info (Anti-Stokes):

WL=617.17, Cnt=3037.44

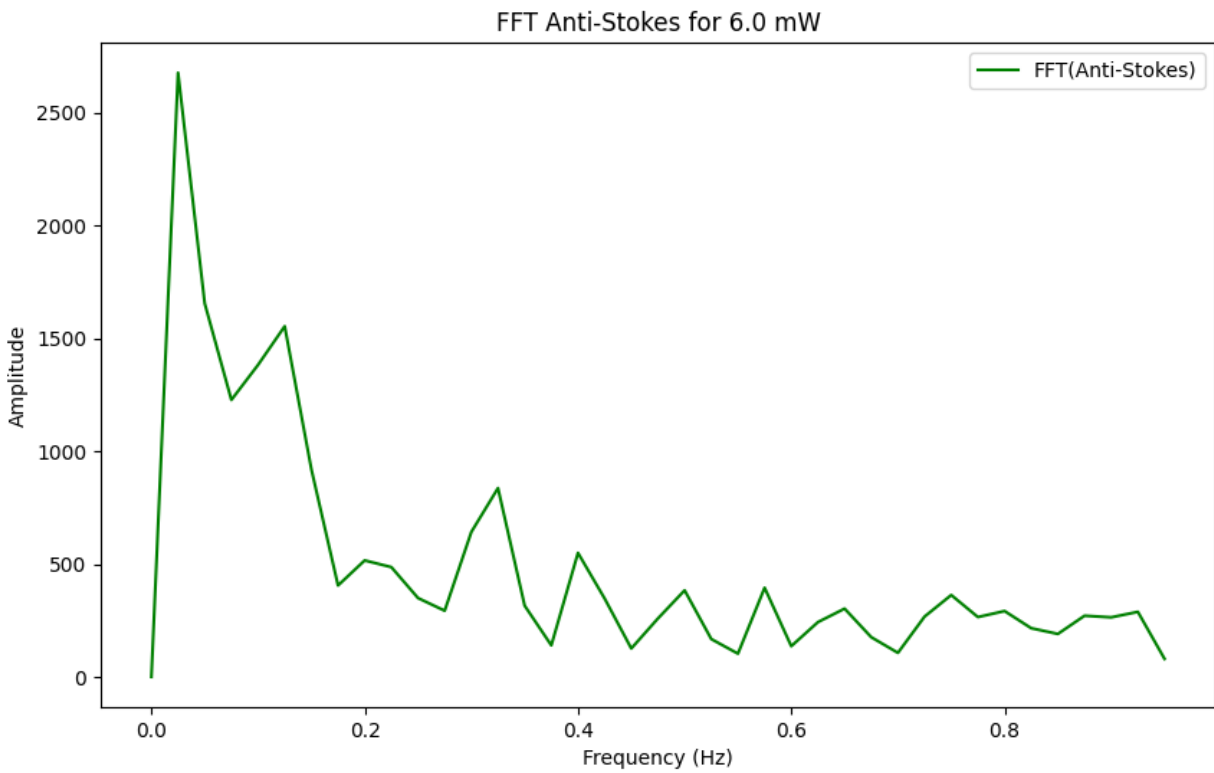
WL=618.19, Cnt=3004.08

WL=609.99, Cnt=2843.67

WL=622.29, Cnt=2815.22

WL=613.07, Cnt=2809.80

### FFT Anti-Stokes for 6.0 mW



Peak Info (FFT Anti-Stokes):

Freq=0.02, Amp=2678.26

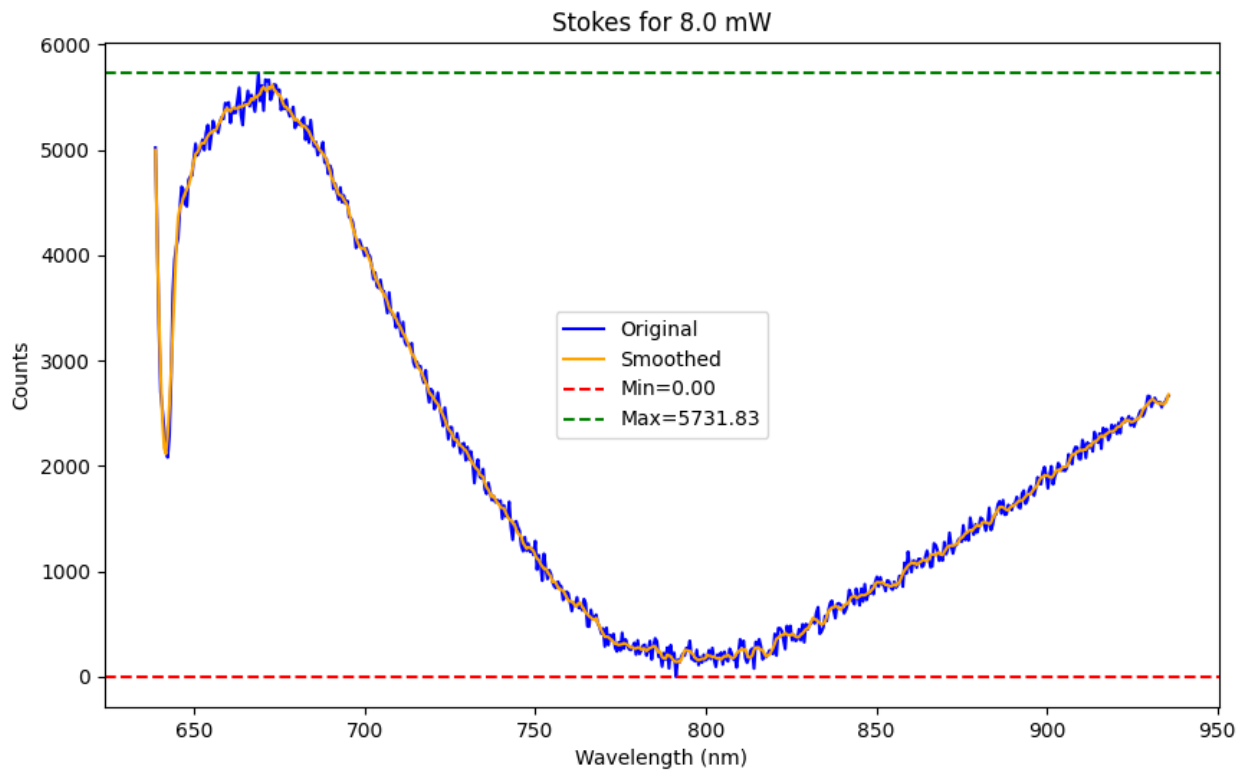
Freq=0.12, Amp=1554.40

Freq=0.32, Amp=836.84

Freq=0.40, Amp=549.53

Freq=0.20, Amp=516.23

## Stokes for 8.0 mW



Integral (Area) = 613917.92

Peak Info (Stokes):

WL=668.87, Cnt=5731.83

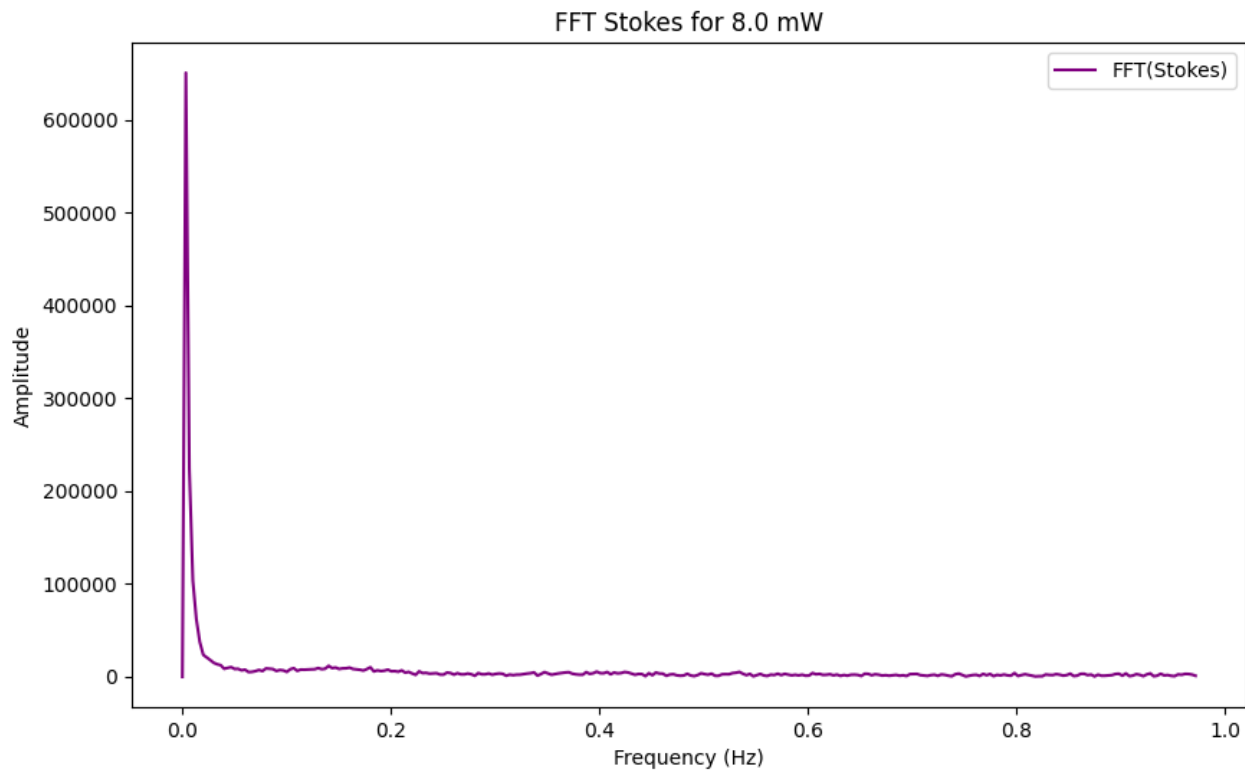
WL=670.91, Cnt=5666.83

WL=671.94, Cnt=5663.99

WL=673.47, Cnt=5620.96

WL=669.89, Cnt=5610.71

### FFT Stokes for 8.0 mW



Peak Info (FFT Stokes):

Freq=0.00, Amp=650712.25

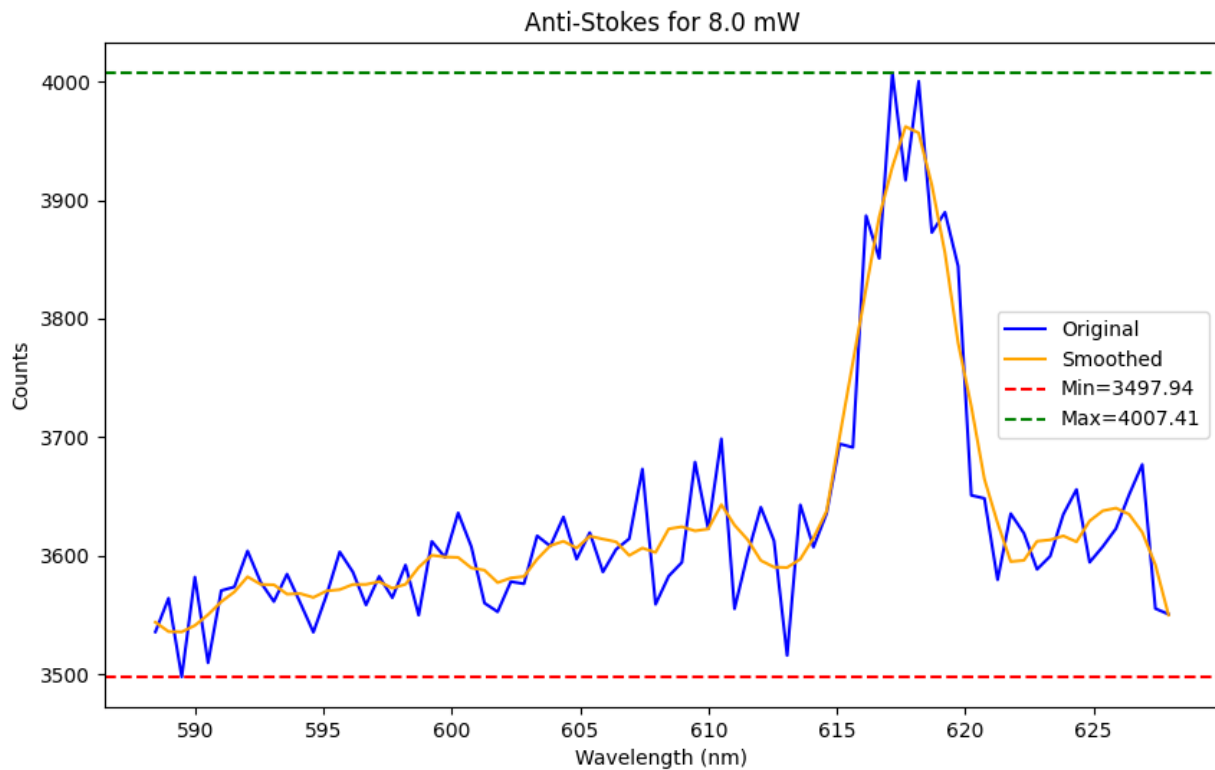
Freq=0.14, Amp=11893.95

Freq=0.05, Amp=10509.92

Freq=0.18, Amp=10321.84

Freq=0.15, Amp=10031.67

## Anti-Stokes for 8.0 mW



Integral (Area) = 143345.90

Peak Info (Anti-Stokes):

WL=617.17, Cnt=4007.41

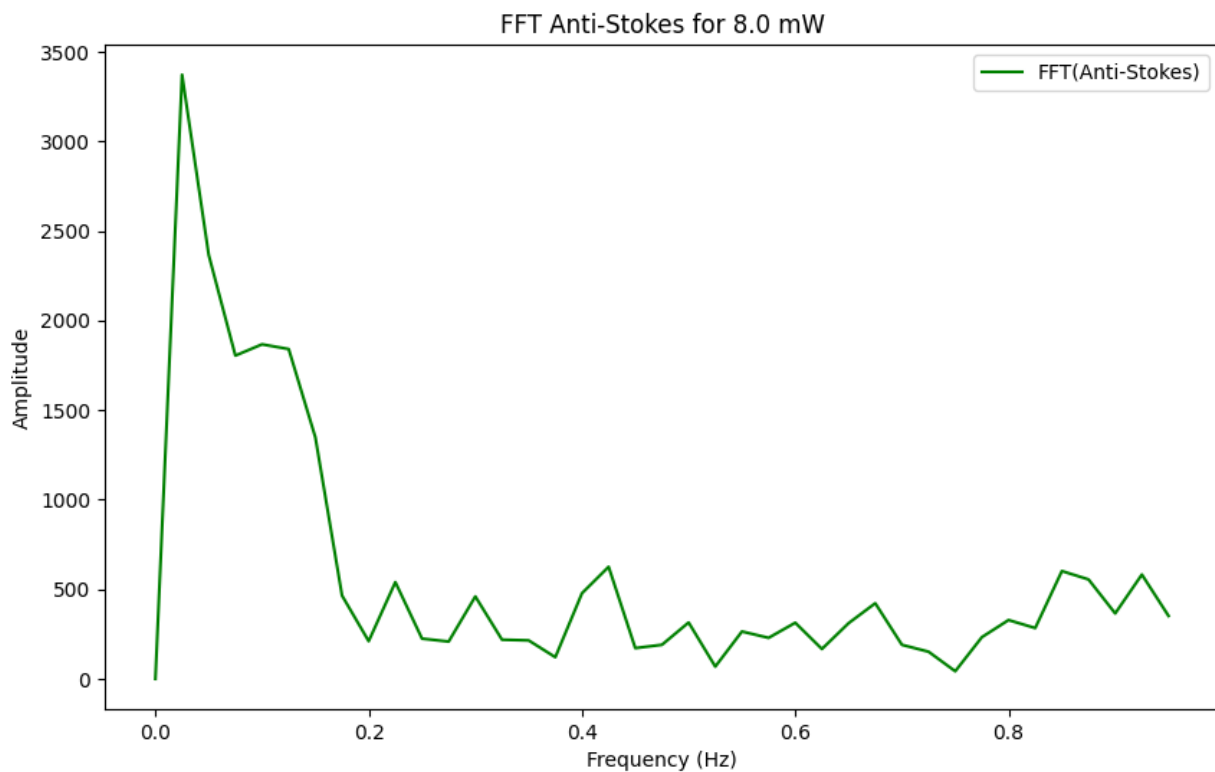
WL=618.19, Cnt=4000.21

WL=619.22, Cnt=3889.76

WL=616.14, Cnt=3886.89

WL=610.50, Cnt=3698.69

### FFT Anti-Stokes for 8.0 mW



Peak Info (FFT Anti-Stokes):

Freq=0.02, Amp=3372.80

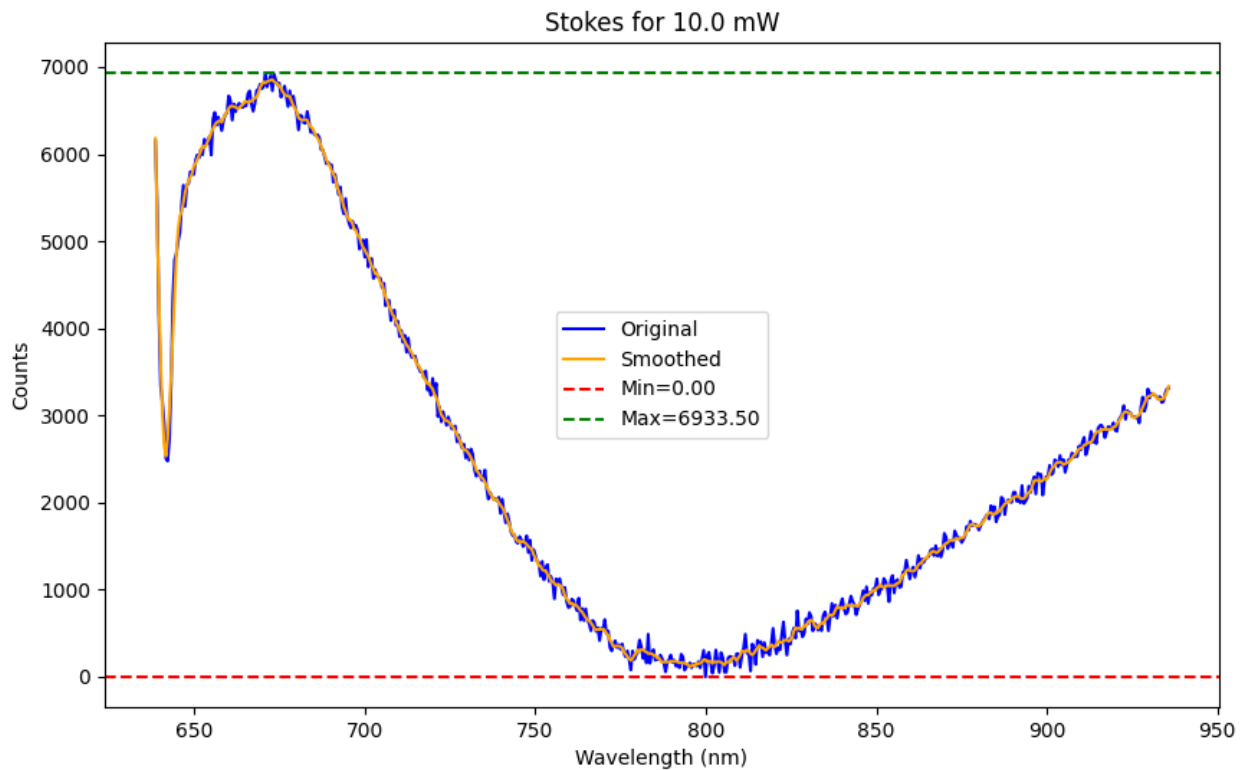
Freq=0.10, Amp=1867.71

Freq=0.42, Amp=625.62

Freq=0.85, Amp=601.86

Freq=0.92, Amp=582.31

## Stokes for 10.0 mW



Integral (Area) = 743936.12

Peak Info (Stokes):

WL=670.91, Cnt=6933.50

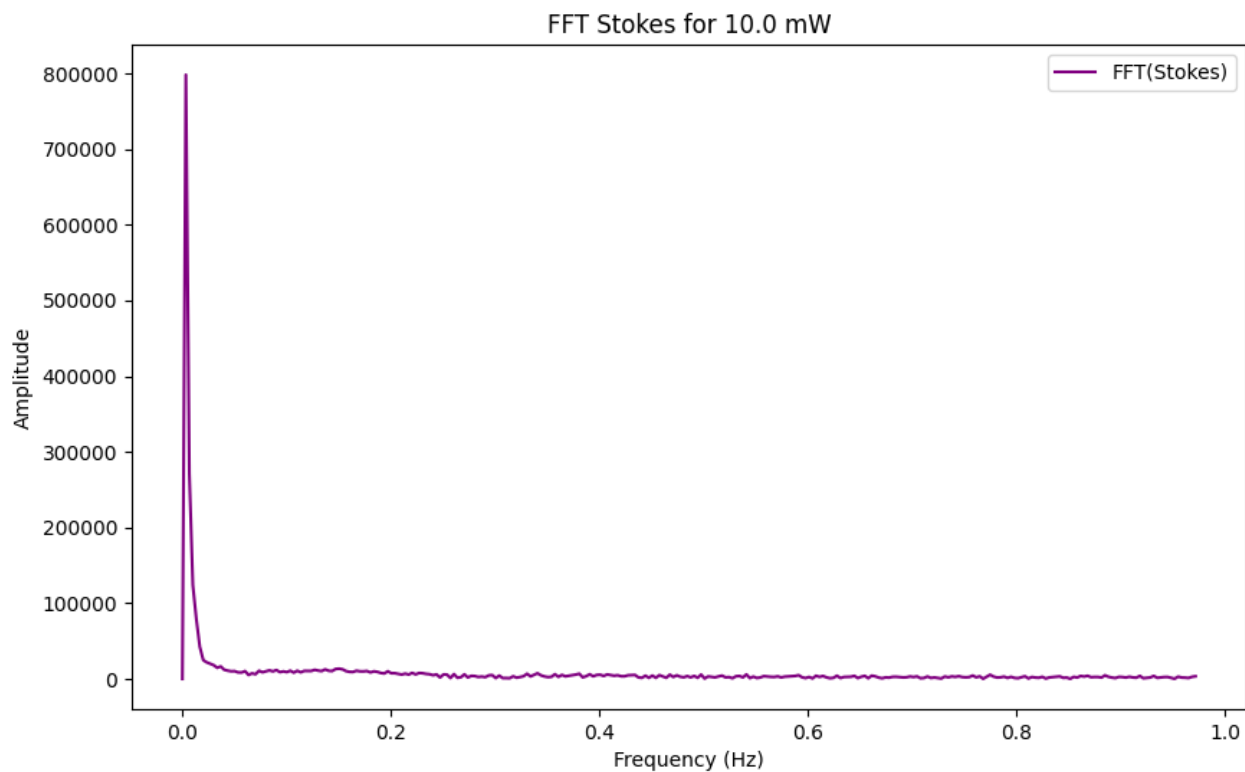
WL=673.47, Cnt=6916.84

WL=672.45, Cnt=6899.93

WL=675.00, Cnt=6813.88

WL=669.38, Cnt=6801.52

## FFT Stokes for 10.0 mW



Peak Info (FFT Stokes):

Freq=0.00, Amp=798269.78

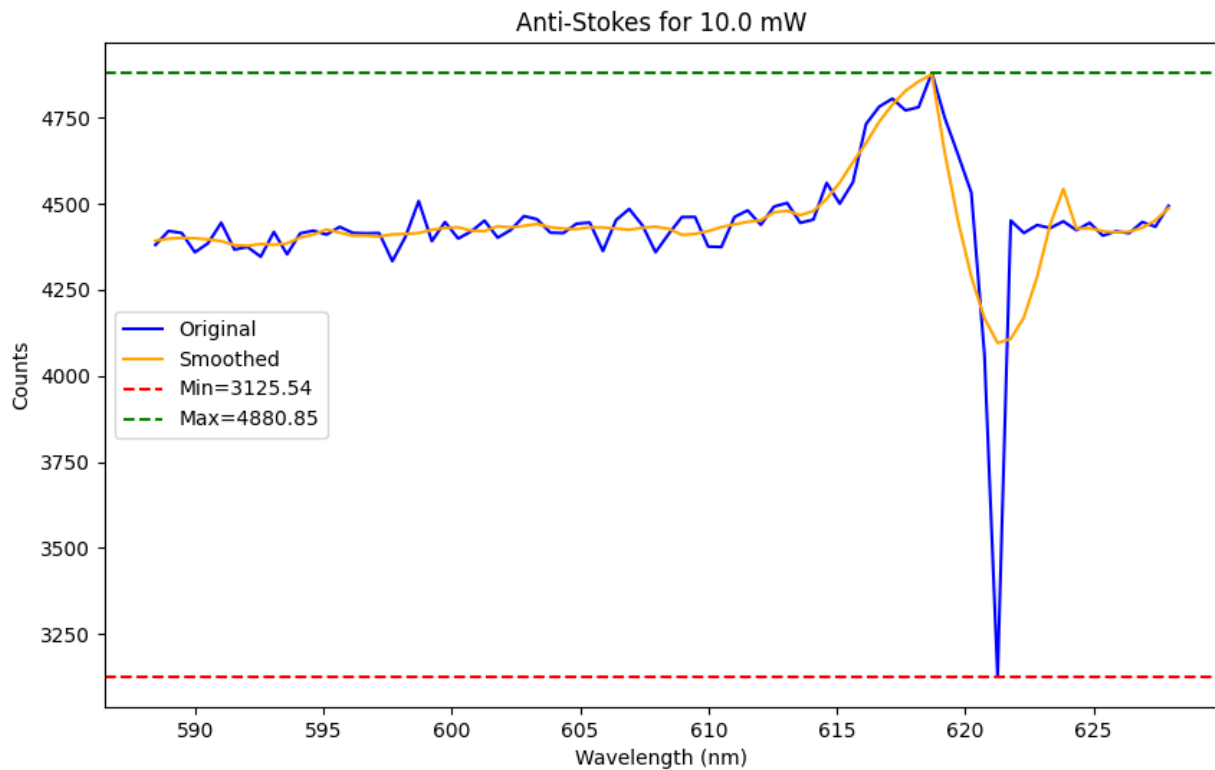
Freq=0.04, Amp=16435.01

Freq=0.15, Amp=13472.43

Freq=0.14, Amp=12538.92

Freq=0.13, Amp=11943.87

## Anti-Stokes for 10.0 mW



Integral (Area) = 175388.86

Peak Info (Anti-Stokes):

WL=618.70, Cnt=4880.85

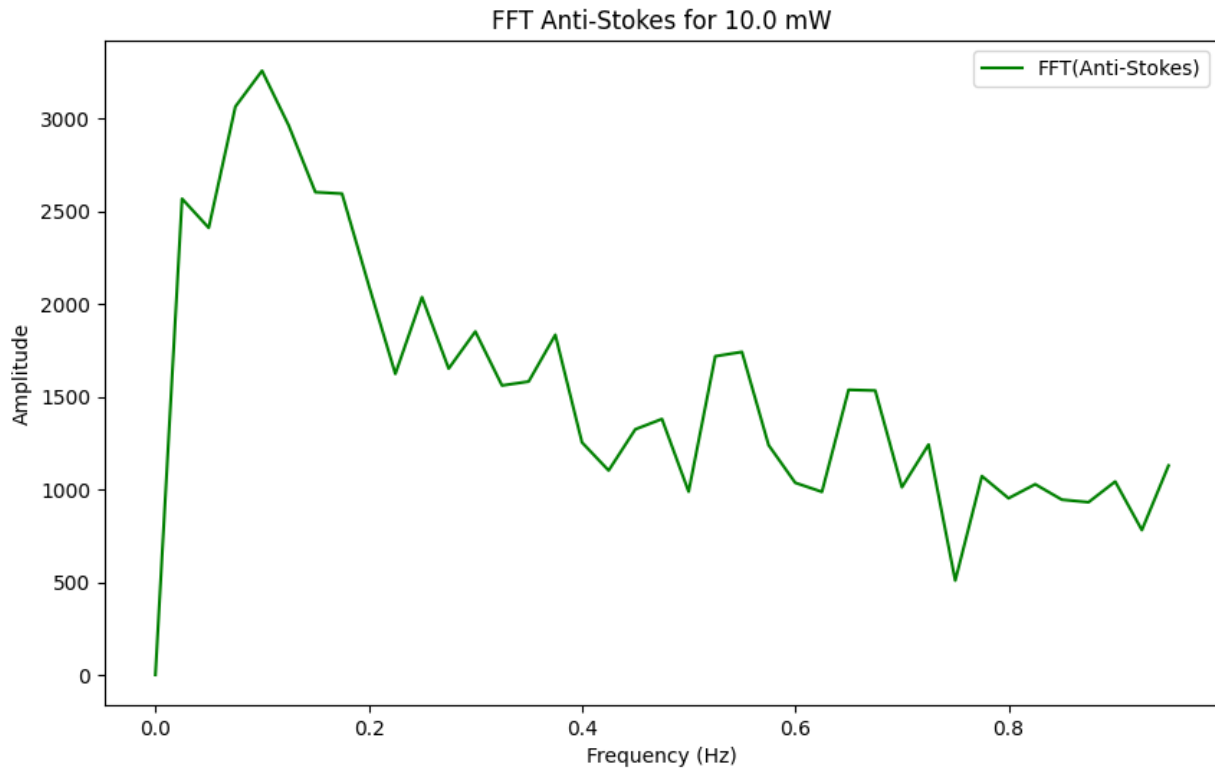
WL=617.17, Cnt=4805.52

WL=614.60, Cnt=4560.89

WL=598.71, Cnt=4508.08

WL=613.07, Cnt=4502.66

### FFT Anti-Stokes for 10.0 mW



Peak Info (FFT Anti-Stokes):

Freq=0.10, Amp=3255.84

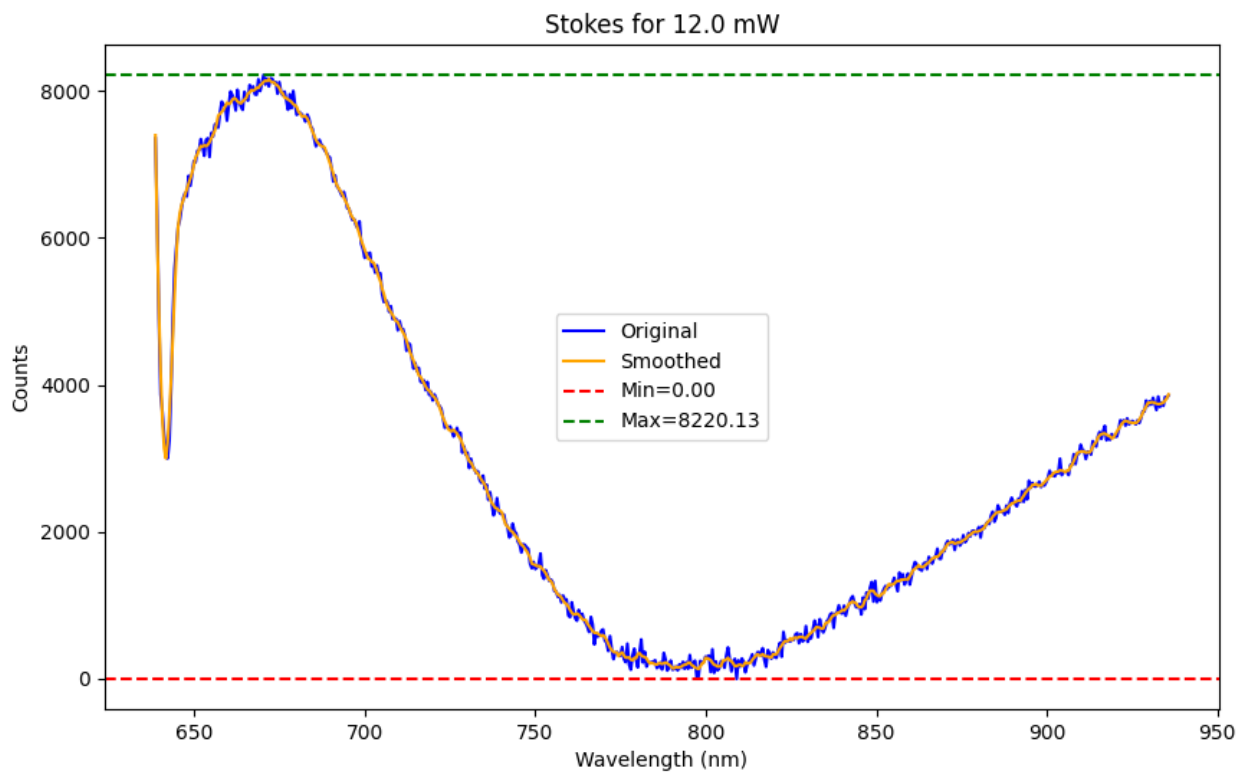
Freq=0.02, Amp=2565.93

Freq=0.25, Amp=2035.62

Freq=0.30, Amp=1850.31

Freq=0.37, Amp=1832.52

## Stokes for 12.0 mW



Integral (Area) = 877826.93

Peak Info (Stokes):

WL=670.40, Cnt=8220.13

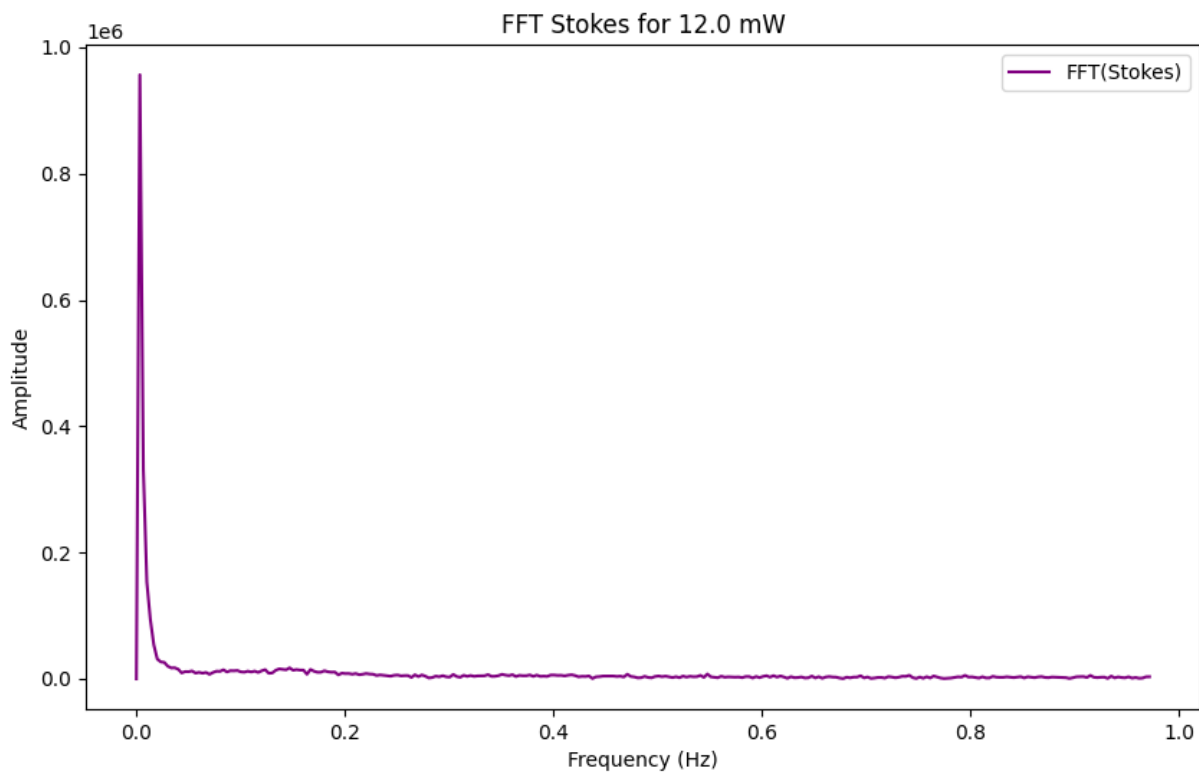
WL=672.45, Cnt=8173.63

WL=671.42, Cnt=8171.77

WL=668.87, Cnt=8157.91

WL=675.00, Cnt=8119.92

## FFT Stokes for 12.0 mW



Peak Info (FFT Stokes):

Freq=0.00, Amp=956706.85

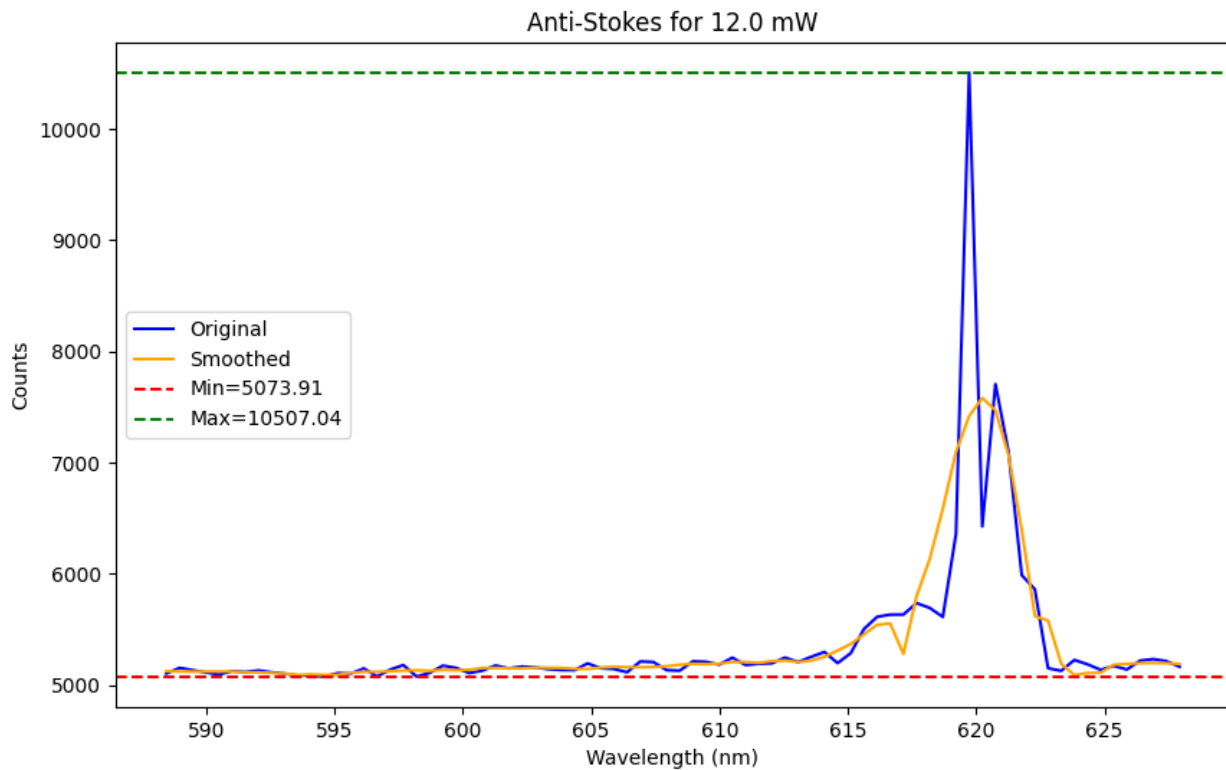
Freq=0.04, Amp=17577.76

Freq=0.15, Amp=17505.77

Freq=0.14, Amp=15812.63

Freq=0.17, Amp=14909.21

### Anti-Stokes for 12.0 mW



Integral (Area) = 212412.49

Peak Info (Anti-Stokes):

WL=619.73, Cnt=10507.04

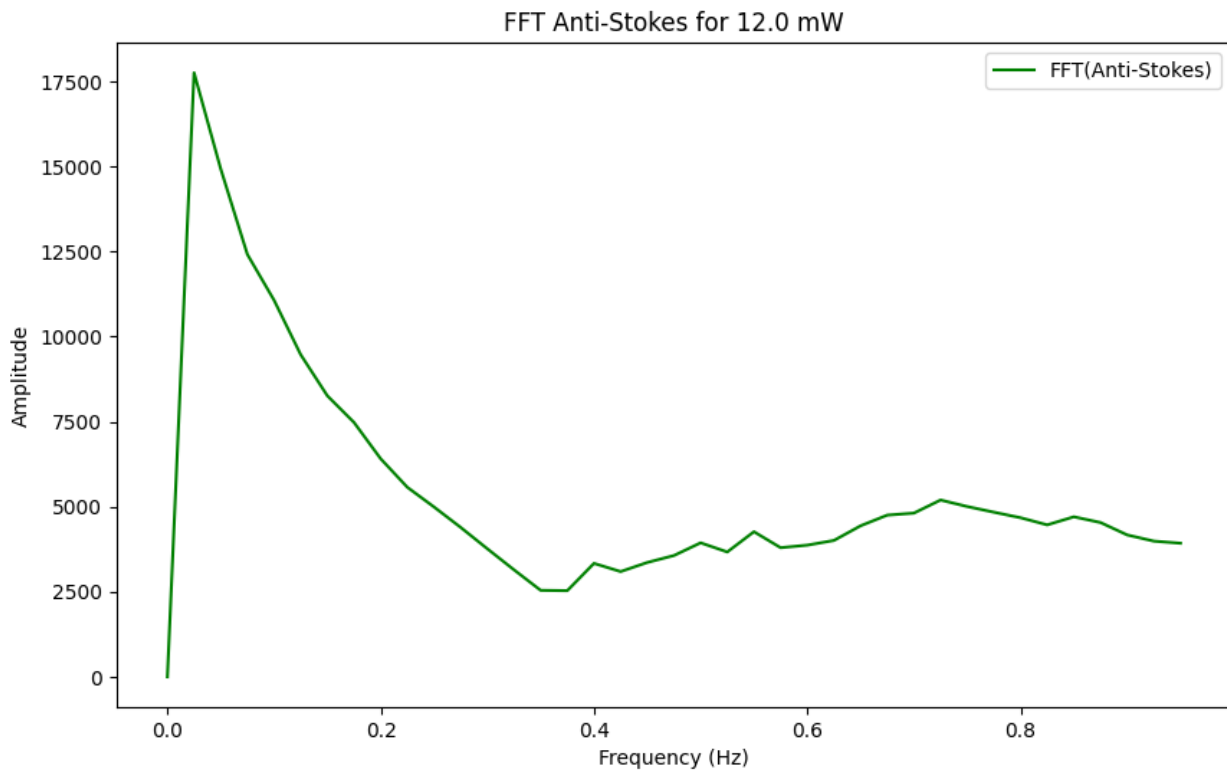
WL=620.75, Cnt=7707.24

WL=617.68, Cnt=5737.12

WL=614.09, Cnt=5297.53

WL=612.55, Cnt=5247.14

### FFT Anti-Stokes for 12.0 mW



Peak Info (FFT Anti-Stokes):

Freq=0.02, Amp=17754.71

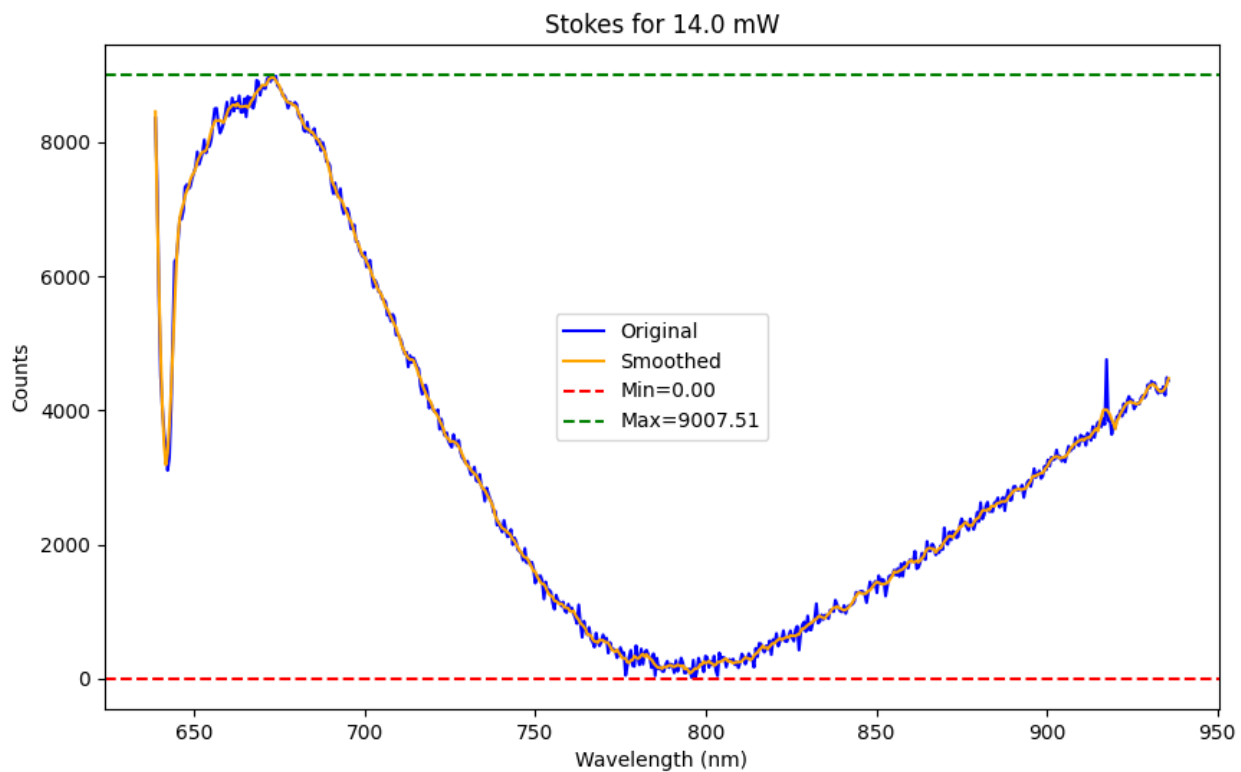
Freq=0.72, Amp=5197.29

Freq=0.85, Amp=4704.00

Freq=0.55, Amp=4266.03

Freq=0.50, Amp=3939.63

## Stokes for 14.0 mW



Integral (Area) = 968822.77

Peak Info (Stokes):

WL=672.96, Cnt=9007.51

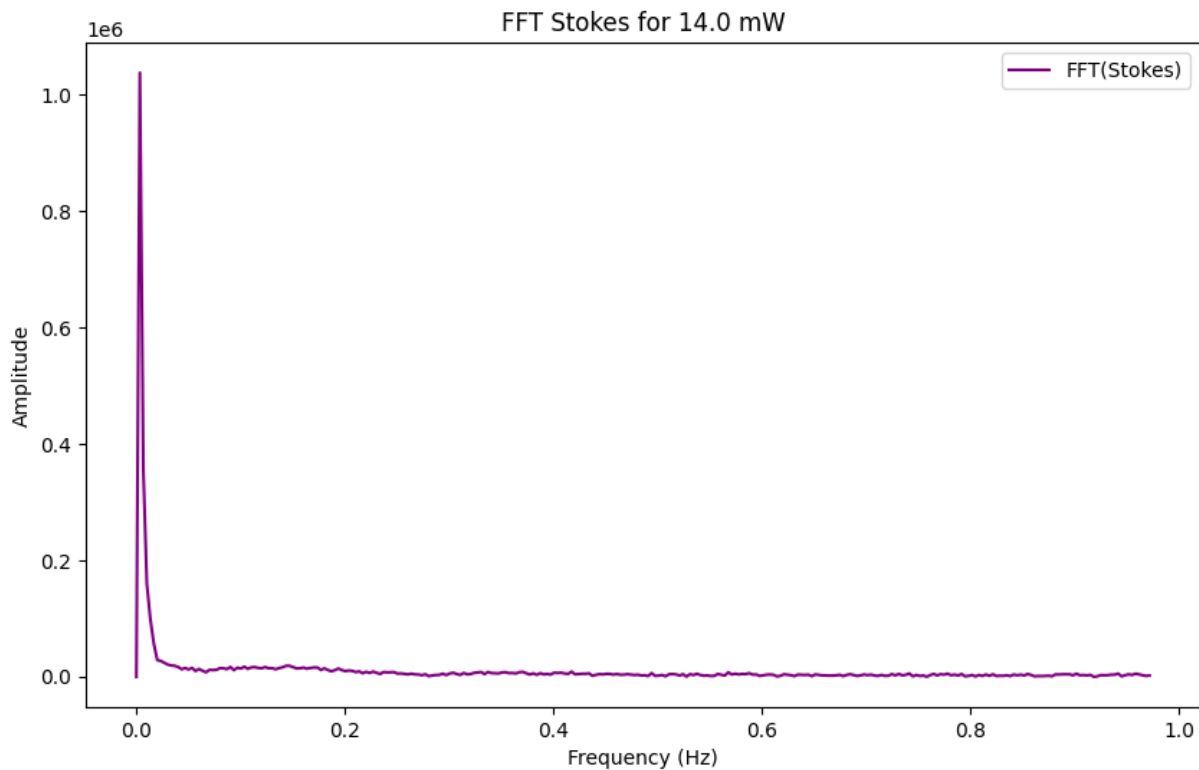
WL=673.98, Cnt=8986.47

WL=671.94, Cnt=8978.02

WL=668.36, Cnt=8925.58

WL=669.89, Cnt=8840.69

## FFT Stokes for 14.0 mW



Peak Info (FFT Stokes):

Freq=0.00, Amp=1037744.26

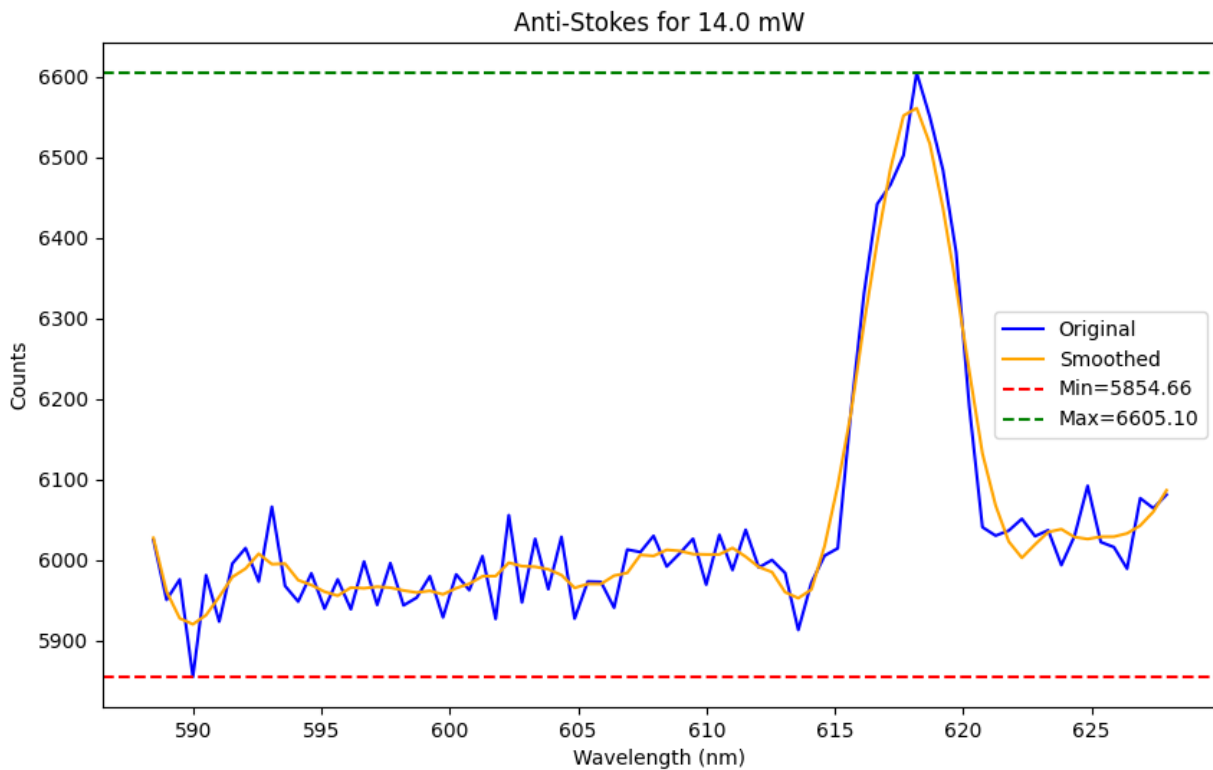
Freq=0.14, Amp=19017.25

Freq=0.10, Amp=17461.13

Freq=0.09, Amp=16990.01

Freq=0.12, Amp=16804.76

### Anti-Stokes for 14.0 mW



Integral (Area) = 238651.01

Peak Info (Anti-Stokes):

WL=618.19, Cnt=6605.10

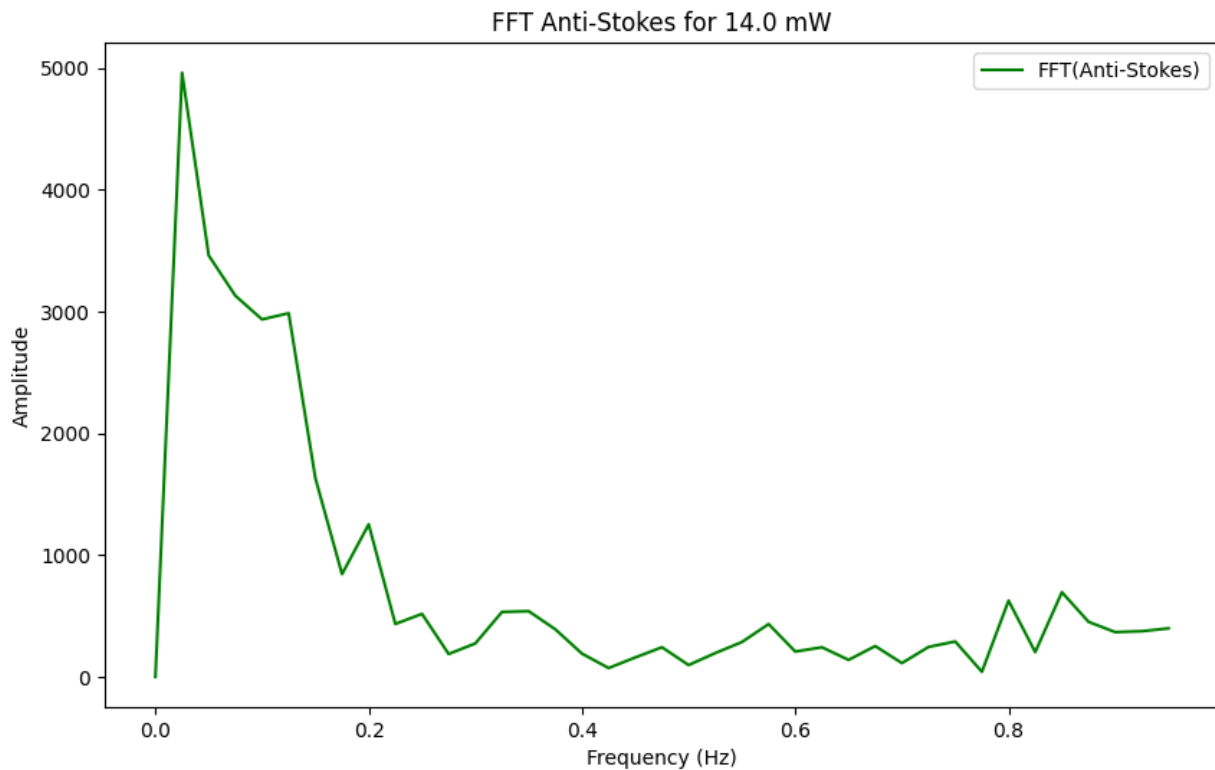
WL=624.85, Cnt=6092.03

WL=626.90, Cnt=6076.58

WL=593.07, Cnt=6065.98

WL=602.30, Cnt=6055.51

### FFT Anti-Stokes for 14.0 mW



Peak Info (FFT Anti-Stokes):

Freq=0.02, Amp=4961.79

Freq=0.12, Amp=2986.70

Freq=0.20, Amp=1252.69

Freq=0.85, Amp=695.32

Freq=0.80, Amp=625.79